Rowan University
Rowan Digital Works

Theses and Dissertations

7-27-2023

EVALUATING THE PERMEABILITY OF POROUS AGGREGATE CONCRETE USING ELECTRICAL RESISTIVITY-BASED MEASUREMENTS

Ariel Miguel Mendez Aragoncillo
Rowan University

Follow this and additional works at: https://rdw.rowan.edu/etd

 Part of the Civil Engineering Commons, and the Transportation Engineering Commons

Recommended Citation

Aragoncillo, Ariel Miguel Mendez, "EVALUATING THE PERMEABILITY OF POROUS AGGREGATE CONCRETE USING ELECTRICAL RESISTIVITY-BASED MEASUREMENTS" (2023). *Theses and Dissertations*. 3145.
https://rdw.rowan.edu/etd/3145

This Dissertation is brought to you for free and open access by Rowan Digital Works. It has been accepted for inclusion in Theses and Dissertations by an authorized administrator of Rowan Digital Works. For more information, please contact graduateresearch@rowan.edu.

EVALUATING THE PERMEABILITY OF POROUS AGGREGATE CONCRETE USING ELECTRICAL RESISTIVITY-BASED MEASUREMENTS

by

Ariel Miguel Mendez Aragoncillo

A Dissertation

Submitted to the
Department of Civil and Environmental Engineering
College of Engineering
In partial fulfillment of the requirement
For the degree of
Doctor of Philosophy in Civil Engineering
at
Rowan University
April 24, 2023

Dissertation Chair: Gilson R. Lomboy, D.Eng, Ph.D., P.E., Assistant Professor, Department of Civil and Environmental Engineering

Committee Members:
Cheng Zhu, Ph.D., P.E., Assistant Professor, Department of Civil and Environmental Engineering
Douglas Cleary, Ph.D., P.E., Professor, Department of Civil and Environmental Engineering
Umashanger Thayasivam, Ph.D., Professor, Department of Mathematics
Yusuf Mehta, Ph.D., P.E., Professor, Department of Civil and Environmental Engineering

© 2023 Ariel Miguel Mendez Aragoncillo

Dedications

For my parents, brothers and sister, and my wife Beah.

For tatay Leo, nanay Conching, tiyo Wilson, and sir Jojo.

For the Department of Civil Engineering – University of the Philippines Los Baños.

Acknowledgments

First and foremost, I would like to express my deepest appreciation to my committee members for their time, expertise, and support throughout my Ph.D. study. Especially to my adviser, Dr. Gilson Lomboy, for guiding me and for being a great role model. I learned a lot from you.

I would also like to acknowledge the people that helped me on this research. To Dr.Shah, thank you for being a friend and for sharing your technical knowledge and expertise. To Paolo, thanks for helping me with the programming part of my research. I am also grateful to Mohsen, Seth, Tasnia, and all the undergraduate clinic students who worked with me on important research activities.

Thank you to the Department of Civil Engineering, University of the Philippines Los Baños, for giving me the opportunity to study in the US. This endeavor could not have been possible without my ERDT scholarship and the people involved in providing me with the funding for four years. I was able to focus on my dissertation research thanks to that.

Thank you to my parents, my wife, my entire family, my old friends, and to the new friends I've met here in New Jersey, for the encouragement, motivation, and fun memories. Special thanks to Beah for her sacrifices and support throughout my Ph.D. journey. Lastly, thanks to the NBA, Netflix, and manga for keeping me out of boredom and homesickness.

Abstract

Ariel Miguel Mendez Aragoncillo
EVALUATING THE PERMEABILITY OF POROUS AGGREGATE CONCRETE USING ELECTRICAL RESISTIVITY-BASED MEASUREMENTS
2022-2023
Gilson R. Lomboy, D.Eng, Ph.D., P.E.
Doctor of Philosophy in Civil Engineering

Recycled concrete aggregates (RCA) and lightweight aggregates (LWA) are popular alternative aggregates for concrete. However, due to their highly porous structure, concrete with RCA and LWA shows a different microstructure and higher permeability than conventional concrete. Thus, the existing relationships used to evaluate the permeability and, consequently, the durability of concrete are not applicable in concretes with RCA and LWA. This research examined the permeation properties of recycled aggregate concrete (RAC) and lightweight aggregate concrete (LWAC). The relationships between electrical resistivity-based measurements in RAC and LWAC and their permeation properties were determined and compared to that of normalweight aggregate concrete (NWAC). At the same electrical resistivity, RAC has higher chloride permeability than LWAC and NWAC. But at the same formation factor, LWAC has higher water permeability than RAC and NWAC. Permeability prediction models for RAC and LWAC were generated using multiple linear regression. Lastly, image analysis was used to determine the air void structure and material composition of the concretes. The air void structure and paste content were found to have significant effects on most permeability measurements.

Table of Contents

Table of Contents (Continued)

Table of Contents (Continued)

Table of Contents (Continued)

Table of Contents (Continued)

List of Figures

List of Figures (Continued)

Figure Page

List of Figures (Continued)

Figure Page

List of Figures (Continued)

Figure Page

List of Figures (Continued)

Figure Page

List of Figures (Continued)

Figure Page

List of Figures (Continued)

Figure Page

List of Tables

List of Tables (Continued)

List of Tables (Continued)

Chapter 1

Introduction[1]

The goal of this research is to be able to use electrical resistivity in predicting the permeability of concrete with porous aggregates. The electrical resistivity of concrete has been correlated to other permeation properties, such as water permeability and rapid chloride permeability. With the electrical resistivity device becoming more commercially available, these correlations made it possible to predict different durability indicators of concrete with simpler and faster testing. However, these relationships were limited to concrete with natural aggregates, which usually have low to moderate permeability. Concrete produced from alternative aggregates such as recycled concrete aggregates (RCA) and lightweight aggregates (LWA) exhibits high permeability and a microstructure different than conventional concrete. A better understanding of the characteristics of recycled aggregate concrete (RAC) and lightweight aggregate concrete (LWAC) will promote their use in the construction industry. Hence, new statistical relationships between the electrical resistivity and the other permeation properties of RAC and LWAC need to be established.

1.1 Background of the Study

1.1.1 Concrete Durability and Permeability

Concrete is the most popular construction material in the world. Concrete-made structures can be found almost everywhere. Because of its high strength and ability to be

[1] Some parts of this chapter are published in [129, 130]

cast into different shapes, it is the most common material for infrastructures such as bridges, buildings, and dams. However, concrete deteriorates. It might take several years or decades, but concrete structures will degrade over time. While deterioration can be considered a natural occurrence, premature deterioration is not desired for any structure as it incites high direct and indirect concrete repair costs.

Producing better and more durable concrete has been a continuous research subject for years. Methods of evaluating concrete durability were established by various codes and research [1, 2, 3, 4]. Since variation in the mixing materials or methods changes the concrete properties, most durability tests are also intended to compare the properties of different concrete mixtures. Many of these developed methods and techniques consider the transport of harmful substances into the concrete to measure its potential for degradation. Thus, these methods measure the permeability characteristics of concrete [5, 4]. Although the term permeability refers to the rate of fluid transport into porous solids under a pressure differential, most frequently, it is used, to include other fluid transport mechanisms such as absorption and diffusion [5, 6]. High permeability combined with the concrete's exposure to the unfavorable environment will adversely affect the durability of concrete through physical effects that include surface wear, cracking, and exposure to extreme temperatures, as well as through chemical effects involving leaching of cement paste, sulfate attack, alkali-aggregate reaction, and corrosion of embedded steel [7].

1.1.2 Electrical Resistivity-Based Tests

Among the methods of quantifying concrete permeability, the electrical resistivity tests are the simplest. By using commercially available apparatus, this method can give instantaneous results. AASHTO T 358 [8] and TP 119-15 [9] provided a guideline for evaluating the likelihood of corrosion using the measured electrical resistivity of the concrete. Several studies [10, 11, 12, 13, 14] also found a strong correlation between the electrical resistivity of the concrete and its other permeation properties, such as rapid chloride penetration and water permeability.

The measurement of the electrical resistivity of saturated concrete is influenced not only by the porosity and pore connectivity of the hardened concrete but also by the conductivity of the pore solution. However, only the porosity and pore connectivity indicate the concrete's resistance to the penetration of ions. Therefore, two concrete types with the same measured electrical resistivity do not necessarily have the same potential durability [15]. The formation factor, FF, was introduced as a better indication of concrete's permeability by disregarding the interference of the pore solution in the electrical resistivity measurement. It is calculated as the ratio between the measured electrical resistivity and the pore solution's resistivity. Likewise, it is also related to the inverse of the product of porosity and pore connectivity, as shown in Equation (1) [16, 17].

$$FF = \frac{\boldsymbol{\rho}}{\boldsymbol{\rho o}} \approx \frac{\mathbf{1}}{\boldsymbol{\phi \beta}} \quad (1)$$

where ρ = bulk resistivity of the saturated concrete, ρo = resistivity of the pore solution in the concrete, ϕ = porosity of the matrix, and β = connectivity of the pores.

For a more accurate determination of the formation factor without directly measuring the conductivity of pore solution inside the concrete, a method called "bucket test" [15] can be used. In this method, the specimens are immersed in a simulated pore solution with known conductivity for at least six days until the pore solution inside the concrete matches the solution in the bucket [18]. The pore solution chemistry is dependent on the cement content, water-cement ratio, degree of hydration, and curing condition. It can be estimated from the online calculator provided by the National Institute of Standards and Technology (NIST) [19]. Using an accurate curing solution is the key point in this method, leading to a lower error in the estimation of pore solution resistivity [15]. The electrical resistivity of the specimens can be measured at desired age, and the formation factor can be calculated immediately since the solution's composition and resistivity are known.

1.1.3 Aggregates in Concrete

Even though aggregates compose the largest volume in the concrete, their direct contribution to the total porosity is usually minimal, as observed in porosity distribution plots presented by Qiao et al. [20]. This minimal effect in total porosity is because most natural aggregates have lower porosity than cement paste. A porosity of up to 2% is typical for intrusive igneous rocks and up to 5% for dense sedimentary rocks [7]. The use of more porous aggregates, such as Recycled Concrete Aggregates (RCA) and Lightweight Aggregates (LWA), might increase the total porosity and the coefficient of

permeability of concrete significantly. Furthermore, use of these aggregates changes the microstructure of concrete, particularly the interfacial transition zone (ITZ), the most porous phase of concrete's microstructure.

1.1.3.1 RCA. In a move towards sustainable development, recycling concrete wastes as aggregate has been a research subject in recent years. Several states produce recycled concrete aggregates in the United States for construction use. These aggregates were filtered and graded like natural aggregates. Several studies have found that recycled aggregate concrete can achieve a strength suitable for common structural uses. However, the microstructure of recycled aggregate concrete is much more complicated than that of natural aggregate concrete. Because RCA is composed of the old mortar and its original aggregate, the new ITZ is divided into the interface between the new cement paste and the old mortar and the interface between the new cement paste and the RCA's rock side [21]. Compared to normalweight aggregate concrete, the RAC was found to reach about two times higher water and air permeability coefficients [22].

RCA is becoming a popular alternative aggregate for concrete to reduce the demand for the declining supply of natural aggregates. However, the concretes made with RCA, or the recycled aggregate concretes (RAC), exhibit high permeability due to the adhered mortar in the RCA. When exposed to other aggressive chemicals, such as magnesium sulfate and sulfuric acid, RAC shows higher mass and compressive strength losses than normalweight aggregate concrete (NWAC) [23]. Significant improvement in RAC durability properties can be achieved either by improving the properties of cement paste and ITZ with the use of supplementary cementitious materials (SCMs) [23, 24, 25]

or with various treatments of the attached mortar in RCA such as the immersion in pozzolan slurry and pre-carbonation [26, 27, 28, 29].

1.1.3.2 LWA. Lightweight aggregates such as pumice, shale, slate, perlite, and volcanic cinders have been used in construction mainly to reduce the dead weight of the structure. The LWA for structural concrete has a bulk density of less than 1120 kg/m^3 compared to normalweight aggregates (NWA), with a bulk density ranging from 1120 kg/m^3 to 1920 kg/m^3 [30]. The use of LWA as partial or full aggregate replacements in concrete is common nowadays. Most mid-rise construction today uses lightweight concrete slabs on steel decks. Reducing aggregate weight allows concrete weight savings of over 20 percent [31]. Lo and Cui [32] have observed a well-bonded ITZ between the lightweight coarse aggregate and hydrated cement paste. Cement paste infiltrated the pores at the surface of LWA, resulting in a better interfacial bond between the cement paste and aggregate at the ITZ and reduced porosity compared to the ITZ of concrete with normal weight aggregates.

An LWAC can still achieve strengths satisfactory for structural concrete even with high LWA volumes [33, 34, 35, 36]. One of the remarkable properties of an LWAC is the improved interfacial transition zone (ITZ) between the cement paste and the aggregates. In regular concrete, the ITZ is the weakest and most porous phase of concrete microstructure. But with the porous surface of LWA, the cement paste can penetrate the LWA to some depth and interlock with it, resulting in a denser and improved ITZ [32, 37]. Furthermore, the relatively similar coefficient of thermal expansion between the LWA and mortar results in fewer microcracks in their interfacial zone [7, 38].

Due to the LWA's very high porosity and large pore sizes, problems regarding the durability of LWACs can be naturally assumed. Increased water absorption and permeability were recorded for concrete mixtures with a high volume of LWA [33, 39, 34, 40, 36]. The recorded high permeability measurements are a concern for concrete's durability. When water can flow easily into the material, several deterioration forms can occur, such as sulfate attack, reinforcement corrosion, frost action, and alkali-aggregate reaction [7, 41]. Therefore, most durability evaluation of concrete uses its permeability as an indicator.

While several studies show that concretes with coarse LWA generally have higher permeability than NWACs, it does not necessarily mean that LWACs are always less durable. A few studies compared the depth of fluid penetration [42, 39, 35] and found that the penetration depth in LWAC is about the same and, in some cases, lower than in NWAC. While it was attributed to the improved ITZ, this can also be because porous aggregates significantly increase the total penetrable area in the concrete. Given the same volume of liquid absorbed, the penetration depth in a more porous concrete will be lower than in the others given the same exposure period. The permeability, however, remains a good measure of concrete's durability when comparing concretes with similar aggregate porosity or when the difference in the measured permeabilities is too high.

1.2 Problem Statement

Among the techniques for evaluating the permeability of concrete, the electrical resistivity tests are the simplest and fastest. The electrical resistivity can be used to predict the permeability of normalweight concrete [43, 44, 12, 13]. However, the

established relationships between permeation properties of concrete are mostly made on ordinary and high-strength concretes with natural aggregates. Although the tested concrete mixtures ranged from the most permeable possible design to the least permeable quality concrete, most concretes are mainly in the low to medium permeability range, and very few are in the high permeability region. Concrete with alternative aggregates, such as RAC and LWAC, shows a different microstructure and higher permeability than conventional concrete. For this reason, the following hypotheses were developed:

1. The relationships between electrical resistivity and permeation properties of concrete with porous aggregates are different from traditional concrete.
2. The permeability of RAC and LWAC will vary based on the properties of the aggregates and the new mortar.
3. The air-void structure of concrete with porous aggregates affects the concrete permeability.

1.3 Significance of the Study

This study will contribute to the body of knowledge about RAC and LWAC, specifically on their durability and permeability. A deeper knowledge on the effect of using high volumes of RCA and LWA on concrete will improve our understanding of their suitable applications in the construction industry. Using these alternative aggregates can be part of a solution to the problem of a declining supply of natural aggregates. Furthermore, the relationships found in this study can be used to estimate the water permeability, rapid chloride permeability, and sorptivity-based measurements of RAC and LWAC using electrical resistivity-based tests. With that, evaluating the durability of

concrete can be faster and easier. The more rapid testing can further increase the research about RAC and LWAC.

1.4 Goals and Objectives

The principal objective of this study is to establish a method of evaluating the permeability of concrete with porous and high permeability coarse aggregates (RCA and LWA) using electrical resistivity-based measurements. The concrete permeability measurements include water permeability, rapid chloride permeability, and water sorptivity, while the electrical resistivity-based measurements include surface resistivity, bulk resistivity, and formation factor. Specific objectives are to:

1. Measure the permeability of concrete with porous aggregates;
2. Determine the correlation of electrical resistivity-based measurements to the water absorption, sorptivity, water permeability, and rapid chloride permeability;
3. Develop permeability prediction models using electrical-resistivity-based measurements as the primary explanatory variable; and
4. Analyze the effect of air void structure on concrete permeability.

1.5 Scope and Limitations

Ordinary portland cement concretes with porous coarse aggregates were analyzed in this research. No supplementary cementitious materials were used. The same cement, water, sand, and admixtures were used. The mix proportions of RAC and NWAC

mixtures were based on ACI 211.1, while LWAC mixtures were designed based on ACI 211.2. The concrete mixing and testing were divided into two stages:

1.5.1 Stage 1: RAC Mixtures (100 % Coarse Aggregate Replacement)

Sixteen RAC mixtures made from eight RCA variations and two varying water-cement ratios (0.48 and 0.38) were examined in this stage. The RCAs were manufactured from parent concretes with known mixture proportions. The RCAs were almost one year old at the time of first mixing. The RCAs also have no presence of foreign materials such as ceramics, masonry, and other building wastes found in RCAs produced from concrete debris.

1.5.2 Stage 2: LWAC Mixtures (0%, 50%, 100% Coarse Aggregate Replacement)

Nine concrete mixes with varying coarse aggregate percent replacements and three water-cement ratios (0.48, 0.38, and 0.28) were prepared. The LWA used is Solite, an expanded shale aggregate produced by NorthEast Solite Corporation, New York, USA. The 0% replacement served as the reference mixture, as all aggregates used were normalweight. The 50% coarse aggregate replacement was based on absolute volume.

The concrete specimens were cured for 28 days before testing for different permeability measurements. The permeability tests include surface resistivity, bulk resistivity, formation factor, rapid chloride permeability, water permeability, and water sorptivity. The permeability tests performed are common indicators of concrete durability.

1.6 Research Organization

This dissertation was divided into seven chapters. Chapter 2 presents the existing methods of permeability measurements and the past studies about permeability relationships and performance of concretes made from RCA and LWA. Chapter 3 presents the materials used and the methods followed in the study, including the concrete mixture design and permeability measurement techniques. The results are discussed in three separate chapters:

1. Chapter 4 shows the fresh concrete properties and permeability measurements on porous aggregate concretes. The effects of the variation in materials used were checked by tests for equality of means. Then, the general relationships between the permeability and electrical resistivity-based measurements were shown.
2. Chapter 5 shows the prediction models developed for water permeability, rapid chloride permeability, water sorptivity, and rate of saturation. Either bulk or surface resistivity, and formation factor, were used as the main explanatory variables, and the models were compared based on the residuals.
3. Chapter 6 shows the air void analysis results measured from the image analysis method. The relations of the air void parameters with the permeability measurements were investigated. The air and paste contents of RCA were also determined in this chapter.

Finally, the conclusions and recommendations for future work based on the results of the study were summarized in Chapter 7.

1.7 Summary of Research Highlights

The permeability of concrete with all coarse RCA was investigated. High chloride ion permeability was observed in all RAC specimens. On the other hand, some of the RAC specimens, particularly those with a low water-cement ratio, were found to have low water permeability. Compared with the established correlation from conventional concrete studies, RAC shows a higher slope of electrical resistivity versus chloride permeability regression line.

The permeability of concrete with coarse LWA at 50% and 100% aggregate replacement was also investigated. The measurements were then compared with the RAC and NWAC permeability. Very high water permeability was observed in all LWAC specimens. Differences in the regression slope of the three concrete types were also found.

A series of multiple linear regressions were performed to improve the permeability regression models, with the electrical resistivity-based properties as main predictors and the aggregate and fresh concrete properties as additional explanatory variables. Most permeability regression models of RAC and LWAC improved, returning low residual standard errors. However, high errors were still observed in the GWT regression models because of the high variability of measurements within the group.

Lastly, a method to calculate the air void structure of the porous aggregate concretes was presented. The air void structure and concrete volume components determined using the image analysis method can be used to characterize the permeability

of RAC and LWAC. There are trends observed between some air void parameters and concrete permeability measurements.

Chapter 2

Literature Review

In the design of structures, engineers or designers should give importance not only to the strength of the material but also to its durability. Every designer should have a good understanding of how environmental factors affects the performance of the concrete. From an economic perspective, the structures should be designed to be serviceable throughout their design life without significant deterioration. Therefore, studies characterizing the concrete properties and how they possibly affect its durability are of great interest.

Several codes and research established methods of evaluating concrete durability based on its permeability. The common methods of measuring concrete permeability are discussed in this section. Furthermore, the related studies that measured the permeability of concrete with porous aggregates, the subject of this dissertation, are summarized. The materials of interest in this research include coarse recycled concrete aggregates (RCA) and coarse lightweight aggregates (LWA).

2.1 Concrete Durability

The durability of concrete is defined as its "ability to resist weathering action, chemical attack, abrasion, and other conditions of service" [45]. Durable concrete can be exposed to its intended environment throughout its service life without deteriorating to the extent that it is unsafe to use. It can be achieved with good design and proper mixing, placing, and concrete curing. Still, there are cases of premature deterioration of concrete. These cases provided lessons on controlling the factors affecting concrete durability [7].

While it is one of the main components in creating concrete, water is also involved in every form of its deterioration [7]. Because of its tiny molecules, water can penetrate extremely fine pores in a material. Since it usually carries some ions and gases, water becomes instrumental in causing chemical deterioration in the concrete. Furthermore, water can cause disruptive volume changes into porous solids due to its moisture movements and structural transformations.

2.1.1 Frost Action

In places with a cold climate, some water inside the concrete freezes and expands, developing internal pressure in the concrete. The progressive expansion of the cement paste matrix due to repeated freezing and thawing could further result in concrete cracking and spalling. Powers [46] described the frost action mechanism in concrete and the use of air entrainment as an effective “escape boundary” for water molecules [7]. As the water inside the concrete freezes, its volume expands by 9% and requires dilation of the cavity or forcing out of the excess water into the boundaries of the specimen. The hydraulic pressure generated during this process depends on the distance of the cavity to an “escape boundary”, the permeability of the intervening material, and the ice formation rate. Damaging pressure can be developed in a saturated cement paste unless an escape boundary is present, not farther than three or four-thousandths of an inch for every capillary cavity. Air voids can provide an effective escape boundary to reduce this pressure. Well-distributed air voids can be achieved using a suitable air-entraining agent.

In addition to the hydraulic pressure, the osmotic pressure generated from the partial freezing of pore solutions can also cause a destructive expansion in cement paste

[46, 7]. Since water in cement paste contains some soluble substances such as alkalies, chlorides, and calcium hydroxides, its freezing point is lower than in pure water. Generally, the higher the concentration of the solution, the lower the freezing point. Partial freezing of the pore solution results in an imbalance in ionic concentrations and hence in osmotic pressure.

2.1.2 Corrosion

Groundwaters, seawater, and some industrial effluents usually contain chloride, sulfate, or bicarbonate of magnesium [7]. The ingress of chloride ions into the concrete is another factor of deterioration and can result in corrosion of the reinforcements in concrete. Corrosion will further cause structural problems due to the loss of bond strength between the steel and the concrete and a reduction in the cross-section of the rebar [7]. Furthermore, the volume increase due to transforming metallic iron to rust would result in concrete expansion and cracking. Ionic diffusion is the movement of ionic species in concrete due to a concentration gradient. It can be used as a measure of the susceptibility of reinforced concrete to corrosion [47].

Corrosion will initiate when a critical amount of oxygen and water reaches the surface of the embedded steel [2]. An adequately thick concrete cover is usually provided to protect the reinforcements from air and water to inhibit corrosion. Naturally, a passive film is formed due to the high alkalinity of the concrete pore solution, which protects the steel reinforcements against corrosion [7]. A well-hydrated Portland cement paste has a high-pH pore solution ranging from 12.5 to 13.5 depending on Na^+, K^+, and OH^- ions concentration. However, when chloride ions can penetrate the concrete and a critical Cl^-

/OH^- molar ratio is met, this passive film becomes either permeable or unstable. Once the passive film is destroyed, the corrosion rate is dictated by the concrete's electrical resistivity and oxygen availability. Chloride ions can come from concrete admixtures, salt-contaminated aggregates, deicing salt solutions, and seawater.

Even with the absence of chloride ions, the passive film protecting the steel reinforcements against corrosion can be destroyed when the alkalinity of the solution is reduced to less than 11.5 [7]. Exposure of the concrete to an acidic environment reduces the pH of the pore solution, which destroys the passivity of the steel and permits the initiation of the corrosion process. The presence of free CO_2 in soft and stagnant water, SO_4^{2-} and Cl^- in groundwater and seawater, and H^+ ions in industrial water are the usual reasons for the lower pH below 6.

2.1.3 Sulfate Attack

The ingress of sulfate ions into concrete may result in the deterioration of concrete, which can manifest in two forms [7]. Sulfate ions react chemically with the alumina-containing hydrates and with calcium hydroxide. These hydrates are converted to high-sulfate form ettringite, which is known to cause an expansion in the concrete. The concrete expansion eventually leads to cracking, increasing the permeability and thus accelerating the deterioration process.

The loss of cohesiveness of hydration products is another form of concrete deterioration by sulfate attack [7]. With concrete exposure to sulfate solutions such as Na2SO4 and MgSO4, the concrete's calcium hydroxide and calcium silicate hydrate (C-S-H) can be converted into gypsum. The gypsum formation lowers the system's pH and

reduces strength and stiffness. It is then followed by expansion, cracking, and eventually turns the cement paste into a mushy or non-cohesive mass [48]. High sulfate concentrations are common in natural and industrial waters such as groundwater, agricultural soil and water, sewer pipes, and cooling towers.

Improper design and poor practice in concrete construction will not only result in a shorter service life but may also result in a high economic cost due to extensive repairs. Because of this, various codes of practice established more restrictive regulations in the design and construction of concrete materials [4]. In American Concrete Institute (ACI) 318-14 [49], Building Code Requirements for Structural Concrete, durability is considered in the design based on the exposure category by limiting the water-cement ratio, specifying the minimum compressive strength, restrictions in the type of cementitious materials, and addition of air content.

2.2 Concrete Permeability

The concrete deterioration rate is usually determined with the ease of water penetration into the material [7]. Permeability is the ease at which fluid flows through a solid material under pressure. Water or moisture ingress in the concrete may result in steel reinforcements' corrosion and the concrete's resaturation, which is critical to freeze-thaw damage.

The size and continuity of pores in the material can be used to evaluate the permeation property of concrete. High permeability and exposure to the unfavorable environment will adversely affect the durability of concrete through physical effects that include surface wear, cracking, and exposure to extreme temperatures, as well as through

chemical effects involving leaching of cement paste, sulfate attack, alkali-aggregate reaction, and corrosion of embedded steel [7].

2.2.1 Porosity

Higher porosity generally means higher, but while porosity pertains to the pore volume over the total material volume, permeability is concerned with the connectivity of the voids. Still, porosity is a good indicator of the material's permeability. The total porosity of concrete can be expressed as the sum of the pores in the hydrated cement paste, the entrained and entrapped air voids, and the pores in the aggregate [50].

For concrete exposed to freezing and thawing cycles, ACI suggests that the total air content shall be designed in the range of 3.5% to 7.5% depending on the maximum size of aggregates and exposure condition [49]. Adding air-entraining agents (AEA) in the concrete mix can ensure sufficient air content. Without AEA, the entrapped air bubbles during the concrete mixing coalesce and are expelled from the mixture. AEAs prevent the bubbles from coalescing and stabilize them to protect the concrete against freezing and thawing cycles.

Porosity in the paste can be classified based on its pore sizes, capillary porosity or the voids contained between the C-S-H and the crystalline hydration products, and gel porosity, which is an intrinsic part of the C-S-H gel. Capillary pore diameter ranges from 50 nm to 10 μm, while the smaller gel pores range from 0.5 nm to 2.5 nm. The large pores are probably more influential in strength and permeability, while the smaller pores influence the drying shrinkage and creep [7].

As the hydration progresses, the hydration products increase and fill up the voids, decreasing the porosity of the cement paste. As a result, the coefficient of permeability of the paste decreases. However, porosity and permeability have no direct proportionality [7]. When the porosity is still high, a decrease in the capillary porosity results in a significant drop in the permeability coefficient. However, when the porosity is below 30 percent, the reduction rate in the permeability coefficient is much lower. At this point, the interconnection between the voids becomes more tortuous that a decrease in the porosity no longer significantly decreases the permeability coefficient [7].

Even though aggregates compose the largest volume in the concrete, they usually have low porosity, and their contribution to the total concrete porosity is mostly minimal. It is because most natural aggregates have low porosity compared to cement paste. A porosity of up to 2% is typical for intrusive igneous rocks and up to 5% for dense sedimentary rocks [7]. However, the coefficient of permeability in aggregate is not necessarily lower. Because of its larger pore sizes, greater than 10 μm on average, compared to the capillary pores in cement paste, some aggregates with only 10 percent porosity show a higher permeability coefficient than the cement paste [7].

The aggregate pores might be significant if very porous aggregates like RCA and LWA are used. In the concrete elementary model studied by Long et al. [51], it was determined that the water porosity of coarse aggregates is one of the main factors affecting the water porosity of concrete. The water porosities of different coarse aggregates used were 0.65% for siliceous quartz, 0.88% for hardened limestone, 1.20% for siliceous calcareous, 12.45% for soft limestone, and 20.03% for recycled concrete.

The ranking of the resulting water porosity of the elementary model was the same as the ranking of the aggregate's water porosity.

2.2.2 Factors Affecting Concrete Permeability

The permeability of concrete is affected by various factors, including the concrete mix proportion, presence of admixture and other cementitious materials, cement type, aggregate properties, curing, degree of hydration, presence of cracks or microcracks, degree of consolidation, finishing methods, and surface treatment [52]. The water-cement ratio is a significant parameter affecting the strength and permeability of concrete.

Generally, a higher water-cement ratio results in a higher porosity of the paste matrix and, consequently, lower strength and higher permeability [7]. The volume of water in the mix is responsible for the volume of empty voids left after the water has been consumed by cement hydration or evaporation. In the early stage of hydration, the void spaces occupied by water are relatively large and well-connected; therefore, the coefficient of permeability is high. As hydration progresses, hydration products occupy these spaces, and the size of voids is reduced, losing their interconnections and resulting in a lower coefficient of permeability. The discontinuity of void spaces in the cement paste can be achieved when the porosity is reduced to about 30 percent [7]. With properly cured concrete mixtures, this porosity can usually be achieved. Although with a higher water-cement ratio, the time it takes to reduce the porosity to this degree takes longer.

Aggregate properties, such as gradation, size, shape, surface texture, absorption, and porosity, directly and indirectly affect concrete's strength and permeability. Conventional aggregates normally have a lower coefficient of permeability than cement

paste. However, using low-permeability aggregates does not necessarily result in a lower coefficient of permeability in concrete. The use of large aggregates results in a higher local water-cement ratio in the interfacial transition zone (ITZ) due to bleeding and thus results in a more porous and weaker ITZ [5]. Microcracks might also develop in the ITZ due to the differential strain between the aggregate and the cement paste [7]. These cracks are larger than most capillary voids present in the cement paste. During the application of external loading, interconnections between these microcracks develop and increase the concrete's permeability.

The porosity of the aggregate can also be significant to the coefficient of permeability of the concrete. It was found that concrete produced from dense limestone aggregates has a significantly lower coefficient of permeability than those made from porous limestone and river gravel [11]. In another study [53] that used four different aggregate types, the lowest permeability measurements were measured in concrete mixtures with granite aggregates. In contrast, the highest permeability results were found in concrete mixes with coarse gravel aggregates. Other aggregates used in the study are limestone and gneiss. Aggregate gradation also affects permeability. Concrete with well-graded aggregates showed lower permeability than gap-graded mixes [53].

2.3 Standard Permeability Tests

Producing better and more durable concrete has been a continuous research subject for years. While concrete deterioration takes years to occur, methods of evaluating its long-term performance within a short time were established by various codes and research. Since variation in the mixing materials or methods results in a

difference in the concrete properties, these tests are also intended to compare the properties of different concrete mixtures. Many of these developed methods and techniques consider the transport of harmful substances into the concrete as the measure of its degradation process [4]. Thus, these methods measure concrete's permeability characteristics and relate them to durability [5]. Although the term permeability refers to the rate of fluid transport into porous solids under a pressure differential, most frequently, it is used, including other fluid transport mechanisms such as absorption and diffusion [5, 6].

2.3.1 Absorption Tests

Absorption is the process in which fluid is drawn into the concrete through capillary suction, filling the permeable voids in the material. Examples of permeability tests that measure the absorption characteristics of concrete are ASTM C642 [54] and ASTM C1585 [52], which measure the absorption capacity and sorptivity, the rate of water absorption of concrete, respectively. Absorption capacity is a measure of the effective porosity of the concrete, while sorptivity describes its ability to absorb water thru capillary suction.

2.3.1.1 Water Absorption Capacity | ASTM C642-13 [54]. By measuring the oven-dried mass, saturated mass after water immersion for at least 48 hours, saturated mass after boiling with tap water for 5 hours, and the apparent mass in the water of a concrete sample with a volume of at least 350 cm^3, the absorption, bulk density, apparent

density, and volume of permeable voids of the hardened concrete can be determined. A 50 mm thick × 100 mm diameter concrete disc satisfies the required sample volume.

2.3.1.2 Water Sorptivity | ASTM C1585-13 [52]. Sorptivity measurement reflects the susceptibility of concrete to the penetration of water. This test is done by immersing the bottom surface of an unsaturated concrete specimen in the water. The other surfaces are sealed to allow the water to be absorbed into the concrete due to capillary suction on one side only.

Concrete discs with 100mm diameter and 50mm thick, obtained from 100 x 200 mm molded cylinder samples, are conditioned for at least 18 days before testing. Conditioning of specimens is an important factor in sorptivity measurements and should be the same for all specimens. At lower relative humidity, more empty pores are available to be filled with water during the test, and the maximum size of pores filled with water is smaller, resulting in higher suction force and a thus higher rate of water absorption [55]. After conditioning the specimens at 50℃ temperature and 80% relative humidity for three days, each sample should be sealed in a container for at least 15 days. It allows the specimens to have a relative humidity of 50 to 70%, similar to the concrete surfaces in some field structures [52].

A water level of 1~3 mm above the support of the concrete sample should be maintained throughout the test. The absorption, I, at given time durations, can be calculated based on the change in mass of the specimens. The absorption rate can be determined by plotting the calculated absorption against the square root of time. A sample plot of absorption over the square root of time is presented in Figure *1*. The initial

rate of water absorption (mm/s$^{1/2}$) is the slope of the plot considering the measurements from 1 min to 6 hours, excluding the time after an apparent change in slope, is observed. The secondary rate of water absorption (mm/s$^{1/2}$) is the slope of the plot using the measurements from 1 day to 7 days of the test.

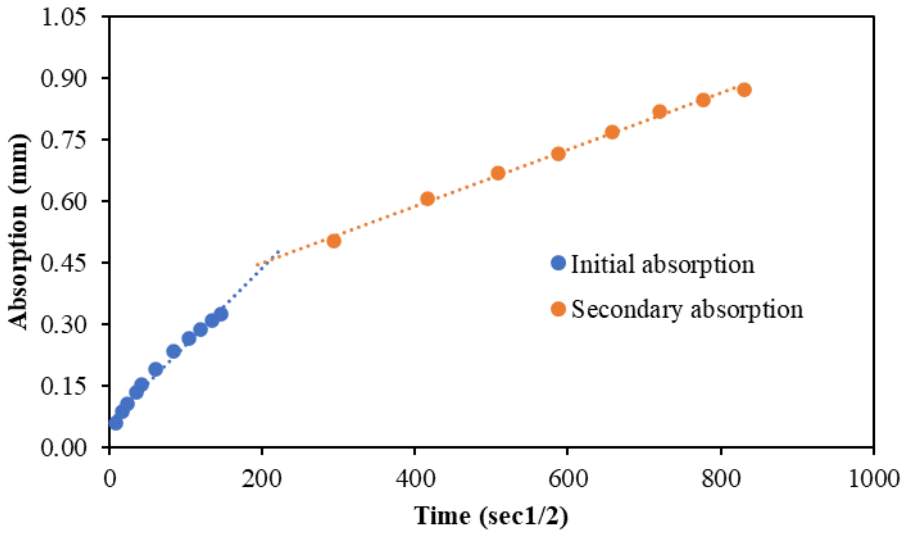

Figure 1. Sample plot of absorption vs. square root of time, sec$^{1/2}$.

The intersection of the slopes of the initial and secondary rate of water absorption represents the state of saturation when the water reaches the top of the sample [56, 47], filling just the gel and capillary pores. During the initial absorption phase, water fills the gel and capillary pores first, from the bottom to the top of the specimen. It seemed that the larger voids, which may include the entrapped or entrained air, were being filled during the secondary absorption rate [47].

The change in mass during the absorption can be converted into the degree of saturation, S, which is the ratio of the absolute volume of absorbed water to the total volume of pores or the total volume of water that the concrete can absorb. The degree of saturation can also be used to predict the performance of concrete against freeze-thaw damage [47]. Apparently, beyond the critical degree of saturation, Scr, the freeze-thaw damage begins to initiate [57, 47]. Li et al. [55] found this level at approximately 86-88% with or without entrained air in concrete.

2.3.2 Absorptivity Tests

The sorptivity test method lets the water be absorbed into the concrete through a one-dimensional flow by sealing the other sides of the concrete specimen. This nature of sorptivity tests makes it difficult to perform on the field. Absorptivity tests determine the absorption characteristic of concrete without control in the flow direction; hence they can be used to test concrete both in the laboratory and on-site [5]. Tests in this category can be classified as surface absorptivity tests and drill hole absorptivity tests. Surface absorptivity tests such as Initial Surface Absorption Test (ISAT), Autoclam sorptivity test, and standpipe absorptivity test have the source water in the form of a reservoir mounted at the surface of the specimen. On the other hand, in drill-hole absorptivity tests like Figg Water Permeability Test and Covercrete Absorption Test, water is allowed to be absorbed into concrete from a hole drilled at the surface of the test specimen [5].

2.3.2.1 Initial Surface Absorption Test (ISAT) | BS 1881: Part 208 [58]. Initial surface absorption is defined in this standard as the water flow rate per unit area of concrete surface at the stated interval and a constant applied head. In this British

standard, a 200 mm water head from a reservoir above the surface of the concrete is maintained, and the initial surface absorption at time intervals of 10 min, 30 min, and 1 hour from the start of the test is measured. The 200 mm head water pressure was said to be worse than the most severe weather exposure in the UK due to driving rain.

A higher ISAT result means that the concrete is more permeable. If, in the 10-minute reading, the ISAT result is less than 0.05 ml/(m^2×s), the concrete can be considered too impermeable. In contrast, if the 10-minute reading is more than 3.60 ml/(m^2×s), the concrete can be regarded as too permeable [58]. In both cases, the test should be stopped as the concrete is not within the sensitivity of a longer-term test.

2.3.2.2 Autoclam Sorptivity Test. "Autoclam" is a test apparatus that can measure the rate of water absorption, water permeability, and air permeability of concrete. The idea of the "Clam" test was first reported by Montgometry and Adams [59] and was initially a water permeability test only [60]. It was then modified into "Universal Clam, " including both water and air permeability tests. The pressure is controlled manually with piston movement. Basheer [61] standardized the test and further developed it into a fully automatic test by adding a microprocessor with a complete data acquisition and transfer facility enabling the computer analysis of results [60].

To measure the sorptivity, constant pressure of 0.02 bar corresponding to a water head of approximately 200 mm, similar to ISAT, is applied. The volume of water absorbed into the concrete every minute for 15 minutes is recorded. Water is filled into the Autoclam test apparatus through the priming valve until the pressure is slightly below 0.02 bar. A stepper motor increases the water pressure to exactly 0.02 bar. As water is

absorbed into the concrete, the piston moves downward to offset the loss of water pressure. The volume of water absorbed can be determined from the movement of the piston and its cross-sectional area. By plotting the cumulative volume of water absorbed over the square root of time, the sorptivity index, which is the slope of the plot, can be determined.

2.3.2.3 Standpipe Absorptivity Test. This test is one of the most straightforward techniques to measure the absorptivity of concrete [60]. The test consists of a suitable diameter vertical tube glued onto the concrete surface and filled with water up to a certain level. The amount of water absorbed into the concrete per unit of time is reported as the water absorptivity index. The diameter, water head, and test duration vary in different versions of the test. In the "chimney method", the standpipe diameter is 67 mm, the water head is constant at 100 mm, and the measurements are taken every 24 hours for six days. In the second method, known as "Karsten's pipe test", the standpipe diameter is 60 mm with a falling head of 100 mm, and measurements were taken between 5 and 15 minutes from the start of the test. Lastly, the "Australian test" has a 100 mm diameter standpipe, a 200 mm falling head, and the test duration either at 2 hours from the start of the test or until the water has fallen by 100 mm. Although these tests are easy to perform, they are not often used because of the low level of sensitivity [60].

2.3.2.4 Figg-Poroscope Method. The Figg Water Permeability Test was first introduced in 1973, based on the Drill Hole Absorptivity Test, which Mercer first developed in 1945 [5]. The method involves drilling a 10mm diameter x 40mm deep hole in the concrete surface, plugged by a special silicon rubber leaving a 10mm diameter x 20mm deep test cavity positioned 20mm from the surface [62]. Water is forced into the

hole until it is filled, and the time it takes for a water volume of 0.01 ml to escape the sealed chamber is recorded. This travel time in seconds is the Figg number and is used as an index to evaluate the quality of the concrete, as shown in Table 1.

Table 1

Relationship between Concrete Protective Quality and Figg Number [5]

Concrete Category	Protective Quality	Measured Time, s
0	Poor	< 20
1	Not very good	2-50
2	Fair	50-100
3	Good	100-500
4	Excellent	> 500

The downsides of this test method are that it does not allow the determination of the sorptivity of concrete because the water penetrates from a cylindrical source and that the drilling of the concrete surface may introduce microcracks and alter the flow mechanism [5].

2.3.3 Permeability Tests

As defined prior, permeability is the material's ability to permit liquids or gases under pressure to pass through. Some test systems, such as Autoclam and Figg-poroscope, can measure both water and gas permeability. Water permeability measurement is important for hydraulic structures where the concrete is exposed to a substantial water depth, such as underground tunnels and dams. On the other hand, gas permeability can give a more rapid index of the material's permeability and is important

to characterize the concrete's vulnerability to gases-induced deterioration such as carbonation.

This property is commonly characterized using the coefficient of permeability, K. For the tests under steady-state flow conditions, wherein the fluid properties in the system do not change over time, K can be determined using the fluid characteristics and sample geometry along with the measured flow rate and applied pressure. However, there are no widely accepted methods for the steady-state water flow test, and several studies have pointed out that a steady-state flow condition is difficult to achieve [5]. With that, most standard methods use a non-steady state condition to determine the permeability index. In some instances, the depth of liquid penetration is measured and used to determine the permeability coefficient.

Water permeability tests in a non-steady state measure either the inflow or outflow of fluids to express the permeability of concrete [5]. German's water permeability test (GWT) and the water permeability test procedure using "Autoclam" are in this category. Meanwhile, water penetration tests such as BS EN 12390-8 are more suitable if the concrete has a comparatively high density or low permeability. Using the outflow method in these types of concrete will not only take a long time to perform the test, but it will also be hard to obtain a measurable quantity of outflow water. In the penetration tests, water under a specified hydrostatic pressure is admitted into the permeability cell containing the concrete sample. At a fixed duration, the concrete sample is removed and split into half along the diameter to measure the water penetration depth.

2.3.3.1 Autoclam Water Permeability Test. In the Autoclam sorptivity test previously discussed, the low water pressure of 0.02 bar is used to ensure that the water penetration is governed by sorptivity. A higher water pressure, i.e., 1.5 bar, is applied in the system [11] for water permeability testing. The setup and procedure are the same with both sorptivity and water permeability tests, wherein the movement of the piston that compensates for the loss of water pressure as the water is being absorbed into the concrete is used to determine the flow rate. In the same way as the sorptivity index, the permeability index is calculated from the cumulative inflow and square root of the time linear plot.

2.3.3.2 Germann Water Permeability Test (GWT). GWT is a commercially available apparatus with a principle similar to the Autoclam test. It evaluates the water resistance ability of a material and can be applied in laboratory tests and in-situ examinations of concrete. A pressure chamber containing a watertight gasket is secured tightly to the specimen's surface, filled with water, and the water is allowed to penetrate the concrete. The selected pressure, usually 100 kPa (1 bar), is maintained by a micrometer gauge that pushes a piston into the chamber as the water is absorbed into the surface. The movement of the piston over time signifies the permeability of the material. The test may be conducted at a constant time, i.e., 10 minutes, or until there is no further piston movement, which usually lasts 5-10 minutes, depending on the concrete quality. The water flux, q, can be calculated from Equation (2):

$$q = B\,(g_1 - g_2) / (A \times t) \qquad \textbf{\textit{(2)}}$$

where B = area of the micrometer pin being pressed into the chamber water, g_1 = micrometer gauge reading before the test, g_2 = micrometer gauge reading after the test, A = water pressure surface area, and t = duration of the test.

A research study by Moczko and Moczko [63] determined the relationship between the values of the average water flux from the GWT and maximum values of water penetration obtained according to BS EN 12390-8. Concrete can be evaluated as water-resistant if the maximum depth of water penetration is not higher than 50 mm. The results have shown that using GWT, concrete can be assessed as water-permeable when the average flux, q_m, is more than 0.32 µm/s [63].

2.3.3.3 Depth of Penetration of Water Under Pressure | BS EN 12390-8 [64]. In part 8 of the British/European standard for testing hardened concrete, a high water pressure of 500 kPa is applied to the specimen's surface, either from the bottom or from the top, for 72 hours. The depth of water penetration is measured after splitting the sample in half. The concrete specimen shall be placed in a permeability cell. The water pressure can act on the surface area, and the pressure applied can be continuously monitored. The concrete specimens can be either cubic, cylindrical, or prismatic with a minimum dimension of 150mm.

2.3.3.4 Autoclam Air Permeability Test [60]. The last type of test Autoclam can perform is the air permeability test. The piston is positioned at the bottom of the cylinder during this test. Air is inserted into the system using a syringe attached to the priming valve until the pressure is slightly above 0.5 bar. As air penetrates the concrete, the air pressure in the system decreases. The apparatus monitors the pressure automatically and

is recorded every minute for 15 minutes or until the pressure becomes zero. The natural logarithm of pressure is plotted against time, and the gradient of the linear regression between the five and 15-minute mark (for tests lasting for 15 minutes) or from the start of the test until the pressure dropped to zero is reported as the air permeability index with units of Ln (Pressure)/min [5].

2.3.3.5 Figg Air Permeability Test. The methods of air permeability test using a poroscope are very similar to the absorptivity test discussed earlier in the chapter. With the same setup as water permeability [62], an air permeability test can be performed just before the water absorptivity or permeability test. A vacuum of less than -55 kPa is applied in the cavity, and the time it takes for the vacuum to change from -55 kPa to -50 kPa is considered the Figg number for air permeability. The relationship between this Figg number and the protective quality of concrete is shown in Table 2.

Table 2

Relationship between Concrete Protective Quality and Figg Number [5, 62]

Concrete Category	Protective Quality	Measured Time, s
0	Poor	< 30
1	Not very good	30-100
2	Fair	100-300
3	Good	300-1000
4	Excellent	> 1000

2.3.4 Diffusion Tests

Another important fluid transport mechanism in concrete is diffusion. It refers to the movement of ions, gas, or vapor into the material due to a concentration gradient from an area of higher concentration to an area of lower concentration. Among the types of diffusion tests, there is a high interest in chloride ionic diffusion because of their significant effect on the corrosion of reinforcements in concrete structures [5]. AASHTO T259 [65] measures the resistance of concrete to chloride ion penetration by subjecting the test specimens to continuous ponding with sodium chloride solution for 90 days. The total chloride content is then analyzed at various sampling depths, then the absorbed chloride ion content is calculated. Higher chloride ion contents absorbed by the specimen mean higher susceptibility of that concrete mixture against corrosion.

Another technique of measuring the chloride diffusion in concrete is according to ASTM C1556 [66]. In this test, the concrete specimen is saturated in a calcium hydroxide solution and immersed in a sodium chloride solution for at least 35 days. Powder samples from various depths of the specimen are obtained by grinding, and the acid-soluble chloride-ion contents of the powder samples for each depth are determined. The values of surface concentration and apparent chloride diffusion coefficient can be determined by curve-fitting the equation of chloride concentration to the measured chloride-ion contents.

A main drawback of AASHTO T259 and ASTM C1556 methods is their long testing duration. AASHTO T277 [67] or ASTM C1202 [68], more commonly known as the Rapid Chloride Permeability Test (RCPT), provides a rapid indication of the

concrete's resistance to chloride ion penetration by relating the electrical conductance of concrete to the results of long-term ponding tests such as AASHTO T259. Including the sample preparation, the test can be completed in only 2 to 3 days. Meanwhile, instantaneous results with less sample preparation can be produced from electrical resistivity tests, either by bulk resistivity presented in AASHTO TP 119 [69] / ASTM C1876 [70] or by surface resistivity in AASHTO T 358 [71]. These tests evaluate the resistance of concrete to chloride ion penetration based on the correlation of electrical resistivity measurements with chloride exposure tests such as ASTM C1556.

2.3.4.1 Rapid Chloride Permeability Test | ASTM C 1202 [68] or AASHTO T 277 [67]. The RCPT determines the electrical conductance of concrete and evaluates its ability to resist chloride ion penetration based on the established correlations between this test procedure and long-term chloride ponding procedures. The concrete samples, 50mm thick x 100mm diameter discs immersed in sodium chloride solution on one end and in sodium hydroxide solution on another, are subjected to dc voltage to determine their electrical conductance. A potential difference of 60 V dc is maintained across the ends of the specimen. The current is recorded at least every 30 minutes up to 6 hours. The total charge passed can be calculated by plotting the current (in amperes) versus time (in seconds) and integrating the area below the curve or by using a formula based on the trapezoidal rule as shown in Equation (3):

$$Q = 900 (I_0 + 2I_{30} + 2I_{60} \ldots + 2I_{300} + 2I_{330} + 2I_{360}) \quad (3)$$

where Q = total charge passed, Coulombs, I_0 = current (Amperes) immediately after voltage is applied; and I_t = current (amperes) at t min after voltage is applied.

Commercially available devices can automatically calculate and report the total charge passed during the RCPT. The level of chloride ion penetrability can then be evaluated using the guideline provided by AASHTO, as shown in Table 3. A "High" chloride ion penetrability is typical on conventional Portland cement concrete (PCC) with a high water-cement ratio (>0.6), while "moderate" penetrability on the moderate water-cement ratio (0.4-0.5) and "low" penetrability on the low water-cement ratio (< 0.4) conventional PCC. The "very low" chloride ion penetrability can be achieved in latex-modified concretes and "negligible" on polymer impregnated concretes [72].

Table 3

Chloride Ion Penetration based on Total Charge Passed [68]

Charge Passed, C	Chloride Ion Penetrability
>4000	High
>2000 to 4000	Moderate
>1000 to 2000	Low
100-1000	Very low
<100	Negligible

2.3.5 Electrical Resistivity Tests

Electrical resistivity is a material property that quantifies how strongly the material opposes the flow of electrical charges applied to it. This intrinsic property can be measured by applying an alternating current (I) in a concrete specimen and measuring the potential drop (V). The general formula for the resistivity is shown in Equation (4). The resistance of the concrete sample, R, is the ratio of the potential drop and the alternating

current applied. At the same time, the resistivity, ρ, can be calculated by applying a geometric factor, K, which is dependent on the specimen's geometry and method of measurement.

$$\rho = R * K = \frac{V}{I} * K \tag{4}$$

For the concrete material, the electrical resistivity tests can be in the form of surface resistivity or bulk resistivity. AASHTO uses electrical resistivity measurements to evaluate the long-term chloride ion penetration in concrete, which measures how susceptible the reinforced concrete is to corrosion. However, this comparison to the chloride penetration applies only to certain types of concrete with an established correlation between the surface resistivity and the long-term chloride diffusion procedures such as ASTM C 1556. Such correlations were presented by Vivas et al. [73] in their technical report for the Florida Department of Transportation about the comparison of results from standard conductivity and diffusion methods for concrete.

The concrete mixtures tested were cast in a laboratory and ranged from the most permeable possible design to the least permeable quality mixtures. Ordinary Portland Cement (Type II), silica sand, and crushed limestone coarse aggregates were the basic materials used. In addition, supplementary cementitious materials (SCM) and admixtures, including fly-ash class, silica fume, metakaolin, slag, calcium nitrate, air entrainer, and superplasticizer (SP), were also used. Although the mixture ranges from the most permeable possible design to the least permeable quality concrete, evaluating chloride ion penetration based on resistivity measurements provided in AASHTO TP 95-11 may not

be applicable for concrete mixtures with different pore structures such as RAC and LWAC.

2.3.5.1 Surface Resistivity | AASHTO T358 [71]. In this test method, the surface resistivity of saturated concrete with standard dimensions of 100 mm x 200 mm or 150 mm x 300 mm cylinders or cores is measured using a 4-pin Wenner probe array. An alternative current (AC) flow is applied in the specimen through the outer probes of the apparatus, and the potential difference is measured from the inner probes.

The surface resistivity, ρ, in kΩ-cm is calculated using Equation (4), wherein the geometric factor, K, is given in Equation (5). In some commercially available apparatuses, such as Proceq Resipod and Giatec's RCON, the applied correction factor is already included in each measurement of concrete resistivity.

$$K = 2\pi a \tag{5}$$

where a = probe/electrode spacing in cm.

In measuring resistivity, several aspects should be monitored to avoid misleading results. It includes the sample age, curing procedure, admixtures used, presence of reinforcing steel, degree of water saturation, and concrete temperature. Depending on the type of concrete and curing procedure, most concretes become less permeable as hydration progresses with time. Unless specified otherwise, the samples should be moist-cured for 28 days in 100 percent relative humidity before testing. If curing by immersion in lime solution is used, the results can be adjusted as it reduces the resistivity by 10 percent on average. The concrete temperature may also affect the electrical resistivity

significantly and should be maintained at 20~25°C (68~77°F) to minimize its effect on the results.

The presence of calcium nitrite in the admixtures reduces the resistivity measurement, which contrasts with the results from long-term chloride diffusion tests, where the presence of calcium nitrite in concrete has no significant effect on its resistance to chloride ion penetration. With this, long-term diffusion tests were recommended for the concrete with admixed calcium nitrite or other admixtures that might affect the results.

Appropriate consideration should also be taken if reinforcing steel is used in the concrete. Since the test is a function of electrical resistance, the presence of electrically conductive materials will affect the results. Although AASHTO stated that this test is not valid for samples containing reinforcement, the Proceq Resipod Instruction manual recommends that measurements be taken between rebars or perpendicular to the rebars if the rebar spacing is so close. Resipod is a modern resistivity meter that operates on the principle of the four-point Wenner probe.

Several studies found that the concrete's electrical resistivity strongly correlates with its resistance to chloride ion penetration. AASHTO T 358 provides a guideline for evaluating the likelihood of corrosion using the measured electrical resistivity of the concrete. The measured resistivity can be assessed in five chloride ion penetrability classifications established in ASTM C1202, as shown in Table 4.

Table 4

Chloride Ion Penetration based on Surface Resistivity [71]

Chloride Ion Penetration	Surface Resistivity (kΩ-cm)	
	100 mm x 200 mm Cylinder α = 3.8 cm	150 mm x 300 mm Cylinder α = 3.8 cm
High	< 12	< 9.5
Moderate	12 to 21	9.5 to 16.5
Low	21 to 37	16.5 to 29
Very Low	37 to 254	29 to 199
Negligible	> 254	> 199

2.3.5.2 Uniaxial or Bulk Resistivity | AASHTO TP 119 [69] or ASTM C 1876 [70].

Both AASHTO TP 119 and ASTM C 1876 provide a guideline to determine hardened concrete's uniaxial or bulk electrical resistivity. Similar to AASHTO T358, AASHTO TP 119-15 also provided a guideline for evaluating the chloride ion penetration based on bulk resistivity measurements, as shown in Table 5. Although applicable to most types of concrete, the applicability of the table, the same as in the surface resistivity, is limited to certain types of concrete with an established correlation between resistivity and long-term chloride penetration. Similarly, ASTM C 1760-12 [74], which provides a guideline for determining the electrical conductivity, the reciprocal of resistivity, can also be used.

Table 5

Chloride Ion Penetrability Classification based on Uniaxial Resistivity [69]

Chloride Ion Penetration	Bulk Resistivity (kΩ-cm)
High	< 5.2
Moderate	5.2 to 10.4
Low	10.4 to 20.8
Very Low	20.8 to 207
Negligible	> 207

Bulk resistivity has the same philosophy as surface resistivity. That is calculating the electrical resistivity of the concrete by applying an alternating current through the specimen and measuring the alternating voltage. Therefore, the required conditioning and factors affecting the resistivity, previously discussed for the surface resistivity, are the same for the bulk resistivity. The main difference is that in the bulk resistivity test, the electrical current passes through the concrete volume from one end surface to another. It is accomplished by placing the electrodes at opposing ends of the specimen, unlike in the surface resistivity test, wherein the probes are placed on one surface of the specimen.

The bulk electrical resistivity, ρ, can be determined using Equation (4), while its geometric factor, K, can be calculated using Equation (6). In some apparatus, the resistance is calculated directly for each specimen.

$$K = \frac{A}{L} \tag{6}$$

where A = cross-sectional area in cm^2, and L = specimen length in cm.

2.3.5.3 Formation Factor. The measured electrical resistivity of saturated concrete is influenced not only by the porosity and pore connectivity of the hardened concrete but also by the conductivity of the pore solution. However, only the porosity and pore connectivity indicate the concrete's resistance to the penetration of ions. Therefore, two concrete types with the same measured electrical resistivity do not necessarily have the same potential durability [15]. The formation factor, F, was introduced in ASTM C1876 [18]. It is the inverse of the product of porosity and pore connectivity and can be determined using Equation (7). The formation factor removes the interference of the pore solution and, therefore, is a better indication of the concrete's ability to resist the penetration of fluids.

$$F = \frac{\boldsymbol{\rho}}{\boldsymbol{\rho o}} = \frac{\mathbf{1}}{\boldsymbol{\phi \beta}} \tag{7}$$

where ρ = bulk resistivity of the saturated concrete, ρo = resistivity of the pore solution in the concrete, ϕ = porosity of the matrix, and β = connectivity of the pores.

Table 6 shows the relationship between the formation factor and the chloride ion penetrability classifications according to AASHTO PP 84-18 [75]. This table assumes a pore solution resistivity of 0.10 Ω-m, which is the typical value for concrete with a water-cement ratio of 0.40, alkali content of approximately 0.59% by mass at 80% hydration, and free alkali factor of 0.75 [76].

Table 6

Chloride Ion Penetrability based on Formation Factor [75]

Chloride Ion Penetration	Formation Factor
High	< 520
Moderate	520 to 1,040
Low	1,040 to 2,080
Very Low	2,080 to 20,700
Negligible	> 20,700

To determine the formation factor, the resistivity of the pore solution can be calculated by [70] (i) the models based on thermodynamics, (ii) the online calculator provided by NIST [19] that was developed based on the report of Snyder et al. [77], (iii) binder or cement composition and assumed degree of hydration, (iv) pore solution extraction and conductivity measurement, or (v) direct measurement of conductivity with an embedded sensor [78]. Additionally, the "bucket test" can be used wherein the specimens are immersed in a "CH-salt" solution with known electrical resistivity until the pore solution matches the solution in the bucket [15].

2.3.5.3.1 Bucket Test. Despite its name, the "bucket test" is not a test but a method for curing and conditioning concrete specimens [15]. In the conventional curing method of placing the specimens in a moist room or lime-saturated water, some alkalis (Na^+ and K^+) that are the main contributors to the electrical conductivity, leach out of concrete. This effect not only increases the error in the resistivity measurement but also changes the composition of the specimen such that it is no longer similar to the concrete placed in the field [15].

In the "bucket test," concrete specimens are immersed in a designed synthetic solution of Na^+, K^+, Ca^{2+}, and OH^-, with the same composition as the expected concrete pore solution to minimize the leaching of alkalis. The pore solution chemistry can be estimated from the online calculator by the National Institute of Standards and Technology (NIST) [19], assuming a sealed curing condition for the specimens. Using an accurate curing solution is the key point in this method which will lead to a lower error in the estimation of pore solution resistivity [15]. Based on ASTM C1876 [70], the specimens should be immersed in a simulated pore solution for at least six days. The electrical resistivity of the specimens can be measured at desired age, and the formation factor can be calculated immediately since the solution's composition and resistivity are known.

However, the "bucket test" has some concerns regarding its results and test safety [79]. Due to curing in simulated pore solution, surface deposits are formed in the concrete specimen, which should be scraped away before testing. As a result, the resistivity measurements of samples cured in pore solution show higher variation than the lime-

saturated specimens. Moreover, proper care and use of personal protective equipment (PPE) should be observed due to the high alkali content of the solution.

2.4 Relationships between Permeability Tests

As discussed earlier, there are several widely accepted methods and techniques to characterize the permeability of concrete. These techniques range from methods with long test duration to methods that can give instantaneous results. Some tests are laborious, while others are relatively easy to perform. Even though there are differences in the transport mechanism being considered and possibly in the accuracy of results for tests in the same category, it will be beneficial to determine the statistical relationship of the measurements from different tests. By doing this, one can estimate or predict the result for a particular permeability test using the measurements from another test, like the correlation between AASHTO T277 and AASHTO T259, as presented in Table 3, and AASHTO TP119/ASTM C1876 and AASHTO TP95 with ASTM C1556 shown in Table 4 and Table 5.

2.4.1 Surface Resistivity (SR) vs. Bulk Resistivity (BR)

A strong correlation between surface and bulk resistivity should be observed as both tests measure the same concrete property. In general, surface resistivity has higher measurements than bulk resistivity. Gudimettla and Crawford [10] found a linear correlation between the two, with a level of agreement (R^2) at 0.98. Using 100 mm ϕ × 200 mm high concrete cylinders cast during the actual concrete production of 11 concrete paving field projects, the results of surface resistivity are about 1.9 times higher than the bulk resistivity. It is a similar ratio found by Spragg et al. [79] and Tibbetts et al. [11]

using laboratory mixtures of concrete. A recent study by Almarshoud et al. [14] observed a linear relationship of SR = 1.73BR.

A comparison of surface and bulk resistivity was also performed by Ghosh and Tran [80] for various binary and ternary-based high-performance concrete (HPC) mixtures, ages 7 to 161 days. Average surface and bulk resistivity increases over time and exhibits moderate to low permeability for all concrete mixes. It was shown that bulk and surface resistivity correlates strongly, linearly, and follows the same trend over time. The average ratio of surface resistivity measurements for the HPC mixtures over the bulk resistivity was 2.63. It was also mentioned that the variability of the measurements increases over time or concrete age.

2.4.2 Chloride Ion Penetration vs. Electrical Resistivity

A relationship between the chloride ion penetration and electrical resistivity is very sensible as the latter represents moving ions in the pore solution in concrete. Many studies show a strong correlation between these two intrinsic properties. With the constant conductivity of concrete samples during the test process, a linear relationship between the electrical resistivity and chloride ion penetration should be expected [12]. However, the comparison study by Ramezanianpour et al. [12] on 57 concrete mixes showed a nonlinear relation between the two properties. A strong power relation between surface resistivity (SR) in kΩ-cm and rapid chloride permeability (RCP) in Coulombs was observed with a high R^2 at 0.898, wherein $SR = 67{,}998(RCP)^{-1.028}$. This result was attributed to the increasing temperature during the RCPT, which increased the electrical

current. The concrete mixes were made of type I Portland cement, crushed calcareous stone, natural sand, and some natural pozzolans.

A similar trend was observed in other studies [11, 13, 10]. Tibbetts et al. [11] have observed a strong relationship with $SR = 15{,}712\ (RCP)^{-0.90}$ and R^2 of 0.98. The concrete samples tested are of varying ages from 28, 56, 91, and up to 182 days, in the report of the Kansas Department of Transportation (KDOT) [13] about the use of surface resistivity as an alternative for RCPT. For same-age measurements at 56 days, the current concrete age requirement for RCPT in the KDOT specifications, there is a strong correlation between the two tests in which $RCP = 31{,}653(SR)^{-0.966}$ with R^2 of 0.86. A comparison of the 56-day RCP to 28-day surface resistivity was also established, showing a slightly lower but still strong correlation at R^2 of 0.84, wherein $RCP = 35{,}352(SR)^{-1.117}$.

The comparison study by Gudimettla and Crawford [10] showed similar results for the RCPT and SR measurements at the same age. The 56-day surface resistivity strongly correlates with the RCPT measurements at 56 days, wherein $SR = 2840.3(RCP)^{-0.625}$ and $R^2 = 0.89$. However, the relationship between the 28-day resistivity and 56-day RCPT, believed to correlate strongly, only showed a moderate correlation ($R^2 = 0.47$). It can be attributed to the improved permeability of the concrete at later ages due to the continuous hydration and the production variability from the sample plant [10]. Their results also demonstrated that the trend lines are close to each other when the permeability is low and tend to drift apart as the concrete permeability increases.

Almarshoud et al. [14] found a strong linear relationship between the RCPT measurements and the inverse of bulk resistivity, the conductivity. The correlation equation is RCP = 223.36*Conductivity with R^2 = 0.93 wherein the RCP is in Coulombs, and the conductivity is in mS/m x 10^{-2}.

2.4.3 Volume of Voids vs. Electrical Resistivity

A weak correlation (R^2 = 0.38) was observed by the KDOT [13] between the surface resistivity and percent permeable voids determined from ASTM C642 boil testing. Meanwhile, no correlation (R^2 = 0.04) was noticed in the investigation of Almarshoud et al. [14] between the two tests. The weak correlation was expected because of the difference in the properties measured. While both tests characterize the permeability of concrete, electrical resistivity measures the flow of current through the concrete, which depends strongly on the size and interconnection of the voids. In contrast, the boil test only measures the total volume of permeable voids.

2.4.4 Water Sorptivity vs. Electrical Resistivity

Almarshoud et al. [14] have found an inverse linear correlation with an R2 value of 0.79 between the bulk resistivity and water sorptivity determined based on ASTM C1585. It could be expected as both properties are heavily affected by the connectivity of concrete pores. However, high residuals or errors can also be observed from the plot. The high errors can be attributed to the difference in concrete conditions during the test. In the electrical resistivity tests, the concrete specimens should be saturated. Meanwhile, the conditioning procedure in water sorptivity simulates the condition of the concrete in the field, which is unsaturated or partially saturated.

The formation factor was also correlated with water sorptivity. Moradllo et al. [81] found a linear relationship between the initial sorptivity and the inverse of the square root of the formation factor ($1/\sqrt{F}$). The regression equation varied depending on the sample conditioning to measure water sorptivity. In their [81] test, the formation factor was calculated based on the estimated pore solution conductivity based on the approach presented by Snyder et al. [77]. They concluded that the formation factor could be used to predict the water absorption in concrete.

2.4.5 Water Permeability vs. Electrical Resistivity

In the study of Ramezanianpour et al. [12], the relationship between electrical resistivity and water permeability was also determined. Water penetration on the 57 concrete mixes was measured based on BS EN-12390-8 [64]. For samples with the same type of cementitious materials, a good power correlation between surface resistivity and water penetration (WP) in mm was observed with $R^2 \approx 0.87$. For concrete mixtures containing metakaolin, the correlation is expressed as $SR = 92.259(WP)^{-0.77}$, while for plain mixture, the surface resistivity measurements are lower as $SR = 69.427(WP)^{-0.595}$. Comparing all the samples regardless of the cementitious materials used results in a slightly lower but still good correlation with R^2 of 0.83.

Tibbetts et al. [11] also compared the electrical resistivity, chloride ion penetration, and water permeability measurements. The water permeability was measured using a uniaxial, steady-flow permeameter test. Data points have consisted of concrete mixtures with traditional secondary cementitious materials (SCMs), including fly ash, silica fume, slag, and metakaolin, and mixtures with alternative SCMs, including ground

glass and sugarcane bagasse ashes. While the overall results show an increasing resistivity with decreasing water permeability, the variability of the data increased when the water permeability was below a threshold of about 6 x 10-14 m/s. It may be accounted to the current limitations of the water permeability test method used, in which the flow becomes too low at lower permeability mixtures to be measured accurately [11]. Moreover, the mixtures with alternative SCMs did not show a significant increase in electrical resistivity values with increasing age. This result suggests that for alternative SCMs, the water permeability may better characterize the change in concrete pore structure over time than the electrical resistivity [11].

Comparing the water permeability results with the ion chloride penetration [11] shows a weak linear relationship resulting in an R^2 of 0.37. However, the mixtures with alternative SCMs can be considered outliers, showing high chloride ion penetration measurements for other mixtures with similar water permeability values. Considering only the mixtures with traditional SCMs, a higher R^2 value of 0.71 was observed in which the total charge passed increases with increasing water permeability.

The water permeability test done by Almarshoud et al. [14] also has a linear correlation with the electrical conductivity, with an R^2 value of 0.76. The water permeability was measured in samples 50 mm thick by 100 mm diameter. An 85 psi (0.59 MPa) pressure was applied to the saturated samples, and the linear discharge through the specimen was monitored for 14 days. The permeability coefficient was then calculated using Darcy's Law.

The Formation Factor was also calculated in [14] by dividing the bulk resistivity measurements by the pore solution resistivity. The pore solution resistivity was estimated using the NIST pore solution conductivity calculator. The resulting correlations of the formation factor with water sorptivity and water permeability were lower than the bulk resistivity. It can be because of the assumptions made in the pore solution estimation that might differ from the actual conditions of the concrete samples.

2.5 Porous Aggregates

2.5.1 Recycled Coarse Aggregates (RCA)

In recent years, recycling concrete wastes as aggregate has been a subject of research. It is primarily because of the substantial volume of concrete waste produced worldwide. In 2017, about 569 million tons of construction and demolition (C&D) wastes were generated in the United States [82]. C&D wastes come from constructing, demolishing, and renovating structures such as buildings and bridges. In 2015, a large percentage of C and D wastes was concrete debris, amounting to 382 million tons or 70% of that year's total C and D wastes. Out of these, 74% were intended for use as aggregates [83]. Recycling concrete wastes promote material cost savings and sustainable development in the construction industry. Additionally, it is an excellent alternative to the disposal of concrete debris.

2.5.1.1 Properties of RCA. Since RCA composition includes old hardened mortar, its basic properties differ from the natural aggregates and thus the recycled aggregate concrete (RAC) from the natural aggregate concrete (NAC). RCA exhibits lower density and higher absorption than natural coarse aggregates (NCA) [21, 22]. The

bulk density of RCA is lower by 12%, while its water absorption at 24 hours is higher by up to 23 times compared to NCA. The high water absorption is the most significant difference between the RCA and NCA [21].

It can also be found that the parent concrete affects the density and water absorption of the RCA. With the increasing strength grade of the parent concrete, the RCA's apparent density increases, and water absorption capacity decreases. The porosity of RCA is up to 20 times higher than NCA. This high porosity may result in lower strength and may lead to some durability issues in RAC [21]. The RCA properties found in the literature are summarized in Table 7.

Table 7

Typical Bulk Unit Weight, Absorption, and Specific Gravity of RCA

Reference	RCA Source	Size	Bulk unit weight, (kg/m^3)	Water Absorption, % weight (% volume)	Specific gravity
Otsuki et al. [84]	-	-	-	2.68~5.13	2.41~2.54
Shaban et al. [29]	C&D wastes	5~37.5 mm	-	≈ 3.25~7.25 (8~17)	2.35~2.50
Gao et al. [85]	-	-	1280~1440	5.3	2.53
Bao et al. [86]	Laboratory waste	5~20 mm	1199~1344	4.3~7.5	2.34~2.53
Pedro et al. [24]	Precast concrete waste	-	-	3.9	2.4
Cantero et al. [87]	Mixed C&D waste	20 mm NMAS	-	5.27~6.28	2.42~2.45
Paul et al. [88]	C&D wastes	-	-	3.2	2.63~2.77
Faella et al. [89]	C&D wastes	0~31.5 mm	-	1.8~12.2	2.37
Xuan et al. [26]	C&D wastes; new designed concrete	5~20 mm	-	5.2~6.4; 5.0~7.2	2.56~2.58; 2.61~2.66
Zaharieva et al. [22]	-	0~6mm; 6~20 mm	1860~2460; 1850~2650	10.5~13.5; 5.5~6.5 (11~14)	-
Somna et al. [25]	Laboratory waste	19mm NMAS	1480	4.81	2.49

2.5.1.2 Strength and Durability Performance. Compared to conventional concrete of the same mix proportion, RAC generally shows lower strength and modulus

of elasticity, indicating lower stiffness. The high porosity of RCA also leads to lower durability as it provides interconnecting paths for harmful substances to penetrate. With this, the serviceability and durability of the concrete should be carefully considered when using RCA [21]. The mechanical and permeability properties of concrete with RCA found in the literature are summarized in Table 8. Even with a high volume of RCA, the RAC mixtures can achieve strengths sufficient for most structural concrete requirements. On the other hand, high permeability properties of RAC were observed. The wide variation in the permeability measurements of the same property, such as in water sorptivity, is due to the different specimen conditioning in the studies.

Table 8

RAC Properties in Literature, Concrete Age at 28 Days Unless Specified

Reference	Properties	Remarks
Otsuki et al. [84]	f'_c = 20~80 MPa Tensile strength = 2~6 MPa Chloride penetration = 1~15 mm	0.25~0.70 w/c
Gao et al. [85]	f'_c = 30.3~33.5 MPa 24h sorptivity = 1245.2~1046.6 g/m^{2}h$^{1/2}$ Chloride diffusion coefficient = 6.83~5.78 ×10^{-12} m^2/s	100~33% RCA by mass
Bao et al. [86]	f'_c = 23~40 MPa 25h sorptivity = 350~850 g/m^{2}h$^{1/2}$ Chloride diffusion coefficient = 4~8.5 ×10^{-12} m^2/s	100~30% RCA by mass; with SCM and SP
Pedro et al. [24]	72h sorptivity = 0.026~0.060 mg/mm^2/min$^{0.5}$	100~50% RCA; with SCM and SP
Cantero et al. [87]	f'_c = 47.78~51.69 MPa ER = 7.9~8.6 kΩ-cm	100~20% RCA; with SP
Paul et al. [88]	f'_c = 33~36 MPa E-modulus = 32~35 GPa Splitting tensile = 3.3~3.6 MPa Chloride conductivity = 1~1.2 mS/cm Water sorptivity = 5.5~6.3 mm/h$^{0.5}$	100~15% RCA
Jaskulski et al. [90]	f'_c = 14.6~54.8 MPa Initial sorptivity = 0.101~0.245 cm/h$^{0.5}$	50% RCA by mass
Kurda et al. [91]	72h sorptivity = 0.48~2.47 ×10^{-3} mm/h$^{0.5}$ ER = 8.8~57 kΩ-cm	100% coarse RCA + 100~0% fine RCA; with SCM and SP
Faella et al. [89]	f'_c = 10~38 MPa Splitting tensile = 1.2~2.75 MPa	100~30% RCA; with SCM
Xuan et al. [26]	Bulk electrical conductivity = 19~25 mS/m Chloride ion permeability = 4500~9500 Coulombs Gas permeability = 5~15 m^2	Age = 56 days; 100~20% RCA by volume
Zaharieva et al. [22]	f'_c = 29.5~43.3 MPa Porosity = 19.7~23.1 %	with SP

Zaharieva et al. [22] found that the water and air permeability of RAC, as compared to NWAC, is two times higher. But while the RAC was considered weakly water permeable, its air permeability is still within the published range for regular concrete not exposed to a strong, aggressive environment. The RAC also shows a higher permeable surface in a factor of 10 to 25 times. It was attributed to the higher actual water-cement ratio in RAC as the water absorbed by RCA before and during mixing was gradually transferred to the cement paste. The measurements found by Otsuki et al. [84] show that the chloride penetration and carbonation depths in RAC are just slightly higher than in NAC. They attributed it to the presence of old ITZ in the RCA and the increased mortar.

While RAC is generally lower in strength when compared to NAC of the same mix proportion, RAC can still achieve an equal or even higher compressive strength than NAC. By decreasing the water-cement ratio with the help of superplasticizers and with the addition of fly ash in the mix, Corinaldesi and Moriconi [92] found that the compressive strength of RAC can achieve the 30 MPa compressive strength, which is adequate for a wide range of common structural uses of concrete. The pore structure was also found to improve by the addition of fly ash, which reduced the carbonation and chloride ion penetration depth in RAC. These results prove that the RCA can be an effective alternative to natural aggregates [92].

2.5.1.3 Microstructure. Concrete's mechanical and durability properties can be better explained by its microstructure composed of the aggregate phase, cement paste, and the interfacial transition zone (ITZ). For the RAC, the microstructure has five phases: the natural aggregate, old mortar, and old ITZ from the RCA, and the new mortar and

new ITZ of the new concrete. The new ITZ can be further divided into (1) the interface between the new cement paste and natural aggregate, (2) the interface between the new and old cement pastes, and (3) the interface between the new cement paste and the surface of the natural aggregate of RCA.

The failure mechanism of RAC is similar to NAC. The cracking starts and develops from the micro-cracks in the ITZ. Similarly, the failure section usually is through the ITZ [21]. Failure through the RCA can also happen in RAC. Otsuki et al. [84] observed that the compressive strength of RAC decreases as the adhesive or residual mortar strength decreases as the old ITZ governs the concrete failure. Corinaldesi and Moriconi [92] have observed this failure section on the RAC produced with fly ash and a low water-cement ratio. In this case, the old cement paste has lower strength than the new cement paste.

2.5.2 Lightweight Aggregates (LWA)

Using lightweight aggregates in concrete is not a new trend in construction. Structures built using lightweight aggregate concrete (LWAC) have existed since ancient times, such as Babylon, which Sumerians built during the 3rd millennium BC. The Greeks and Romans used pumice, a natural aggregate of volcanic origin, in building construction. Some of these ancient structures still exist, such as the St. Sofia Cathedral in Istanbul, Turkey (4th century A.D.); the Roman temple, Pantheon (A.D. 118 to 128); Pont du Gard (A.D. 14); and the great Roman Amphitheatre, Colosseum (A.D. 70 and 82) [93].

In today's construction, lightweight aggregates are utilized mostly in buildings and bridges. In the United States, several hundreds of steel-frame commercial buildings are constructed yearly using lightweight concrete and steel composite decking. Most mid-rise construction today uses lightweight concrete slabs on steel decks. Reducing weight allows concrete weight savings of over 20 percent [31].

2.5.2.1 Properties of LWA. As defined in ASTM C125 (Standard Terminology Relating to Concrete and Concrete Aggregates) [52], lightweight aggregates are "aggregates with a bulk density less than 1120 kg/m3 (70 lb/ft3), such as pumice, scoria, volcanic cinders, tuff, and diatomite; expanded or sintered clay, shale, slate, diatomaceous shale, perlite, vermiculite, or slag; and end products of coal or coke combustion". The low density is due to the high porosity of these aggregates. In a study by Liu et al. [53], the porosity of commercially available expanded clays used in the experiment was more than 50% by volume, and the water absorption by mass reached 11% to 13%. The other coarse LWA properties in the literature are summarized in Table 9.

Table 9

Typical Bulk Unit Weight, Water Absorption, and Specific Gravity of LWA

Reference	LWA type	Particle Size (mm)	Bulk unit weight, (kg/m^3)	Water Absorption, % weight (% volume)	Specific gravity
Patel et al. [42]	Sintered fly ash	4.75~20	937~998	16.95	1.89
Lo and Cui [32]	Expanded clay (synthetic)	10 (MAS)	800	-	1.7
Youm et al. [36]	Expanded clay; Slate	-	-	14; 6	1.13; 1.47
Real and Bogas [34]	Expanded clay; Sintered fly ash; Expanded Slate	-	330~624; 750; 760	15.8~21.4 (40.7~58.0); 17.9 (39.8); 3.6 (14.9)	5.97~1.08; 1.34; 1.48
Gesoğlu et al. [40]	Hardened fly ash	0.25~4; 4~16	-	21%; 17%	1.76
Liu et al. [39]	Expanded clay	4.75~9.50; 2.36~4.75; 1.18~2.36; <1.18	450~650	13.0 (25.8); 11.6 (28.1); 12.8 (36.6); 25~30 (40)	1.2; 1.3; 1.05; 1.6
Chia and Zhang [35]	Expanded clay	4~8	625~675	7	1.2

2.5.2.2 Strength and Durability. Due to the highly porous structure of LWA, the LWAC mixtures show lower strength than the normalweight concretes. Concrete durability is also of concern due to the increased permeability. Patel et al. [42] have observed an up to 50% decrease in the compressive strength of concrete with coarse and fine LWA compared to the reference concrete with no LWA. They also observed lower

durability in the LWAC mixtures against sulfate and acid attack. Compared to the reference concretes, the strength losses in LWAC due to sulfate and acid attack were up to 5 and 7 times higher, respectively.

The strength and durability properties of LWAC can be improved by adding SCMs. A lower water-cement ratio can also be achieved by using superplasticizers. Table 10 summarizes the strength and permeability properties of concrete with LWA found in the literature. The LWAC mixtures can achieve strengths applicable to most structural uses.

Table 10

Summary of LWAC Properties in Literature

Reference	Properties	Remarks
Patel et al. [42]	f'_c = 17.5~33 MPa Strength loss due to sulfate attack = 3.16~11.55% Strength loss due to acid attack = 8.44~18.42% Chloride ingress = 4.06~7.68 mm	100~50% LWA replacement by volume
Hornakova et al. [94]	SR = 8.52 kΩ-cm BR = 3.65 kΩ-cm Diffusion coefficient = 2.03 $\times 10^{-11}$ ms^{-2}	
Youm et al. [36]	f'_c = 46~72 MPa Splitting tensile strength = 3.6~4.7 MPa E = 19~27 GPa RCPT = 1160~9750 Coulombs Chloride diffusion coefficient = 2.5~11.9 $\times 10^{-12}$ m^2/s	With SCM and SP
Real and Bogas [34]	Oxygen permeability, K_{02} = 0.59~303.4 $\times 10^{-18}$ m^2	With SCM
Gesoğlu et al. [40]	f'_c = 43~70 MPa Splitting tensile strength = 2.1~3.7 MPa Sorptivity = 0.08~0.20 $mm/min^{0.5}$ Water penetration = 16~33.5 mm RCPT = 2200~5000 Coulombs Gas permeability = 2.9~7.8 $\times 10^{-16}$ m^2	100~10% LWA replacement by volume; with SP
Liu et al. [39]	f'_c = 34~50 MPa E = 15~23 GPa Water porosity = 10.9~21.5% 24h sorptivity = .05~0.14 $kg/m^2h^{0.5}$ RCPT = 2400~3600 Coulombs Chloride penetration = 12.3~17.9 mm Chloride migration = 6.5~8.9 $\times 10^{-12}$ m^2/s Surface chloride content = 13~25 kg/m^3 Chloride diffusion = 5.3~9 $\times 10^{-12}$ m^2/s	100~50% LWA replacement by volume; with SP
Chia and Zhang [35]	f'_c = 34~56 MPa Water penetration = 20 mm Chloride penetration = 3.5~14 mm RCPT = 300~5100 Coulombs	With SCM and SP; Permeability tests at 30 days of concrete age

It was observed from some studies [39, 35, 42], that the fluid or ion penetration depth in concretes with LWA are similar and sometimes lower than with the reference concrete specimens. It was attributed to the improved ITZ between the cement paste and LWA. The chloride ingress in LWAC from the study of Patel et al. [42] is about 52% lower than the chloride ingress in reference concrete. Some LWAC water and chloride penetration results of Liu et al. [39] are lower than reference concretes by up to 40% and 33%, respectively. Lastly, some LWAC test results in the study of Chia and Zhang [35] showed up to 63% and 12.5% reduction in water and chloride penetration depth, respectively.

2.5.2.3 LWAC Microstructure. In the study of Lo and Cui [32], a well-bonded interfacial zone (IZ) between the lightweight coarse aggregate and hydrated cement paste was observed. The "wall effect" does not seem to occur in lightweight aggregate concrete resulting in a better bond between the aggregate and the cement paste. The Scanning Electron Microscope (SEM) view of the lightweight aggregate concrete showed that the LWA shell is not distinct, and a tight and continuous bond between the aggregate and cement paste was noticed. Further examination under back-scattered electron imaging (BSEI) displayed a thin layer of IZ of about 10μm. The porous and rough surface properties of LWA provided sites for the cement paste to merge with the IZ and improve its interaction with the aggregate [32].

The fractured section of the LWC was further examined under high-power magnification, and a 20μm thick shell of LWA was noticed. At the contact layer, on the surface of the aggregate, is a 5-10 μm layer of a porous network of ettringite followed by a layer of dense C-S-H with less ettringite. The 5-10 μm layer of the porous band is

considered the C-S-H/LWA interface. The sizes of pores found in the IZ are about 0.3 to 1 μm, bigger than the capillary voids (10 nm – 5 μm) but smaller than entrained air voids (50-500 μm) in the cement paste [32].

From the enlarged view of the ITZ, it was further seen that ettringites have formed on the aggregate shell. Cement paste infiltrated the pores at the surface of LWA, resulting in a better interfacial bond between the cement paste and aggregate at the ITZ and reduced porosity. As a result, the ITZ of LWAC is smaller than that of NWAC [32].

Chapter 3

Materials and Methods[2]

3.1 Materials

3.1.1 Coarse Aggregates

The study used two types of porous aggregates: recycled concrete aggregates (RCA) and lightweight aggregates (LWA). Reference concrete specimens were also prepared using normal-weight aggregates (NWA).

3.1.1.1 Recycled Concrete Aggregates (RCA). RCAs were manufactured from four different parent or source concretes with known properties. The parent concretes' mixture proportions are shown in Table 11, where the varying water-cement ratio, coarse aggregate type, concrete components, and air content can be observed. To obtain RCA with different aggregate properties, the parent concretes were made with either granite or limestone aggregates and at water-cement ratios of 0.48 or 0.38. The RCAs manufactured from the four parent concretes were sized into two gradations, with nominal maximum aggregate sizes (NMAS) of 25mm (1 inch) and 19mm (3/4 inch), producing a total of eight (8) RCA variations. An image of a sample RCA is shown in Figure *2*, where a high volume of adhered mortars for each piece of RCA can be seen.

[2] Some parts of this chapter are published in [129, 130, 131]

Table 11

RCA Parent Concrete Mixture Proportions in kg/m3 (% Volume) and Properties

Parent Concrete	w/c	CA type	Cement	Water	FA	CA	AC
PC1	0.48	G	341 (10.4)	164 (16.1)	777 (34.1)	1038 (42.9)	(7.2)
PC2	0.38		433 (13.6)	166 (16.1)	700 (30.1)	1032 (41.4)	(4.5)
PC3	0.48	L	341 (10.5)	164 (16.0)	777 (33.9)	1041 (43.0)	(6.8)
PC4	0.38		433 (13.3)	166 (16.2)	700 (30.3)	1035 (42.2)	(5.0)

Note: w/c = water to cement ratio by weight; CA = coarse aggregate; FA = fine aggregate; and AC = Air Content in % Volume; G = Granite, L = Limestone

Figure 2. Pieces of recycled concrete aggregates.

The required coarse aggregate properties for mixture design were determined based on ASTM C33 [95], C29 [96], C127 [97], and C330 [98], and are summarized in Table 12. For the lightweight aggregates, the absorption was determined by immersing the samples in water for 72 ± 4 hours.

Table 12

Coarse Aggregate Properties

CA	Source	Size/Gradation (mm)	γ_{bulk} (kg/m^3)	Water Absorption (weight %)	Water Porosity (volume %)	SG
RCA1	PC1	25.0 to 4.75	1304	4.32	9.89	2.389
RCA2		19.0 to 4.75	1303	5.22	11.62	2.343
RCA3	PC2	25.0 to 4.75	1340	3.62	8.61	2.461
RCA4		19.0 to 4.75	1385	4.45	10.56	2.480
RCA5	PC3	25.0 to 9.5	1324	5.19	11.78	2.389
RCA6		19.0 to 9.5	1323	4.92	11.31	2.411
RCA7	PC4	25.0 to 4.75	1335	5.06	11.69	2.425
RCA8		19.0 to 4.75	1320	4.09	9.64	2.454
LWA	Expanded Shale	19.0 to 4.75	795	14.94	20.86	1.604
NWA	Traprock	25.0 to 9.5	1664	0.22	0.60	2.746

Note: NMAS = nominal maximum aggregate size; γ_{bulk} = bulk or dry-rodded unit weight; and SG = specific gravity at saturated surface dry condition.

The coarse aggregate gradation plots shown in Figure *3* are for RCAs with 25 mm NMAS, while Figure 4 plots are for RCAs with 19 mm NMAS. The aggregates are of similar size distributions, mostly at #57 and #67 ASTM C33 [95] gradations. Among the RCA types, only the RCA5 and RCA6 have gradation sizes of #56 and #6, respectively, with fewer fine particles than the #57 and #67 size gradations.

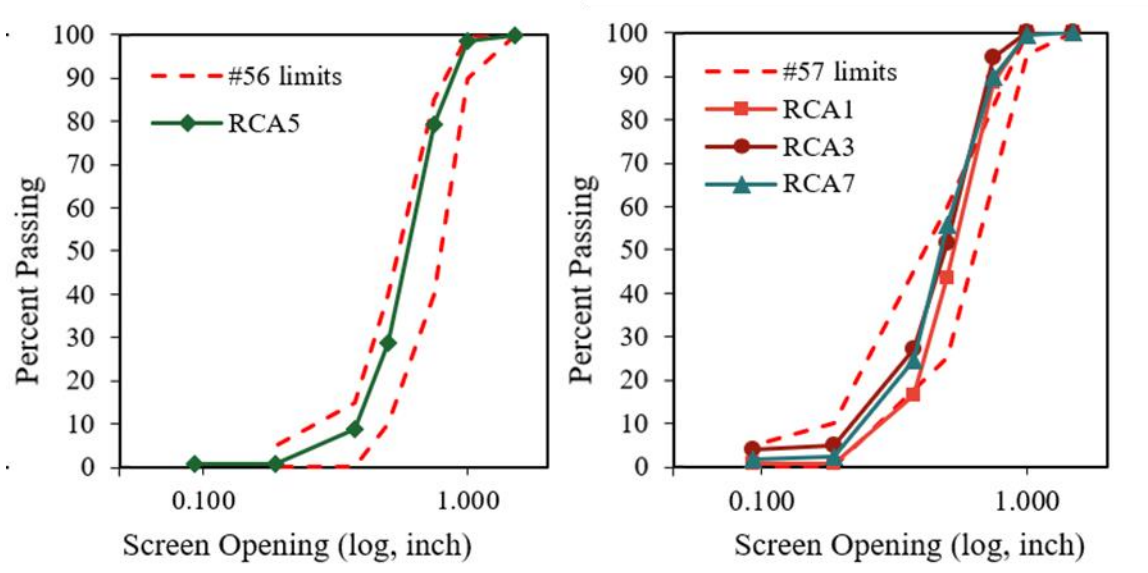

Figure 3. Gradation of RCA coarse aggregates with 25.0 mm NMAS. Limits for size #56 and #57 gradations according to ASTM C33 are included.

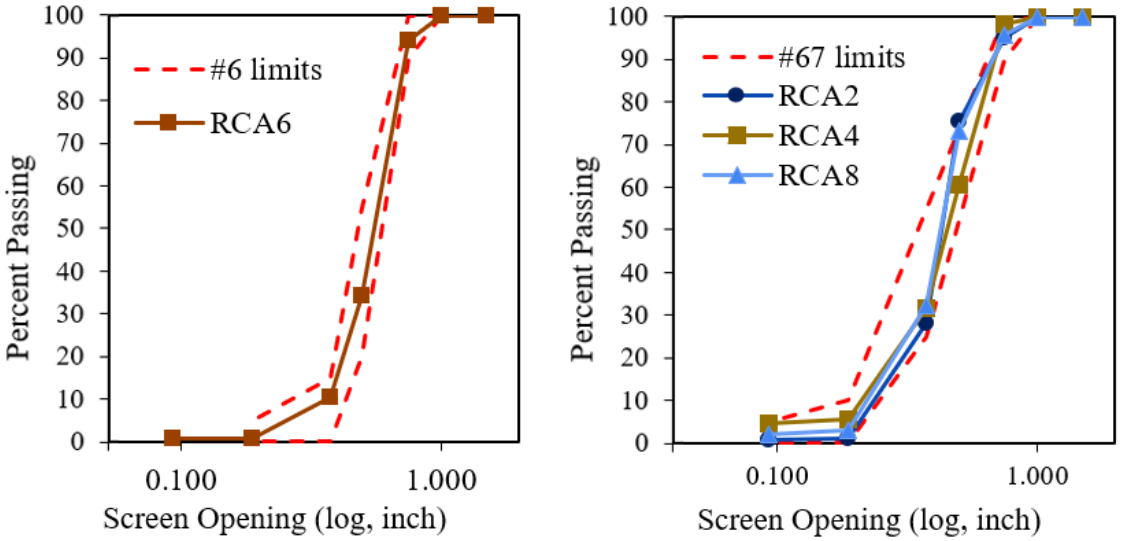

Figure 4. Gradation of RCA coarse aggregates with 19.0 mm NMAS. Limits for size #6 and #67 gradations according to ASTM C33 are included.

3.1.1.2 Lightweight Aggregates (LWA). The LWA is an expanded shale supplied by the Northeast Solite Corporation, New York. The expanded shale aggregates were processed in kiln temperatures of 2100°F, resulting in a stronger and lighter material than a common shale [99]. Before concrete mixing, the LWAs were immersed in water for three days to allow water enough time to penetrate the highly porous aggregate. An image of the LWA used is shown in Figure 5, where the high porosity of the LWA can be observed. The LWA properties are included in Table 12. Figure 6 shows the gradation of LWA with limits provided in ASTM C330. The LWA is at the maximum limits of gradation for 19.0 mm NMAS.

Figure 5. Expanded shale LWA.

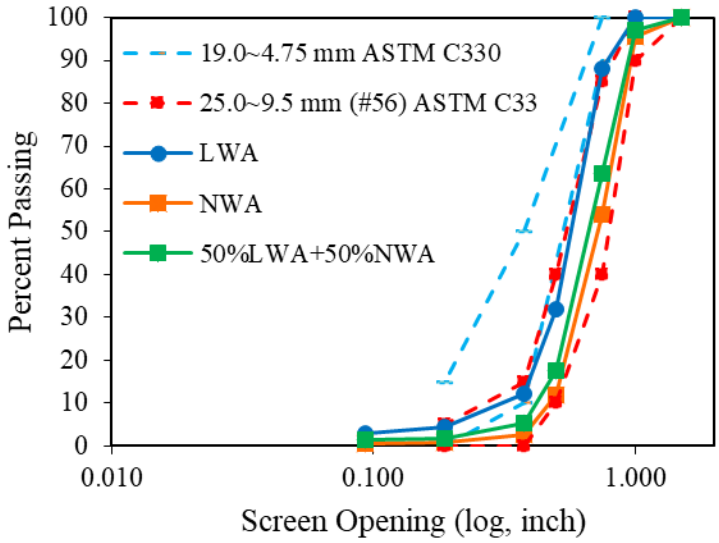

Figure 6. Gradation of LWA, NWA, and combined LWA+NWA. Limits for LWA and NWA gradations according to ASTM C330 and ASTM C33 are included.

3.1.1.3 Normal-Weight Aggregates (NWA). The NWA used is a trap rock, an extrusive igneous rock. It is one of the excellent aggregate materials for concrete construction due to its high strength and very low porosity [7]. An image of the NWA used is shown in Figure *7*. Compared to the RCA and LWA, the NWA has a less porous structure. The NWA properties are also included in Table 12. The NWA gradation and the combined LWA and NWA (50% by volume) are included in Figure 6. The NWA shows the coarsest particle distribution but is still within the ASTM C33 #56 gradation limit. Moreover, the combined LWA and NWA are within the #56 ASTM C33 gradation limits.

Figure 7. Trap rock NWA.

3.1.2 Cement, Fine Aggregate, and Admixtures

The other concrete materials used are Type I portland cement (PC), concrete sand with a fineness modulus of 2.81 and water absorption of 1.4%, and tap water. The cement used conformed to the requirements of ASTM C150. The cement composition from the vendor data is shown in Table 13. The gradation of fine aggregates is shown in Figure *8*, where it can be observed that the fine aggregates used satisfied the gradation requirements of ASTM C33 [95]. An air-entraining admixture, Sika AIR, was used to entrain air in the concrete as required for structures exposed to cyclic freezing-thawing. A water-reducing admixture, Sikament 686, was used in concretes with a 0.28 water-cement ratio to achieve a workable concrete even with low mixing water.

Table 13

Chemical Composition (%) of Type 1 Portland Cement

Cement	SiO_2	Al_2O_3	Fe_2O_3	CaO	MgO	SO_3	Na_2O	K_2O	LOI
Type 1	19.32	5.77	2.38	61.55	2.63	4.56	0.33	0.97	2.50

Source: Keystone Cement Company

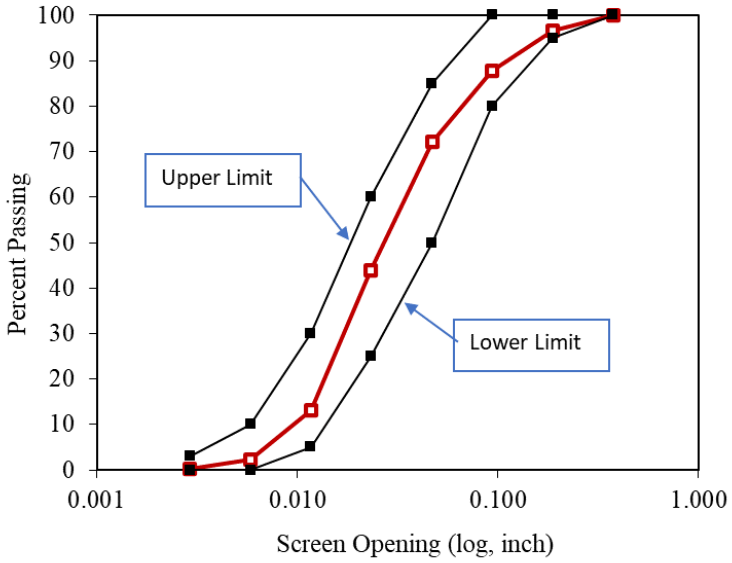

Figure 8. Gradation of fine aggregate. Limits provided by ASTM C33 [95].

3.1.3 Concrete Mix Proportions

The recycled aggregate concrete (RAC) mixtures, concrete mixtures with coarse RCA, were prepared first. To achieve a wide range of permeability measurements, two water-to-cement ratios for each RCA variation were used in the mix design: 0.48 and 0.38. The coarse aggregates for the RAC mixtures were 100% RCA. The material proportions in kilograms per cubic meter of concrete (kg/m^3), including the volume

proportion, of the 16 RAC mixtures are shown in Table 14. The mixture proportions were derived based on the ACI 211.1 procedure [100], which considers the coarse aggregates' dry-rodded unit weight and specific gravity. A target air content of 6% and a slump of 2 inches were used in the design calculations.

Table 14

Mixture Proportions of RAC Mixtures, in kg/m3 (% Volume)

Mixture	**Cement**	**Water**	**Sand**	**RCA**	**AEA,** ml/ m^3 (% Volume*)
0.48-RCA1	340 (10.8)	163 (16.3)	794 (30.3)	874 (36.6)	155 (6)
0.38-RCA1	429 (13.7)	163 (16.3)	720 (27.5)	874 (36.6)	279 (6)
0.48-RCA2	350 (11.1)	168 (16.8)	827 (31.6)	808 (34.5)	160 (6)
0.38-RCA2	442 (14.1)	168 (16.8)	750 (28.6)	808 (34.5)	288 (6)
0.48-RCA3	340 (10.8)	163 (16.3)	797 (30.4)	898 (36.5)	155 (6)
0.38-RCA3	429 (13.7)	163 (16.3)	722 (27.6)	898 (36.5)	279 (6)
0.48-RCA4	350 (11.1)	168 (16.8)	823 (31.4)	859 (34.6)	160 (6)
0.38-RCA4	442 (14.1)	168 (16.8)	746 (28.5)	859 (34.6)	288 (6)
0.48-RCA5	340 (10.8)	163 (16.3)	779 (29.7)	887 (37.1)	155 (6)
0.38-RCA5	429 (13.7)	163 (16.3)	705 (26.9)	887 (37.1)	279 (6)
0.48-RCA6	350 (11.1)	168 (16.8)	839 (32.0)	820 (34.0)	160 (6)
0.38-RCA6	442 (14.1)	168 (16.8)	762 (29.1)	820 (34.0)	288 (6)
0.48-RCA7	340 (10.8)	163 (16.3)	786 (30.0)	894 (36.9)	144 (6)
0.38-RCA7	429 (13.7)	163 (16.3)	712 (27.2)	894 (36.9)	279 (6)
0.48-RCA8	350 (11.1)	168 (16.8)	857 (32.7)	818 (33.4)	160 (6)
0.38-RCA8	442 (14.1)	168 (16.8)	780 (29.8)	818 (33.4)	288 (6)

* Designed air content

The same water-cement ratios from RAC mixtures of 0.48 and 0.38 were used for lightweight and normalweight aggregate concretes (LWAC and NWAC). Concrete mixtures at a lower water-cement ratio of 0.28 were added to achieve lower permeability measurements. Furthermore, partial lightweight aggregate concretes (PLWAC) with 50% LWA and 50% NWA by volume were also prepared. The material proportions in kilograms per cubic meter of concrete (kg/m3) and percent volume are shown in Table 15. The mixture proportions were derived based on the ACI 211.1 [100] and ACI 211.2 [101] procedures for the normal-weight aggregate and lightweight aggregate concrete. Like the RCA mixture design, the target air content is 6% while the target slump is 2 inches. The lightweight aggregates were immersed in water for three days and brought to SSD condition before being included in the mix.

Table 15

Concrete Mixture Proportion for Lightweight, Partial Lightweight and Normal-Weight Aggregate Concretes (LWAC, PLWAC, and NWAC) in kg/m3 (% Volume)

Mixture	Cement	Water	Sand	NWA	LWA
LWAC48	354 (11.3)	170 (17.0)	701 (26.8)	0 (0)	555 (34.6)
LWAC38	447 (14.2)		744 (28.4)		
LWAC28	607 (19.3)		448 (17.1)		
50LWAC48	350 (11.1)	168 (16.8)	814 (31.1)	480 (17.5)	280 (17.5)
50LWAC38	442 (14.1)		737 (28.1)		
50LWAC28	600 (19.1)		606 (23.1)		
NWAC48	340 (10.8)	163 (16.3)	689 (26.3)	1115 (40.6)	0 (0)
NWAC38	429 (13.7)		614 (23.4)		
NWAC28	582 (18.5)		486 (18.6)		

The slump and temperature of the fresh concrete mixtures were measured according to ASTM C143 [102] and ASTM C1064 [103], respectively. The unit weights were measured using the air meter measuring bowl. The air contents of RAC, LWAC, and PLWAC mixtures were measured using the volumetric method according to ASTM C173 [104], while the air contents of NWAC mixtures were measured based on the pressure method according to ASTM C231 [105].

3.2 Methods

The flow chart of research experiments is shown in Figure 9. After the aggregate property measurements and the concrete mixing, casting, and curing, the concrete specimens were subjected to different permeability tests shown below. After the bulk resistivity, surface resistivity, and Germann water permeability tests, the concrete specimens were cut for rapid chloride and water sorptivity tests.

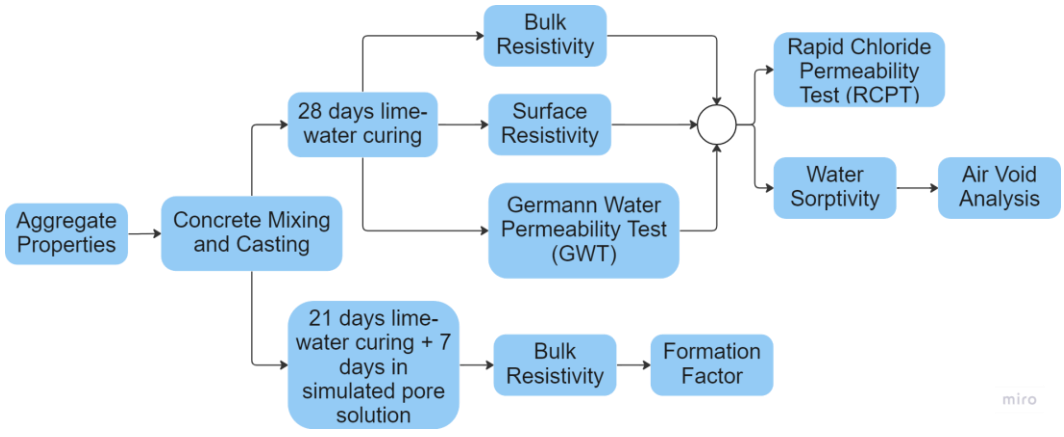

Figure 9. Research methodology outline.

For each concrete mixture, a minimum of 6 – 100 mm ϕ × 200 mm) cylinders were cast and cured in a saturated lime-water solution. Seven days before testing, six samples were cut thinly at both ends to ensure a leveled surface and to expose the concrete cross-section that would better represent the permeability of the concrete. An image of the concrete specimens with uncut and cut surfaces is shown in Figure *10*. The aggregates are exposed on the cut surface.

Figure 10. Concrete specimens (left) before and (right) after cutting the surface.

After 21 days of curing, two cut cylindrical samples were immersed in a simulated pore solution to condition the samples to determine the formation factor. The other four cut samples were subjected to different permeability tests: surface resistivity according to AASHTO T 358 [8], bulk resistivity according to AASHTO TP 119 [9], and

water permeability using the Germann water permeability test (GWT). Three specimens tested for electrical resistivity and GWT were sliced to obtain two 50 mm thick concrete discs. The concrete discs from the top and middle parts of the cylindrical specimens were conditioned and tested for rapid chloride permeability according to ASTM C1202 [68] and water sorptivity according to ASTM C1585 [52], respectively. Figure *11* was provided to visualize the specimens used for each permeability testing, including the location of RCPT and sorptivity specimens from the cylinders. The average measurements for each concrete mixture were used in the analysis.

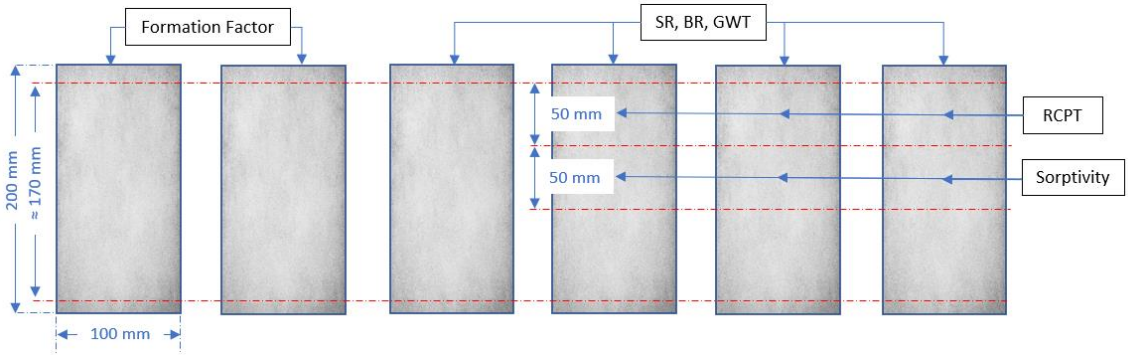

Figure 11. Cylindrical concrete specimens used for each permeability test; red dashed lines show the cutting locations.

3.2.1 Permeability Tests

3.2.1.1 Surface and Bulk Electrical Resistivity. A commercially available resistivity meter with a probe spacing of 38 mm was used for surface resistivity testing. The schematic of the surface resistivity device shown in Figure 12 is similar to the test set-up provided in AASHTO T 358-15 [8], where an alternating current is applied in the

outer probes, and the potential drop is measured in the inner probes. The resistance is calculated by dividing the potential drop by the applied current. Then, the resistance is multiplied by the geometric factor to determine the electrical resistivity. The readings in the device already include the geometric factor for cylindrical specimens, which is 2π times the probe spacing.

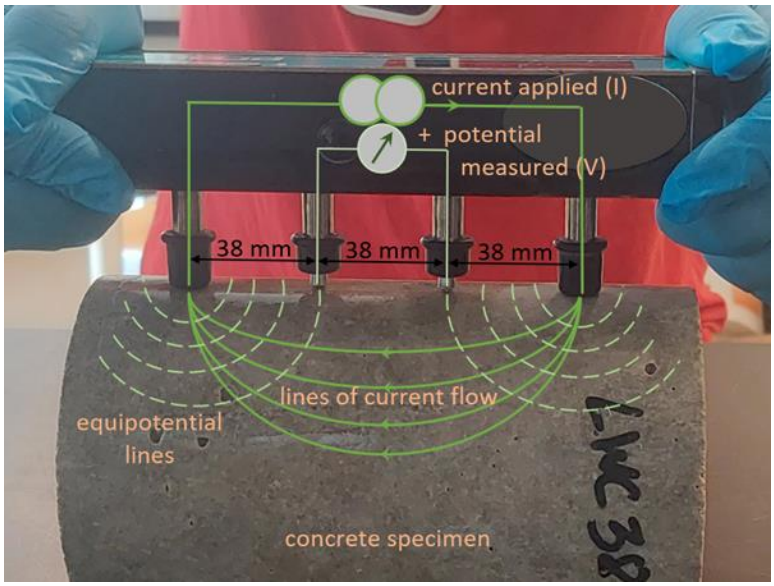

Figure 12. Surface Resistivity testing with the schematic of the Wenner probe.

The same device from surface resistivity was used for bulk resistivity testing shown in Figure *13*. The probes of the resistivity meter were removed and replaced by connectors for the two metal plates with conductive foam inserts. Since the device readings already include the geometric factor for surface resistivity of cylindrical specimens, the bulk resistivity measurements were adjusted, as shown in Equation (8), to

replace the geometric factor for surface resistivity (2πa) with the geometric factor for bulk resistivity (A/L).

$$\boldsymbol{\rho_{bulk}} = \frac{\boldsymbol{R_{measured}}}{\boldsymbol{2\pi a}}\left(\frac{\boldsymbol{A}}{\boldsymbol{L}}\right) \tag{8}$$

where: ρ_{bulk} = bulk resistivity, $R_{measured}$ = device reading, a = probe spacing, A = cross-sectional area, and L = length of the specimen.

Figure 13. Bulk electrical resistivity test set-up.

The specimens were kept in saturated condition before testing to evaluate the concrete's permeability more accurately. Electrical resistivity measurements are higher when the concrete specimens are not saturated. Furthermore, the temperature of the samples also affects the readings [106]. At lower temperatures, the ionic mobility is

lower; thus, the electrical resistivity readings will be higher. The temperature correction factor shown in Equation (***9***) [18] was applied to normalize the results to a reference temperature of 21°C. The 10% increase for lime water-cured concrete samples, as suggested by ASHTO T 358 [8], was also included.

$$\boldsymbol{\rho_{Tref} = \rho_T \, exp\,[\frac{-E_{a-cond}}{R}(\frac{1}{T+273} - \frac{1}{T_{ref} + 273})]} \quad (9)$$

where ρ_{Tref} = adjusted resistivity of concrete at reference temperature T_{ref}, ρ_T = measured resistivity at testing temperature T, E_{a-cond} = the activation energy of conduction, 15.8 kJ/mol, and R = the universal gas constant, 8.314 J/(mol*K).

3.2.1.2 Formation Factor. The composition of the simulated pore solution containing NaOH, KOH, and $Ca(OH)_2$ is provided in ASTM C1876 [18] to determine the formation factor. However, the pore solution varies depending on the cement composition, water-cement ratio, and degree of hydration. For a more accurate determination of the formation factor, the simulated pore solution should be close to the actual pore solution. The pore solution conductivity can be estimated based on the cement composition and the concrete mixture proportion, particularly the water-cement ratio [107]. A lower water-cement ratio means higher cement content and, thus, a higher concentration of leaked alkali ions in the pore solution. The simulated pore solution compositions shown in Table 16 were calculated using the online calculator for pore solution conductivity provided by NIST [19] to consider these factors. The degrees of hydration on the 28th day were assumed to be 0.83, 0.73, and 0.63 for the 0.48, 0.38, and

0.28 w/c, respectively. The degrees of hydration were interpolated from the assumptions of Qiao et al. [20].

Table 16

Chemical Composition (in g/L) of Simulated Pore Solution

w/c	NaOH	KOH	$Ca(OH)_2$	Pore Solution Resistivity (kΩ-cm)
0.48	9.6	25.8	3.0	0.0073
0.38	12.4	33.7	3.0	0.0058
0.28	18.4	49.9	3.0	0.0041

3.2.1.3 Germann Water Permeability Test (GWT). GWT measures the water permeability of concrete in a relatively shorter time than the other standard water permeability tests. This test can be classified as a non-steady water flow test, wherein the flow rate changes over time. The testing time should be consistent for all the samples and was set at 10 minutes, as recommended by Moczko & Moczko [63]. The samples were also kept in saturated condition before testing. The GWT system is shown in Figure *14*.

Figure 14. Germann Water Permeability Test (GWT) set-up.

In the GWT, the water chamber was clamped tightly at the top of the concrete cylinder. This chamber was filled with water, and 100 kPa hydrostatic pressure was applied by closing the valves and turning down the lid. As water is absorbed into the concrete, the pressure is maintained by turning the micrometer gauge. The initial and final micrometer gauge readings were recorded upon applying pressure and 10 minutes later. The volume absorbed was calculated as the product of the micrometer gauge movement and its internal area. The average flux was then computed by dividing the volume of absorbed water by the area of the exposed surface (internal area of the chamber) and the testing time (10 minutes).

3.2.1.4 Rapid Chloride Permeability Test (RCPT). Three 50mm-thick concrete discs from each concrete mixture were tested for rapid chloride permeability according to ASTM C1202 [68]. The RCPT device reports the total charge passed for each specimen. In some cases, when the test was stopped before the 6-hour period, the equivalent total

charge passed was calculated by determining the regression equation of the current vs. time plot curve and integrating it from 0 to 6 hours. The RCPT test set-up is shown in Figure *15*.

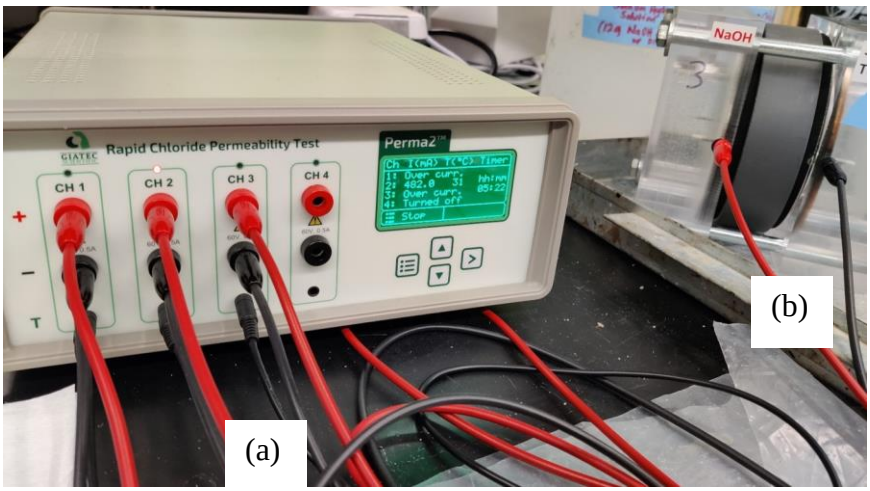

Figure 15. RCPT test set-up, showing the (a) laboratory device and (b) voltage cell.

3.2.1.5 Rate of Water Absorption (Sorptivity). The sample conditioning guideline provided in ASTM C1585 [52] (drying at 50 °C temperature and 80% RH for three days, sealing in individual containers for at least 15 days) was strictly followed. A mist humidifier connected to an RH sensor and controller was placed inside an environmental chamber to control the RH at 80% ± 3%. The water absorption test set-up and the calculation of initial and secondary sorptivities were done according to the standard [52]. The sorptivity conditioning set-up is shown in Figure *16*, while the test set-up is shown in Figure 17. During conditioning, the socket connected to the humidifier turns off when RH reaches the target RH of 80% and turns on when RH drops to 78%.

The sorptivity was also expressed as a single parameter by plotting the absorption to the fourth root of time ($t^{0.25}$), as proposed by Zaccardi et al. [20].

Figure 16. Sorptivity conditioning set-up showing (a) concrete specimens, (b) mist humidifier, (c) humidity sensor inside the environmental chamber, (d) humidity controller, and (e) humidifier power plug.

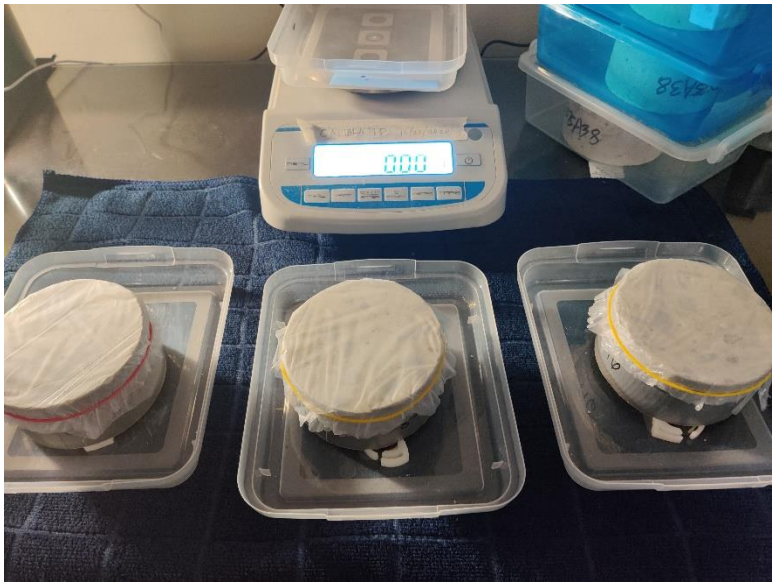

Figure 17. Water sorptivity set-up, showing the sealed concrete specimens immersed in shallow water.

After the sorptivity test, the oven-dried mass of the samples was determined by placing them in the oven at 105 °C for at least two days. The samples were then fully immersed in water for at least three days to determine the saturated-surface-dry (SSD) weight. The difference between the SSD and oven-dried weights is assumed to be the water absorption capacity of the specimen. The sample's water content before testing is the difference between its initial and oven-dried weight. The increase in saturation was determined as the ratio of the absorbed water over the absorption capacity.

3.2.2 Air Void Structure

After the sorptivity testing, some concrete specimens were polished to determine the air-void structure. The samples were polished by grinding the surface with a set of fine abrasives with nominal grit sizes of 125, 52, 40, 15, 10, and 8 μm (No. 120, 240,

320, 600, 800, and 1200, respectively). Then, phenolphthalein solution was sprayed onto the concrete surface. The cement paste reacts to the phenolphthalein and turns its grayish color into pink, thus separating the color of the cement paste component from the aggregates. Finally, the air voids were filled with a mixture of fine particle-size white powder and petroleum jelly to separate the color of the air voids from the other concrete components. The sample images for each process are shown in Figure *18*. The specimens were scanned using a high-resolution scanner producing images at 4800 dpi.

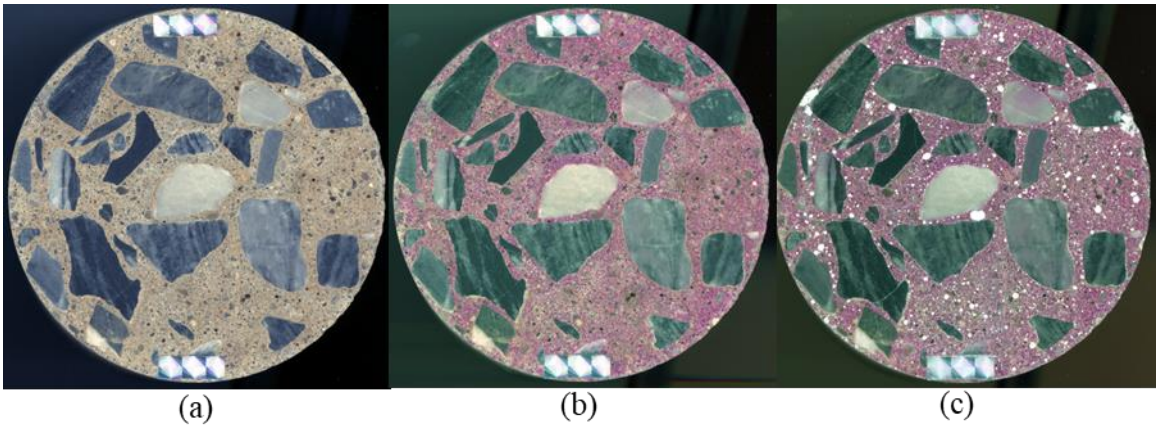

Figure 18. Scanned images of a 100 mmØ normal-weight concrete specimen after (a) polishing, (b) spraying of phenolphthalein, and (c) filling of white powder.

The air void structure of the concrete specimens, including the air content, spacing factor, and percent volume of other concrete components, were calculated using the image analysis method. Software verification was done by comparing the results to the traditional way of determining the concrete air void structure, the linear traverse method according to ASTM C457 [108].

3.2.2.1 Image Analysis Algorithm. The image analysis software that calculates the percent volume of concrete components was written in Python. Visual Studio, an integrated development environment, was used to write, edit, debug, and run the program. The Open-Source Computer Vision Library, commonly known as OpenCV, was utilized to perform image processing tasks. The high-resolution image of concrete is loaded in the program and cropped at the user-defined dimensions. Then, image thresholding was done using the user-defined HSV range for the air voids and cement paste, converting the image into multilevel (black, white, and gray). In the multilevel image, air voids are white, cement pastes are gray, and aggregates are black. A screenshot of the program interface, including the source and multilevel images, is shown in Figure 19.

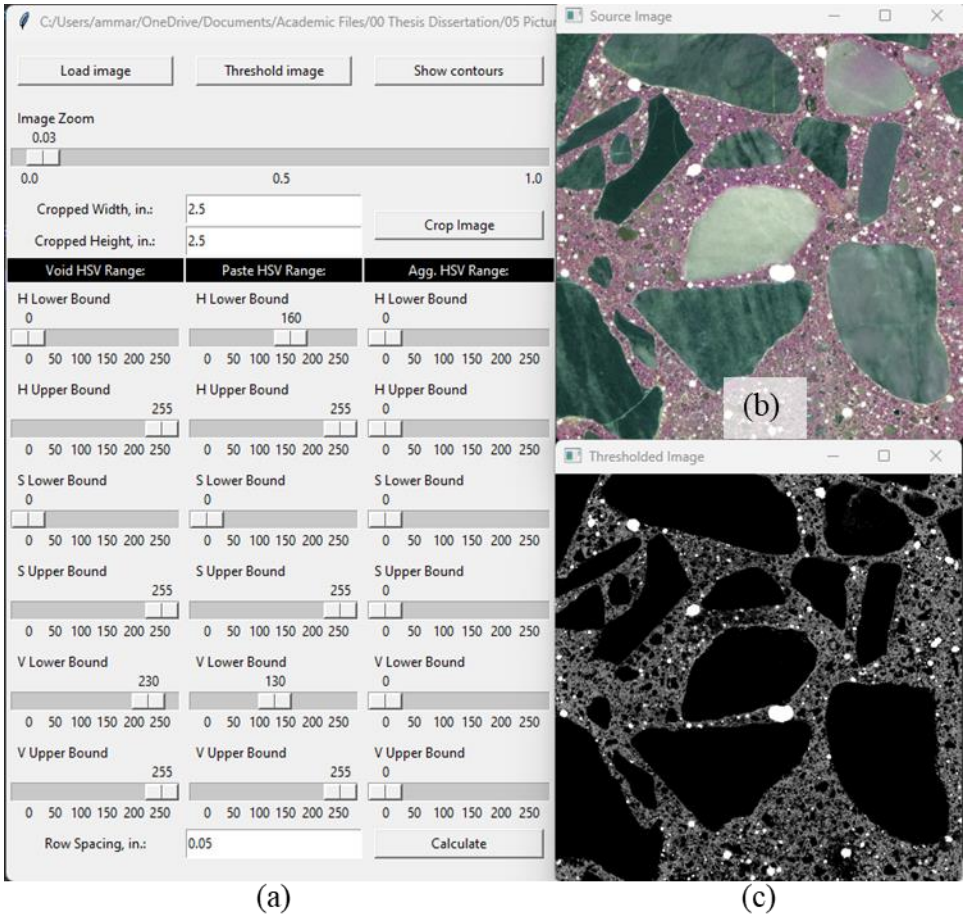

Figure 19. Image analysis program (a) user interface, (b) source image, and (c) multilevel image.

In the multilevel image, the concrete composition was calculated based on the color of the pixels in a series of regularly spaced lines. The pixels were counted from leftmost to rightmost and from top to bottom of the cropped image. The counting algorithm is shown in Figure *20*, while the calculation of air voids, cement paste, and aggregate percents, including the spacing factor, is shown in Equations *(*11)-(*17*). The line spacing was modified to satisfy the minimum length of traverse for the linear traverse method required by ASTM C457 [108], as shown in Table 17.

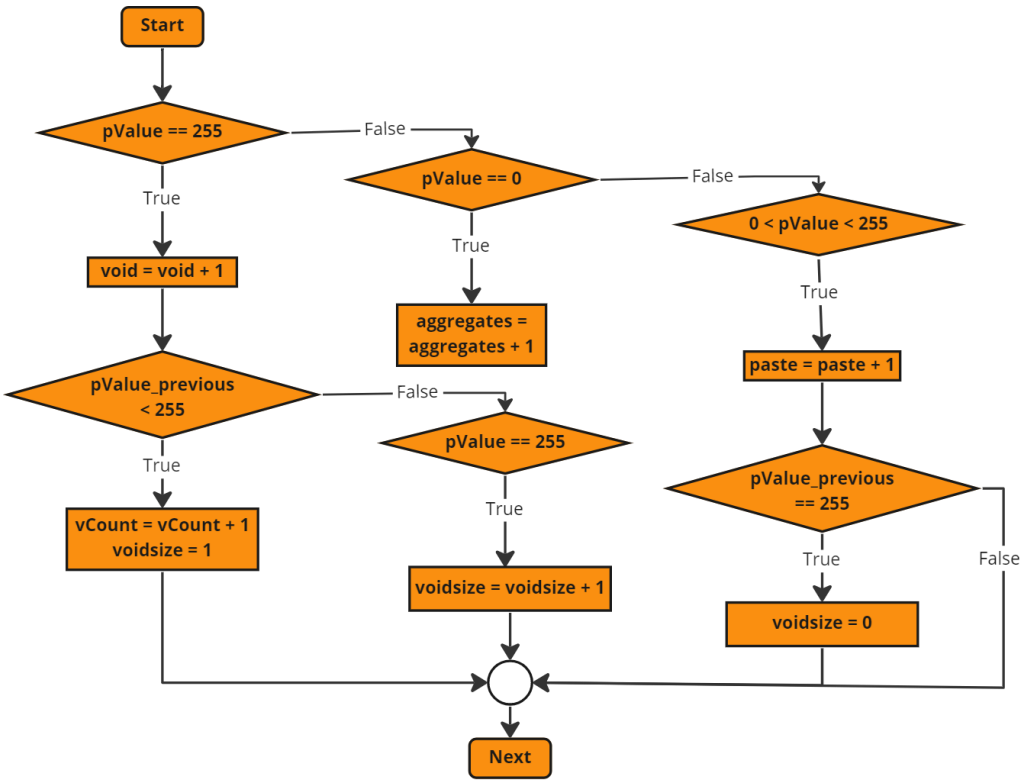

Figure 20. Pixel counting algorithm of air voids, aggregates, and cement paste.

$$\boldsymbol{Total\ length\ of\ traverse\ (T_t), in\ mm} = (\boldsymbol{void} + \boldsymbol{paste} + \boldsymbol{aggregates})\frac{\boldsymbol{25.4 \times 1000}}{\boldsymbol{dpi}} \quad (10)$$

$$\boldsymbol{Air\ Content\ (A), in\ \%} = \frac{\boldsymbol{void \times 100}}{(\boldsymbol{void} + \boldsymbol{paste} + \boldsymbol{aggregates})} \quad (11)$$

$$\boldsymbol{Void\ frequency\ (n), in\ \%\ =\ \frac{vCount}{T_t}} \tag{12}$$

$$\boldsymbol{Paste\ Content\ (p), in\ \%\ =\ \frac{paste \times 100}{(void\ +\ paste\ +\ aggregates)}} \tag{13}$$

$$\boldsymbol{Aggregate\ Content, in\ \%\ =\ \frac{aggregates \times 100}{(void\ +\ paste\ +\ aggregates)}} \tag{14}$$

$$\boldsymbol{specific\ surface\ (\alpha) = \frac{4 \times vCount}{void \times 25.4 \times 1000 \div dpi}} \tag{15}$$

$\boldsymbol{if\ p/A\ <=\ 4.342}$:

$$\boldsymbol{spacing\ factor\ (\bar{L}), in\ mm\ =\ \frac{paste}{(4 * vCount)} \times \frac{25.4 \times 1000}{dpi}} \tag{16}$$

$\boldsymbol{else}$:

$$\boldsymbol{\bar{L} = \frac{3}{\alpha} \times [1.4\ \left(1 + \frac{p}{A}\right)^{\frac{1}{3}}\ -\ 1]} \tag{17}$$

where: void, paste, and aggregates are the number of pixels for each concrete component, vCount = total number of air voids, and dpi = image resolution at dots per inch.

Table 17

Minimum Length of Traverse according to ASTM C457 [108]

Nominal or Observed Maximum Size of Aggregate in the Concrete, mm	Minimum Length of Traverse, mm
25.0	2413
19.0	2286

3.2.2.2 Software Results Verification. One concrete specimen was also analyzed through the linear traverse method to verify the image analysis results. The linear traverse method provided in ASTM C457 [108] is a traditional method of determining concrete surface's air void structure using a microscope. In this method, the concrete cross-section is polished with fine abrasives and viewed in a stereoscopic microscope with at least 50x magnification. Then, the volumetric composition of concrete is determined by summing the distances of each concrete component (aggregate, cement paste, and air void) traversed under the microscope along a series of regularly spaced lines. The linear traverse set-up with the machine and microscope connected to the computer is shown in Figure 21.

Figure 21. Linear traverse machine set-up.

3.2.2.3 Determining the RCA and LWA Components. The air void structures of RAC and LWAC are more complicated than that of regular concrete, as the porous aggregates also contain a significant number of voids that are large enough to be considered air voids. The RAC components include the new cement paste, the air voids in the new cement paste, natural aggregates from RCA, the old cement paste from RCA, and the air voids from the old cement paste in RCA. In Figure 22*a*, the RCA and the new mortar can be easily distinguished, with the RCA being darker than the new mortar. But in Figure 22*b*, after applying phenolphthalein, the RCA and new mortar have the same color and are no longer separable. When the final processed sample shown in Figure 22*c* is analyzed in the image analysis software, the total air voids, natural aggregates, and

cement paste are determined. However, the percent of RCA cannot be determined, and the air voids for new mortar and RCA's adhered mortar cannot be separated.

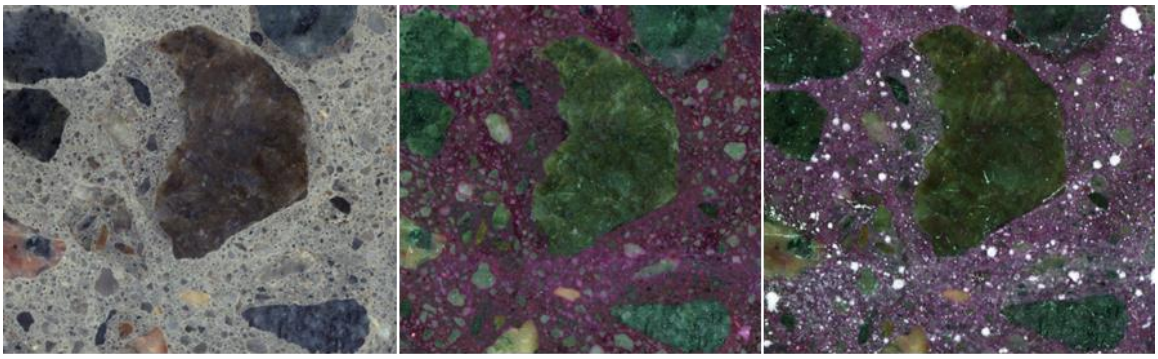

Figure 22. Scanned images of recycled aggregate concrete (RAC) specimen after (a) polishing, (b) spraying of phenolphthalein, and (c) filling of white powder.

Image overlays were done in an image editing software, GitHub, to determine RCA's residual mortar and air voids percentage. The RCA boundaries were traced from the polished section image like in Figure *22*a, then overlayed to the final processed cross-section. Figure *23* shows the (a) original or source image and the overlayed images in which the RCA boundaries were filled with (b) black color and (c) pink color. The same methods were also done in the LWAC image to determine the air voids contributed by the LWA and by the cement paste separately. Table 18 shows how the concrete components can be distinguished from the three different images. Using those results in Equations (*18*)-(*21*) returns the percent of RCA/LWA in the mixture, the concrete air content considering only the voids from RCA/LWA, paste content in RCA, and the percent of air voids in the RCA/LWA.

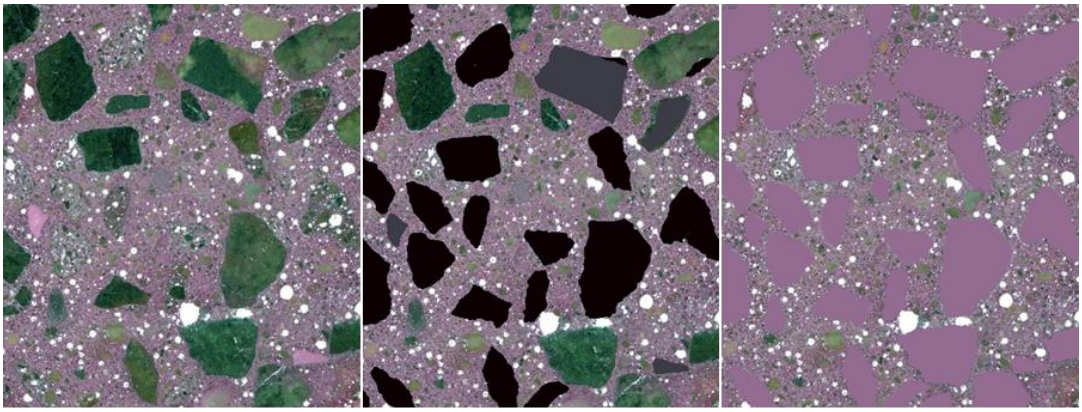

Figure 23. Image overlay of recycled aggregate concrete (RAC) specimen: (a) original, (b) RCA as aggregates, and (c) RCA as cement paste.

Table 18

Interpretation Of Image Analysis Results in RCA Image Overlays

Image	Air Content, A	Paste Content, P	Aggregate Content, Agg
(a)	$A_{(a)} = A_{NM} + A_{RCA/LWA}$	$P_{(a)} = P_{NM} + P_{RCA}$	$Agg_{(a)} = FA_{NM} + (CA + FA)_{RCA} + (LWA - A_{LWA})$
(b)	$A_{(b)} = A_{NM}$	$P_{(b)} = P_{NM}$	$Agg_{(b)} = FA_{NM} + RCA/LWA$
(c)	$A_{(c)} = A_{NM}$	$P_{(c)} = P_{NM} + RCA/LWA$	$Agg_{(c)} = FA_{NM}$

Note: NM = new mortar, FA = fine aggregates, CA = coarse aggregates (RCA or LWA), A_{NM} = air concrete considering only the voids in new mortar, $A_{RCA/LWA}$ = air concrete considering only the voids in RCA/LWA

$$\boldsymbol{RCA/LWA\ content, in\ \%\ =\ Agg_{(b)} - Agg_{(c)}} \quad (18)$$

$$\boldsymbol{A_{RCA/LWA}, in\ \%\ =\ Agg_{(b)} - Agg_{(c)}} \quad (19)$$

$$\boldsymbol{RCA\ Paste\ content\ (P_{RCA}), in\ \%\ =\ P_{(a)} - P_{(b)}} \quad (20)$$

$$\boldsymbol{RCA/LWA\ air\ content, in\ \%\ =\ \frac{100[A_{RCA/LWA}]}{RCA/LWA}} \quad (21)$$

3.2.3 Statistical Analysis

The bivariate regressions between permeability measurements were determined in Microsoft Excel 365. The statistical analyses, including the test for equality of means and the multiple linear regression, were performed in R [109], a statistical programming language . The assumptions in multiple linear regression analysis [110], including linearity, multicollinearity, normality, homoscedasticity, and independence, were checked.

The measurements from all samples were treated as independent observations. The multicollinearity was checked using the variance inflation factors (VIF). The chosen predictors have VIFs of less than 5. A stepwise regression analysis was performed to remove the variables and interactions between variables that are insignificant to the regression model. The normality and homoscedasticity of the residuals were checked using the Shapiro-Wilk normality test and the Breusch-Pagan test, respectively. Multivariate outliers were removed to satisfy the assumptions of normality and homoscedasticity of the residuals. The R packages used are car [111], olsrr [112], and lmtest [113].

Chapter 4

Concrete Permeability and its General Relation to Electrical Resistivity and Formation Factor[3]

This research aims to establish the relation of water permeability, rapid chloride permeability, and rate of water absorption, with the electrical resistivity-based measurements of concrete with porous aggregates (RCA and LWA). With porous aggregates, higher permeability measurements are expected for RACs and LWACs. In this chapter, the fresh concrete properties are first presented, and the possible effect of the porous aggregates is examined. Then the results of the permeability tests are discussed. The effects of the water-cement ratio, RCA variation, and LWA percent replacement on the concrete permeability measurements are determined. Finally, the relation of the different types of permeability measurements to the electrical resistivity-based tests (surface resistivity, bulk resistivity, and formation factor) is shown.

4.1 Fresh Concrete Properties

4.1.1 Slump, Air Content, and Temperature

The fresh concrete properties shown in Table 19 were measured and recorded after each mix. The fresh concrete temperature varied from 14.9~26.7 °C. The slump ranged from 20~190 mm, while the air content ranged from 3.0~10.4%. The varying values of fresh concrete properties resulted in a wide range of permeability measurements which is essential in determining the trend of the permeability plots.

[3] Some parts of this chapter are published in [129, 130, 131]

Table 19

Fresh Concrete Properties

Mixture	Slump (mm)	Air Content (%)	Temperature (°C)
RAC48*	110	6.2	18.8
RAC38*	73	5.3	20.4
LWAC48	125	9.7	19.9
LWAC38	140	8.75	22.2
LWAC28	25	3.75	21.3
50LWAC48	120	10.4	19.3
50LWAC38	75	5.75	26.6
50LWAC28	20	3.25	21.6
NWAC48	95	6.5	22.0
NWAC38	50	5.5	23.5
NWAC28	45	3	24.6

*Average of 8 RAC mixtures per w/c.

The effect of the decreasing water-cement ratio on the fresh concrete properties was probably reduced by the increasing cement paste volume (CPV) as they have contrasting effects on the concrete workability. Studies have shown that concrete workability increases as the CPV increases [114, 115, 116]. But in this study, the fresh concrete properties followed the common trends related to the water-cement ratio, wherein the slump and air content decrease as the water-cement ratio decreases.

A high air content for the concrete with a 0.28 water-cement ratio was hard to achieve even with a higher amount of air-entraining admixture. Thus, the slump and air content of concretes with 0.28 w/c only ranged from 20~45mm and 3~3.75%, respectively. There was no clear trend on the effect of porous aggregates on the

workability of concrete, but the air content is generally higher for concrete with LWA. Due to their high porosity and large pores, there may be more air bubbles produced on the surface of lightweight aggregates.

4.1.2 Fresh Concrete Unit Weight

The fresh concrete unit weights are summarized in Figure *24*, where the unit weight reduction in using LWA can be observed. The bulk unit weight of LWA is less than half of the bulk unit weight of NWA; thus, the unit weight of concrete significantly decreases as the LWA content increases. On average, the fresh concrete unit weight was reduced by 24% for LWAC and 12% for PLWAC. On the other hand, the fresh concrete unit weight of RAC mixtures does not significantly differ from the NWAC mixtures of the same water-cement ratio because the specific gravity and bulk unit weight of RCA is slightly lower than that of NWA. The fresh concrete unit weight also increases as the water-cement ratio decreases, which can be attributed to the increased amount of cement, the concrete component with the highest specific gravity.

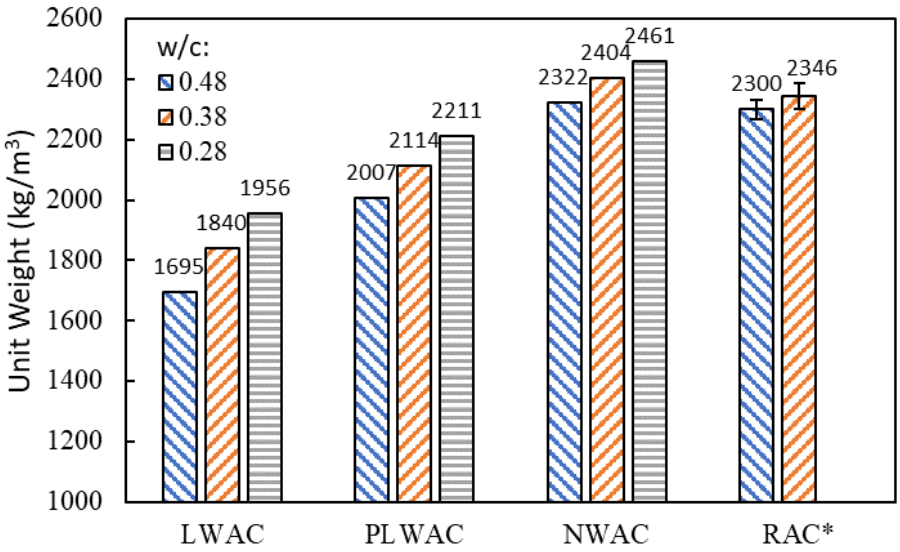

Figure 24. Fresh concrete unit weight in kg/m^3. Error bars in RAC represent the standard deviation for the average of 8 RAC mixtures per w/c.

4.2 Concrete Permeability

The permeability measurements for the 16 RAC (100% coarse RCA), 3 LWAC (100% coarse LWA), 3 50LWAC (50% LWA), and 3 NWAC (control) mixtures are discussed in this section.

4.2.1 Recycled Aggregate Concrete (RAC)

4.2.1.1 Surface and Bulk Electrical Resistivity. The electrical resistivity tests indirectly evaluate concrete's permeability by measuring its resistance to the flow of electrons. Higher electrical resistivity means lower permeability and vice versa. For each concrete mixture, four specimens were tested for surface resistivity according to

AASHTO T358 [8] and bulk resistivity according to AASHTO TP 119 [9]. Figure *25* shows the average electrical resistivity measurements in 16 RAC mixtures.

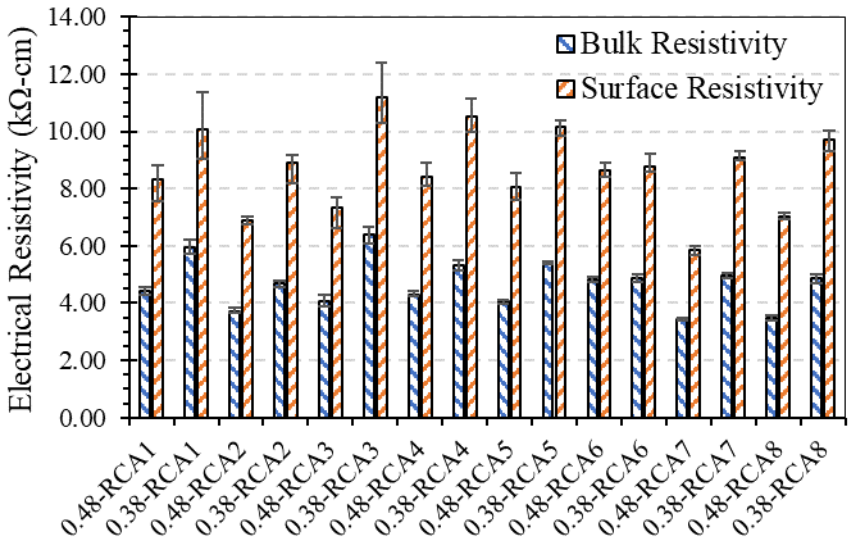

Figure 25. Electrical Resistivity (kΩ-cm) of RAC Mixtures on the 28th day. Error bars represent the range of values for four specimens.

The RAC bulk resistivity values ranged from 3.45 kΩ-cm to 6.40 kΩ-cm, while the surface resistivity ranged from 5.84 kΩ-cm to 11.19 kΩ-cm. The bulk electrical conductivity, the inverse of resistivity, values observed by Xuan et al. [26] in RAC are within the range of values found in this study. In their study, one type of RCA used is an old RCA sourced from a local laboratory of C&D waste. The other type is a new RCA, sourced from a newly designed concrete made specifically for the study. They have observed 56-day bulk electrical conductivity measurements of about 25 mS/m (4 kΩ-cm bulk resistivity) and 23.5 mS/m (4.26 kΩ-cm bulk resistivity) for concretes with new and

old RCAs, respectively, at 100% replacement. The electrical resistivity improved when they used carbonated RCAs.

4.2.1.2 Formation Factor. The formation factor of each mixture was calculated by measuring the bulk resistivity of the concrete specimens immersed in the simulated pore solution and dividing it by the pore solution's resistivity. A higher formation factor means the material has lower permeability and vice versa. The results in the plot were the average of two specimens immersed in a bucket of simulated pore solution for each concrete mixture to determine the formation factor. The average calculated formation factor measurements in the 16 RAC mixtures are presented in Figure *26*.

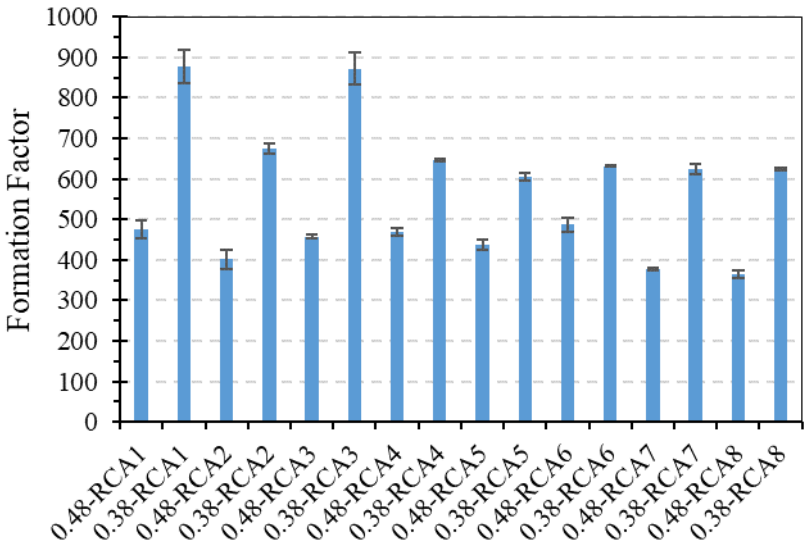

Figure 26. Formation factor of RAC Mixtures at the 28th day. Error bars represent the range of values for two specimens.

4.2.1.3 Germann Water Permeability. The average GWT measurements are shown in Figure *27*. Most RAC specimens with a lower water-cement ratio also have lower water permeability. While there are no universally accepted limits for maximum water penetration in concrete for practical applications, German national standards suggest that concrete can be evaluated as water-resistant when the average maximum depth of water penetration measured is not higher than 50 mm [8]. Based on an established correlation between the GWT and BS EN 12390-8 standard by Moczko and Moczko [8], the 50 mm depth in the 72-hour water penetration test corresponds to a 10-minute average water flux of 0.32 μm/s. However, the average water flux calculated from this study are a magnitude lower than the values found by Moczko and Moczko [8]. The lower measurements could be because the testing was done in laboratory specimens saturated under water curing, while the testing done by Moczko and Moczko [8] was in "in-situ" concrete specimens. The GWT measurements found in this study are more comparable to the values found by Trezos et al. [117], where the mean water flux for underwater cured specimens of various concrete mixtures ranged from $0.3\sim0.6 \times 10^{-4}$ mm/sec.

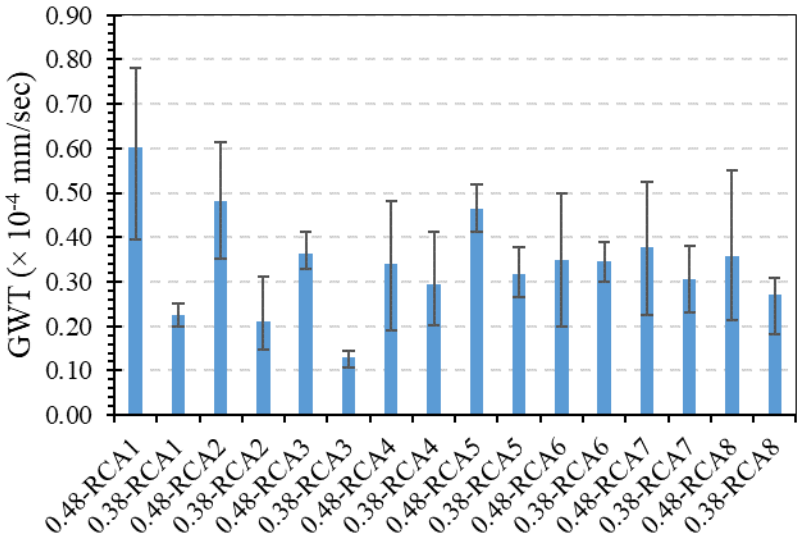

Figure 27. Germann water permeability of RAC specimens on the 28th day. Error bars represent the range of values for at least three specimens except 0.38-RCA1.

4.2.1.4 Rapid Chloride Permeability. A higher total charge passed during the 6-hour RCPT means higher concrete permeability. Consequently, higher electrical resistivity corresponds to lower RCPT measurement and vice versa. The total charge passed can be calculated by determining the area under the current versus time chart and is expressed in Coulombs (C). The RCPT results of RAC mixtures are shown in Figure *28*, where very high total charges passed were measured. If evaluated based on ASTM C1202 [68] criteria, the RAC mixtures are considered to have high chloride ion penetrability.

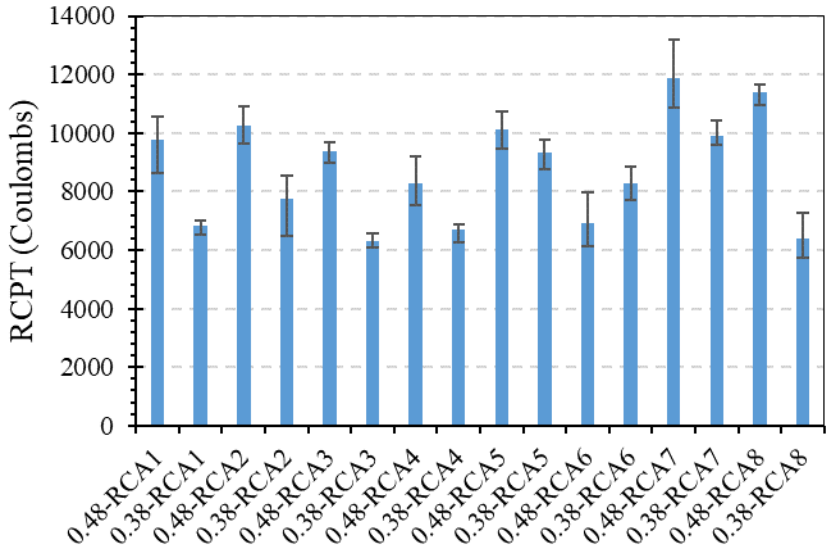

Figure 28. Average total charge passed (Coulombs) in RAC specimens on the 28th day. Error bars represent the range of values for three specimens.

The RCPT should run for 6 hours. However, most samples have their test terminated only after 2 to 4 hours. The test stoppage is because the maximum current of 500mA allowed by the measuring device was exceeded during the testing, suggesting that the samples have very high chloride ion permeability. A sample of this occurrence is shown in Figure *29*, where the test for a 0.48-RCA1 specimen was stopped at 224 minutes. The total charge passed (C) for those samples was estimated by integrating the current-time regression equation from 0 to 360 minutes.

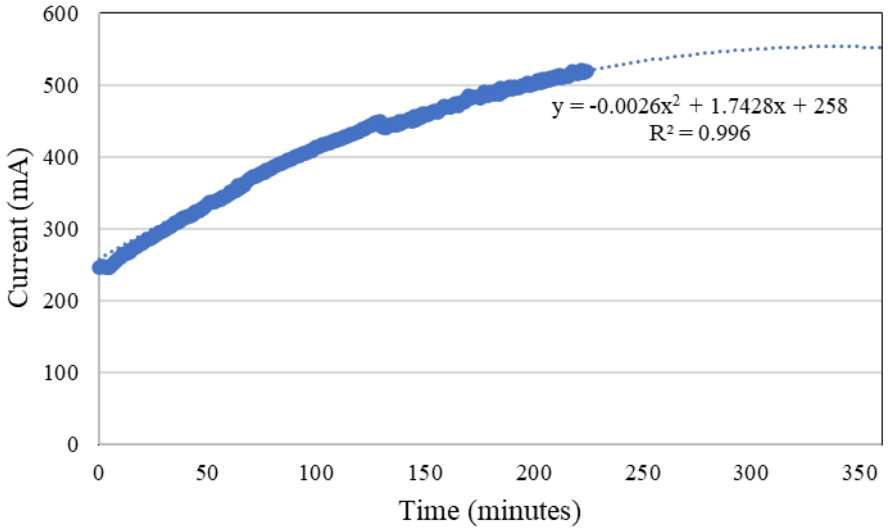

Figure 29. RCPT result of one sample from 0.48-RCA1 mixture, where the test was stopped due to overcurrent.

4.2.1.5 Water Sorptivity Test. During the early phase of absorption, water is absorbed and fills the tiny pores through capillary suction. Then, the larger pores and air voids are filled during the second phase, which involves other fluid flow mechanisms such as diffusion [118] [119]. As a result, the rate of absorption is divided into initial and secondary sorptivity. The change in mass during the absorption was also divided by the water absorption capacity to calculate the increase in the degree of saturation of concrete.

The rate of water absorption or sorptivity measures how fast the water penetrates the concrete without significant hydrostatic pressure. Three specimens from each of the 16 RAC concrete mixtures were tested for water sorptivity according to ASTM C1585 [52]. In this subsection, the water sorptivity measurements in RAC specimens are

discussed. Comparison of the sorptivity measurements with the other concrete types was shown in the Section 4.2.2.5.

4.2.1.5.1 Water Sorptivity Values. The initial sorptivities were calculated as the slope of the plot of absorption versus the square root of time using the data from the first 6 hours of testing. Similarly, the secondary sorptivity was calculated using the data from day 1~8. ASTM C1585 [52] requires a correlation coefficient of at least 0.98 between the absorption and square root of time to determine the initial and secondary sorptivity. A regression plot of one RAC specimen is shown in Figure *30*. In the figure, the initial sorptivity is 0.4159 mm/day$^{0.5}$ while the secondary sorptivity is 0.2354 mm/day$^{0.5}$.

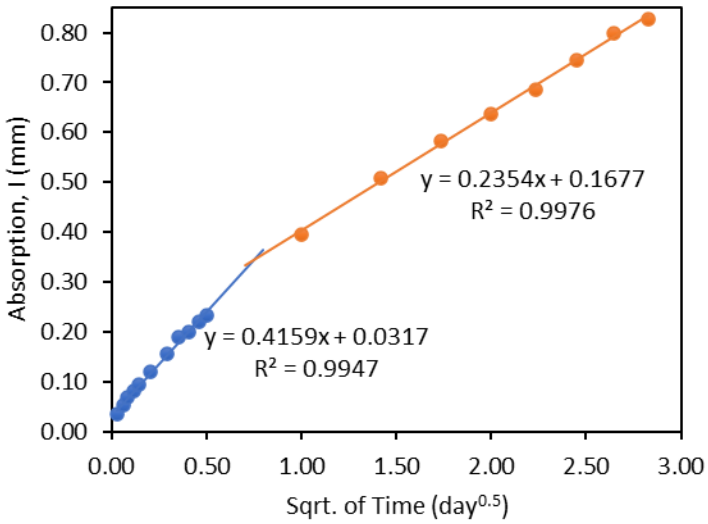

Figure 30. Absorption versus square root of time plot of a 0.48-RCA1 specimen. The slopes of the regression lines are the sorptivity measurements.

Figure *31* shows the average sorptivity measurements of the 16 RAC mixtures. Sorptivity is expressed as the volume of absorbed water (mm^3) over the area of the specimen (mm^2) and the square root of time ($day^{1/2}$), $mm^3/mm^2/day^{1/2}$ or simply $mm/day^{1/2}$. The results show a wide range of initial sorptivity (0.28~1.68 $mm/day^{1/2}$) and secondary sorptivity (0.20~0.78 $mm/day^{1/2}$) values of the RAC specimens. The sorptivity values measured by Cantero et al. [87] (0.48~0.68 $mm/day^{1/2}$) for 90-day RAC are within the range of sorptivity values measured in this study.

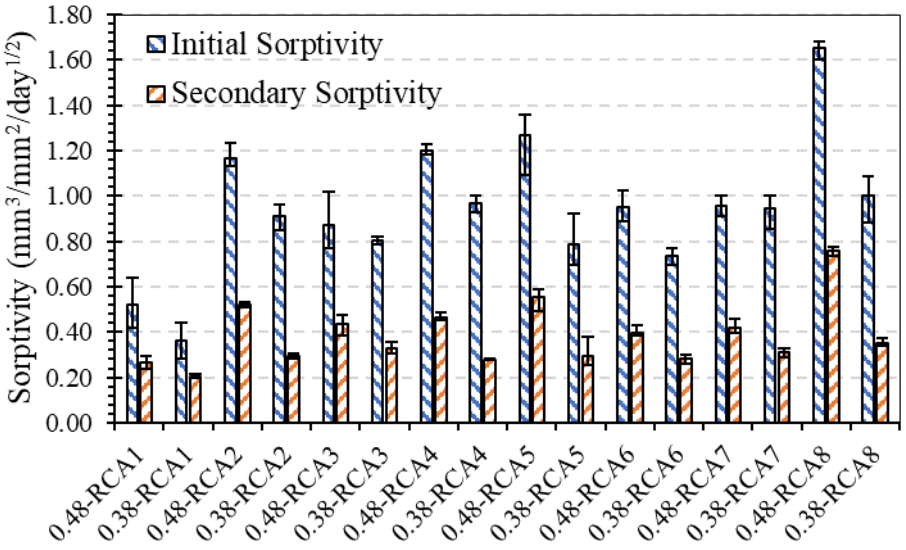

Figure 31. Average initial and secondary sorptivity of 16 RAC mixture. Error bars represent the range of values for three specimens.

4.2.1.5.2 Sorptivity Based on the Fourth Root of Time ($t^{0.25}$).

The correlation coefficients of the absorption versus square root of time plot for the initial and secondary sorptivity ranged from 0.9822~0.9997 and 0.9842~0.9993, respectively. The required correlation coefficient in the standard [52] of at least 0.98 was satisfied in both cases. In Figure 30**,** the slope difference between the initial and secondary absorptions is evident. When sorptivity is based on a single parameter combining the data of initial and secondary absorptions, the correlation coefficients will only range from 0.9747~0.9975; therefore, some of the measurements will be invalid.

The data for the initial and secondary absorptions cannot be combined using the square root of time, but expressing the sorptivity using a single parameter can be done by determining the slope of absorption versus the fourth root of time ($t^{0.25}$) instead of $t^{0.5}$. Cantero et al. [87] used the sorptivity measurements based on $t^{0.25}$, as Zaccardi et al. [21] proposed, and found that the correlation coefficients are higher than when expressed based on $t^{0.5}$. Based on the data from this study, the correlation coefficients improved to 0.9897~0.9999 when the single sorptivity parameter based on $t^{0.25}$ was used. The linear relationship between the absorption in RAC mixtures from 1 minute to 8 days of testing and $t^{0.25}$ is shown in Figure 32. Due to the improved linear relationship and simplicity, this single-parameter sorptivity can be used instead of the initial and secondary sorptivity. The values of the $t^{0.25}$-based sorptivity are shown in Figure *33*.

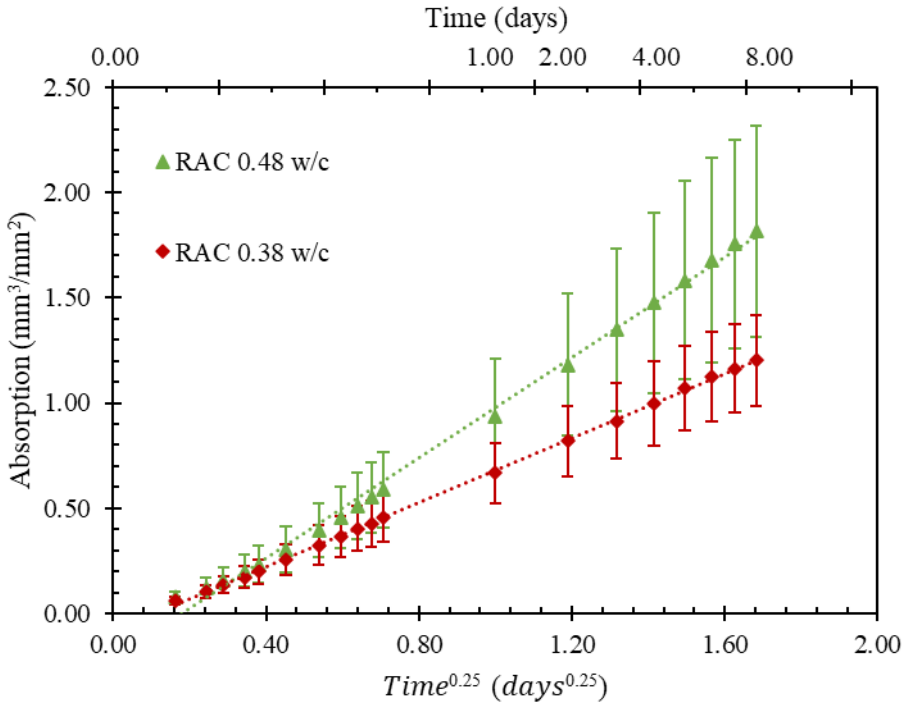

Figure 32. Average water absorption versus time$^{0.25}$ plot of RAC mixtures. Error bars represent the standard deviation for the average of 8 RAC mixtures per w/c.

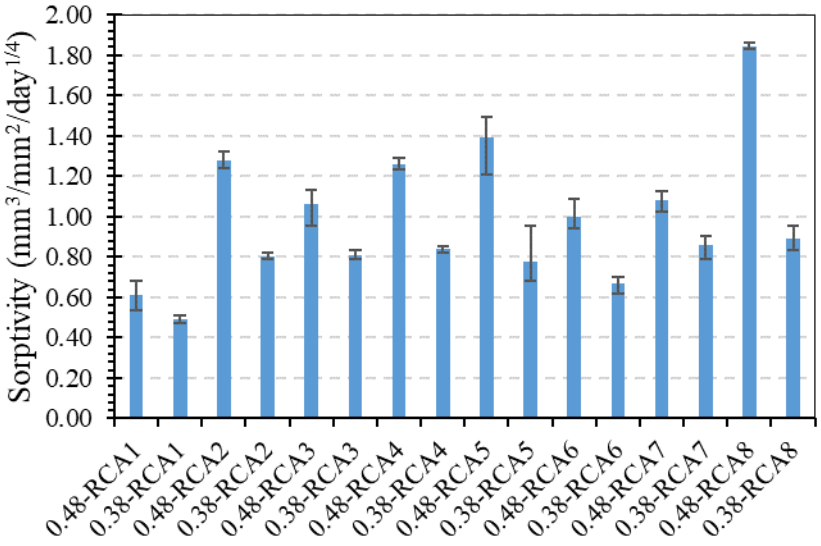

Figure 33. Average t$^{0.25}$-based sorptivity of RAC mixtures. Error bars represent the range of values of three specimens.

4.2.1.5.3 Rate of Water Saturation. As water is absorbed into the concrete, the degree of saturation increases. The higher the rate of saturation, the more susceptible the concrete is to freeze-thaw damage. There is a critical degree of saturation, Scr, beyond which freeze-thaw damage begins to initiate [57]. Luan et al. [118] found that the critical degree of saturation of RAC specimens is approximately 81~83%, which is lower than that of regular concrete (86~88%) [55]. Therefore, determining the rate of increase in saturation, in addition to sorptivity, is necessary. Similar to the determination of sorptivity, the rate of water saturation was determined from the plot of the degree of saturation and the fourth root of time. The average rate of water saturation in (%)/day0.25 is shown in Figure *34*. The trends are similar to the trends observed in sorptivity measurements. The rate of saturation decreases as the water-cement ratio decreases.

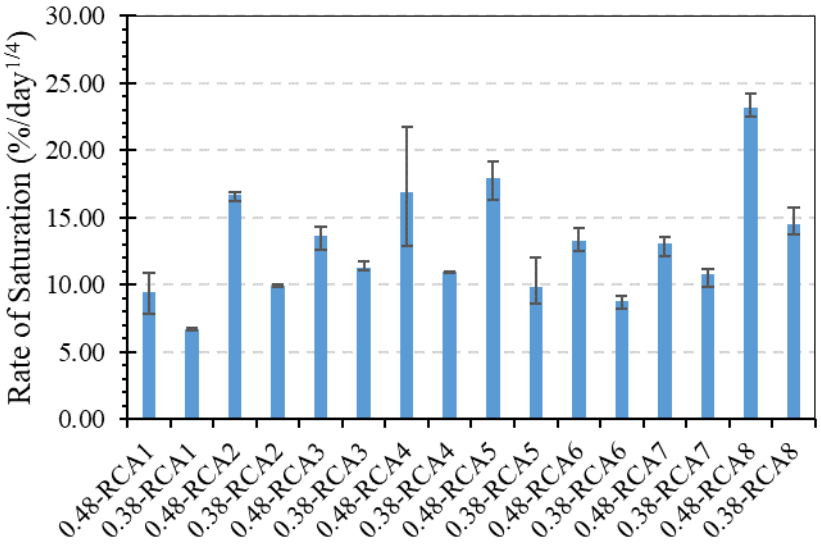

Figure 34. Average rate of water saturation in 16 RAC mixtures. Error bars represent the range of values for three specimens.

4.2.1.6 Effect of Varying Water-Cement Ratio and RCA Variation. Eight variations of RCA was used in this study. Then, to achieve a range of permeability measurements from a less permeable to a more permeable concrete, each RCA variation was combined with 2 water-cement ratios (0.48 and 0.38) to produce 16 RAC mixtures. To determine if the permeability measurements in the 16 RAC mixtures produced from two factors (water-cement ratio and RCA variation) are statistically different, two-way analysis of variance (ANOVA) was conducted.

There are three assumptions in ANOVA. The first two assumption are that the observations from each RAC mixture are normally distributed and that their variances are equal. For each mixture, the measurements were gathered from separate specimens, and so the requirement in ANOVA that the measurements are independent was satisfied. The normal distribution assumption was checked by applying Shapiro-Wilk normality test in the ANOVA residuals, while the equal variance assumption was checked using Levene's Test. The analyses were performed using RStudio 2022.12.0+353.

During the normality test, some variables particularly the surface and bulk resistivity were needed to be transformed to satisfy the normal distribution requirement. The Shapiro-Wilk normality tests performed on the ANOVA residuals for the variables 1/SR ($W = 0.981$, p-value = 0.455), 1/BR ($W = 0.981$, p-value = 0.446), GWT ($W = 0.980$, p-value = 0.509), RCPT ($W = 0.992$, p-value = 0.985), and Sorptivity ($W = 0.974$, p-value = 0.365) did not show any evidence that the permeability measurements are not normally distributed. Meanwhile, the result for the rate of saturation, RS, ($W = 0.787$, p-value = 6.836e-07) suggests that the distribution of RS is non-normal. But since the

number of observations in RS is greater than 30 (48 specimens), the distribution of residuals is approximately normal, and so, two-way ANOVA is still applicable.

The results of Levene's tests imply that there is homogeneity of variances in all permeability measurements: p-value = 0.07 for 1/SR, p-value = 0.57 for 1/BR, p-value = 0.06 for GWT, p-value = 0.95 for RCPT, p-value = 0.91 for Sorptivity (S), and p-value 0.22 for rate of saturation (RS). All p-values are greater than 0.05, which means that the variances between groups are not statistically different.

The results of two-way ANOVA for surface resistivity is summarized in Table 20, where the p-values of w/c, RCA variation, and their interaction are all less than 0.05. The summary of two-way ANOVA for the other permeability tests are shown in Appendix. The p-values returned from the series of two-way ANOVA performed on different permeability tests are presented in Table 21. The 16 RAC mixtures is the result of interaction between two w/c and eight RCA variations. All p-values of w/c are less than 0.05, which indicates that the differences between the 0.48 and 0.38 w/c measurements on surface resistivity, bulk resistivity, GWT, RCPT, sorptivity, and saturation rate, are statistically significant. Moreover, all p-values of RCA variation and its interaction with w/c, except in GWT, are less than 0.05. The low p-values mean that the RCA variations resulted in statistically different values of surface resistivity, bulk resistivity, RCPT, sorptivity, and saturation rate. Moreover, the RCA variation affected the relationship between the w/c and permeability measurements, except in GWT.

Table 20

Two-Way ANOVA of the Inverse of RAC Mixture's Surface Resistivity (1/SR)

Source of Variation	Df	SS	MS	F	p-value
water-cement ratio	1	0.015191	0.015191	437.05	< 2e-16
RCA variation	7	0.007060	0.001009	29.02	5.08e-15
Interaction (RAC Mixture)	7	0.004520	0.000646	18.58	1.35e-11
Residuals	47	0.001634	0.000035		

Table 21

Summary of p-Values from the Two-Way ANOVA in RAC Permeability Measurements

Source of Variation	1/SR	1/BR	GWT	RCPT	S	RS
w/c	< 2e-16	< 2e-16	4.94e-06	1.68e-11	< 2e-16	1.14e-13
RCA	5.08e-15	<2e-16	0.1536	5.96e-09	< 2e-16	1.50e-11
Interaction (RAC Mixture)	1.35e-11	<2e-16	0.0729	9.70e-07	9.66e-10	0.0010

The p-value of RCA variation in GWT measurements suggests that there is not enough evidence that the GWT measurements at different RCA variations are different. Moreover, the p-value of the interaction between RCA variation and w/c indicates that the RCA variation does not have significant effect on the relationship between the water-cement ratio and GWT measurements. This result can be attributed to the high variation in GWT measurements, which can be observed from Figure *27*. In summary, the varying RCA types and water-cement ratio resulted in statistically different measurements in most types of permeability assessed in this study.

4.2.2 Lightweight and Normalweight Aggregate Concretes (LWAC, NWAC, and 50LWAC)

4.2.2.1 Surface and Bulk Electrical Resistivity. Figure *35* shows the average values in three LWAC, three 50LWAC, and three NWAC mixtures. Also included in Figure *35* are the average measurements of RAC specimens at 0.48 and 0.38 w/c. Compared to NWAC, the average electrical resistivity values of RAC are lower by 41%, while the average electrical resistivities of LWAC and 50LWAC are lower by about 50% and 38%, respectively.

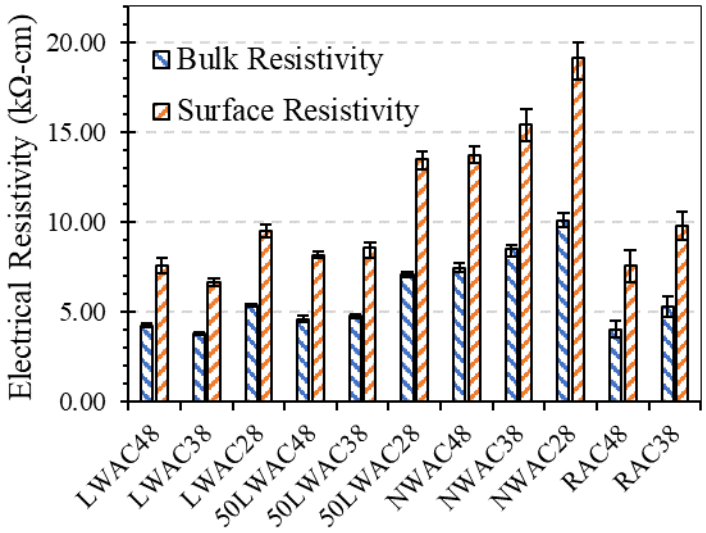

Figure 35. Electrical Resistivity (kΩ-cm) of all concrete mixtures on the 28th day. Error bars represent the range of values for four specimens each in LWAC, 50LWAC, and NWAC mixtures and the standard deviation for the average of 8 RAC mixtures per w/c.

It can be observed from Figure *35* that the electrical resistivity decreases as the LWA content increases. The surface resistivity of the lightweight aggregate concretes

(100% and 50% coarse LWA) ranged from 6.7~13.5 kΩ-cm, and the bulk resistivity ranged from 3.8~7.1 kΩ-cm. The electrical resistivity values measured for LWACs are similar to those of Hornakova et al. [94] for structural concrete made from expanded clay coarse aggregate. They measured a 28th-day surface and bulk resistivity values of 8.52 kΩ-cm and 3.65 kΩ-cm, respectively.

In general, the electrical resistivity increases as the water-cement ratio decreases. However, the increase in CPV could have reduced the effect of the lower water-cement ratio on electrical resistivity. The trend was the same for most of the tested concretes, but the recorded electrical resistivities at 0.48 and 0.38 w/c are relatively close. A slightly higher resistivity for 0.48 w/c than 0.38 w/c can even be observed in LWAC. Both cement paste and coarse aggregates have high permeability at high water-cement ratios. It is also possible that the effect of the pore solution conductivity in the electrical resistivity measurement is more evident in this case. The cement paste becomes less porous at a lower water-cement ratio, and thus significant improvements in the electrical resistivity were recorded.

4.2.2.2 Formation Factor. The average formation factors of 8 RAC mixtures for each water-cement ratio are included in Figure *36*, where the average formation factors in 3 LWAC, 3 50LWAC, and 3 NWAC mixtures are shown. The formation factors calculated in RAC mixtures were lower by 29% and 22% than NWAC, with 0.48 and 0.38 w/c, respectively. On the other hand, the formation factors of lightweight concrete mixtures are lower than the RAC mixtures. As compared to NWAC with 0.48, 0.38, and 0.28 w/c, the formation factor decreased by 38%, 52%, and 28%, respectively, when 100% LWA coarse aggregates were used and decreased by only 37%, 39%, and 5%,

respectively, for the 50% coarse aggregate replacement. Like the electrical resistivity, the formation factor increases as the percent replacement of LWA decreases.

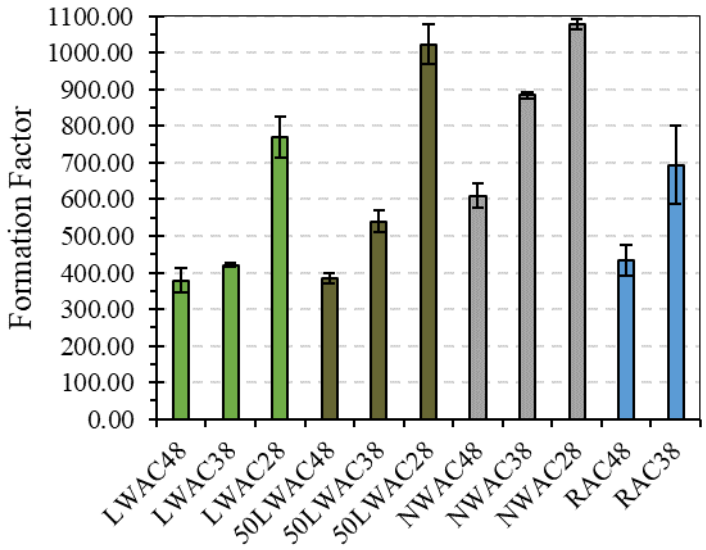

Figure 36. Formation factor of all concrete mixtures on the 28th day. Error bars represent the range of values for two specimens each in LWAC, 50LWAC, and NWAC mixtures and the standard deviation for the average of 8 RAC mixtures per w/c.

It is evident in all concrete mixtures that the formation factor increases as the water-cement ratio decreases. The permeability trend with the water-cement ratio is more apparent than the observations for electrical resistivity since, in the formation factor, the effect of the pore solution's resistivity was removed. The concrete permeability can be divided by the permeability of its microstructure phases: aggregates, cement paste, and ITZ. It can be observed that the increase in the formation factor between 0.48, 0.38, and 0.28 w/c is uniform for NWAC. The uniform increase could be because the normalweight aggregate permeability is too low, and the cement paste and ITZ are mainly affected by

the water-cement ratio. But for LWAC and PLWAC, there is a sudden increase from 0.38 to 0.28 w/c. It seems that at 0.28 w/c, the permeability of the cement paste and ITZ for lightweight concretes are very low, and the impact of the LWA on the permeability of the concrete is reduced.

4.2.2.3 Germann Water Permeability. Figure *37* shows the average results in the 3 LWAC, 3 50LWAC, and 3 NWAC mixtures, including the average values for the RAC mixtures with 0.48 and 0.38 w/c. The measurement variations within-group of NWACs are low, but the high variations within-group of porous aggregate concretes are noticeable. The high within-groups variance in RAC, LWAC, and 50LWAC mixtures is due to the difference in aggregates exposed to the surface during the test. GWT does not consider the whole depth or volume of the concrete specimen. Instead, the test can only measure the permeability of the surface and up to a certain depth that the water can reach in 10 minutes of testing. When the tested surface has more porous aggregates exposed than the other specimens in the same mixture, it will return a higher permeability measurement than the others. With that, the Germann water permeability of porous aggregate concretes should be evaluated as the average measurement for at least two or three specimens.

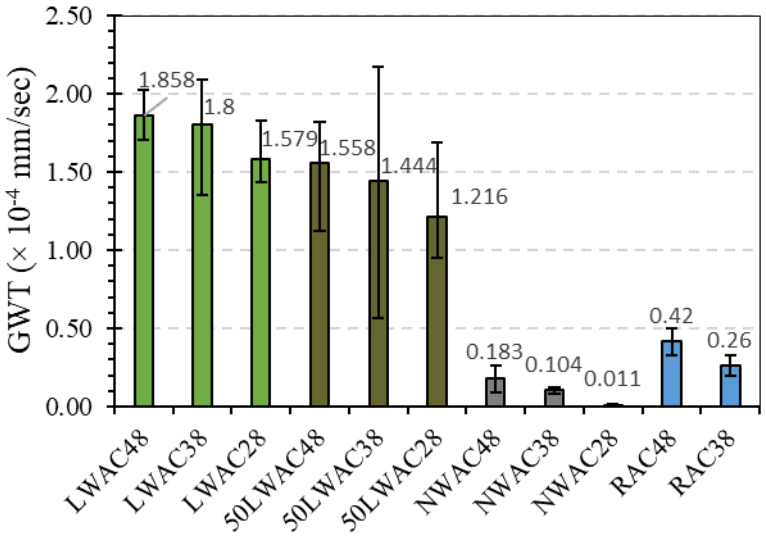

Figure 37. Germann water permeability of all concrete mixtures. Error bars represent the range of values for at least three specimens each in LWAC, 50LWAC, and NWAC mixtures and the standard deviation for the average of 8 RAC mixtures per w/c.

All NWACs can be considered water-resistant since their average water flux only ranged from 1.1 x 10^{-6} mm/s to 1.8 x 10^{-5} mm/s. The RACs average water flux is 2 to 3 times higher than NWAC. At the same water absorption rate as the normalweight concretes, the porous aggregate concretes will possibly have a lesser depth of water penetration since the porous aggregates can absorb the water.

As observed in Figure *37*, the concrete water permeability decreases as the water-cement ratio decreases since the cement paste becomes less porous. Like in the formation factor, the change in water permeabilities from 0.38 w/c to 0.28 w/c is abrupt. It is also evident that the water permeability increases when the percentage of LWA increases. Very high water permeability was observed for LWAC and 50LWAC ranging from 1.2 x 10^{-4} mm/s to 1.85 x 10^{-4} mm/s. LWACs and 50LWACs can be regarded as water permeable as their water permeabilities are 10~100 times higher than NWACs.

A slight improvement in the water permeability can be observed when the LWA content is reduced from 100% to 50%. The average flux in 50LWAC is lower by 16%, 20%, and 23% for 0.48, 0.38, and 0.28 w/c, respectively, than LWAC. The very high permeability can be attributed to the pore structure of LWA. Since LWA has large pores, the head loss for fluid flow is low, resulting in a high flow rate. Even though LWAs have high water absorption that will reduce the depth of water penetration, the measured water permeabilities are too high. The results infer that the LWACs would not be suitable for concrete structures subjected to high hydrostatic forces, such as dams and tunnels.

The coarse LWA percent replacement can also be expressed by the weighted coarse aggregate (CA) porosity, the total porosity attributed to the CA per unit volume of concrete. It can be calculated as the sum of the products of CA volume and its porosity, as shown in Equation (22). The calculated values are 7.30% and 3.76% for LWAC and PLWAC, respectively, and only 0.24% for the NWAC. Based on the values, even if the volume of LWA is further reduced, the water permeability will probably still be high. The RACs have an average weighted CA porosity of 3.77%, almost equal to PLWAC. Still, the RAC has a lower water permeability than PLWAC because, unlike the LWA, the RCA has tiny pores and a tortuous pore structure.

$$\phi_{WeightedCA} = \sum (V_{CAi} * \phi_{CAi}) \ / \ 100 \tag{22}$$

where $\phi_{WeightedCA}$ = the weighted coarse aggregate porosity (%), V_{CAi} = % volume of coarse aggregate *i* in concrete, and ϕ_{CAi}= porosity of coarse aggregate *i* (%).

4.2.2.4 Rapid Chloride Permeability. Figure *38* shows the average RCPT measurements in all concrete mixtures. Based on the evaluation table provided in ASTM C1202 [9], the chloride ion penetrability of NWAC with 0.48 w/c (4504 C) can be classified as "high," while those with 0.38 w/c (2966 C) and 0.28 w/c (2414 C) are in "moderate" classification. The RACs recorded the highest readings and were 2.2~2.6 times higher than NWACs. The LWACs were about 1.6~2.7 times higher than NWACs, while the 50LWACs were only 1.2~1.6 times higher than NWACs. While the LWA is more porous than RCA, the ITZ of LWAC is improved due to the cement paste-aggregate interlock [32] [37]. On the other hand, the ITZ of RAC has a less compact and more porous structure. RCA contains un-hydrated cement and during hydration of the new concrete, it produces some amount of calcium hydroxide resulting to an increased net formation of calcium hydroxide in RAC than in NWAC [23]. The calcium hydroxide leaches out of the paste, leaving more voids in the ITZ.

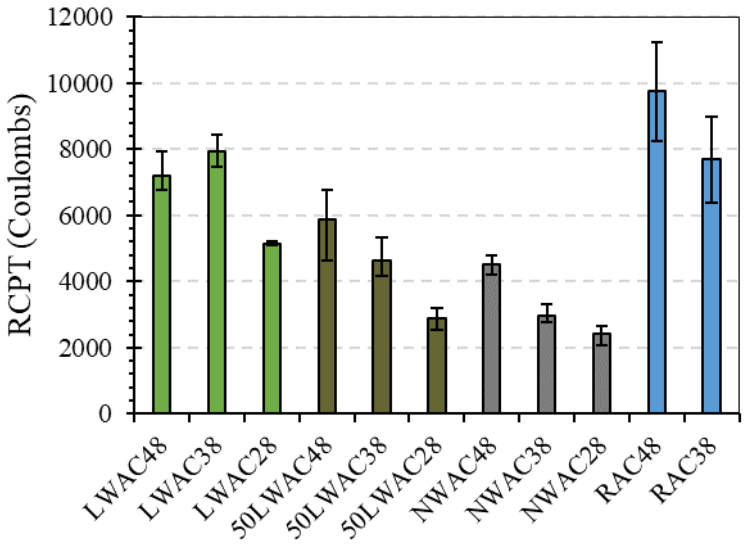

Figure 38. Average total charge passed (Coulombs) of all concrete mixtures. Error bars represent the range of values for three specimens each in LWAC, 50LWAC, and NWAC mixtures and the standard deviation for the average of 8 RAC mixtures per w/c.

The RCPT measurements for NWAC are comparable with the measurements made by Liu et al. [39] for 0.38 w/c (2528 C) and 0.54 w/c (6199 C) control NWACs and are lower than the measurements by Youm et al. [36] for 0.28 w/c (4612 C) NWAC without silica fume. Because of the significant difference in the aggregate porosity, the porous aggregate concretes show very high RCPT measurements. The LWACs ranged from 5148~7941 C, while the 50LWACs ranged from 2879~5890. These measurements are higher than the total charge passed measured by Liu et al. [39] for LWAC at 0.38 w/c (2496~3278 C) but lower than the measurements by Youm et al. [36] for LWAC without silica fume at 0.24 w/c (9751 C).

The water absorptions of the LWAs used in this study and the others [36, 39] are approximately equal at 13~15%, but the nominal maximum aggregate size (NMAS), air

content, and slump of the LWACs differ. A 19 mm NMAS was used in this study, while the others used 9.5 mm [39] and 8 mm [36] NMAS. The use of large aggregates can result in a higher localized water-cement ratio in the ITZ due to bleeding and thus results in a more porous and weaker ITZ [7]. The other studies measured non-air-entrained concrete, while this study prepared air-entrained concrete. Higher slumps were recorded in [36] at 220~230 mm, compared to the slumps in [39] and in this study at 20~140 mm. The RCPT measurements in this study could be higher than [39] because of increased air content and larger NMAS but lower than [36] because of the lower slump.

The evaluation table provided in ASTM C1202 can evaluate the chloride penetration in NWAC but cannot be used for LWAC and RAC. While permeability is a good indicator of the concrete's durability, care should be taken when comparing concretes with different aggregates. The LWACs and RACs, while having higher permeability than NWACs, provide additional flow paths and increase the concrete's penetrable area. The higher permeable area might result in a lower depth of fluid penetration. In [39], the penetration depth measured in the rapid migration test of LWAC is 3% lower than NWAC, even when the LWAC has a 30% higher rapid chloride permeability. Still, the RCPT measurements of LWAC and RAC are too high and can be considered vulnerable to chloride ion penetration.

The resistances to chloride ion penetration were improved at a lower percentage of LWA and water-cement ratio. Smaller coarse aggregates can be used in the concrete mixtures to improve the RCPT measurements further. Moreover, to make these materials more appropriate for structures exposed to water or soil containing aggressive chemicals, using SCMs to improve the cement paste and ITZ is recommended.

4.2.2.5 Water Sorptivity. In this subsection, the average water permeability measurements of the LWAC, 50LWAC, and NWAC mixtures were presented. The measurements in RAC mixtures were also included in the discussion.

4.2.2.5.1 Water Absorbed during the Sorptivity Test. The change in mass of the specimens is the amount of water absorbed in the concrete. The average values of water absorbed for each concrete mixture and water-cement ratio were plotted against the square root of time, as shown in Figure *39*.

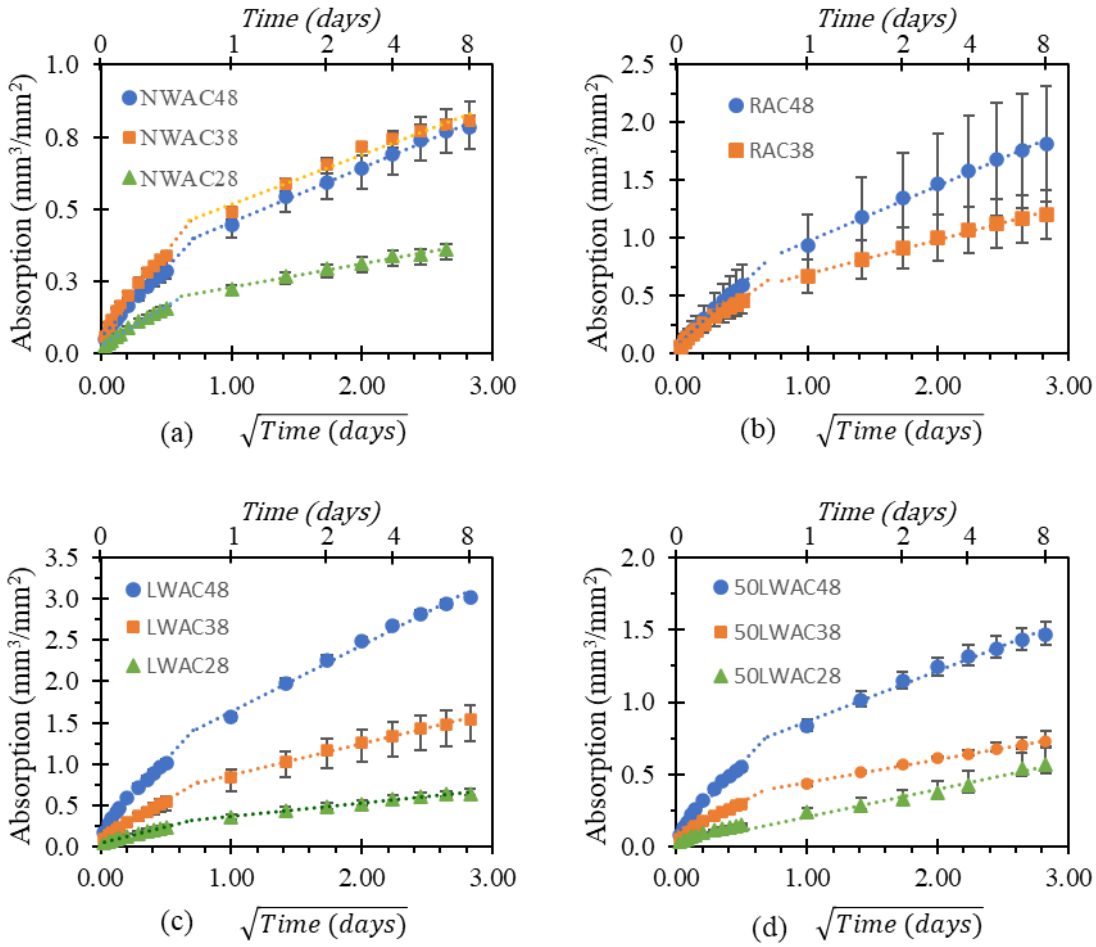

Figure 39. Average water absorption versus time$^{0.5}$ plots of (a) NWAC, (b) RAC, (c) LWAC, and (d) 50LWAC mixtures. Error bars represent the range of values for three specimens each in LWAC, 50LWAC, and NWAC mixtures and the standard deviation for the average of 8 RAC mixtures per w/c.

The difference in the water absorbed in NWAC with 0.48 and 0.38 w/c is not statistically significant, but the water absorbed in 0.28 w/c concrete is expectedly lower. On the other hand, there is a clear trend in the water absorption results of RAC, LWAC, and 50LWAC specimens indicating that the water absorption decreases as the water-cement ratio decreases. Furthermore, when compared to NWAC of the same water-cement ratio, the percent difference in the water absorbed in RAC and LWAC mixtures

increases as the water-cement ratio increases, as shown in Table 22. Since the quality of the mortar depends on the water-cement ratio, the results suggest that the new mortar's quality significantly affects the concrete's water sorptivity. These results were expected since the increased porosity due to the RCA and LWA provides a higher number of pathways for water transport.

Table 22

Increase in Water Absorption as Compared to NWACs with the same Water-Cement Ratio

Mixture	NWAC		
	0.48w/c	0.38w/c	0.28w/c
RAC	131%	49%	-
LWAC	285%	91%	74%
50LWAC	87%	-10% (decreased)	50%

4.2.2.5.2 Water Sorptivity Values. Sixteen mixtures of RAC were tested to achieve a range of sorptivity values from less permeable to more permeable concrete. Lightweight concretes at 50% and 100% coarse aggregate replacement and varying water-cement ratios were also tested for the same objective. The NWAC mixtures, which have no RCA or LWA, were also prepared to compare the measurements in the porous aggregate concretes to the regular concrete mixtures. Figure 40 shows the results for the 3 LWAC, 3 50LWAC, and 3 NWAC mixtures, including the average results for RAC mixtures. The secondary sorptivity of 50LWAC with 0.28 w/c returned a correlation coefficient of less than 0.98 and therefore was not determined.

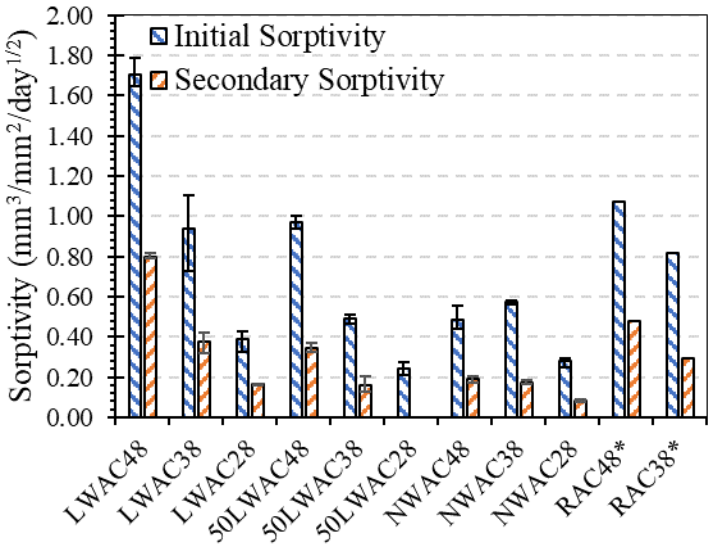

Figure 40. Average initial and secondary sorptivity of LWAC, 50LWAC, NWAC, and RAC mixtures. Error bars in LWAC, 50LWAC, and NWAC mixtures represent the range of values for three specimens.

The results show a wide range of initial sorptivity (0.28~1.68 mm/day$^{1/2}$) and secondary sorptivity (0.20~0.78 mm/day$^{1/2}$) values of the RAC specimens. The sorptivity values measured by Cantero et al. [87] (0.48~0.68 mm/day$^{1/2}$) for 90-day RAC are within the range of sorptivity values measured in this study. On average, the initial and secondary water sorptivity of RAC were higher than NWAC by 1.8 and 2.1 times, respectively. A wider range of sorptivity measurements was observed in lightweight concretes (50% and 100% replacement). The LWAC specimens have initial and secondary sorptivity measurements of 0.33~1.78 mm/day$^{1/2}$ and 0.16~0.82 mm/day$^{1/2}$, respectively. On the other hand, the 50LWAC specimens generally have lower values than LWAC with initial and secondary sorptivity measurements of 0.21~1.00 mm/day$^{1/2}$ and 0.13~0.37 mm/day$^{1/2}$, respectively.

In all specimens tested for water sorptivity, the secondary sorptivity is lower than the initial sorptivity. It was found that there is a strong correlation between the two sorptivity measurements. In Figure *41*, where all sorptivity measurements except 50LWC28 were plotted, the secondary sorptivity increases by about 0.45 mm^3/mm^2/day$^{1/2}$ per unit increase of the initial sorptivity.

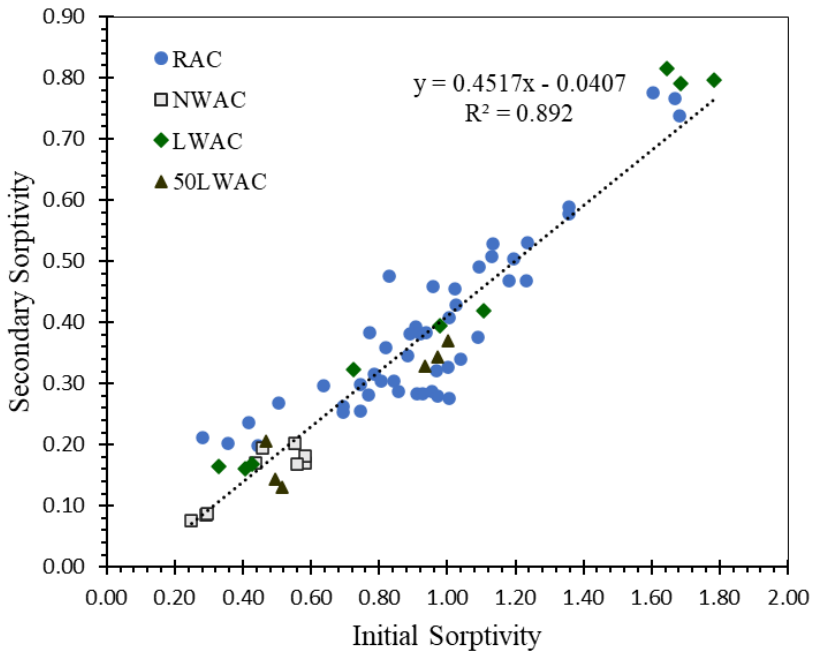

Figure 41. Relationship between initial and secondary sorptivity of 72 concrete specimens (48 RAC, 9 NWAC, 9 LWAC, and 6 50LWAC).

4.2.2.5.3 Sorptivity Based on the Fourth Root of Time ($t^{0.25}$).

The values of the $t^{0.25}$-based sorptivity are shown in Figure *42*. Like the water absorbed, the sorptivity values also increase as the water-cement ratio increases. The trend can be observed in Table 23, where the percent increase in water sorptivity as compared to NWAC of the same water-cement ratio is shown. The LWAC mixtures recorded the highest sorptivity measurements, followed by the RAC and 50LWAC.

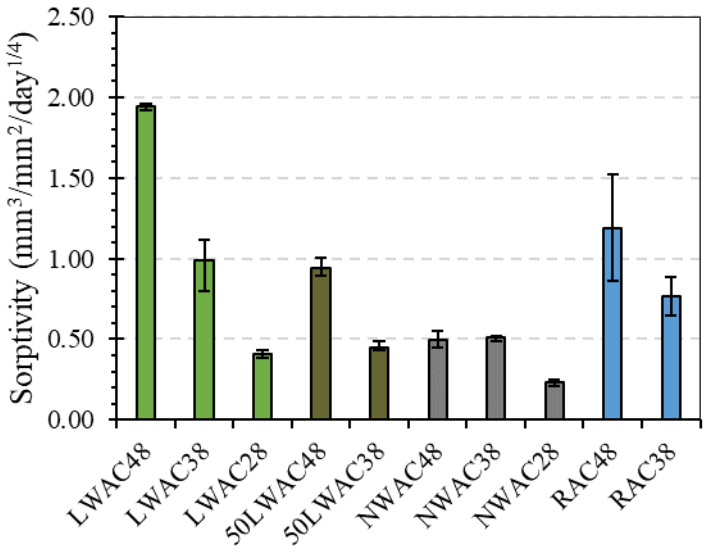

Figure 42. Average $t^{0.25}$-based sorptivity of LWAC, 50LWAC, NWAC, and RAC mixtures. Error bars represent the range of values for three specimens each in LWAC, 50LWAC, and NWAC mixtures and the standard deviation for the average of 8 RAC mixtures per w/c.

Table 23

Increase in Water Sorptivity as compared to NWACs with the same Water-Cement Ratio

Mixture	NWAC		
	0.48w/c	0.38w/c	0.28w/c
RAC	139%	51%	-
LWAC	289%	94%	76%
50LWAC	89%	-11% (decreased)	-

4.2.2.5.4 Degree of Saturation.

The water sorptivity can be used as an indicator of the concrete durability as the water absorbed possibly contains chemicals harmful to the concrete. Another concrete deterioration related to the water sorptivity results is freeze-thaw damage. During freeze-thaw damage, the water expands by about 9%. If the concrete is highly saturated, the water expansion will result in stress development in the concrete pores. If the developed stress exceeds the tensile capacity of the concrete, the concrete will be damaged. Therefore, concrete specimens with a high degree of saturation are more vulnerable to freeze-thaw damage. The total amount of water in the specimens during the sorptivity tests can be divided into the water absorption capacity to calculate the degree of saturation.

The plots of average values of the degree of saturation during the sorptivity test are shown in Figure 43. In all concrete types, it can be observed that the slope of the trendlines increases as the water-cement ratio increases. This trend is due to the higher water absorption in specimens with a higher water-cement ratio. Meanwhile, it is also noticeable that the initial degree of saturation increases as the water-cement ratio decreases. Since the rate of water absorption in low water-cement ratio concretes are lower, it can be that the water desorption is also lower. During the sample conditioning, less water was removed in concrete specimens with a lower water-cement ratio. After the test, the degree of saturation of the concrete specimens are almost the same regardless of the water-cement ratio.

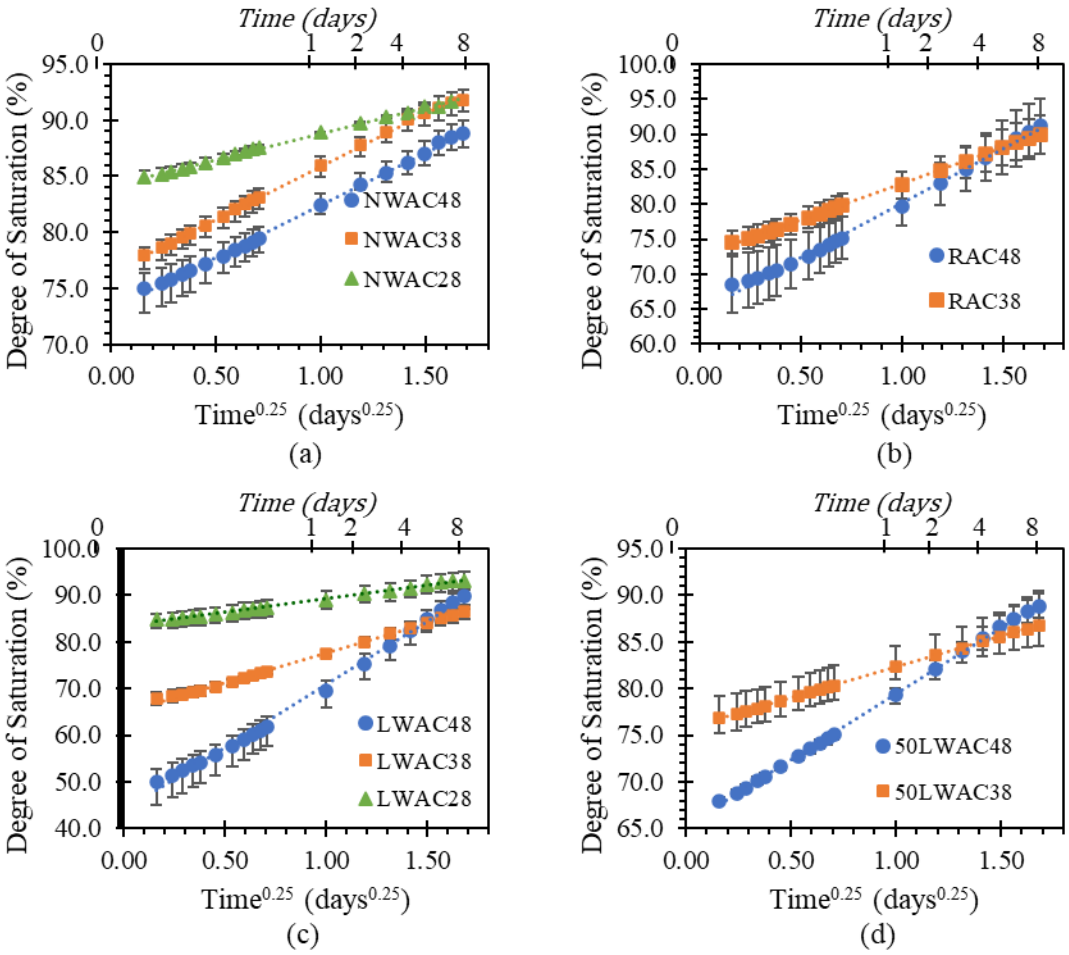

Figure 43. Average degree of saturation versus time$^{0.25}$ plots of (a) NWAC, (b) RAC, (c) LWAC, and (d) 50LWAC mixtures. Error bars represent the range of values for three specimens each in LWAC, 50LWAC, and NWAC mixtures and the standard deviation for the average of 8 RAC mixtures per w/c.

4.2.2.5.5 Rate of Water Saturation. The average rate of water saturation in (%)/day$^{0.25}$ is shown in Figure *44*. The trends are similar to the trends observed in sorptivity measurements. The rate of saturation increases as the water-cement ratio increases. The LWA mixtures recorded the highest rate of saturation due to the increased porosity. However, it should be noted that LWA is highly porous and contains larger pores compared to other aggregates. In addition to absorbing some of the penetrating water, the LWA can provide additional air voids where water can escape before freezing, resulting in lesser damage to the cement paste.

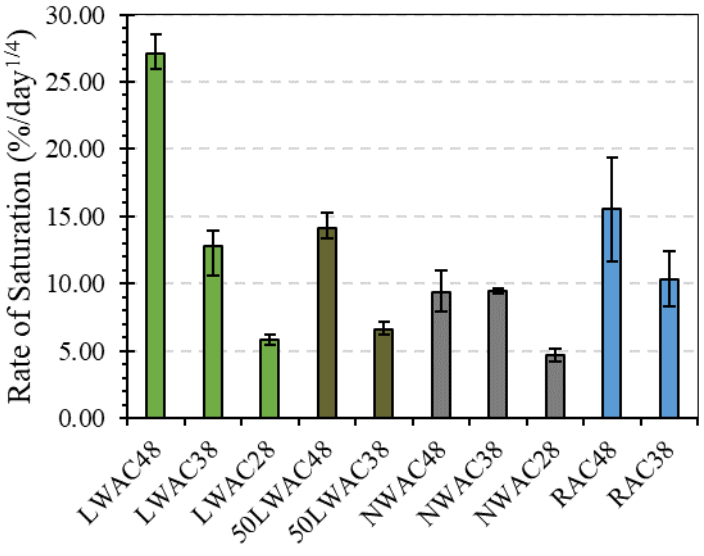

Figure 44. Average rate of water saturation of LWAC, 50LWAC, NWAC, and RAC mixtures. Error bars represent the range of values for three specimens each in LWAC, 50LWAC, and NWAC mixtures, and the standard deviation for the average of 8 RAC mixtures per w/c.

4.2.2.6 Effect of Varying Water-Cement Ratio and Coarse LWA Replacement

. Two-way ANOVA was also conducted for each permeability

measurements to evaluate the effect of water-cement ratio, LWA percent replacement, and their interaction. As compared to RAC mixtures, there are fewer total number of observations (specimens) for the LWA, 50LWA, and NWAC mixtures combined. Therefore, the normality of the residuals should be satisfied.

Like in the RAC mixtures, some variables were needed to be transformed to satisfy the normal distribution requirement. In this case, the inverse of sorptivity was used. The Shapiro-Wilk normality tests performed on the ANOVA residuals for the variables SR ($W = 0.979$, p-value = 0.705), BR ($W = 0.976$, p-value = 0.614), GWT ($W = 0.955$, p-value = 0.253), RCPT ($W = 0.962$, p-value = 0.408), 1/S ($W = 0.948$, p-value = 0.284), and RS ($W = 0.968$, p-value = 0.612), did not show any evidence that the permeability measurements are not normally distributed.

The results of Levene's tests for SR (p-value = 0.062), GWT (p-value = 0.103), RCPT (p-value = 0.746), 1/S (p-value = 0.700), and RS (p-value = 0.783), imply that there is homogeneity of variances in those permeability measurements. The p-values in surface resistivity, bulk resistivity, GWT, RCPT, and rate of saturation (RS) are greater than 0.05, which means that the variances between groups are not statistically different. Welch's ANOVA was used for bulk resistivity because its p-value ($0.0004 < 0.05$) implies that the variances between mixtures are statistically different. Separate Welch's ANOVA was performed for water-cement ratio, LWA replacement, and their interaction.

The results of each test on equality of means (two-way ANOVA and Welch-ANOVA) for each permeability test is shown in the Appendix. The p-values retuned from each test were then summarized in Table 24. All p-values of w/c are less than 0.05,

except in GWT, which indicates that the differences between the 0.48, 0.38, and 0.28 w/c permeability measurements are statistically significant. Moreover, all p-values of coarse LWA percent replacement (0, 50, and 100%) are less than 0.05, which means that the LWA percent replacement resulted in statistically different permeability measurements. Except in GWT where the p-value is greater than 0.05, the p-values of the interaction for the other tests indicates that the LWA percent replacement affected the relationship between the water-cement ratio and permeability measurements. The insignificant effect of water-cement ratio in GWT measurements can be attributed to the high variations in GWT measurements in each concrete mixture.

Table 24

Summary of p-Values from the Two-Way ANOVA and Welch-ANOVA in LWAC, 50LWAC, and NWAC Permeability Measurements

Source of Variation	SR	BR*	GWT	RCPT	1/S	RS
w/c	< 2e-16	0.03039	0.331	7.96e-08	8.04e-13	2.20e-12
LWA replacement	< 2e-16	5.584e-09	9.41e-09	2.52e-10	8.69e-11	9.74e-11
Interaction	3.07e-07	5.81e-13	0.993	0.0051	7.84e-05	2.53e-09

*Welch-ANOVA was performed

In summary, the varying coarse LWA percent replacement resulted in statistically different permeability measurements. Except in GWT where the variation in measurements between specimens of the same mixture is high, the varying water-cement ratio also affected the permeability measurements significantly.

4.3 General Relation to Electrical Resistivity and Formation Factor

Among the permeability tests performed, the surface and bulk resistivity tests are the fastest and simplest to operate. While determining the formation factor requires additional curing procedures and chemicals, it removes the effect of the pore solution on the electrical resistivity. It, therefore, could improve the relationship between electrical resistivity and permeability. This section discusses the relation of bulk resistivity and formation factor with the other permeability tests. Since surface and bulk resistivity has a strong linear relationship, it can be expected that they will have similar goodness of fit when plotted with the other permeability tests.

The regression between the surface and bulk resistivity measurements is shown in Figure 45. It was observed that there is a strong linear correlation between the two tests with an R^2 of 0.998. A strong correlation between the two tests was expected since they both measure electrical resistivity and only differ in the geometry considered in the measurement. While the surface resistivity was determined from the side faces of the concrete cylinder specimens, the bulk resistivity was measured from the end-to-end faces. With the application of the geometric factors, the surface resistivity measurements were observed to be about 1.84 times greater than the computed bulk resistivity values. This ratio is similar to the theoretical ratio of surface-to-bulk resistivity, which is approximately 1.85. The theoretical ratio of SR over BR can be determined using Equation (*23*) [14, 79].

$$\frac{SR}{BR} = 1.10 - \frac{0.730}{\frac{d}{a}} + \frac{7.34}{\left(\frac{d}{a}\right)^2} \quad (23)$$

where d = specimen diameter, 102 mm, and a = probe spacing, 38 mm.

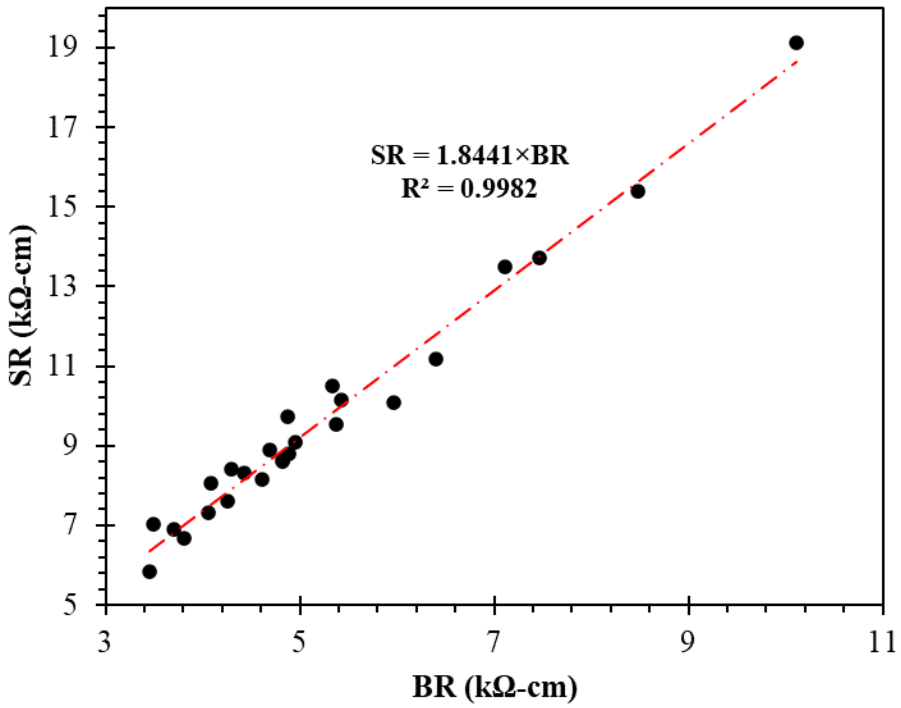

Figure 45. Bulk resistivity (BR) vs. surface resistivity (SR).

4.3.1 Germann Water Permeability

The range of GWT measurements or the average water flux is 1×10^{-6} ~ 1.86×10^{-4} mm/sec, with the highest measurements recorded from the LWAC and 50LWAC specimens. Figure *46* shows the relation of GWT results with the electrical resistivity tests (surface and bulk). In all concretes the water permeability decreases as the surface

or bulk resistivity increases. The data clustering based on the concrete type can be observed. As the percent volume of coarse LWA increases from 0% (NWAC) to 100% (LWAC), the regression slope and the intercept also increases. On the other hand, the RAC mixtures have the lowest regression slope of the mixes with porous aggregates.

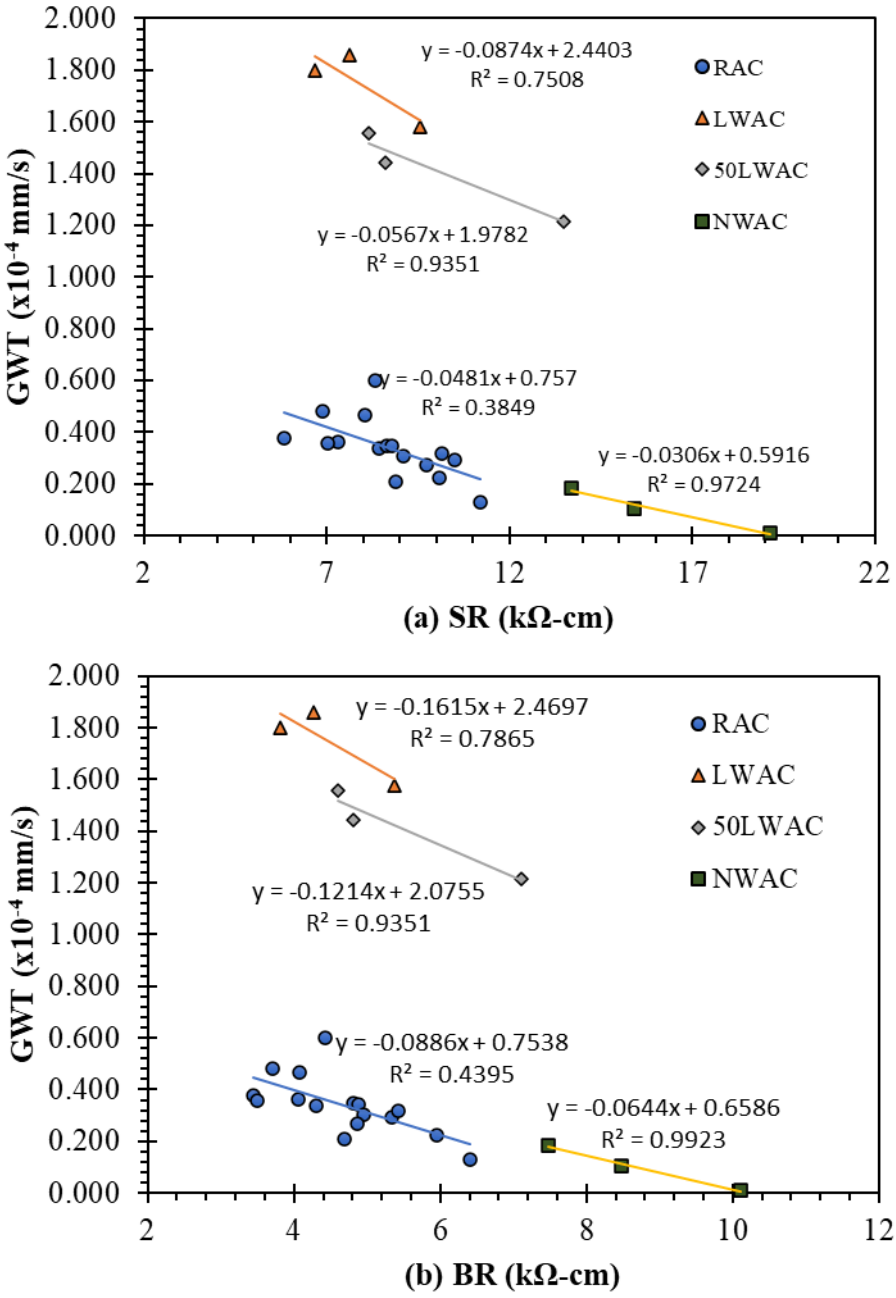

Figure 46. Relation of the GWT results with the (a) surface resistivity and (b) bulk resistivity.

The lower R^2 in RAC mixtures compared to different concrete types is due to the higher number of observations in RAC, resulting in higher variation in the measurements.

Similar trends from the surface and bulk resistivity can be observed in the relationship with formation factor. As shown in Figure *47*, except for NWAC, it can be observed that the R^2s improved when the formation factor was used instead of the surface or bulk resistivity. The improved R^2s imply that for porous aggregate concretes, the formation factor effectively removed the effect of the pore solution's conductivity in the electrical resistivity measurements and is indeed a better indicator of the concrete's water permeability.

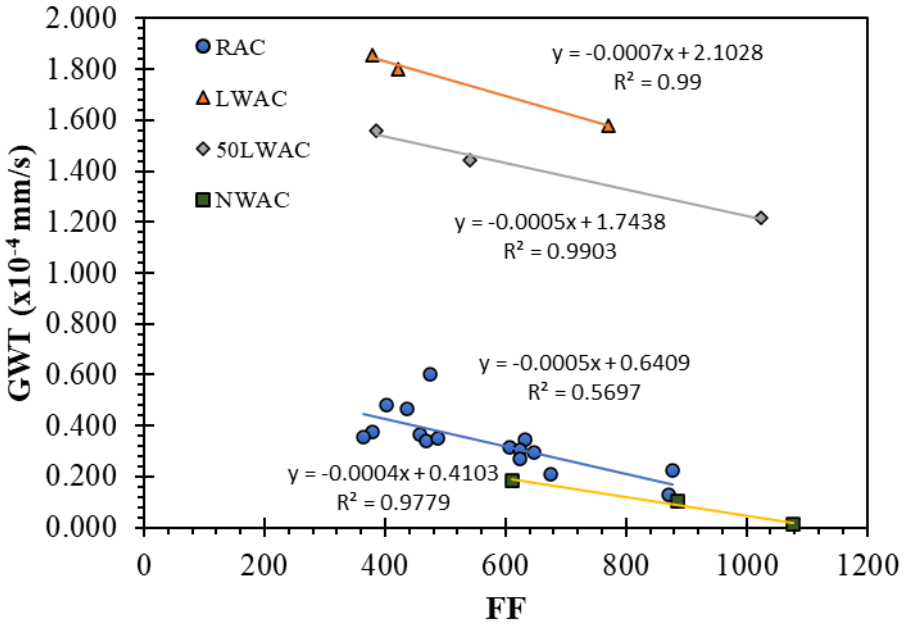

Figure 47. Relation between the inverse of formation factor and the GWT results.

For LWAC, PLWAC, and NWAC mixtures, the change in water permeability per unit increase of the formation factor is almost the same. However, the y-intercepts are different, which suggests that even at the same formation factor, the water permeability

increases as the percentage of LWA increases. For RAC, the GWT measurements decrease by about 5×10^{-8} $mm^3/mm^2/sec$ in every unit increase of the formation factor. The range of formation factor of RAC is just the same as the lightweight concretes; however, its water permeability is closer to NWAC than in the lightweight concretes. The RACs only have 0.48 and 0.38 water-cement ratios, but their water permeability is far below the lightweight concretes with 0.28 w/c. At the same formation factor, the water permeability of RAC is lower than that of lightweight aggregate concretes.

The very high water permeability can be attributed to the large pores of LWA. While also porous because of the adhered mortar, the RCA has tiny pores and a tortuous structure, making water transport more difficult.

4.3.2 Rapid Chloride Permeability

The RCPT results range from 2414 Coulombs to 11864 Coulombs, with the highest measurements recorded from the RAC specimens. Several studies have presented the relationship between the RCPT and electrical resistivity test results [14, 10, 11, 12, 13]. In the standards, a table was provided to evaluate the chloride ion penetration in concrete from the measured electrical resistivity [9] [8] or total charge passed [68]. Table 25 shows the limiting values set by ASTM C1202, AASHTO TP 119, and AASHTO T358 for each chloride ion penetration classification. Also included in Table 25 is the relationship presented in a recent study by Almarshoud et al. [14] for different mixtures of normalweight concrete.

Table 25

Rapid Chloride Permeability and Electrical Resistivity Relationships

Chloride Ion Penetrability Classification	ASTM C 1202 RCPT Charge Passed (Coulombs)	AASHTO TP 119 Bulk Resistivity (kΩ-cm)	AASHTO T 358 Surface Resistivity (kΩ-cm)
High	> 4000	< 5.2	< 12
Moderate	2000-4000	5.2-10.4	12-21
Low	1000-2000	10.4-20.8	21-37
Very Low	100-1000	20.8-207	37-254
Negligible	< 100	> 207	> 254
Almarshoud et al. 2021	RCP = 223.36*(1/BR) = 457.92*(1/SR) = 2.13E+06*(1/FF)		

Figure *48* shows the relationship between the electrical conductivity (inverse of electrical resistivity) and RCPT measurements. Since the RCPT results in RAC mixtures are higher than the other concrete types, a separate trendline was generated for RAC mixtures, while the LWAC, 50LWAC, and NWAC were combined in one trendline. Also shown in the figures are the established relationships for normalweight concretes. One was the relationship established by Almarshoud et al. [14], while the other was generated from plotting the limiting values set by ASTM C 1202 and AASHTO TP 119 for different classifications of chloride ion penetrability.

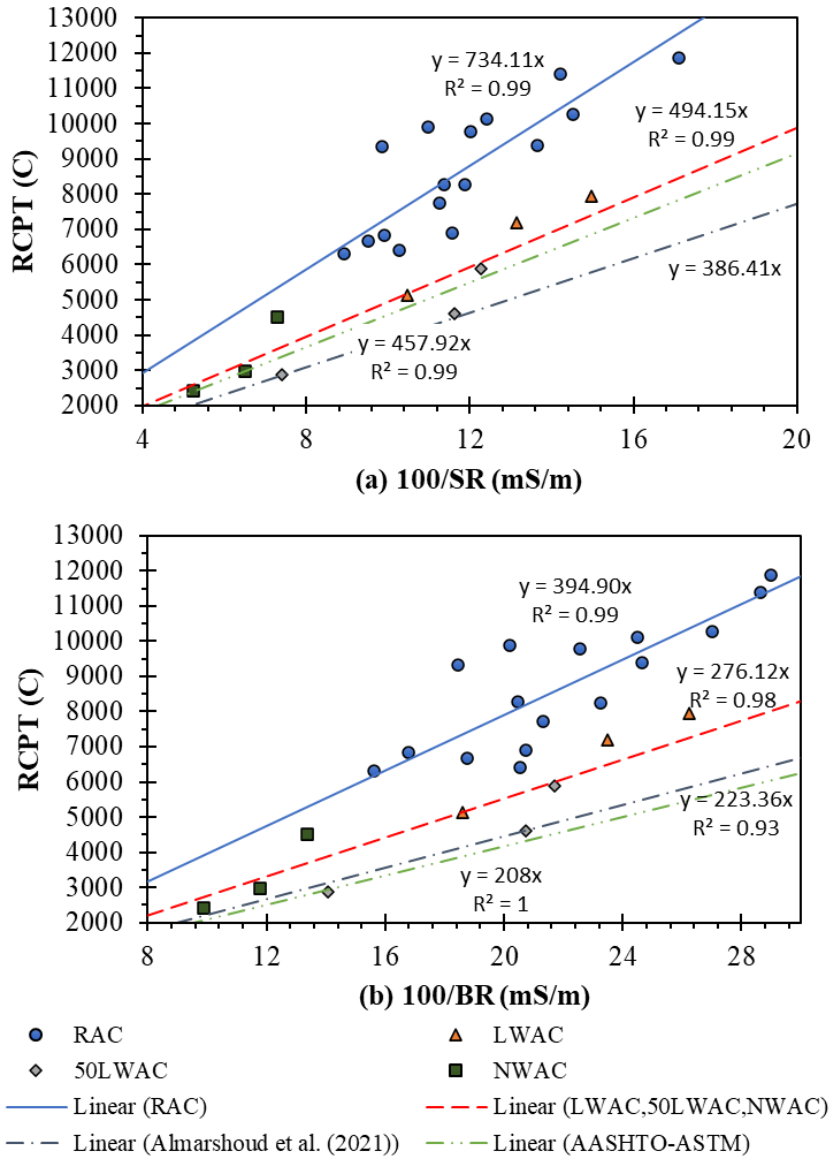

Figure 48. Relation of the RCPT results with the (a) surface resistivity and (b) bulk resistivity.

The intercepts of the trendlines were set to 0, the same as how Almarshoud et al. [14] presented their results. As a result, higher R^2 values are observed. A separate analysis determined that the correlation coefficient in RAC mixtures is 0.82, while the correlation coefficient of the combined LWAC, 50LWAC, and NWAC mixtures, is 0.94.

The high correlation coefficients indicate a strong linear relationship between the electrical conductivity and RCPT measurements.

The data from the NWAC38, NWAC28, and 50LWAC28 mixtures (three observations with low RCPT values) are close to the previously established relationships for normal-weight concretes. But as higher permeability measurements and bulk conductivity (lower bulk resistivity) was observed, the plotted values tended to move away from the established trendlines. This observation can also be noticed in the plots presented by Almarshoud et al. [14], where the residuals in higher permeability measurements are higher than those with lower permeability. In their study, most concrete types measured have low permeability, but in this study, the concrete mixtures are distributed from more permeable to less permeable concrete. As a result, the trendlines generated in this study are higher than the referenced trendlines. For LWAC, 50LWAC, and NWAC mixtures, the RCPT measurement or total charge passed in concrete increased by about 276 Coulombs per unit increase of the bulk conductivity (mS/m). The trendline for the RAC mixtures is highest, where the total charge passed increases by about 395 Coulombs per unit increase of the bulk conductivity (mS/m).

The higher trendlines generated in this study suggest that the existing relationships between the RCPT and electrical resistivity are not applicable for the porous aggregate concretes, RAC, and LWAC. Furthermore, the RAC mixtures' trendline is higher than in the other concrete types. The reason for higher RCPT measurements of RCA even at the same resistivity as the other concretes is that a larger increase in current over time was observed during the RCPT test. Most of the RAC samples, particularly those with 0.48 w/c, have exceeded the current limit of 500 mA before the 6-hour period,

resulting in the test's stoppage. The current increases as more ions transfer from one side of the migration cell to the other. The RCA has tiny pores compared to LWA due to the adhered mortar and a more porous ITZ. And thus, even at the same porosity, RCA might have provided a higher number of flow paths for the ion transfer, increasing the migration rate and RCPT readings.

The RCPT results are also plotted against the inverse of the formation factor, as shown in Figure *49*. The established relationship by Almarshoud et al. [14] is also included. As a result of immersing the concrete specimens in a simulated pore solution, higher R^2s can be observed from our data than in the referenced study. It was determined that the correlation coefficient in RAC mixtures is 0.80, while the correlation coefficient of the combined LWAC, 50LWAC, and NWAC mixtures is 0.89.

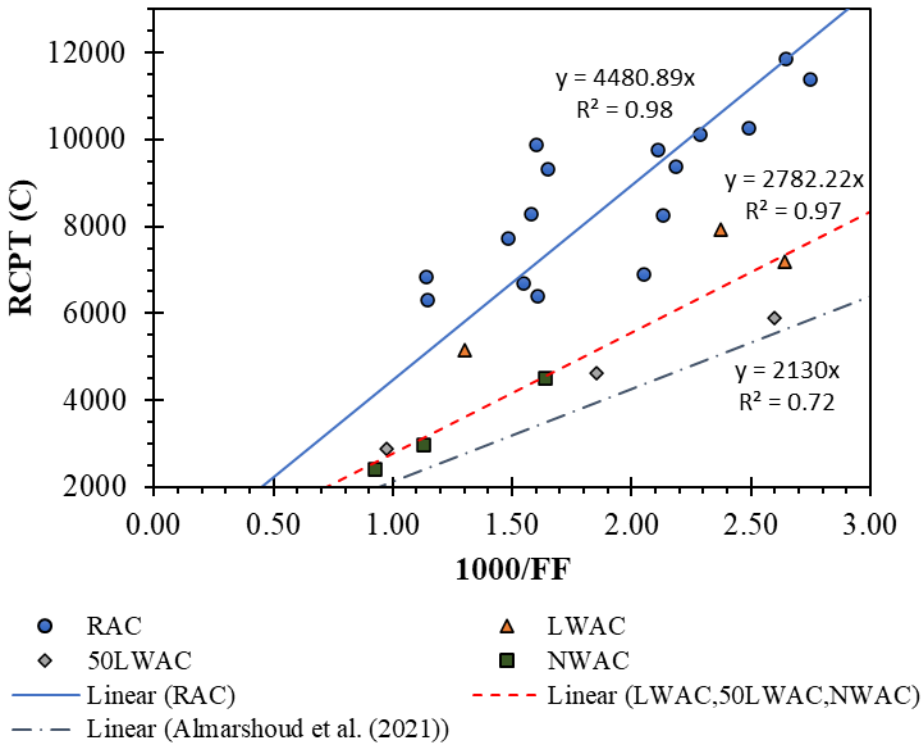

Figure 49. Relation between the inverse of formation factor and the GWT results.

Similar trends with the electrical conductivity and RCPT relationship can be observed when the formation factor replaces surface or bulk conductivity. But unlike in the GWT, the RCPT has a slightly better fit to the electrical conductivity than the formation factor. The reason is that the RCPT measurement, like the electrical resistivity, is affected by the pore solution's conductivity [107]. Therefore, while the formation factor strongly correlates with the RCPT measurements, the surface and bulk resistivity tests are still the better predictor of the total charge passed in concrete during the RCPT.

4.3.3 Water Sorptivity and Rate of Water Saturation

The water sorptivity test results showed water sorptivity values in the range of 0.234~1.941 mm/day$^{0.25}$ and rate of saturation values in the range of 4.156~28.553 %/ day$^{0.25}$. The highest measurements were recorded from the RAC and LWAC specimens. Figure *50* and Figure *51* show the relations of electrical conductivity (surface and bulk) with the water sorptivity and rate of saturation, respectively. Unlike in the previous regression plots, the relation between the sorptivity test results and electrical conductivity for all concrete types can be expressed in a single trendline. The water sorptivity and electrical conductivity measurements for all concrete types tested show a strong linear relationship. Still, a weaker linear relationship (lower R^2) was observed in the rate of saturation and electrical conductivity plot. For every unit increase of surface conductivity (mS/m), the water sorptivity increases by 0.10 mm/ day$^{0.25}$, and the rate of saturation increases by 1.07 %/ day$^{0.25}$. Meanwhile, for every unit increase of bulk conductivity (mS/m), the water sorptivity increases by 0.06 mm/ day$^{0.25}$, and the rate of saturation increases by 0.68 %/ day$^{0.25}$.

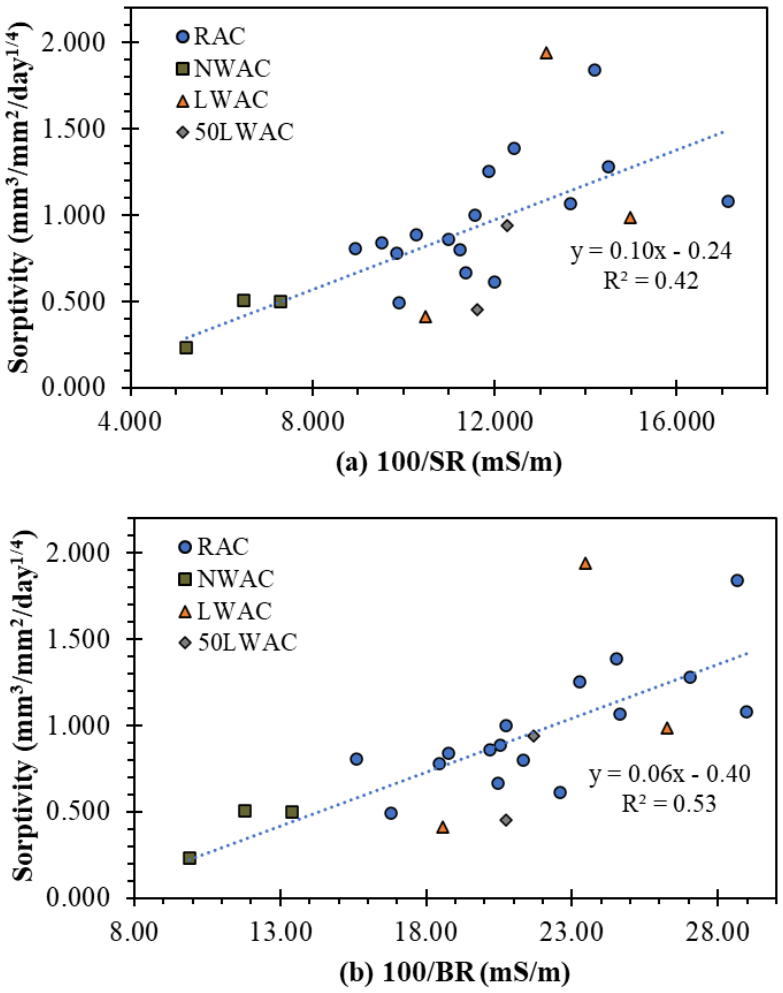

Figure 50. Relation of sorptivity with the (a) surface conductivity and (b) bulk conductivity.

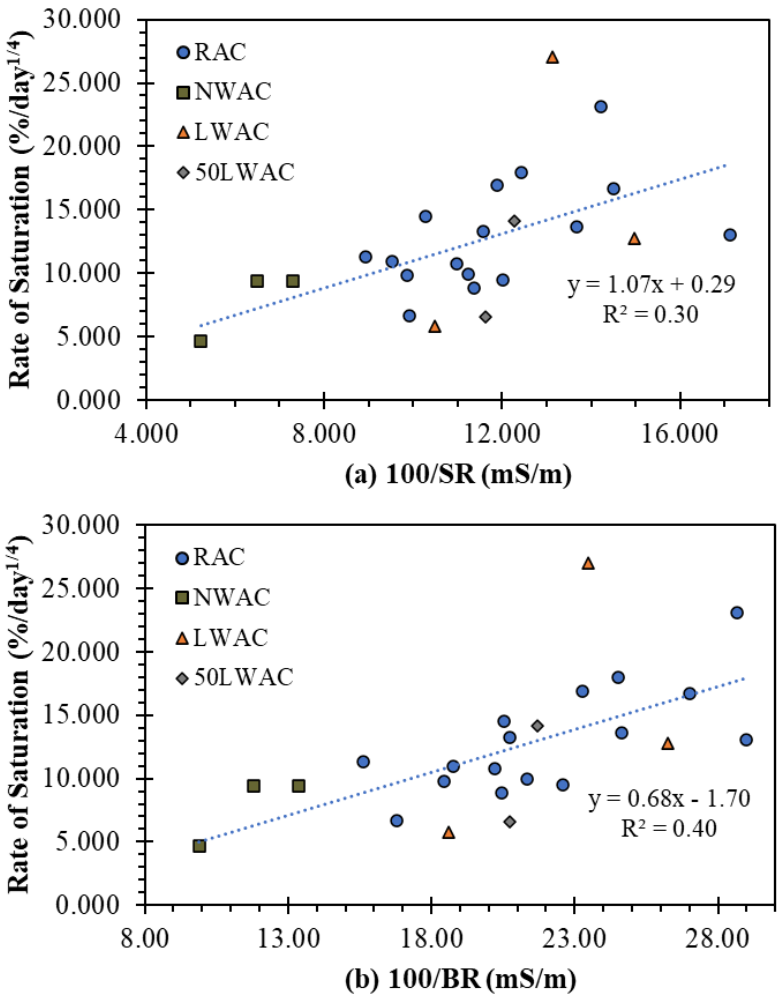

Figure 51. Relation of rate of saturation with the (a) surface conductivity and (b) bulk conductivity.

Figure *52* shows the relation of the inverse of formation factor with the water sorptivity and rate of saturation. Like in the GWT results, a higher R^2 was observed when the formation factor was used instead of surface or bulk resistivity. GWT and water sorptivity test results are unaffected by the pore solution's conductivity. By effectively removing the effect of pore solution in the electrical resistivity measurements, the formation factor was confirmed to be a better indicator of water permeability and water

sorptivity. For every unit increase of the inverse of the formation factor (1000/FF), the water sorptivity increases by 0.60 mm/day$^{0.25}$, and the rate of saturation increases by 7.27 %/day$^{0.25}$.

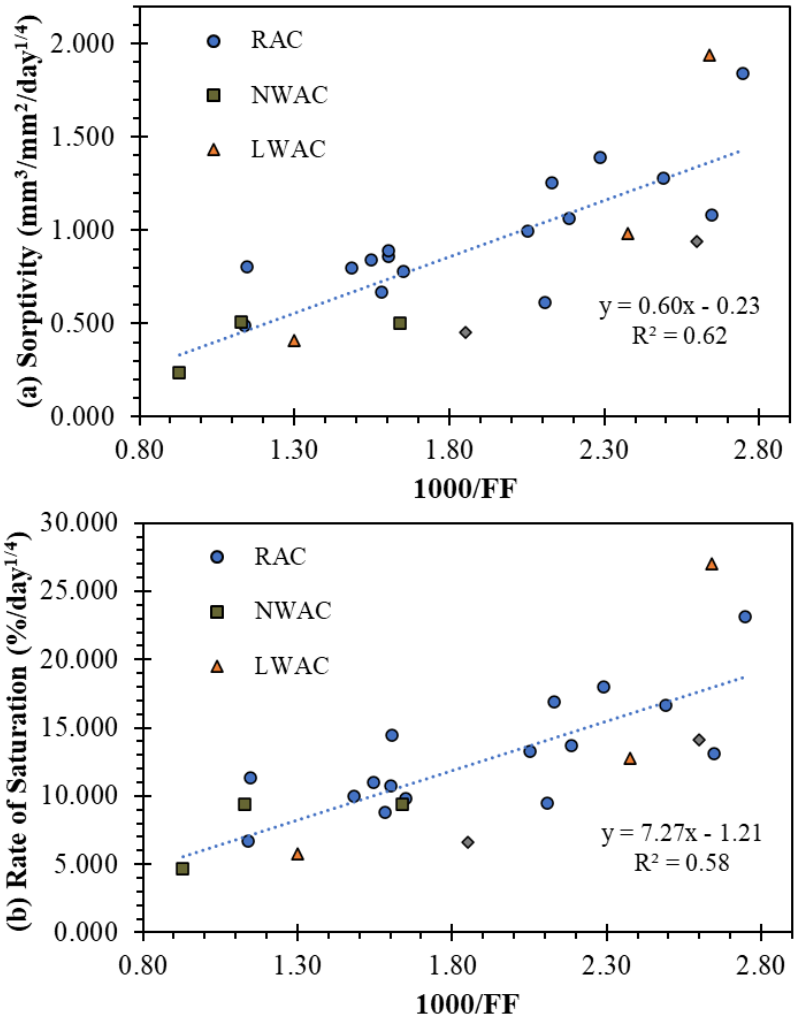

Figure 52. Relation of the inverse of formation factor (bulk conductivity) with the (a) water sorptivity and (b) rate of saturation results.

4.3.4 Comparison of Electrical Resistivity (Surface or Bulk) and Formation Factor

The general relations of the electrical resistivity with the other permeability measurements were shown. In conclusion, it was proven that there is a strong correlation between the electrical resistivity-based tests and the water permeability, rapid chloride permeability, water sorptivity, and saturation rate, of concrete with porous aggregates. Furthermore, it was observed that the formation factor is a better indicator of the concrete's water permeability and water sorptivity than the bulk or surface resistivity. The immersion of concrete specimens in the simulated pore solution to calculate the formation factor effectively minimized if not totally removed the influence of pore solution's conductivity in the electrical resistivity measurements. For the total charge passed in RCPT, the bulk or surface resistivity is still the better indicator since both tests are affected by the pore solution's conductivity.

Chapter 5

Multiple Linear Regression Models of Porous Aggregate Concrete's Permeability[4]

Most regression results showed a linear relationship between the permeability measurements and the surface resistivity, bulk resistivity, or formation factor. However, some coefficients of determination in the regression analyses (R^2) are low. In this chapter, additional explanatory variables were considered, and the fit of the permeability regression models was improved by multiple linear regression.

Based on the average measurements per mixture, the formation factor is a better indicator of the concrete's water permeability, sorptivity, and water saturation rate. However, the formation factor was measured from specimens immersed in simulated pore solution, different from the specimens used in other permeability tests. Therefore, the formation factor can only be used as average values. As a result, the multiple linear regression using the formation factor may not be able to capture the variation in measurements between specimens within the same group or concrete mixture. The bulk resistivity, measured on the same specimens of GWT, RCPT, and water sorptivity measurements, was also used as an explanatory variable.

The multiple linear regressions with the GWT, RCPT, sorptivity, and saturation rate as dependent variables were done two times. The first is using the formation factor as the main explanatory variables, followed by the regression using bulk resistivity as main explanatory variable. The regression models were also separated for RAC mixtures (Section 5.1) and for LWAC, 50LWAC, and NWAC mixtures (Section 5.2). The analysis

[4] Some parts of this chapter are published in [131]

for RAC is shown first, followed by the models for LWAC, 50LWAC, and NWAC mixtures.

5.1 Recycled Aggregate Concrete (RAC)

The surface and bulk resistivity measurements in RAC specimens have means of 8.70 kΩ-cm and 4.67 kΩ-cm, respectively, and standard deviations of 1.487 kΩ-cm and 0.821 kΩ-cm, respectively. There is a strong correlation between the surface and bulk resistivity measurements. Therefore, in regression analyses presented in this chapter, only bulk resistivity was used as it has lower coefficient of variation than the surface resistivity. On the other hand, the mean and standard deviation of the formation factor are 560 and 155, respectively. Additional variables are needed to improve the precision of the regression models.

Along with the bulk resistivity (BR) and formation factor (FF), the aggregate properties of RCA and fresh concrete properties of RAC were considered as possible predictors for GWT, RCPT, water sorptivity (S), and rate of saturation (RS) measurements. The included aggregate properties of RCA are the water porosity (wp), bulk density, specific gravity (sg), absorption, and residual mortar air content (RM_{air}). The fresh concrete properties of RAC mixtures are the air content, slump, and density.

During the air content determination using the volumetric method, the measuring bowl was shaken vigorously to break the concrete inside and allow the air occupying the voids to escape to the surface. Because the cement paste adhered in RCA is already hardened, it can be assumed that the air content measurement only captured the air voids in the fresh mortar and did not include the air content from the RCA itself. Some mortars

were pulverized and removed when the parent concrete was crushed to manufacture RCA. Thus, the proportion of concrete material components was changed. While the ratio of air voids to concrete will be lower, we can assume that there is no significant change in the ratio of air voids to the residual mortar. The air content of RCA residual mortar was calculated by dividing the parent concrete's air content by the mortar volume (cement, water, sand) in the parent concrete mixture. A scanned image was prepared in Figure 53 to visualize the components of the air content of RAC. The boundaries of the coarse RCA were marked by black ink. Phenolphthalein was sprayed to separate the color of the cement paste from the natural aggregates, and the air voids were filled with white paste.

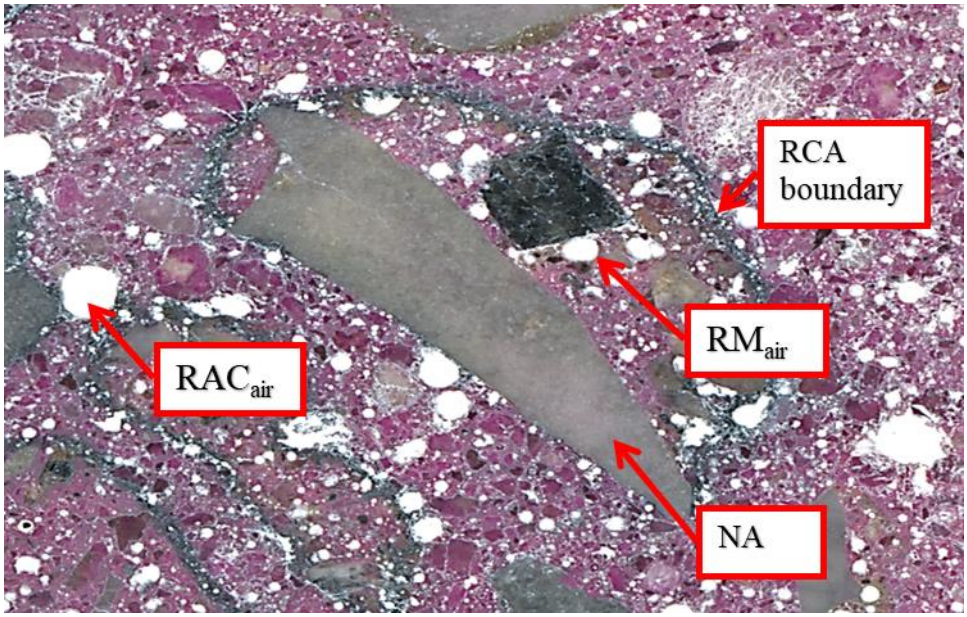

Figure 53. Scanned image of recycled aggregate concrete (RAC).

The volume of RCA in the RAC mixture was also considered. The RCA volume was adjusted to the air content measured from the fresh concrete. Since the RAC

mixtures were designed assuming an air content of 6%, the actual percent volume of RCA in the mixture is higher than the designed proportion when the RAC air content is lower than 6% and lower than the designed proportion when the RAC air content is higher than 6%. The RCA volume for each RAC mixture was adjusted as shown in Equation (24).

$$V_{rca} = V_{rca,design} \times \frac{\left(1 - {RAC_{air}}/{100}\right)}{0.94} \quad (24)$$

where V_{rca} = percent volume of RCA (adjusted) in %, $V_{rca,design}$ = percent volume of RCA (design) in %, and RAC_{air} = air content of the RAC mixture measured using the volumetric method in %.

The linear relationship between the permeability measurements and explanatory variables is listed in Table 26. The main effects of each explanatory variable can be conceived from their correlation to the permeability measurements. A positive correlation coefficient means that the variables increase or decrease linearly with each other. On the other hand, a negative correlation means that the variable decreases linearly as the other variable increases and vice versa. Using the correlation table, we can select different explanatory variables that show linear relationships, based on the correlation coefficient, to each of the response variables (GWT, RCPT, S, and RS).

Table 26

Correlation Coefficients of RAC Permeability and Explanatory Variables

Variables	SR	BR	FF	RAC_{air}	RAC_{slump}	$RAC_{density}$
GWT	-0.47	-0.5	-0.58	0.61	0.5	-0.58
RCPT	-0.74	-0.75	-0.72	0.58	0.7	-0.72
S	-0.61	-0.7	-0.71	0.55	0.43	-0.28
RS	-0.54	-0.65	-0.67	0.49	0.36	-0.17

Variables	RCA_{wp}	$RCA_{bulk\_density}$	RCA_{sg}	$RCA_{absorption}$	RM_{air}	V_{rca}
GWT	0.11	-0.18	-0.2	0.13	0.25	-0.07
RCPT	0.31	-0.18	-0.2	0.31	0.04	0.07
S	0.03	0.14	0.2	0	-0.29	-0.44
RS	-0.06	0.13	0.24	-0.09	-0.3	-0.48

The multicollinearity in the regression models was checked based on the variance inflation factors (VIF), as it can make the variable coefficients unstable and difficult to interpret. Therefore, the variables that are highly correlated to each other were not used simultaneously. A set of variables was considered independent when the VIF were all less than 5. The possible interactions between the predictors were also considered in the linear regression. Even though the other predictors have a weak correlation with permeability, their interaction with bulk resistivity or formation factor can improve the overall model. Stepwise regression was performed with a significance level set to $\alpha = 0.05$ to eliminate the variables and interactions that are not statistically significant to the permeability measurements.

Before stepwise regression analysis, the permeability measurements were investigated for possible univariate outliers. The boxplots of GWT, RCPT, sorptivity, and water saturation rate are shown in Figure 54. There are possible outliers for sorptivity and saturation rate measurements. There are no univariate outliers in GWT and RCPT measurements.

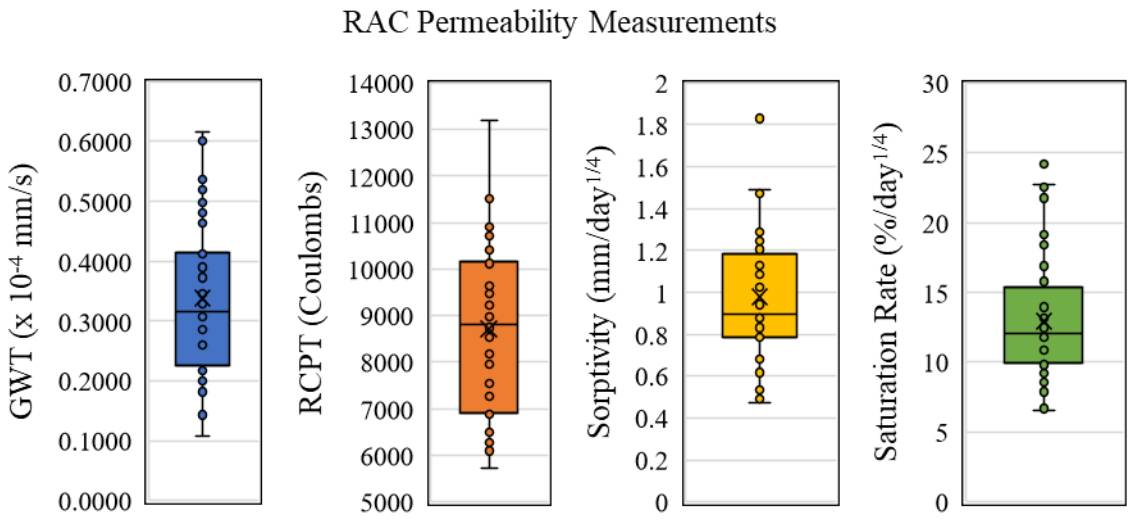

Figure 54. Boxplots of RAC specimens' measurements for GWT, RCPT, sorptivity, and water saturation rate.

5.1.1 Regression of GWT Measurements

The 10-minute average water flux measured in RAC specimens using GWT has a mean of 0.339 $\times 10^{-4}$ mm/s and a standard deviation of 0.135 $\times 10^{-4}$ mm/s . Based on the test for equality of means using two-way ANOVA, the water-cement ratio significantly affects the GWT measurements. However, the effect of the RCA variation in the GWT measurements is insignificant. It was attributed to the wide range of values measured

within each RAC mixture. Due to that, high residuals can be expected from the regression models of GWT measurements.

5.1.1.1 Using Formation Factor. The range of GWT measurements in RAC mixtures is 0.108 $\times 10^{-4}$ ~ 0.615 $\times 10^{-4}$ mm/s , while the formation factor is 360~880. A scatter plot with data ellipses at 50% and 95% confidence levels, shown in Figure 55, was generated to check for possible bivariate outlier/s between GWT and formation factor. Since all measurements are inside the data ellipse with a 95% confidence level, no possible bivariate outlier was observed.

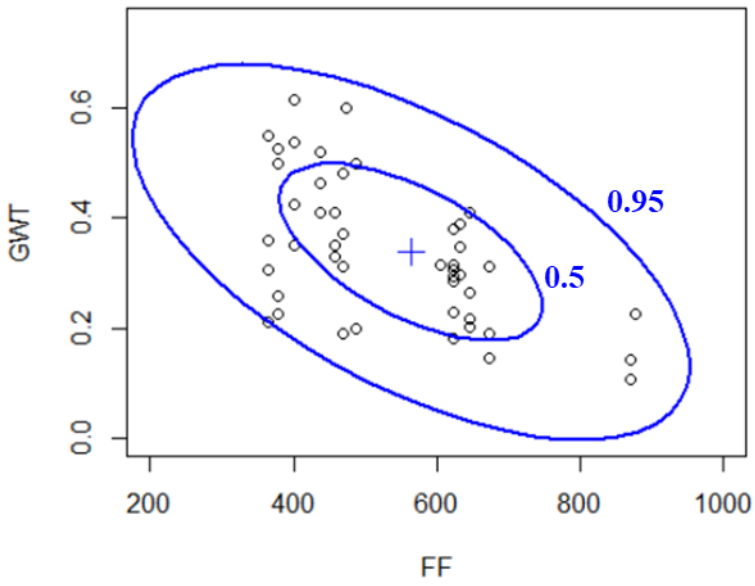

Figure 55. Scatter plot of RAC's GWT and formation factor measurements with data ellipses at 0.5 and 0.95 confidence levels. One possible outlier was detected.

Based on the correlation coefficients in Table 26, the RAC fresh concrete properties (air content, slump, and density) correlate well with the GWT measurements.

A set of five independent variables with VIF < 5 were considered as predictors, consisting of the formation factor (FF), RAC fresh concrete properties (air, slump, and density), and the air content of the RCA residual mortar (RM_{air}).

The multiple linear regression model of RAC's GWT is summarized in Table 27. The regression model is statistically significant with a very low p-value. It shows that about 60% of the variance in the GWT measurements can be explained by the formation factor, the air content of the new concrete, and the air content of the RCA residual mortar, with a residual standard error of 0.085 $\times 10^{-4}$ mm/s. The multiple linear regression model shows a slightly better model fit than when the formation factor was used as the lone predictor (R^2 = 0.44, RSE = 0.1017 $\times 10^{-4}$ mm/s). The final model's Shapiro-Wilk normality test on the residuals (W = 0.9606, p-value = 0.06882) did not show enough evidence that the residuals are not normally distributed.

Table 27

Regression Result for the RACs' GWT Measurements ($\times 10^{-4}$ mm/s) using Formation Factor, RAC Air Content, and Residual Mortar Air Content

Intercept	-1.014** (0.306)
1000/FF	0.494** (0.158)
RAC_{air}	0.153** (0.048)
RM_{air}	0.024** (0.007)
(1000/FF): RAC_{air}	-0.060* (0.024)
Residual standard error (RSE)	0.0848 on 50 df
Adjusted R^2	0.6097
p-value	1.508e-10
No. outliers removed	3
Remaining no. observations	55 RAC specimens

Notes: Standard errors are reported in parentheses; *,**, and *** indicate significance levels at 0.05, 0.01, and 0.001, respectively.

Furthermore, the studentized Breusch-Pagan test (BP = 7.4373, df = 4, p-value = 0.1145) in the final regression did not show the presence of heteroscedasticity in the regression model. The regression model is heteroscedastic when the variance in residual is not constant and changes with the expected value of the response variable [110]. Three observations were considered outliers and removed from the regression model to satisfy the model's homoscedasticity requirements. The three outliers came from different RAC mixtures and were the lowest measurements within their respective group of specimens.

The regression model shows how the 10-minute average water flux in RAC specimens measured using GWT changes with the changes in explanatory variables. The average water flux in RAC specimens increases by 0.023×10^{-4} mm/s per percent increase in the RCA residual mortar air content. An increase in the inverse of the formation factor and RAC air content resulted in an increase in GWT measurements. There is a significant interaction between the formation factor and RAC air content. The change in GWT measurement per unit change in the inverse of the formation factor is lower when the RAC air content is high.

5.1.1.2 Using Bulk Resistivity Measurements. The same set of outliers removed from the previous model was also removed in this regression model using bulk resistivity as an explanatory variable. The same set of additional explanatory variables was also considered, except for the formation factor, which was replaced by the bulk resistivity. A scatter plot with data ellipses at 50% and 95% confidence levels, as shown in Figure *56*,

was generated to check for possible bivariate outlier/s between GWT and electrical resistivity measurements. No other possible outliers were found.

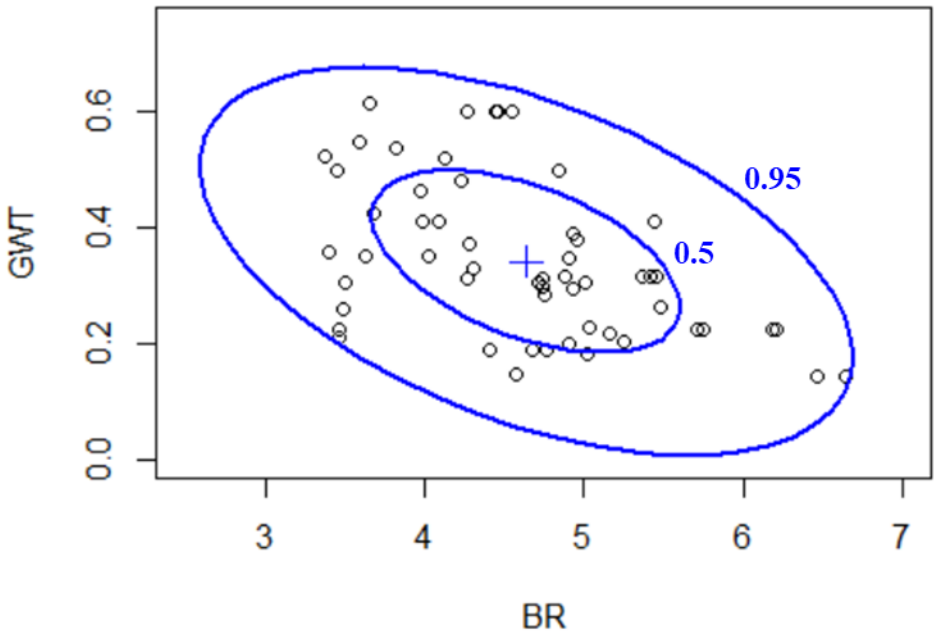

Figure 56. Scatter plot of paired measurements of RAC's bulk resistivity and GWT with data ellipses at 0.5 and 0.95 confidence levels.

The GWT regression model using bulk resistivity as an explanatory variable is summarized in Table 28. The results imply that about 47% of the variance in the average water flux can be explained by the bulk conductivity (100/BR) and the fresh RAC unit weight or density, with a residual standard error of 0.098 $\times 10^{-4}$ mm/s. The Shapiro-Wilk normality test on the residuals (W = 0.97174, p-value = 0.2201) showed no evidence that the residuals are not normally distributed. Furthermore, the studentized Breusch-Pagan test (BP = 4.3198, df = 2, p-value = 0.1153) did not show enough evidence of

heteroscedasticity in the regression model. The multiple linear regression model shows a slightly better model fit than when the bulk resistivity was used as the lone predictor (R^2 = 0.31, RSE = 0.1126 $\times 10^{-4}$ mm/s).

Table 28

Regression Result for the RACs' GWT's Average Water Flux (×10-4 mm/s) using Bulk Resistivity and Fresh Concrete Density

Intercept	3.434*** (0.826)
100/BR	0.009** (0.003)
$RAC_{density}$	0.0015*** (0.0004)
Residual standard error (RSE)	0.0984 on 52 df
Adjusted R^2	0.474
p-value	2.059e-08
No. outliers removed	3
Remaining no. observations	55 RAC specimens

Notes: Standard errors are reported in parentheses; *,**, and *** indicate significance levels at 0.05, 0.01, and 0.001, respectively.

Based on the above regression model, the average water flux in RAC increases by 0.009 $\times 10^{-4}$ mm/s per unit increase of the bulk conductivity (100/BR) and by 0.0015 $\times 10^{-4}$ mm/s per unit increase of the fresh RAC unit weight or density.

5.1.2 Regression of RCPT Measurements

High RCPT measurements were recorded in RAC mixtures at 6300~12000 Coulombs. The total charge passed in RAC specimens measured during the 6-hour RCPT has a mean of 8700 Coulombs and a standard deviation of 1850 Coulombs. Based on the test for equality of means using two-way ANOVA, both the RCA variation and water-

cement ratio significantly affect the RCPT measurements and the electrical resistivity measurements. Therefore, it can be assumed that an RCPT regression model for RAC specimens can be generated from the formation factor/electrical resistivity.

Based on the correlation coefficients in Table 26, the RAC fresh concrete properties (air content, slump, and density) also correlate well with the RCPT measurements. Unlike in the GWT, the residual mortar air content is not correlated to the RCPT measurements. A set of six independent variables with VIF < 5 were considered as RCPT predictors, consisting of the SR/BR/FF, the two RCA properties (water porosity and specific gravity), and the three fresh concrete properties of RAC mixtures (slump, unit weight, and air content).

5.1.2.1 Using Formation Factor. Unlike the water permeability and sorptivity tests, the RCPT results showed a better correlation with the bulk resistivity than the formation factor. Still, the formation factor has a strong correlation with the RCPT measurements. No univariate outlier was seen in the boxplot of RCPT measurements, and there is also no possible bivariate outlier detected in the scatter plot with data ellipses for the RCPT and formation factor shown in Figure *57*.

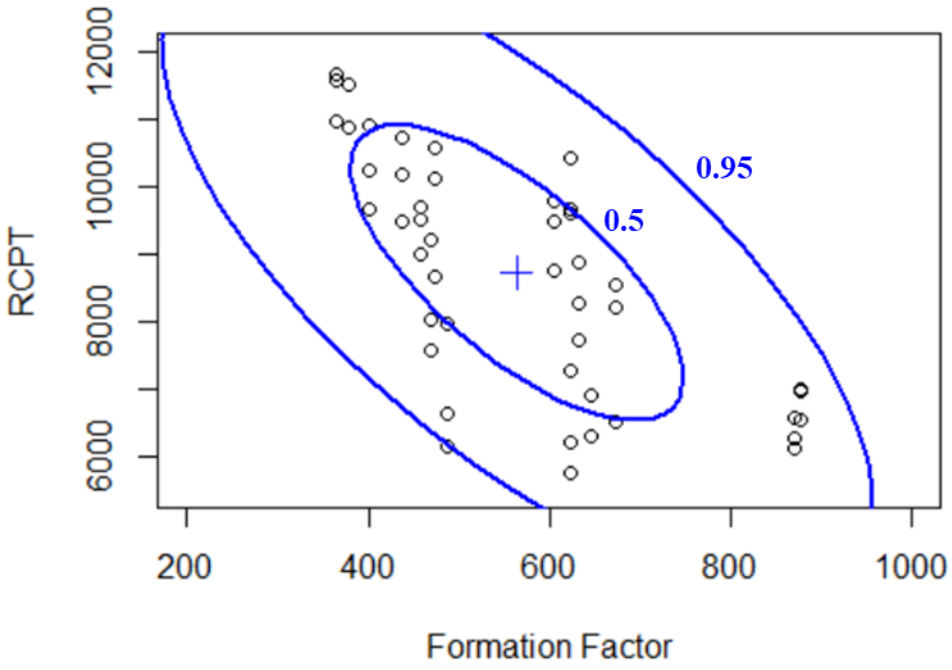

Figure 57. Scatter plot of RAC's RCPT and formation factor measurements with data ellipses at 0.5 and 0.95 confidence levels. No possible outlier was detected.

The selected multiple linear regression model summary is shown in Table 29. The regression model is statistically significant with a very low p-value. The inverse of the formation factor and the RAC fresh concrete properties, including slump, unit weight, and air content can explain about 84% of the variance in the RCPT measurements. The residual standard error is 729.8 Coulombs. This multiple linear regression model shows a much better model fit than when the formation factor was used as the lone predictor (R^2 = 0.57, RSE = 1213 Coulombs). The Shapiro-Wilk normality test on the residuals (W = 0.98443, p-value = 0.7676) did not show enough evidence that the residuals are not normally distributed. Furthermore, the studentized Breusch-Pagan test (BP = 4.5619, df = 6, p-value = 0.6011) did not show the presence of heteroscedasticity in the regression model.

Table 29

Regression Results for the RACs' RCPT Measurements (Coulombs) using Formation Factor and Fresh Concrete Properties

Intercept	-1.791e+04 (2.715e+04)
(1000/FF)	7.098e+04*** (1.954e+04)
RAC_{air}	-1.072e+03*** (1.769e+02)
RAC_{slump}	-8.202e+02*** (2.161e+02)
$RAC_{density}$	1.137e+01 (1.227e+01)
(1000/FF):$RAC_{density}$	-3.075e+01** (8.838e+00)
$RAC_{density}$:RAC_{slump}	3.837e-01*** (9.885e-02)
Residual standard error (RSE)	729.8 on 41 df
Adjusted R^2	0.8444
p-value	3.062e-16
No. outliers removed	0
Remaining no. observations	48 RAC specimens

Notes: Standard errors are reported in parentheses; *,**, and *** indicate significance levels at 0.05, 0.01, and 0.001, respectively.

Based on the model, the total charge passed in RAC specimens increases as the RAC air content increases. The RAC density has significant interaction effects with the inverse of the formation factor and the RAC slump. The slump's effect in the model seemed to differ from its main effect in RCPT due to the negative coefficient. But considering the value of the fresh concrete unit weight (2150~2300 kg/m^3), a higher slump will result in higher RCPT measurement. Furthermore, the change in RCPT measurement per unit increase in the inverse of the formation factor is lower when the fresh concrete unit weight is high. The RAC air content has a negative coefficient. However, an increase in the air content will decrease the formation factor, increase the slump, and decrease the unit weight, all resulting in an increase in RCPT measurements.

5.1.2.2 Using Bulk Resistivity Measurements. Like in the average values, no univariate outlier was seen in the boxplot of individual RCPT measurements. No possible

bivariate outlier is detected in the scatter plot with data ellipses for the GWT and bulk resistivity measurements shown in Figure *58*.

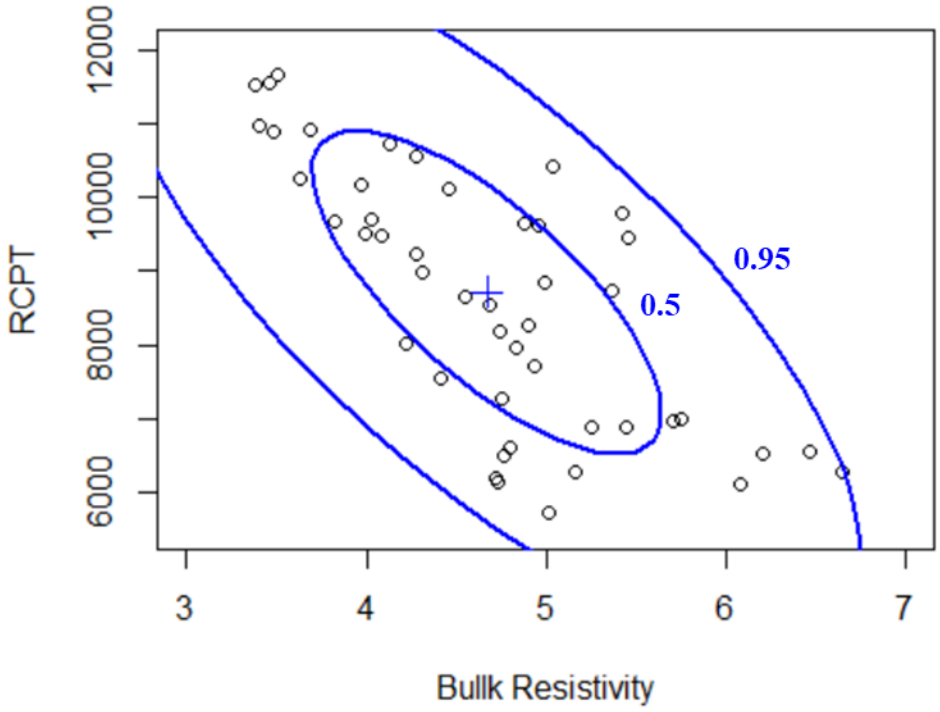

Figure 58. Scatter plot of paired measurements of RAC's bulk resistivity and RCPT with data ellipses at 0.5 and 0.95 confidence levels. No possible outlier was detected.

The same explanatory variables from the previous model were used except for the formation factor, which was replaced by the bulk resistivity. The multiple linear regression model of RCPT using bulk resistivity is summarized in Table 30. The regression model is statistically significant with a very low p-value. The model shows that 83% of the variance in the RCPT measurements can be explained by the bulk conductivity and the RAC fresh concrete properties, including slump, unit weight, and air

content, with a residual standard error of 765 Coulombs. The Shapiro-Wilk normality test on the residuals (W = 0.99026, p-value = 0.9581) showed no evidence that the residuals are not normally distributed. Furthermore, the studentized Breusch-Pagan test (BP = 2.4795, df = 6, p-value = 0.8708) did not show the presence of heteroscedasticity in the regression model. The multiple linear regression model shows a much better model fit than when the bulk conductivity was used as the lone predictor (R^2 = 0.5984, RSE = 1172 Coulombs).

Table 30

Regression Result for the RACs' RCPT Measurements (Coulombs) using Bulk Resistivity and Fresh Concrete Properties

Intercept	57365.809*** (10973.921)
Bulk conductivity (100/BR)	-317.272 (248.066)
RAC_{air}	-3984.359** (1198.915)
RAC_{slump}	107.604*** (40.811)
$RAC_{density}$	-18.086* (4.469)
(100/BR):RAC_{air}	159.428** (58.787)
(100/BR):RAC_{slump}	-4.368* (1.890)
Residual standard error (RSE)	764.3 on 41 df
Adjusted R^2	0.8293
p-value	1.975e-15
No. outliers removed	0
Remaining no. observations	48 RAC specimens

Notes: Standard errors are reported in parentheses; *,**, and *** indicate significance levels at 0.05, 0.01, and 0.001, respectively.

Some interactions were found to be significant in the regression model. It shows that the effect of bulk conductivity in the RCPT measurements changes depending on the value of RAC air content and slump. Although the coefficient of the bulk conductivity is

negative, an increase in bulk conductivity will result in an increase in RCPT measurement when the values of RAC air content and slump are considered. The RCPT measurement increases as the slump increases and decreases as the fresh concrete unit weight decreases. Like in the previous model with the formation factor, RAC air content has a negative coefficient. However, it somehow affects the measurement for other variables such that an increase in RAC air content will eventually result in an increase in RCPT when the other variables are considered. The previous regression model where the formation factor was used had a slightly better model fit than this regression model that uses bulk resistivity.

5.1.3 Regression of Water Sorptivity and Rate of Saturation

Based on the correlation table in Table 26, the water sorptivity (S) and rate of water saturation (RS) have high to low correlation coefficients with the variables SR/BR/FF, RAC air content and slump, RCA volume, and RCA residual mortar air content. The set of independent variables with VIF < 5 includes SR/BR/FF, RAC_{air}, V_{rca}, and RM_{air}. The correlation coefficient between BR and S/RS is better than between SR and S/RS. Therefore, BR was used in the regression analysis involving electrical resistivity.

Naturally, we can assume that the sorptivity increases as the RCA volume increase, but in this study, the variation in RCA volume is small. This regression model is only valid for concrete with 100% coarse RCA. The variation in the RCA volumes is only due to the varying RCA properties such as NMAS, bulk density, and specific gravity. Furthermore, the RCA percent volumes were adjusted based on the measured air contents

of the new mortars such that when the measured air content is higher than the designed air content (6%), the RCA volume will be lower. Therefore, an increase in RCA volume could also mean a decrease in new mortar's air content and, thus, lower sorptivity.

The air content of the RCA's residual mortar also affects the water sorptivity and water saturation rate. The air content of the concrete is known to affect water sorptivity. In RCA's case, the aggregate also has air voids, which can influence the sorptivity test results.

5.1.3.1 Using Formation Factor. During the regression analysis for water sorptivity and rate of water saturation, some observations were considered outliers and removed from the model to satisfy the normality requirements in residuals and remove the presence of heteroscedasticity in the model. One of the outliers is a specimen from the 0.48-RCA4 mixture, which has a lower initial degree of saturation, thus resulting in much higher sorptivity than the other two specimens of the same mixture. The other three outliers are from the same mixture of 0.48-RCA5, which can be identified as multivariate outliers from the bulk resistivity and RCA volume interaction.

5.1.3.1.1 Water Sorptivity. The scatter plot of water sorptivity and formation factor measurements with data ellipses at 50% and 95% confidence levels are shown in Figure *59*. Even though the highest sorptivity measurements are outside the 95% ellipse, they are not too far from the other data and were not immediately considered outliers.

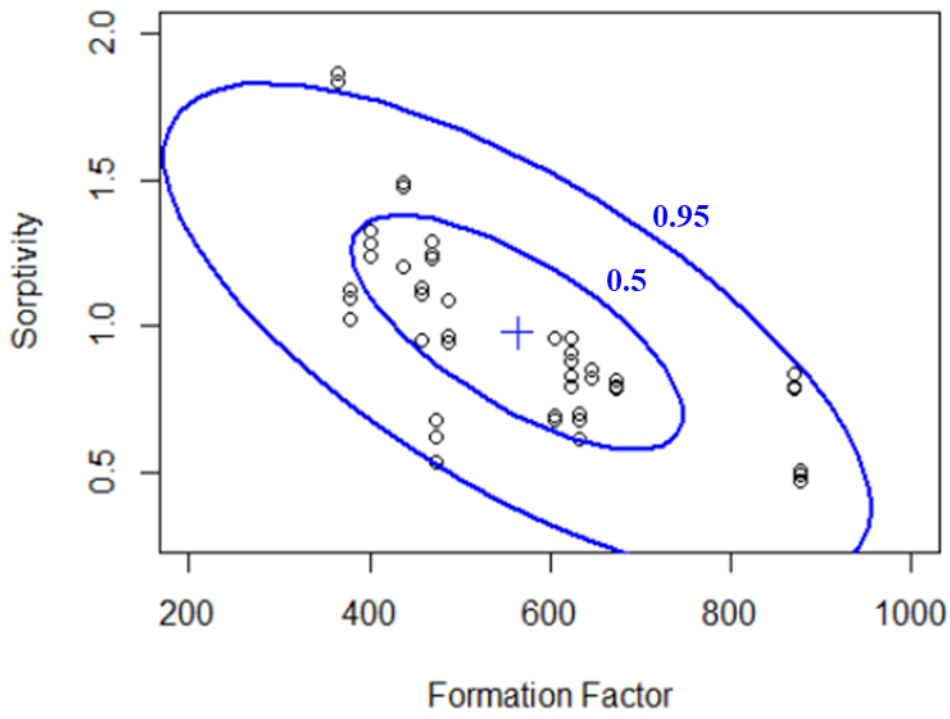

Figure 59. Scatter plot of RAC's sorptivity and inverse of formation factor measurements with data ellipses at 0.5 and 0.95 confidence levels.

The final multiple linear regression model of sorptivity based on individual measurements is shown in Table 31. The regression model is statistically significant, showing that 92% of the variance in the sorptivity (S) can be explained by the formation factor, RCA percent volume, RCA residual mortar air content, and RAC mixture air content, with RSE of only 0.092 mm/day$^{0.25}$. The Shapiro-Wilk normality test on the residuals (W = 0.97751, p-value = 0.5369) showed no evidence that the residuals are not normally distributed. Furthermore, the studentized Breusch-Pagan test (BP = 10.205, df = 5, p-value = 0.06963) did not show the presence of heteroscedasticity in the regression model. The interaction between the variables also shows that the change in sorptivity with the change in formation factor is lower when the RCA volume is high. The multiple

linear regression model shows a much better R^2 and standard error than when the formation factor was used as the lone predictor (R^2 = 0.56, RSE = 0.212 mm/day$^{0.25}$).

Table 31

Regression Result for the RACs' Water Sorptivity (mm/day$^{0.25}$) using Formation Factor, RCA Volume, Residual Mortar Air Content, and RAC Air Content

Intercept	-7.098*** (1.227)
(1000/FF)	6.116*** (0.607)
V_{rca}	0.225*** (0.034)
RM_{air}	-0.056*** (0.009)
RAC_{air}	-0.075*** (0.021)
(1000/FF):V_rca	-0.158*** (0.017)
Residual standard error	0.092 on 38 df
Adjusted R-squared	0.9212
No. outliers removed	4
Remaining no. observations	44 RAC specimens

Notes: Standard errors are reported in parentheses.
*** indicate significance level at 0.001

5.1.3.1.2 Rate of Water Saturation (RS). The scatter plot with data ellipses for the rate of saturation and inverse of the formation factor is shown in Figure *60*. Like in the sorptivity, no outlier was considered in the regression analysis of RS even though one data was observed outside the data ellipse.

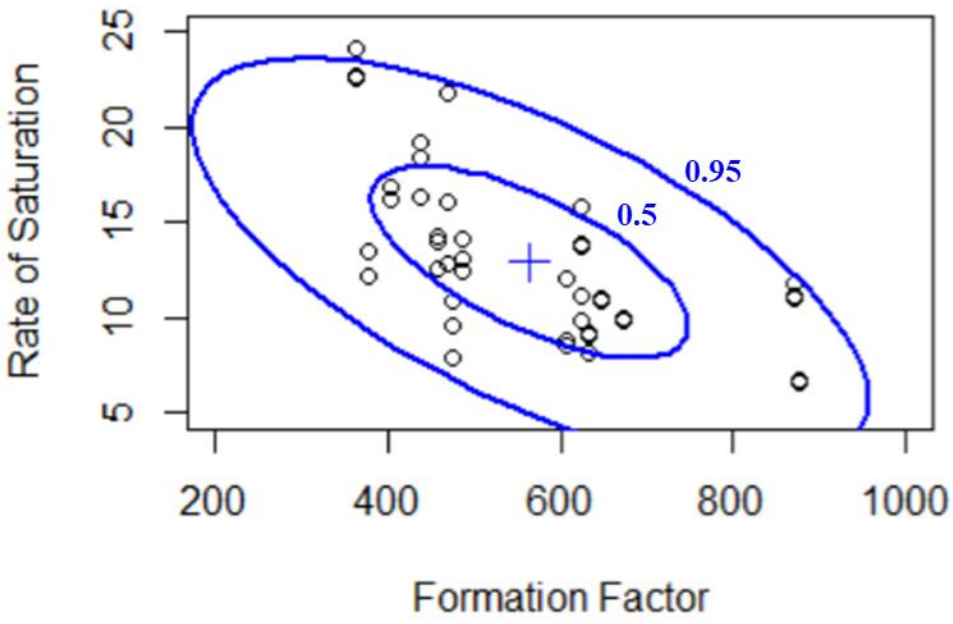

Figure 60. Scatter plot of RAC's rate of saturation and formation factor measurements with data ellipses at 0.5 and 0.95 confidence levels.

In the regression analysis for the rate of water saturation, the same set of outliers from the sorptivity regression model was removed. Furthermore, the same set of explanatory variables was also used. The RS prediction model summary is shown in Table 32. The explanatory variables explained about 92% of the variance in RS values, with a standard error of 1.116 %/day$^{0.25}$. The Shapiro-Wilk normality test on the residuals (W = 0.9515, p-value = 0.06256) did not show enough evidence that the residuals are not normally distributed.

Table 32

Regression Result for the RACs' Rate of Saturation (%/day0.25) using Formation Factor, RCA Volume, Residual Mortar Air Content, and RAC Air Content

Intercept	-60.5495*** (15.3411)
(1000/FF)	66.9066*** (7.5481)
V_{rca}	2.3747*** (0.4147)
RM_{air}	-1.7876*** (0.4245)
RAC_{air}	-1.3827*** (0.2933)
(1000/FF):V_rca	-1.8597*** (0.2066)
(1000/FF): RM_{air}	0.6460* (0.2406)
Residual standard error	1.112 on 37 df
Adjusted R-squared	0.9216
No. outliers removed	4
Remaining no. observations	44 RAC specimens

Notes: Standard errors are reported in parentheses. *,**, and *** indicate significance levels at 0.05, 0.01, and 0.001, respectively.

Furthermore, the studentized Breusch-Pagan test (BP = 4.5625, df = 6, p-value = 0.601) did not show the presence of heteroscedasticity in the regression model. The interaction between the variables also shows that the change in RS with the change in formation factor is lower when the RCA volume is high and higher when the air content of the RCA residual mortar is high. Compared to the RS regression model using only the formation factor ((R^2 = 0.52, RSE = 2.754 %/day$^{0.25}$), the multiple linear regression model has a much better fit.

5.1.3.2 Using Bulk Resistivity Measurements. The same set of additional explanatory variables from the previous sorptivity and rate of saturation models using the

formation factor was used in this regression, replacing the formation factor with bulk resistivity. Furthermore, the same set of outliers was also removed from the models.

5.1.3.2.1 Water Sorptivity. The scatter plot of individual water sorptivity and bulk resistivity measurements with data ellipses at 50% and 95% confidence levels are shown in Figure *59*. Even though five observations are outside the data ellipse, they are still close to the other values and, therefore, not immediately considered outliers.

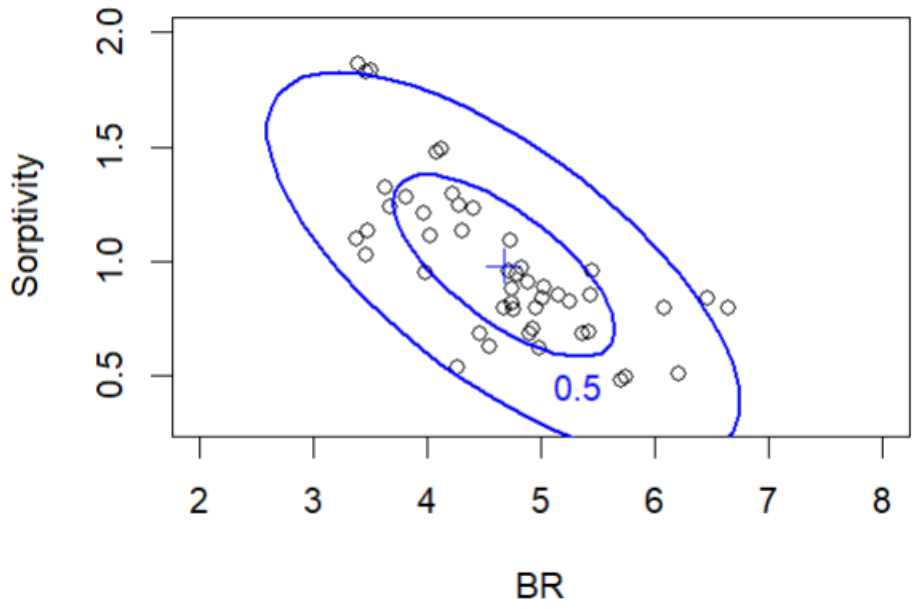

Figure 61. Scatter plot of paired measurements of RAC's bulk resistivity and sorptivity with data ellipses at 0.5 and 0.95 confidence levels. Five possible outliers were detected.

The final multiple linear regression model of sorptivity based on individual measurements is shown in Table 33. The regression model is statistically significant with a very low p-value. It shows that 90% of the variance in the sorptivity (S) can be explained by the bulk resistivity, RCA percent volume, and RCA residual mortar air

content, with RSE of only 0.1014 mm/day$^{0.25}$. The Shapiro-Wilk normality test on the residuals (W = 0.95463, p-value = 0.08193) showed no evidence that the residuals are not normally distributed. Furthermore, the studentized Breusch-Pagan test (BP = 3.7708, df = 4, p-value = 0.4379) did not show the presence of heteroscedasticity in the regression model. The interaction between the explanatory variables means that the change in sorptivity per unit change in bulk resistivity is lower when the RCA volume is high. The multiple linear regression model shows a much better R^2 and standard error than when bulk resistivity was used as the lone predictor (R^2 = 0.46, RSE = 0.24 mm/day$^{0.25}$).

Table 33

Regression Results for RACs' Water Sorptivity (mm/day$^{0.25}$) using Bulk Resistivity, RCA Volume, and Residual Mortar Air Content

Intercept	25.449*** (1.992)
BR	-4.669*** (0.425)
V_rca	-0.640*** (0.056)
RM_air	-0.074*** (0.009)
BR:V_rca	0.124*** (0.012)
Residual standard error	0.1014 on 39 df
Adjusted R-squared	0.9039
p-value	< 2.2e-16
No. outliers removed	4
Remaining no. observations	44

Notes: Standard errors are reported in parentheses; *,**, and *** indicate significance levels at 0.05, 0.01, and 0.001, respectively.

5.1.3.2.2 Rate of Water Saturation. The scatter plot with data ellipses for the rate of saturation and rate of water saturation is shown in Figure *62*. Like in the sorptivity, there are measurements outside the data ellipse, but they were not immediately considered outliers as they are not far from the other data.

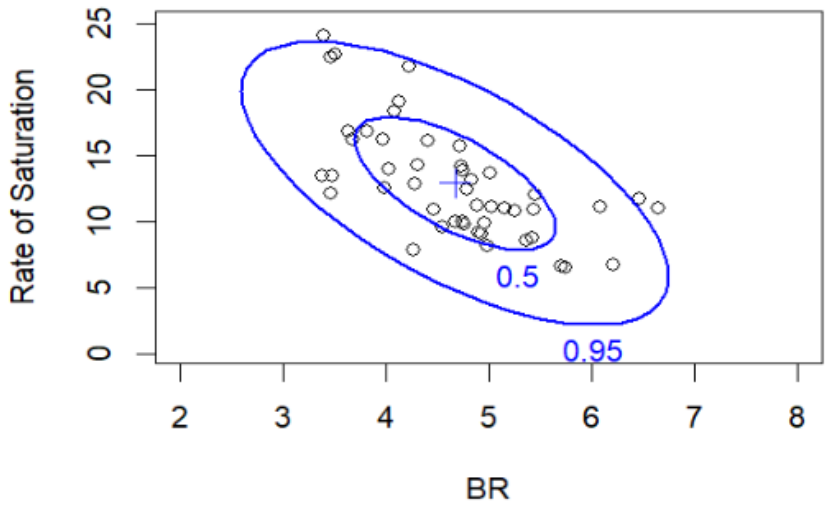

Figure 62. Scatter plot of paired measurements of RAC's bulk resistivity and rate of saturation with data ellipses at 0.5 and 0.95 confidence levels. Five possible outliers were detected.

The RS prediction model summary using bulk resistivity as an explanatory variable is shown in Table 34. The model explained almost 90% of the variance in RS values with a standard error of 1.282 %/day$^{0.25}$. The Shapiro-Wilk normality test on the residuals (W = 0.97773, p-value = 0.5454) showed no evidence that the residuals are not normally distributed. Furthermore, the studentized Breusch-Pagan test (BP = 1.5717, df = 4, p-value = 0.8139) did not show the presence of heteroscedasticity in the regression model. The interaction between the variables also shows that the change in RS with a unit

change in bulk conductivity is lower when the RCA volume is high. The multiple linear regression model shows a much better R^2 and standard error than when bulk resistivity was used as the lone predictor (R^2 = 0.41, RSE = 3.05 %/day$^{0.25}$).

Table 34

Regression Results for the RAC's Rate of Saturation (%/day$^{0.25}$) using Bulk Resistivity, RCA Volume, and Residual Mortar Air Content

Intercept	311.192*** (25.127)
BR	-55.049*** (5.364)
V_rca	-7.861*** (0.703)
RM_air	-0.912*** (0.114)
BR:V_rca	1.476*** (0.149)
Residual standard error	1.278 on 39 df
Adjusted R-squared	0.8963
No. outliers removed	4
Remaining no. observations	44

Notes: Standard errors are reported in parentheses.
*** indicate significance level at 0.001

5.1.4 Linear Regression Models of RAC Permeability

To summarize the results of multiple linear regression analyses on the RAC permeability measurements, the regression equations for the permeability of RAC specimens using the formation factor as an explanatory variable are shown in Equations (25) to (28). The regression equations for the RAC specimens with bulk resistivity as main explanatory variable are shown in Equations (29) to (32).

Using formation factor:

$$GWT = -1.014 + 0.494 \times \frac{1000}{FF} + 0.153 \times RAC_{air} + 0.024 \times RM_{air} - 0.060 \times \frac{1000}{FF} \times RAC_{air} \pm \varepsilon_{(25)} \quad (25)$$

$$RCPT = -17910 + 70980 \times \frac{1000}{FF} - 1072 \times RAC_{air} - 820.2 \times RAC_{slump} + 11.37 \times RAC_{density} - 30.75 \times \frac{1000}{FF} \times RAC_{density} + 0.384 \times RAC_{density} \times RAC_{slump} \pm \varepsilon_{(26)} \quad (26)$$

$$S = -7.098 + 6.116 \times \frac{1000}{FF} + 0.225 \times V_{rca} - 0.056 \times RM_{air} - 0.075 \times RAC_{air} - 0.158 \times \frac{1000}{FF} \times V_{rca} \pm \varepsilon_{(27)} \quad (27)$$

$$RS = -60.550 + 66.907 \times \frac{1000}{FF} + 2.375 \times V_{rca} - 1.788 \times RM_{air} - 1.383 \times RAC_{air} - 1.860 \times \frac{1000}{FF} \times V_{rca} + 0.646 \times \frac{1000}{FF} \times RM_{air} \pm \varepsilon_{(28)} \quad (28)$$

Using bulk resistivity:

$$GWT = 3.434 - 0.0015 \times RAC_{density} + 0.009 \times \frac{100}{BR} \pm \varepsilon_{(29)} \quad (29)$$

$$RCPT = 57366 - 317.272 \times \frac{100}{BR} - 3984.359 \times RAC_{air} + 107.604 \times RAC_{slump} - 18.086 \times RAC_{density} + 159.428 \times \frac{100}{BR} \times RAC_{air} - 4.368 \times \frac{100}{BR} \times RAC_{slump} \pm \varepsilon_{(30)} \quad (30)$$

$$S = 25.449 - 4.669 \times BR - 0.640 \times V_{rca} - 0.074 \times RM_{air} + 0.124 \times BR \times V_{rca} \pm \varepsilon_{(31)} \quad (31)$$

$$RS = 311.192 - 55.049 \times BR - 7.861 \times V_{rca} - 0.912 \times RM_{air} + 1.476 \times BR \times V_{rca} \pm \varepsilon_{(32)} \quad (32)$$

where GWT = average flux from GWT (0.108~0.615 $\times 10^{-4}$ mm/s), $RCPT$ = total charge passed from RCPT (5700~13200 Coulombs), S = sorptivity (0.475~1.864 mm/day$^{0.25}$), RS = rate of saturation (6.59~24.17 %/day$^{0.25}$), FF = formation factor (364~878), BR = bulk resistivity (3.38~6.65 kΩ-cm), RAC_{air} = air content of the new concrete or RAC mixture (4.5~8.25 %, air voids from the RCA excluded), RAC_{slump} = slump of the fresh concrete (34~188 mm), $RAC_{density}$ = fresh concrete unit weight (2150~2300 kg/m^3), RM_{air} = air content of residual mortar of RCA (7~11 %), V_{rca} = percent volume of RCA in the mixture (32.8~37.6 %), and the normally distributed errors $\varepsilon_{(25)} \sim N(0,0.085^2) \times 10^{-4}$ mm/s, $\varepsilon_{(26)} \sim N(0,729.8^2)$ Coulombs, $\varepsilon_{(27)} \sim N(0,0.092^2)$ mm/day$^{0.25}$, $\varepsilon_{(28)} \sim N(0,1.112^2)$ %/day$^{0.25}$, $\varepsilon_{(29)} \sim N(0,0.098^2) \times 10^{-4}$ mm/s, $\varepsilon_{(30)} \sim N(0,764.3^2)$ Coulombs, $\varepsilon_{(31)} \sim N(0,0.1014^2)$ mm/day$^{0.25}$, and $\varepsilon_{(32)} \sim N(0,1.278^2)$ %/day$^{0.25}$.

The high formation factor or electrical resistivity indicates that the RAC mixture has high resistance against the flow of electrons. Thus, RAC specimens with high resistivity and formation factor generally showed low permeability measurements. The fresh concrete properties (air content, slump, and density) influenced the permeability measurements. The air content of the fresh concrete consisted of larger air voids which probably provided less resistance to the flow of fluid and ions in the concrete than the smaller and tortuous capillary pores. The slump and density are both affected by the cement paste content. Higher cement paste content resulted in a lower slump, and higher cement content resulted in higher density. The high air content also increases the slump and decreases concrete density.

The RCA property, residual mortar air content, and the adjusted volume of RCA in the mixture were significant factors in RAC sorptivity and saturation rate. The residual mortar's air voids seemed to have delayed water penetration due to capillary suction in the concrete. On the other hand, the adjusted RCA volume is a function of the RCA properties (SG, bulk density, and nominal maximum aggregate size) and the RAC air content. Considering that all coarse aggregates in the mixture are RCA and the mixture design is based on ACI 211.1 [100], higher RCA volume resulted in lower sorptivity and saturation rate in concrete.

Although most RAC permeability models show that the residual standard error is lower in the models that used the formation factor, there are little differences in the residuals between the formation factor and bulk resistivity-based models. The formation factor is a better indicator of the concrete’s permeability. Still, considering the additional

work required to determine the formation factor of concrete, the use of electrical resistivity as an indicator of RAC permeability is more practical.

5.1.5 Nomograms

Nomograms were also prepared in some RAC permeability models with 3 variables for a more convenient way of estimating the permeability. Nomogram, or nomograph, is a two-dimensional diagram representing the relations between three or more variables. Figure 63 shows how the 10 minute GWT measurements can be estimated with the formation factor and the air contents. As shown in Figure 64, the nomogram can be used to approximate the sorptivity and rate of saturation based on the bulk resistivity, CA percent volume, and residual mortar air content. Furthermore, the nomogram limits the user to only input values that were in the range of measurements observed in this study.

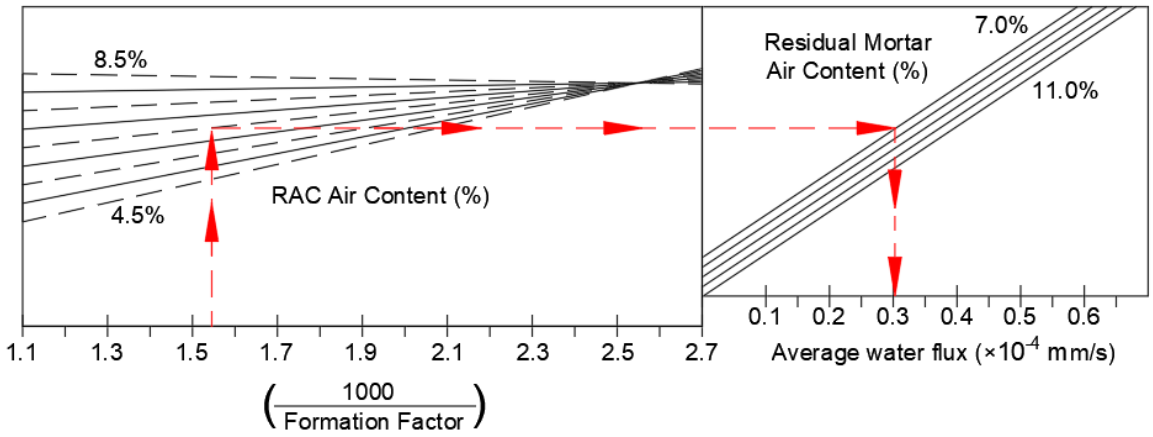

To use this chart:

1. Enter with the inverse of formation factor (1000/FF), move up to new mortar or RAC air content
2. Move right to residual mortar air content
3. Move down for approximate GWT measurement (× 10^{-4} mm/s) with error ~ N(0,0.085^2)

Figure 63. Nomogram for estimating the RAC average water flux (×10^{-4} mm/s) using formation factor, RAC air content, and residual mortar air content.

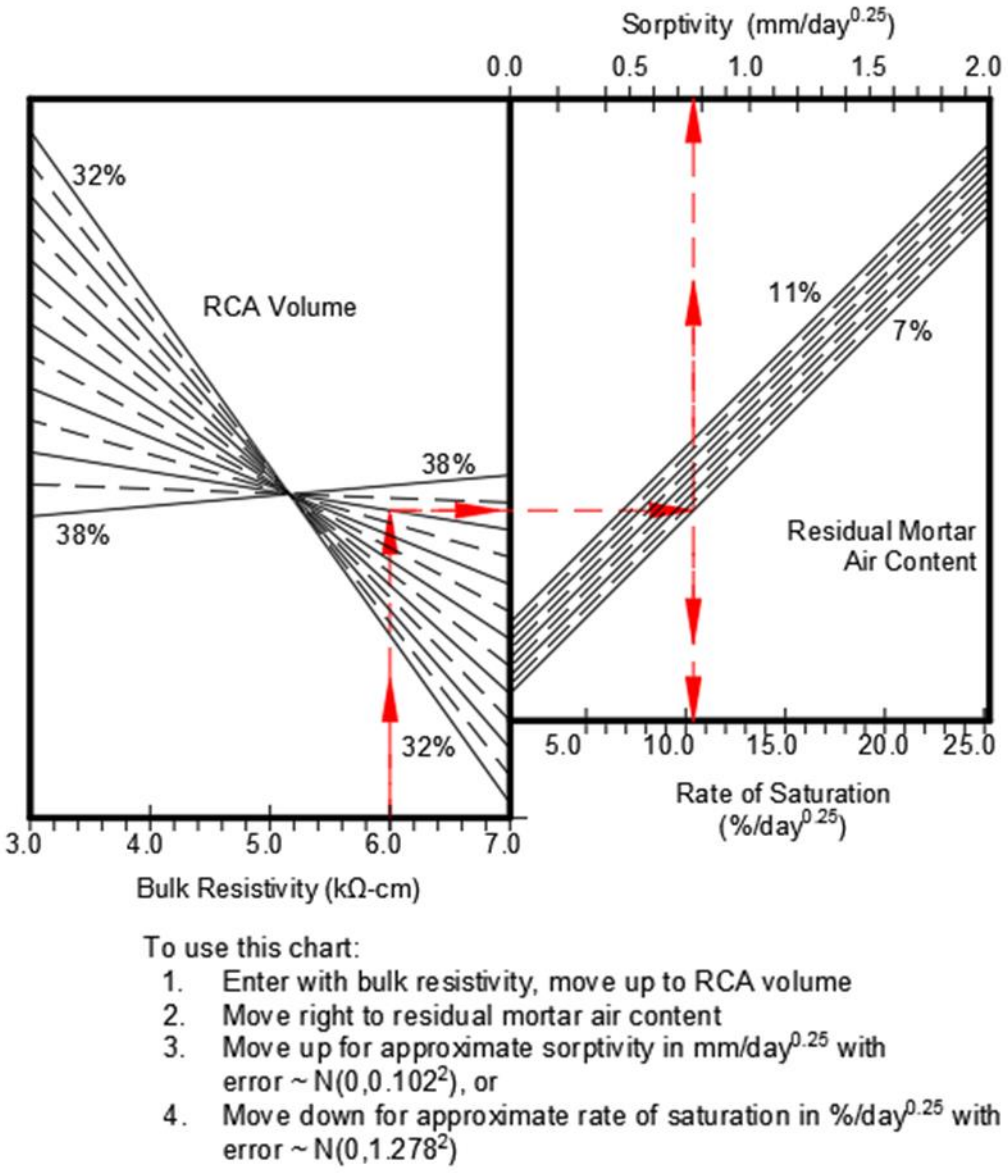

Figure 64. Nomogram for estimating the RAC sorptivity and rate of saturation using bulk resistivity, RCA volume, and residual mortar air content.

5.2 NWAC, LWAC, and 50LWAC

The tests for equality of means in Chapter 4 showed that most permeability measurements of concretes at different water-cement ratios and coarse LWA replacement have a significant difference. With three water-cement ratios and three coarse LWA

replacements, nine total concrete mixtures are produced. The regression plots of GWT and electrical resistivity/formation factor measurements in the previous chapter showed different trendlines for coarse LWA replacements. And while the regressions of RCPT, sorptivity, and saturation rate were expressed in a single trendline, high residuals can be observed from the graphs. Like in the RAC permeability measurements, the regression models of NWAC, LWAC, and 50LWAC could be improved if additional explanatory variables are considered. In this case, where only one type of LWA used, the other variables can be expressed by the water-cement ratio and the coarse LWA replacement. The coarse LWA percent replacement can also be expressed by the weighted coarse aggregate (CA) porosity, the total porosity attributed to the CA per unit volume of concrete. It can be calculated as the sum of the products of CA volume and its porosity, as shown in Equation (**33**). The calculated values are 7.22% and 3.75% for LWAC and PLWAC, respectively, and only 0.24% for the NWAC.

$$\phi_{WeightedCA} = \sum (V_{CAi} * \phi_{CAi}) \ / \ 100 \qquad (33)$$

where $\phi_{WeightedCA}$ = the weighted coarse aggregate porosity (%), V_{CAi} = % volume of a coarse aggregate *i* in concrete, and ϕ_{CAi} = porosity of coarse aggregate *i* (%).

Like in the RAC, multiple regression analyses were done twice, one for formation factor and another for electrical resistivity. The boxplots of GWT, RCPT, sorptivity, and water saturation rate measurements in LWAC, 50LWAC, and NWAC mixtures are shown in Figure *65*. Three measurements far from the other data can be observed in the sorptivity and saturation rate boxplots (it looks like just one point in the sorptivity

boxplot because the measurements are almost equal). These measurements came from the 0.48-LWAC specimens.

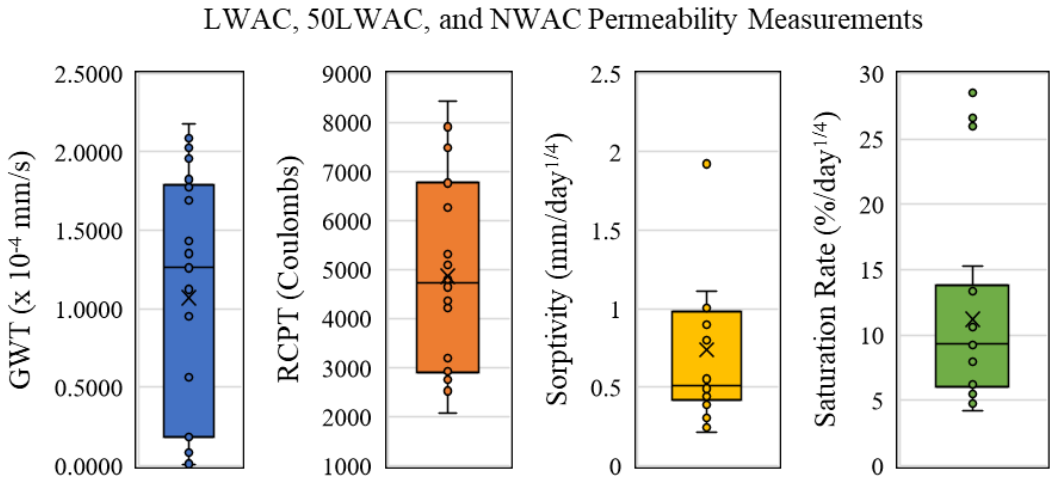

Figure 65. Boxplots of GWT, RCPT, sorptivity, and water saturation rate measurements in LWAC, 50LWAC, and NWAC specimens.

5.2.1 Regression of GWT Measurements

The 10-minute average water flux measured using GWT has a mean of 1.070 $\times 10^{-4}$ mm/s and a standard deviation of 0.776 $\times 10^{-4}$ mm/s . Based on the test for equality of means using two-way ANOVA, the coarse LWA percent replacement significantly affects the GWT measurements. However, the effect of the water-cement ratio in the GWT measurements is insignificant, and the water-cement ratio did not affect the relationship between the coarse LWA percent replacement and the GWT measurements. It was attributed to the wide range of values measured within each concrete mixture. Particularly for LWAC and 50LWAC specimens, the within-the-group variances are

high. Due to that, high residuals can also be expected from the regression models of GWT measurements.

5.2.1.1 Using Formation Factor. It was determined from Chapter 4 that for porous aggregate concretes, the average water flux measured through GWT has a better correlation with the formation factor than in surface or bulk resistivity. A scatter plot between the formation factor and GWT measurements with data ellipses at 50% and 95% confidence levels are shown in Figure *66.* All measurements are inside the data ellipses; therefore, no bivariate outlier was found.

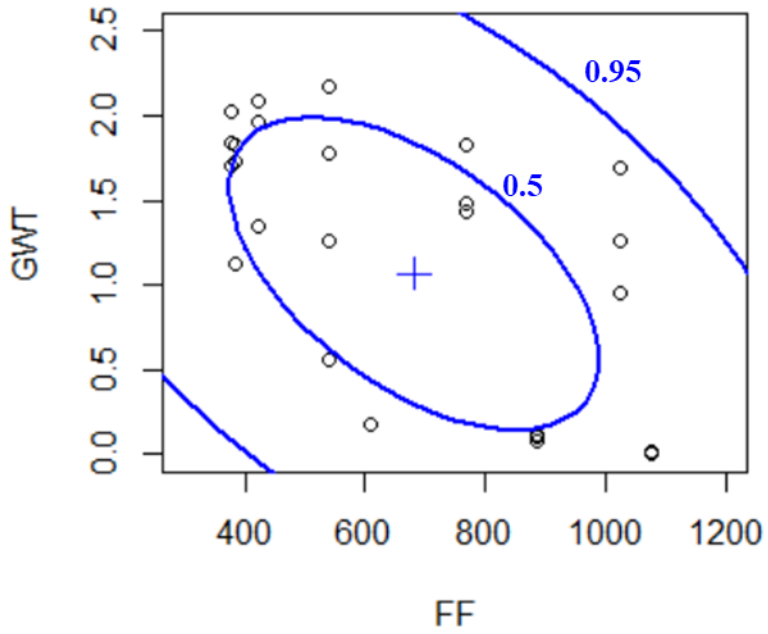

Figure 66. Scatter plot of LWAC, 50LWAC, and NWACs' GWT and formation factor measurements with data ellipses at 0.5 and 0.95 confidence levels.

In the scatter plot between the GWT measurements and the formation factor in Chapter 4, individual trendlines separated by the y-intercept were observed for LWAC, 50LWAC, and NWAC mixtures. Higher y-intercept corresponded to higher coarse LWA replacement. Furthermore, the change in y-intercept is not linear, such that the difference from 100% to 50% coarse LWA replacement is small, but the difference from 50% to 0% is large. With that, the regression of GWT measurements with the formation factor can be expressed as a function of the formation factor and coarse LWA percent replacement. The coarse LWA percent replacement was represented by the logarithm of the weighted coarse aggregate porosity to account for the difference in porosity of LWA and NWA and the non-linear change in the y-intercept of their regression trendlines.

The linear regression model of the lightweight and normalweight concrete's GWT is summarized in Table 35. The regression model is statistically significant with a very low p-value. It shows that about 84% of the variance in the GWT measurements in LWAC, 50LWAC, and NWAC can be explained by the formation factor and the weighted coarse aggregate porosity, with a residual standard error of 0.308×10^{-4} mm/s. The Shapiro-Wilk normality test on the residuals ($W = 0.94493$, p-value = 0.1235) did not show enough evidence that the residuals are not normally distributed. Furthermore, the studentized Breusch-Pagan test ($BP = 2.6166$, $df = 2$, p-value = 0.2703) did not show the presence of heteroscedasticity in the regression model.

Table 35

Regression Result for LWACs' GWT Measurements (×10-4 mm/s) using Formation Factor and Weighted CA Porosity

Intercept	0.45135* (0.17312)
log($\phi_{WeightedCA}$)	0.43001*** (0.04475)
1000/FF	0.21255 (0.10381)
Residual standard error (RSE)	0.3083 on 27 df
Adjusted R^2	0.8421
p-value	5.722e-12
No. outliers removed	0
Remaining no. observations	30 concrete specimens

Notes: Standard errors are reported in parentheses; *,**, and *** indicate significance levels at 0.05, 0.01, and 0.001, respectively.

As expected, the residuals in the GWT regression model are high. Even though the Breusch-Pagan test indicated no presence of heteroscedasticity in the model, the high value of residuals occurred on the measurements for LWAC and 50LWAC. In contrast, low residual values occurred in the NWAC specimens. The results infer that for porous aggregate concretes, either full or 50% partial LWA replacement, the GWT measurements do not change significantly with the formation factor.

5.2.1.2 Using Bulk Resistivity Measurements. The scatter plot with data ellipses at 50% and 95% confidence levels for GWT and bulk resistivity measurements are shown in Figure *67*. Like with the formation factor, no bivariate outlier was found.

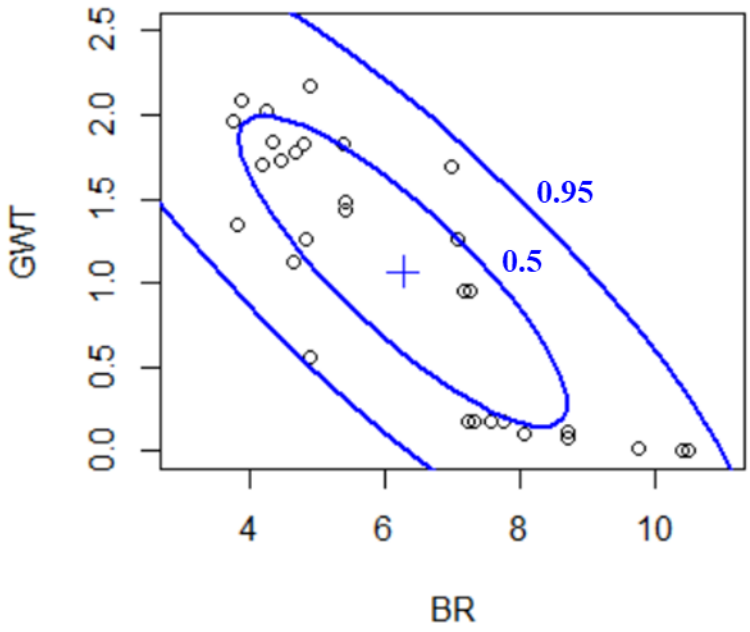

Figure 67. Scatter plot of LWAC, 50LWAC, and NWACs' GWT and bulk resistivity measurements with data ellipses at 0.5 and 0.95 confidence levels.

The linear regression model of the lightweight and normalweight concrete's GWT is summarized in Table 36. The regression model is statistically significant and shows that about 84% of the variance in the GWT measurements in LWAC, 50LWAC, and NWAC can be explained by the bulk resistivity and the weighted coarse aggregate porosity. The residual standard error of 0.310 $\times 10^{-4}$ mm/s is almost equal to the result when the formation factor was used (RSE = 0.308 $\times 10^{-4}$ mm/s). The Shapiro-Wilk normality test on the residuals (W = 0.94356, p-value = 0.1134) did not show enough evidence that the residuals are not normally distributed. Furthermore, the studentized Breusch-Pagan test (BP = 2.7688, df = 2, p-value = 0.2505) did not show the presence of heteroscedasticity in the regression model.

Table 36

Regression Result for LWACs' GWT Measurements (×10-4 mm/s) using Bulk Resistivity and Weighted CA Porosity

Intercept	0.20398 (0.30263)
log($\phi_{WeightedCA}$)	0.36841*** (0.06754)
100/BR	0.03664 (0.01875)
Residual standard error (RSE)	0.3102 on 27 df
Adjusted R^2	0.8402
p-value	6.73e-12
No. outliers removed	0
Remaining no. observations	30 concrete specimens

Notes: Standard errors are reported in parentheses; *,**, and *** indicate significance levels at 0.05, 0.01, and 0.001, respectively.

Similar to the regression model using the formation factor, the residual standard error is also high in the model using bulk resistivity measurements. Furthermore, the inverse of bulk resistivity has a p-value of 0.06 > 0.05, which means that its effect in GWT measurements is not statistically significant at a 95% confidence level.

5.2.2 Regression of RCPT Measurements

The total charge passed during the 6-hour RCPT has a mean of 4800 Coulombs and a standard deviation of 1900 Coulombs. Based on the test for equality of means using two-way ANOVA, the coarse LWA percent replacement and water-cement ratio significantly affect the RCPT measurements and the electrical resistivity measurements. Therefore, it can be hypothesized that an RCPT regression model can be generated from the formation factor and bulk resistivity.

5.2.2.1 Using Formation Factor. The scatter plot between the formation factor and RCPT measurements with data ellipses at 50% and 95% confidence levels are shown

in Figure *68*. All measurements are inside the data ellipses; therefore, no bivariate outlier was found.

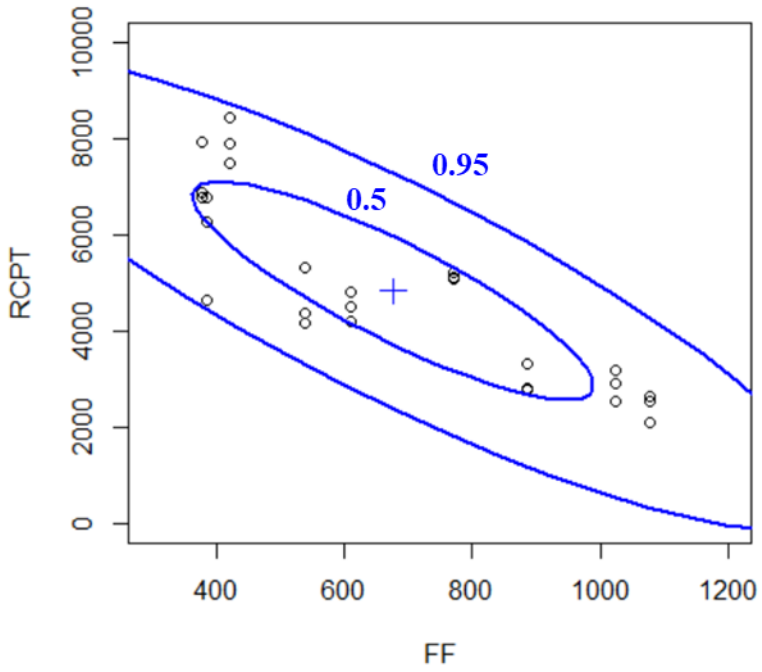

Figure 68. Scatter plot of paired measurements of LWAC, 50LWAC, and NWACs' formation factor and RCPT with data ellipses at 0.5 and 0.95 confidence levels. No possible outlier was detected.

Unlike in the GWT measurements, the scatter plot between the GWT and electrical resistivity/formation factor measurements presented in Chapter 4 shows that the RCPT regression can be expressed in a single trendline. However, it can also be observed that the measurements in LWAC specimens are in the upper part of the trendline, while the measurements in 50LWAC specimens are in the lower part. Because of that difference between the LWAC and 50LWAC specimens, the weighted coarse aggregate porosity was considered an additional explanatory variable.

The linear regression model of the lightweight and normalweight concrete's RCPT measurements is summarized in Table 37. The regression model is statistically significant with a very low p-value. The regression model involving the formation factor and weighted coarse aggregate porosity explained 85% of the variance in the RCPT measurements of LWAC, 50LWAC, and NWAC specimens, with a residual standard error of 729 Coulombs. This result is similar to the regression analysis for the RAC specimens, where the RSE is about 700 Coulombs. The Shapiro-Wilk normality test on the residuals (W = 0.97837, p-value = 0.8239) did not show enough evidence that the residuals are not normally distributed. Furthermore, the studentized Breusch-Pagan test (BP = 4.4395, df = 2, p-value = 0.1086) did not show the presence of heteroscedasticity in the regression model.

Table 37

Regression Result for LWACs' RCPT Measurements (Coulombs) using Formation Factor and Weighted CA Porosity

Intercept	643.35 (398.18)
1000/FF	1875.62*** (259.58)
$\phi_{WeightedCA}$	261.77*** (58.97)
Residual standard error (RSE)	729.2 on 24 df
Adjusted R^2	0.8537
p-value	3.687e-11
No. outliers removed	0
Remaining no. observations	27 concrete specimens

Notes: Standard errors are reported in parentheses; *, **, and *** indicate significance levels at 0.05, 0.01, and 0.001, respectively.

Based on the RCPT regression results, the total charge passed increases by about 1875 Coulombs per unit increase in the inverse of formation factor (1000/FF) and increases by about 260 Coulombs per unit increase of the weighted coarse aggregate porosity.

5.2.2.2 Using Bulk Resistivity Measurements. The scatter plot with data ellipses for the RCPT and bulk resistivity measurements is shown in Figure *69*. Like in the boxplots where no univariate outlier was found in RCPT measurements, there is also no bivariate outlier between RCPT and bulk resistivity measurements.

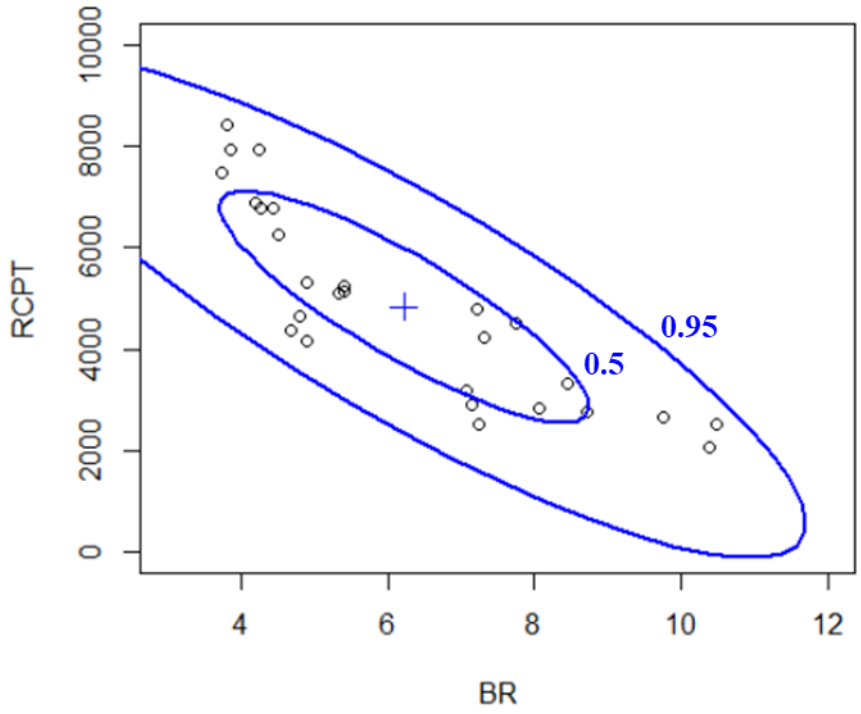

Figure 69. Scatter plot of paired measurements of LWAC, 50LWAC, and NWACs' bulk resistivity and RCPT with data ellipses at 0.5 and 0.95 confidence levels. No possible outlier was detected.

The linear regression model of the lightweight and normalweight concrete's RCPT measurements is summarized in Table 38. The regression model is statistically significant with a very low p-value. The regression model explained 87% of the variance in the RCPT measurements of LWAC, 50LWAC, and NWAC specimens, with a residual standard error of 687.5 Coulombs. This result is similar to the regression analysis for the RAC specimens, where the RSE is about 700 Coulombs. The Shapiro-Wilk normality test on the residuals (W = 0.98114, p-value = 0.8871) did not show enough evidence that the residuals are not normally distributed. Furthermore, the studentized Breusch-Pagan test (BP = 6.8569, df = 3, p-value = 0.0766) did not show the presence of heteroscedasticity in the regression model.

Table 38

Regression Result for LWACs' RCPT Measurements (Coulombs) using Bulk Resistivity and Weighted CA Porosity

Intercept	943.47 (851.55)
100/BR	192.73** (64.20)
$\phi_{WeightedCA}$	-587.45* (209.81)
(100/BR):$\phi_{WeightedCA}$	33.47** (11.44)
Residual standard error (RSE)	687.5 on 23 df
Adjusted R^2	0.8699
p-value	5.92e-11
No. outliers removed	0
Remaining no. observations	27 concrete specimens

Notes: Standard errors are reported in parentheses; *,**, and *** indicate significance levels at 0.05, 0.01, and 0.001, respectively.

Based on the regression results, the total charge passed increases by about 190 Coulombs per unit increase in bulk conductivity (100/BR). The relationship between bulk

resistivity and RCPT measurements is significantly affected by the weighted coarse aggregate porosity, which means that the main effect of bulk resistivity on the RCPT measurement varies between the LWAC, 50LWAC, and NWAC specimens. The interaction between explanatory variables shows that the increase in RCPT measurement per unit increase of bulk conductivity is higher when the weighted coarse aggregate porosity is low such as in NWAC specimens. On the other hand, the increase in RCPT measurement per unit increase of bulk conductivity is lower for LWAC specimens.

5.2.3 Water Sorptivity and Rate of Saturation

The water sorptivity in LWAC, 50LWAC, and NWAC specimens have a mean of 0.9789 mm/day$^{0.25}$ and a standard deviation of 0.336 mm/day$^{0.25}$. For the rate of water saturation, the mean is at 12.94 %/day$^{0.25,}$ and the standard deviation is 4.25 %/day$^{0.25}$. It was shown in the boxplots that there are three univariate outliers on the sorptivity and rate of saturation measurements. Those outliers are the three specimens from the LWAC48 mixture. After the sorptivity test, it was found that the initial degree of saturation in the LWAC48 specimens was only 45~53 %. The initial degree of saturation in the LWAC48 was much lower than that of other concrete specimens (66.5~87% degree of saturation). Since the LWAC48 specimens are relatively drier than the other concrete specimens, the capillary suction is stronger, and consequently, the sorptivity measurements are higher. Since the initial condition of these three specimens differs from the other concrete specimens, these can be considered outliers. In this section, regression analysis, including all measurements, was performed first, then compared to the regression analysis results with the outliers removed from the data.

5.2.3.1 Using Formation Factor. Based on the average values, the sorptivity measurements correlate better with the formation factor than with the surface or bulk resistivity.

5.2.3.1.1 Water Sorptivity. A scatter plot with data ellipses at 50% and 95% confidence levels shown in Figure *70*, was generated to check for possible bivariate outlier/s between water sorptivity and formation factor. The three measurements from LWAC48 with the highest values are within the boundary of the outer ellipse. There are no other possible outliers detected in the plot.

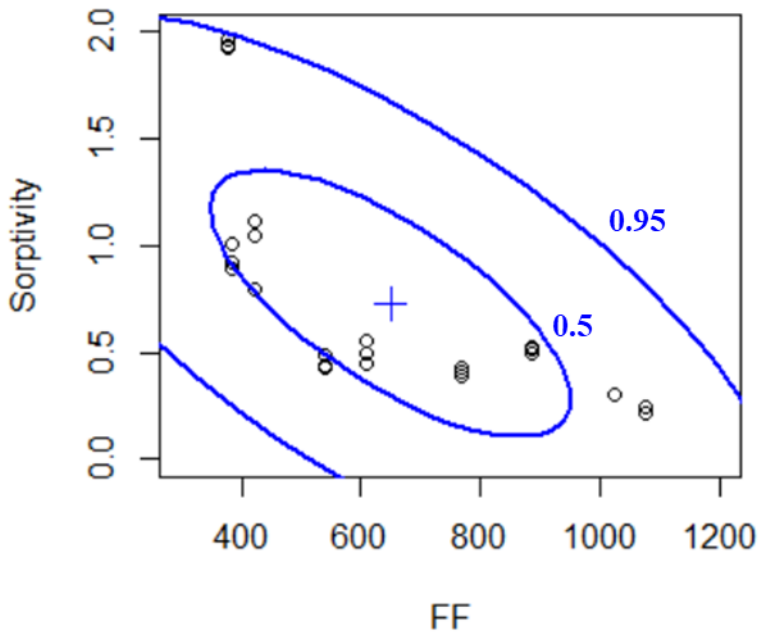

Figure 70. Scatter plot of LWAC, 50LWAC, and NWACs' formation factor and sorptivity with data ellipses at 0.5 and 0.95 confidence levels. No bivariate outlier was detected.

The linear regression model of the lightweight and normalweight concrete's sorptivity is summarized in Table 39. The regression model is statistically significant with a very low p-value. The regression model shows that about 81% of the variance in the sorptivity measurements of LWAC, 50LWAC, and NWAC specimens can be explained by the inverse of formation factors and the weighted coarse aggregate porosity, with a residual standard error of 0.228 mm/day$^{0.25}$. The Shapiro-Wilk normality test on the residuals (W = 0.95597, p-value = 0.34) did not show enough evidence that the residuals are not normally distributed. However, the studentized Breusch-Pagan test (BP = 13.834, df = 3, p-value = 0.003141) shows the presence of heteroscedasticity in the regression model. The high residual standard error is mainly due to the high sorptivity measurements recorded in LWAC48 specimens. As a result, the residuals seemed to be higher when the sorptivity measurements were high, and therefore, heteroscedasticity was observed in the model.

Table 39

Regression Result for LWACs' Water Sorptivity (mm/day$^{0.25}$) using Formation Factor and Weighted CA Porosity

Intercept	0.42997 (0.23203)
1000/FF	-0.03114 (0.16344)
$\phi_{WeightedCA}$	-0.18820** (0.05218)
1000/FF:$\phi_{WeightedCA}$	0.13687*** (0.03086)
Residual standard error (RSE)	0.2279 on 21 df
Adjusted R^2	0.8099
p-value	2.299e-08
No. outliers removed	0
Remaining no. observations	25 concrete specimens

Notes: Standard errors are reported in parentheses; *, **, and *** indicate significance levels at 0.05, 0.01, and 0.001, respectively.

The linear regression model of sorptivity with the outliers removed is summarized in Table 40. The regression model is statistically significant with a very low p-value. The regression model shows that about 82% of the variance in the sorptivity measurements of LWAC, 50LWAC, and NWAC specimens can be explained by the inverse of formation factors and the weighted coarse aggregate porosity, with a residual standard error of 0.115 mm/day$^{0.25}$. With the removal of outliers, the residual standard error was reduced to half. This result is comparable to the regression analysis for the RAC specimens, where the RSE is about 0.1014 mm/day$^{0.25}$. The Shapiro-Wilk normality test on the residuals (W = 0.93212, p-value = 0.1358) did not show enough evidence that the residuals are not normally distributed. Furthermore, the studentized Breusch-Pagan test (BP = 4.1241, df = 3, p-value = 0.2484) did not show enough evidence of heteroscedasticity in the regression model.

Table 40

Regression Result for LWACs' Water Sorptivity (mm/day$^{0.25}$) using Formation Factor and Weighted CA Porosity

Intercept	0.13920 (0.12252)
1000/FF	0.21101* (0.08779)
$\phi_{WeightedCA}$	-0.06642* (0.03038)
1000/FF:$\phi_{WeightedCA}$	0.04717* (0.01916)
Residual standard error (RSE)	0.115 on 18 df
Adjusted R^2	0.8215
p-value	1.504e-07
No. outliers removed	3
Remaining no. observations	22 concrete specimens

Notes: Standard errors are reported in parentheses; *, **, and *** indicate significance levels at 0.05, 0.01, and 0.001, respectively.

Based on the regression results, the water sorptivity increases by about 0.211 $mm/day^{0.25}$ per unit increase in the inverse of the formation factor (1000/FF). There is also a significant interaction effect between the inverse of the formation factor and weighted coarse aggregate porosity, which means that the change in sorptivity with the change in formation factor varies depending on the coarse LWA percent replacement. Like in the RCPT regression model with bulk conductivity, the main effect of the formation factor on the RCPT measurement varies between the LWAC, 50LWAC, and NWAC specimens. The increase in sorptivity per unit increase of the inverse of the formation factor is higher when the weighted coarse aggregate porosity is low such as in NWAC specimens. On the other hand, the increase in RCPT measurement per unit increase of the inverse of formation factor is lower for LWAC specimens.

5.2.3.1.2 Rate of Water Saturation (RS). The scatter plot with data ellipses at 50% and 95% confidence levels for the rate of water saturation, and formation factor is shown in Figure *71*. Aside from the highest measurements recorded in LWAC48 specimens, no other outliers were detected.

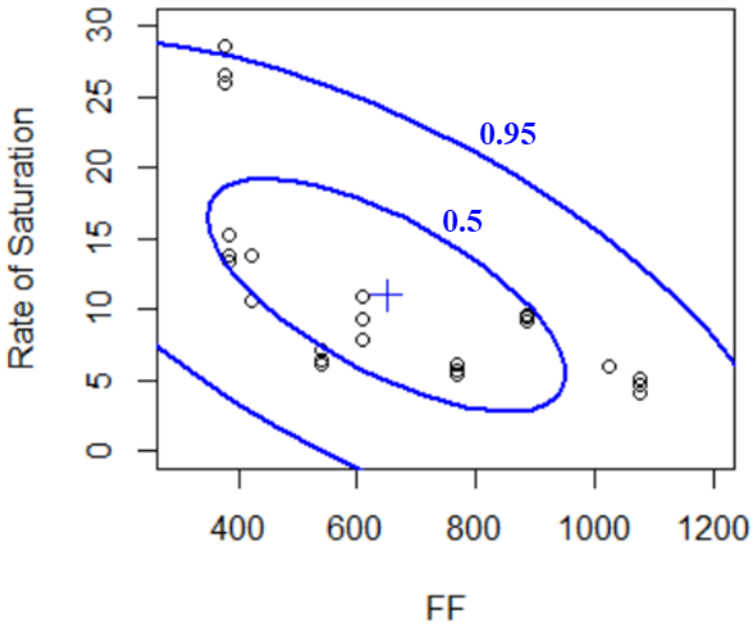

Figure 71. Scatter plot of LWAC, 50LWAC, and NWACs' formation factor and sorptivity with data ellipses at 0.5 and 0.95 confidence levels. No bivariate outlier was detected.

The linear regression model of the lightweight and normalweight concrete's sorptivity is summarized in Table 41. The regression model is statistically significant with a very low p-value. The regression model shows that about 70% of the variance in the sorptivity measurements of LWAC, 50LWAC, and NWAC specimens can be explained by the bulk conductivity (inverse of bulk resistivity) and the water-cement ratio used, with a residual standard error of 1.906 %/day$^{0.25}$. Even with removing outliers, the residuals in this regression model are higher than the regression result for the RAC specimens, where the RSE is only 1.28 %/day$^{0.25}$. The Shapiro-Wilk normality test on the residuals (W = 0.94189, p-value = 0.2165) did not show enough evidence that the residuals are not normally distributed. Furthermore, the studentized Breusch-Pagan test

(BP = 1.0056, df = 2, p-value = 0.6048) did not show enough evidence of heteroscedasticity in the regression model.

Table 41

Regression Result for LWACs' Rate of Saturation (%/day$^{0.25}$) using Formation Factor and Water-Cement Ratio

Intercept	-2.3858 (2.0470)
1000/FF	3.3338** (0.9394)
w/c	15.1701* (7.1903)
Residual standard error (RSE)	1.906 on 19 df
Adjusted R^2	0.6962
p-value	4.7e-06
No. outliers removed	3
Remaining no. observations	22 concrete specimens

Notes: Standard errors are reported in parentheses; *, **, and *** indicate significance levels at 0.05, 0.01, and 0.001, respectively.

The regression results imply that the rate of water saturation increases by about 3.33 %/day$^{0.25}$ per unit increase in the inverse of formation factor (1000/FF) and by about 15.17 %/day$^{0.25}$ per unit increase in the water-cement ratio. Although the change in water-cement ratio can already be reflected in the formation factor measurements, using it as an additional explanatory variable slightly improved the residual standard error from 2.064 %/day$^{0.25}$ when the formation factor was used alone to 1.906 %/day$^{0.25}$.

5.2.3.2 Using Bulk Electrical Resistivity Measurements. The regressions of water sorptivity and water saturation rate with the bulk electrical resistivity were also analyzed.

5.2.3.2.1 Water Sorptivity. The scatter plot with data ellipses at 50% and 95% confidence levels, shown in Figure *72*, was generated to check for other possible bivariate outliers between water sorptivity and bulk resistivity. Same with the formation factor, the three measurements from LWAC48 with the highest values are within the boundary of the outer ellipse. There are no other possible outliers detected in the plot.

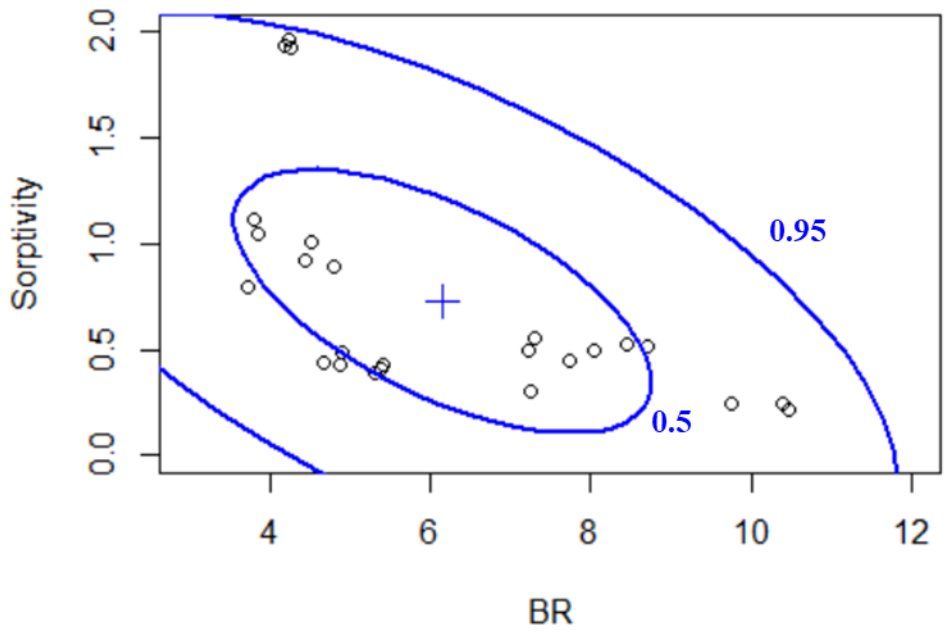

Figure 72. Scatter plot of paired measurements of LWAC, 50LWAC, and NWACs' bulk resistivity and sorptivity with data ellipses at 0.5 and 0.95 confidence levels. No bivariate outlier was detected.

The linear regression model of the lightweight and normalweight concrete's sorptivity is summarized in Table 42. The regression model is statistically significant with a very low p-value. The regression model shows that about 73% of the variance in the sorptivity measurements of LWAC, 50LWAC, and NWAC specimens can be explained by the bulk conductivity (inverse of bulk resistivity) and the water-cement ratio used, with a residual standard error of 0.142 mm/day$^{0.25}$. This result is comparable to the regression analysis for the RAC specimens, where the RSE is about 0.1014 mm/day$^{0.25}$. The Shapiro-Wilk normality test on the residuals (W = 0.98284, p-value = 0.9544) did not show enough evidence that the residuals are not normally distributed. Furthermore, the studentized Breusch-Pagan test (BP = 5.4468, df = 2, p-value = 0.06565) did not show enough evidence of heteroscedasticity in the regression model.

Table 42

Regression Result for LWACs' Water Sorptivity in (mm/day$^{0.25}$) using Bulk Resistivity and Water-Cement Ratio

Intercept	-0.535376** (0.162323)
100/BR	0.032060*** (0.005723)
w/c	1.445761** (0.408448)
Residual standard error (RSE)	0.1419 on 19 df
Adjusted R^2	0.728
p-value	1.641e-06
No. outliers removed	3
Remaining no. observations	22 concrete specimens

Notes: Standard errors are reported in parentheses; *, **, and *** indicate significance levels at 0.05, 0.01, and 0.001, respectively.

Based on the regression results, the water sorptivity increases by about 0.032 mm/day$^{0.25}$ per unit increase in the bulk conductivity (100/BR), and by about 1.446

mm/day$^{0.25}$ per unit increase in the water-cement ratio. By including the water-cement ratio as an explanatory variable, the regression model for water sorptivity slightly improved to a residual standard error of 0.142 mm/day$^{0.25}$ from a residual standard error of 0.178 mm/day$^{0.25}$ when bulk resistivity was used as a lone predictor. However, the regression model using the formation factor still showed a better model fit with a residual standard error of only 0.115 mm/day$^{0.25}$.

5.2.3.2.2 Rate of Water Saturation. The scatter plot with data ellipses at 50% and 95% confidence levels for the rate of water saturation and bulk resistivity is shown in Figure *73*. Same with the formation factor, the three measurements from LWAC48 with the highest values are close to the boundary of the outer ellipse, and no other possible outliers were detected in the plot.

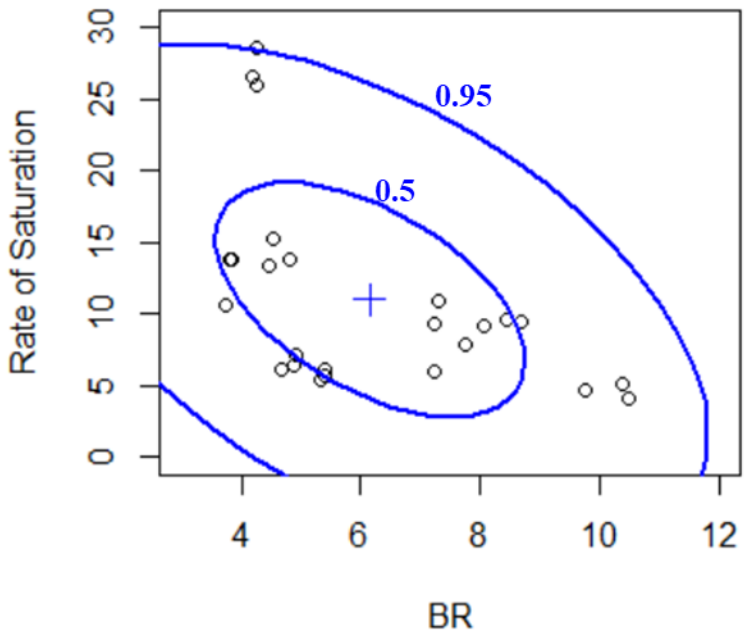

Figure 73. Scatter plot of paired measurements of LWAC, 50LWAC, and NWACs' bulk resistivity and rate of water saturation with data ellipses at 0.5 and 0.95 confidence levels. No bivariate outlier was detected.

The linear regression model of the lightweight and normalweight concrete's saturation rate is summarized in Table 43. The regression model is statistically significant with a very low p-value. The regression model shows that about 66% of the variance in the rate of saturation in LWAC, 50LWAC, and NWAC specimens can be explained by the bulk conductivity (inverse of bulk resistivity) and the water-cement ratio used, with a residual standard error of 2.017 %/day$^{0.25}$. Even with removing outliers, the residuals in this regression model are higher than the regression result for the RAC specimens, where the RSE is only 1.28 %/day$^{0.25}$. The Shapiro-Wilk normality test on the residuals (W = 0.98284, p-value = 0.9544) did not show enough evidence that the residuals are not normally distributed. Furthermore, the studentized Breusch-Pagan test (BP = 3.7472, df =

2, p-value = 0.1536) did not show enough evidence of heteroscedasticity in the regression model.

Table 43

Regression Result for LWACs' Rate of Saturation (%/day0.25) using Bulk Resistivity and Water-Cement Ratio

Intercept	-5.90275* (2.30683)
100/BR	0.24681** (0.08134)
w/c	27.83932*** (5.80461)
Residual standard error (RSE)	2.017 on 19 df
Adjusted R^2	0.6597
p-value	1.38e-05
No. outliers removed	3
Remaining no. observations	22 concrete specimens

Notes: Standard errors are reported in parentheses; *, **, and *** indicate significance levels at 0.05, 0.01, and 0.001, respectively.

Based on the regression results, the rate of water saturation increases by about 0.247 %/day$^{0.25}$ per unit increase in the bulk conductivity (100/BR) and by about 27.839 %/day$^{0.25}$ per unit increase in the water-cement ratio. Including the water-cement ratio as an explanatory variable significantly improved the regression model and reduced the residual standard error to 2.017 %/day$^{0.25}$ from the residual standard error of 2.923 %/day$^{0.25}$ when bulk resistivity was used as the lone predictor. However, the regression model using the formation factor still showed a slightly better model fit with a residual standard error of only 1.906 %/day$^{0.25}$.

5.2.3.3 Using Concrete Air Content and Weighted Coarse Aggregate Porosity.

Surprisingly, regression models for sorptivity and rate of water saturation

without either the formation factor or bulk resistivity returned better results. The air content of the concrete significantly affects the sorptivity measurements in the LWAC, 50LWAC, and NWAC specimens. As summarized in Table 44 and Table 45, a better model fit was generated when the air content of the concrete was used as a predictor.

Table 44

Regression Result for LWACs' Water Sorptivity (mm/day$^{0.25}$) using Weighted CA Porosity and Air Content

Intercept	-0.082341 (0.050499)
$\phi_{WeightedCA}$	0.022338** (0.006692)
Air Content	0.093967*** (0.007768)
Residual standard error (RSE)	0.08647 on 19 df
Adjusted R^2	0.899
p-value	1.34e-10
No. outliers removed	3
Remaining no. observations	22 concrete specimens

Notes: Standard errors are reported in parentheses; *, **, and *** indicate significance levels at 0.05, 0.01, and 0.001, respectively.

Table 45

Regression Result for LWACs' Rate of Saturation (%/day$^{0.25}$) using Air Content

Intercept	0.9790 (0.7270)
Air Content	1.2873*** (0.1106)
Residual standard error (RSE)	1.271 on 20 df
Adjusted R^2	0.8649
p-value	1.641e-06
No. outliers removed	2.326e-10
Remaining no. observations	22 concrete specimens

Notes: Standard errors are reported in parentheses; *, **, and *** indicate significance levels at 0.05, 0.01, and 0.001, respectively.

The sorptivity regression model shows that about 90% of the variance in the sorptivity measurements of LWAC, 50LWAC, and NWAC specimens can be explained by the air content of the concrete and the weighted coarse aggregate porosity, with a residual standard error of only 0.086 mm/day$^{0.25}$. The Shapiro-Wilk normality test on the residuals (W = 0.94816, p-value = 0.2903) did not show enough evidence that the residuals are not normally distributed. Furthermore, the studentized Breusch-Pagan test (BP = 5.7358, df = 2, p-value = 0.05682) did not show enough evidence of heteroscedasticity in the regression model. Based on the model, the sorptivity increases by 0.022 mm/day$^{0.25}$ per unit increase of weighted coarse aggregate porosity and by 0.094 mm/day$^{0.25}$ per unit increase in concrete's air content.

The linear regression model of the lightweight and normalweight concrete's rate of saturation shows that more than 86% of the variance in the rate of water saturation in LWAC, 50LWAC, and NWAC specimens can be explained by the air content of the concrete alone, with a residual standard error of only 1.271 %/day$^{0.25}$. The Shapiro-Wilk normality test on the residuals (W = 0.9398, p-value = 0.196) did not show enough evidence that the residuals are not normally distributed. Furthermore, the studentized Breusch-Pagan test (BP = 2.0353, df = 1, p-value = 0.1537) did not show enough evidence of heteroscedasticity in the regression model. Based on the model, the rate of water saturation increases by 1.287 %/day$^{0.25}$ per unit increase in the concrete's air content.

The air content of concrete significantly affects the water sorptivity and water saturation rate. However, evaluating the concrete permeability based only on fresh concrete properties might be wrong. The formation factor and bulk resistivity

measurements reflect the microstructure of the hardened concrete and therefore are better indicators of the concrete permeability, even with the sorptivity and saturation rate. Furthermore, the effect of air content might be misleading as there is a general trend of increasing air content as the coarse LWA percent replacement and the water-cement ratio increase. When concrete with 100% coarse LWA and a high water-cement ratio was produced with lower air content, the trend of sorptivity with air content might differ.

5.2.4 Linear Regression Models of LWAC, 50LWAC, and NWAC Permeability

To summarize the results of multiple linear regression analyses of the LWAC permeability measurements, the regression equations using formation factor as an explanatory variable for the RCPT, sorptivity, and water saturation rate of LWAC, 50LWAC, and NWAC mixtures are shown in Equations (34) to (36). On the other hand, the regression equations involving bulk resistivity as an explanatory variable are shown in Equations (37) to (39). Individual measurements were used in the regression models based on bulk resistivity. Still, the average predicted values of at least two specimens are suggested to be used as the estimated measurement.

Using formation factor:

$$RCPT = 643.35 + 1875.62\times \frac{1000}{FF} + 261.77 \times \phi_{WeightedCA} \pm \varepsilon_{(34)} \quad (34)$$

$$S = 0.139 + 0.211 \times \frac{1000}{FF} - 0.066 \times \phi_{WeightedCA} + 0.047 \times \frac{1000}{FF} \times \phi_{WeightedCA} \pm \varepsilon_{(35)} \quad (35)$$

$$RS = -2.386 + 3.334 \times \frac{1000}{FF} + 15.170 \times w/c \pm \varepsilon_{(36)} \quad (36)$$

Using bulk resistivity:

$$RCPT = 943.47 + 192.73 \times \frac{100}{BR} - 587.45 \times \phi_{WeightedCA} + 33.47 \times \frac{100}{BR} \times \phi_{WeightedCA} \pm \varepsilon_{(37)} \quad (37)$$

$$S = -0.535 + 0.032 \times \frac{100}{BR} + 1.446 \times (^{w}/_{c}) \pm \varepsilon_{(38)} \quad (38)$$

$$RS = -5.903 + 0.247 \times \frac{100}{BR} + 27.839 \times (^{w}/_{c}) \pm \varepsilon_{(39)} \quad (39)$$

where *RCPT* = total charge passed from RCPT (2080~8430 Coulombs), S = sorptivity (0.210~1.960 mm/day$^{0.25}$), RS = rate of saturation (4.15~28.55 %/day$^{0.25}$), *FF* = formation factor (380~1100), $\phi_{WeightedCA}$ = weighted coarse aggregate porosity (0.2~7.4 %), w/c = water-cement ratio (0.28~0.48), and the normally distributed errors $\varepsilon_{(34)} \sim N(0,730^2)$ Coulombs, $\varepsilon_{(35)} \sim N(0,0.115^2)$ mm/day$^{0.25}$, $\varepsilon_{(36)} \sim N(0,1.906^2)$ %/day$^{0.25}$, $\varepsilon_{(37)} \sim N(0,670^2)$ Coulombs, $\varepsilon_{(38)} \sim N(0,0.142^2)$ mm/day$^{0.25}$, and $\varepsilon_{(39)} \sim N(0,2.017^2)$ %/day$^{0.25}$.

Like in the RAC, the regression equation for the GWT measurements has a poor model fit and therefore was not included in this summary. The high residuals in the GWT measurements were attributed to the high variation in RCPT measurements in concretes with LWA. It also agrees with the observations in Chapter 4, where two-way ANOVA was performed in GWT measurements of LWAC, 50LWAC, and NWAC specimens and

found that the water-cement ratio and its interaction with the coarse LWA percent replacement are not statistically significant.

The RCPT regression equation with bulk resistivity as an explanatory variable has a lower residual standard error than the regression with the formation factor. Using the formation factor as an explanatory variable will result in lower errors in the case of sorptivity and saturation rate regression equations. However, the differences in the respective residual standard errors of the permeability models are small. Like in the RAC specimens, while the formation factor proved to be a better permeability indicator, electrical resistivity is more practical.

5.3 Comparison of Univariate and Multiple Linear Regression of Permeability

To visualize the improvement of the permeability regression models, the plots of the observed versus predicted values are presented below. The y-axis of the plots are the observed or the values measured from the experiments. On the x-axis are the predicted values using the univariate linear regression and the multiple linear regression equations. The closer the data points to the 1:1 line, the better the model. Figure *74* shows slight improvement of the prediction model when additional variables aside from formation factor or electrical resistivity were considered. On the other hand, significant improvements can be observed from Figure *75* to Figure *77*.

For LWAC permeability measurements, Figure 78 and Figure 79 shows slight improvement in the RCPT and sorptivity regression models, respectively, when the weighted coarse aggregate porosity and water-cement ratio were considered as additional predictors. For the GWT and saturation rate multiple linear regression models of LWAC

measurements, there are no significant improvements than when using electrical resistivity or formation factor as a lone predictor.

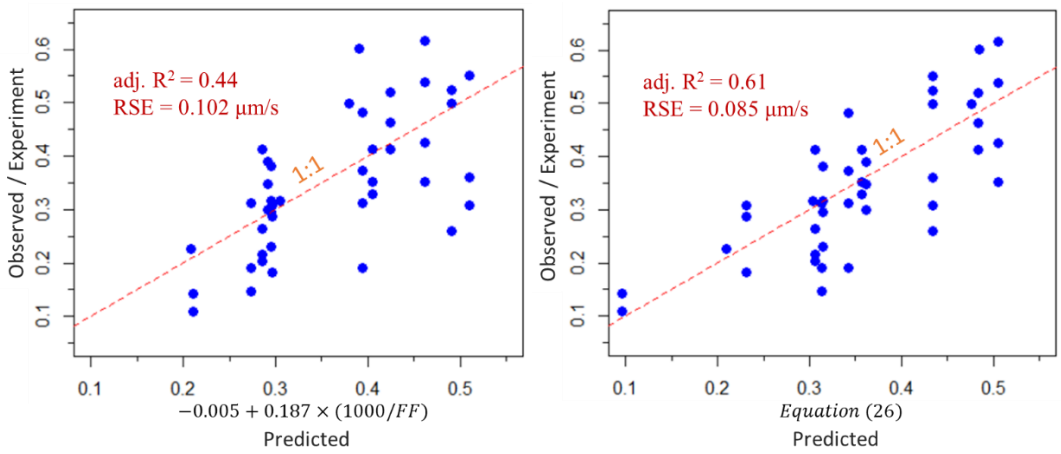

Figure 74. Observed vs. predicted values of GWT measurements in RAC.

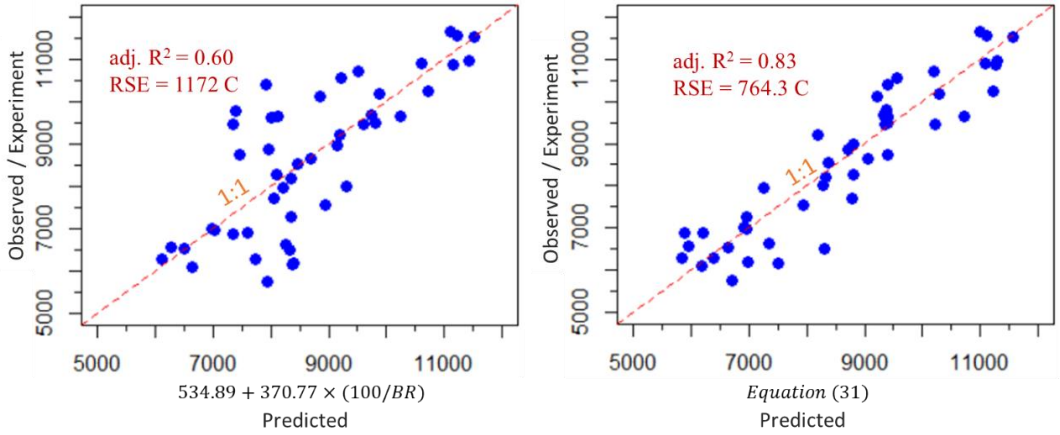

Figure 75. Observed vs. predicted values of RCPT measurements in RAC.

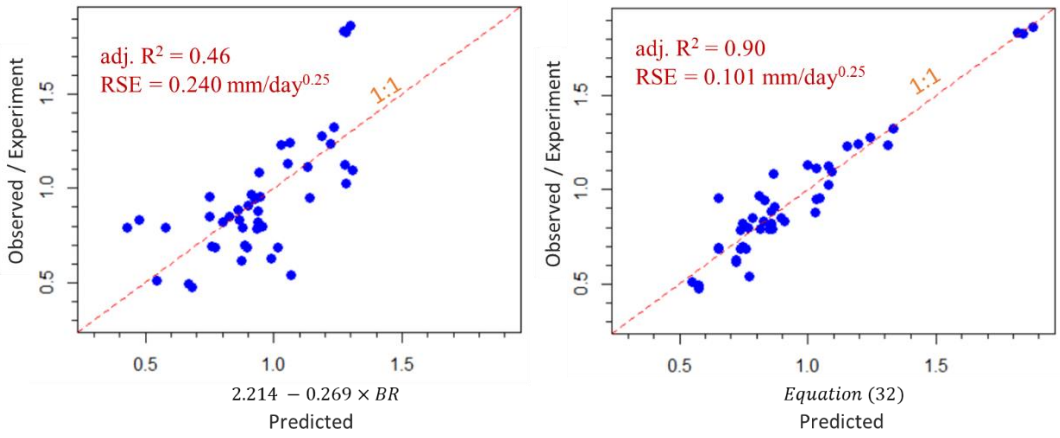

Figure 76. Observed vs. predicted values of water sorptivity measurements in RAC.

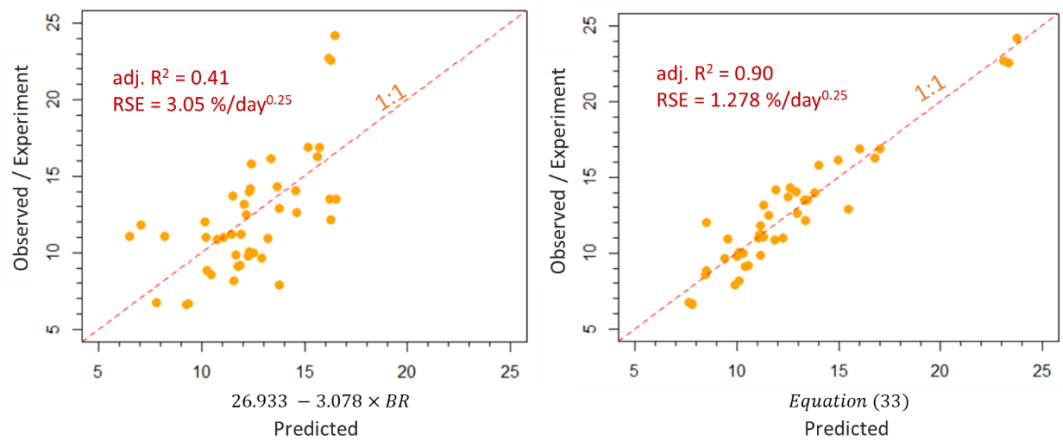

Figure 77. Observed vs. predicted values of water saturation rate in RAC.

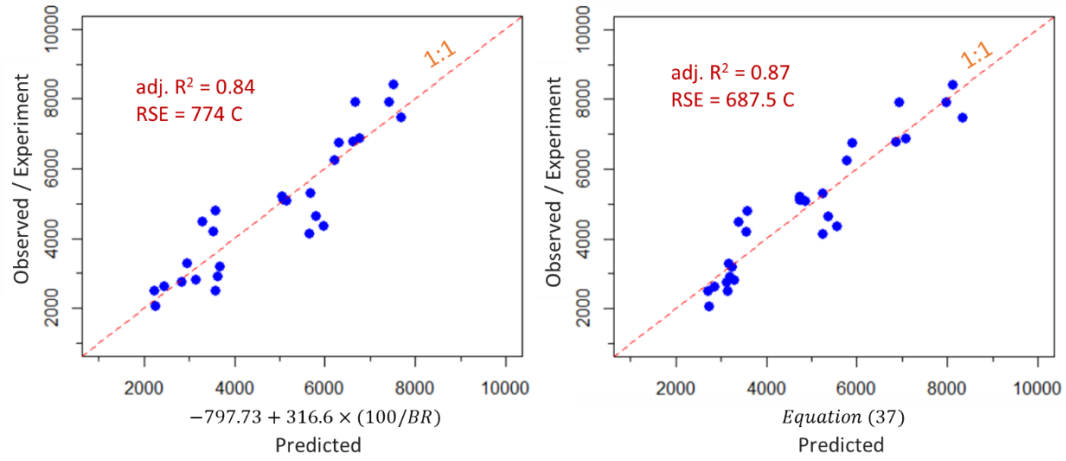

Figure 78. Observed vs. predicted values of RCPT measurements in NWAC, LWAC, and 50LWAC.

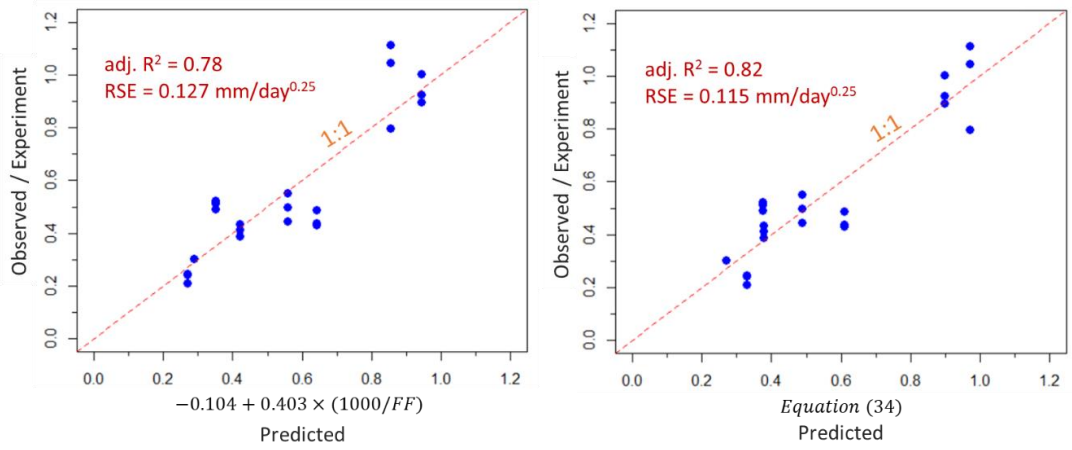

Figure 79. Observed vs. predicted values of water sorptivity in NWAC, LWAC, and 50LWAC.

5.3 Applicability and Limitations of the Permeability Regression Models

The permeability regression models established in this study can be used to quickly compare the quality of 28th day concretes with coarse RCA or LWA. The standard methods of determining the electrical resistivity or formation factor, whichever the user prefers, should be followed. Furthermore, if the specimens were not at room temperature during testing, the temperature correction factor shown in Equation (9) should be applied in the electrical resistivity measurements.

The regression models are only applicable to the range of values observed in this study. The range of values for each variable are already stated in the previous subsections. The interferences specified in the AASHTO and ASTM standards for the electrical resistivity and RCPT measurements should also apply. It includes the effect of admixtures and reinforcements in the electrical resistivity measurements that might produce misleading results.

Chapter 6

Relation to Concrete Permeability of the Air Void Structure and Paste Content Determined using Image Analysis

Determining the air void structure of concrete is vital in evaluating the concrete's durability, particularly against freeze-thaw damage. Standard methods of quantifying the air void system of hardened concrete are provided in ASTM C457, where the air content parameters are determined microscopically. Alternative methods of concrete air void determination were presented by several studies [120, 121, 122, 123, 124, 125] to expedite the process, such as automated air void analysis and the image analysis method. In this study, we developed an image analysis program that could differentiate the concrete components (air voids, cement paste, and aggregates). The program development was discussed in Chapter 3. The image analysis results are presented in this chapter. The relation of the concrete permeability with the air void parameters and paste content was also investigated.

Seven specimens from different concrete mixtures were polished and scanned in a high-resolution scanner at 4800 dots per inch (dpi). The percentage of each concrete component was determined using the image analysis method, including the air content, cement paste, and aggregates. The concrete specimens analyzed include one NWAC (NWAC48), five RAC (0.38-RCA1, 0.38-RCA3, 0.48-RCA2, 0.38-RCA5, and 0.38-RCA8), and one LWAC (LWAC48).

6.1 Determination of Air Void Structure and Cement Paste Content

6.1.1 Image Processing Results

The cement paste was pigmented by spraying phenolphthalein on the polished concrete surface to differentiate the cement paste from the aggregates. The phenolphthalein reacts with the cement paste and turns it pink, thus, separating the paste from the aggregates, which should have remained in its original color. However, some aggregates either reacted to phenolphthalein or were stained by the excess solution in the cement paste; thus, it was hard to segregate them from the cement paste using the developed program. There are also cases where some parts of the cement paste did not significantly change its color. For those specimens, digital editing was done using GIMP, an image manipulation program, to segregate the concrete components better. A sample raw image beside its pre-processed image is shown in Figure *80*. In the raw image, some of the natural aggregates, which are limestone, were stained pink. Furthermore, some of the pastes were still gray. These areas of the cement pastes and aggregates were overlayed by the colors pink and black, respectively.

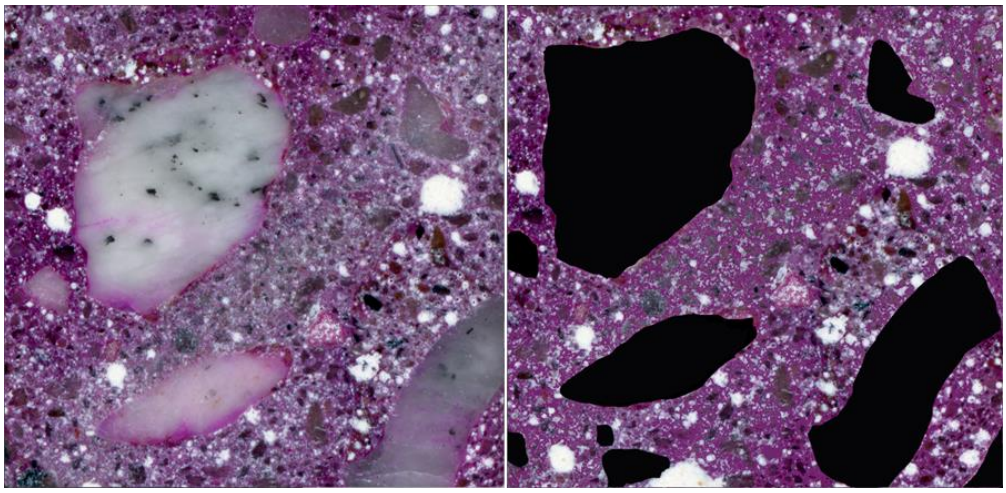

Figure 80. Microscopic images of concrete specimen: (left) original scanned image and (right) pre-processed image in GIMP.

The pre-processed images of concrete were loaded in the image analysis software, and image thresholding was performed using the HSV ranges shown in Table 46. The source and the multilevel (black, white, gray) images of one type each of NWAC, RAC, and LWAC specimens are shown in Figure *81* to Figure *83*. In the multilevel images, the air voids are white, the cement pastes are gray, and the aggregates are black. For the LWAC specimen, it can be observed that the aggregates in the multilevel image are not entirely black in color. The LWA is highly porous and contains large pores. The large pores of LWA were filled by the white powder intended for the air voids in cement paste. As a result, many air voids were found in the multilevel image of LWAC. The digital image was edited, and the LWA areas were filled with black color to analyze the air voids attributed only to the mortar, as shown in Figure *84*. The LWAC images with and without the black-filled aggregates were analyzed separately.

Table 46

Range of Hue, Saturation, Value (HSV) used for Image Thresholding of each Concrete Specimen

Specimen	Air Voids HSV range	Cement Paste HSV range
0.48-NWAC	0-255, 0-255, 200-255	120-255, 30-255, 120-255
0.38-RCA1	0-255, 0-255, 150-255	130-165, 50-255, 50-255
0.38-RCA3	0-255, 0-255, 165-255	100-160, 50-255, 50-255
0.48-RCA2	0-255, 0-255, 175-255	110-165, 50-255, 50-255
0.38-RCA5	0-255, 0-255, 200-255	130-160, 50-255, 100-255
0.38-RCA8	0-255, 0-255, 180-255	120-160, 50-255, 80-255
0.48-LWAC	0-255, 0-255, 190-255	110-255, 0-255, 125-255

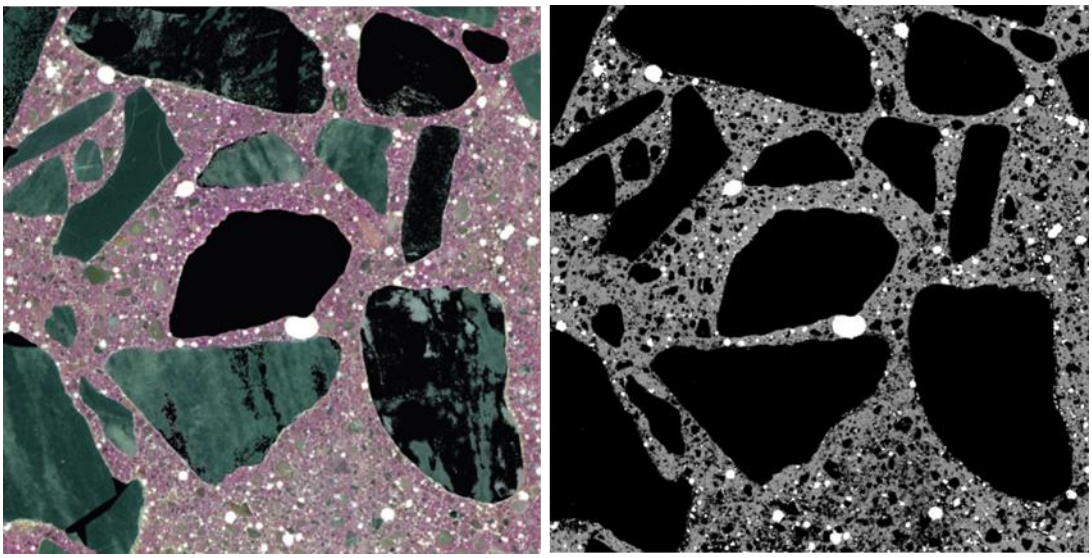

Figure 81. (Left) Source and (right) multilevel images of NWAC specimen.

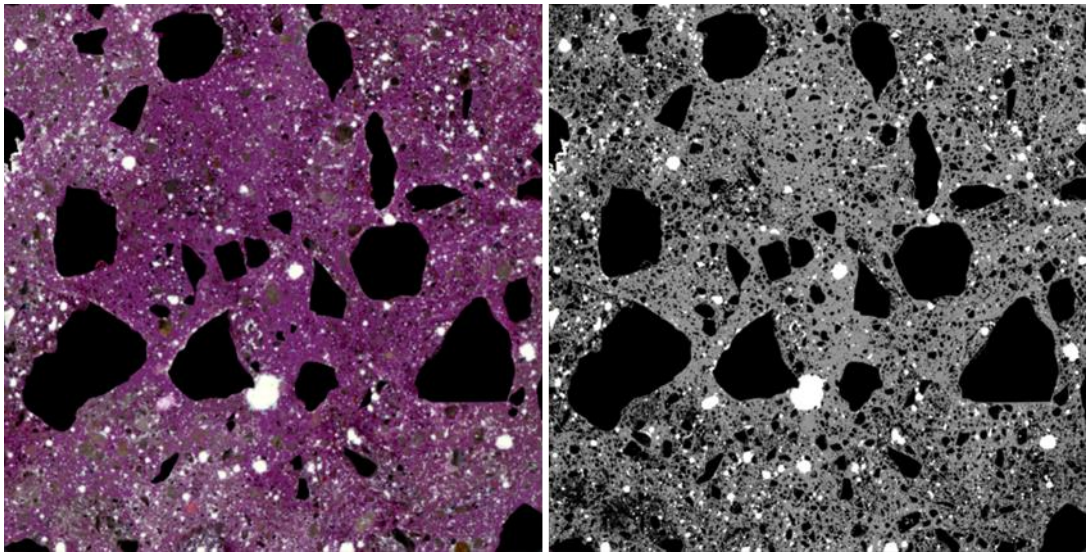

Figure 82. (Left) Source and (right) multilevel images of an RAC specimen, 0.38-RCA8.

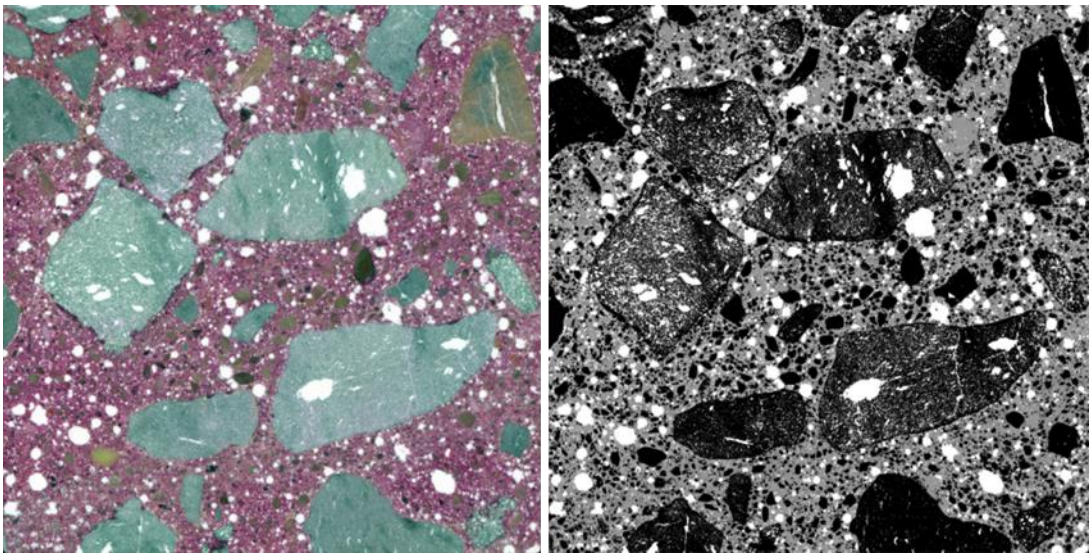

Figure 83. (Left) Source and (right) multilevel images of LWAC specimen.

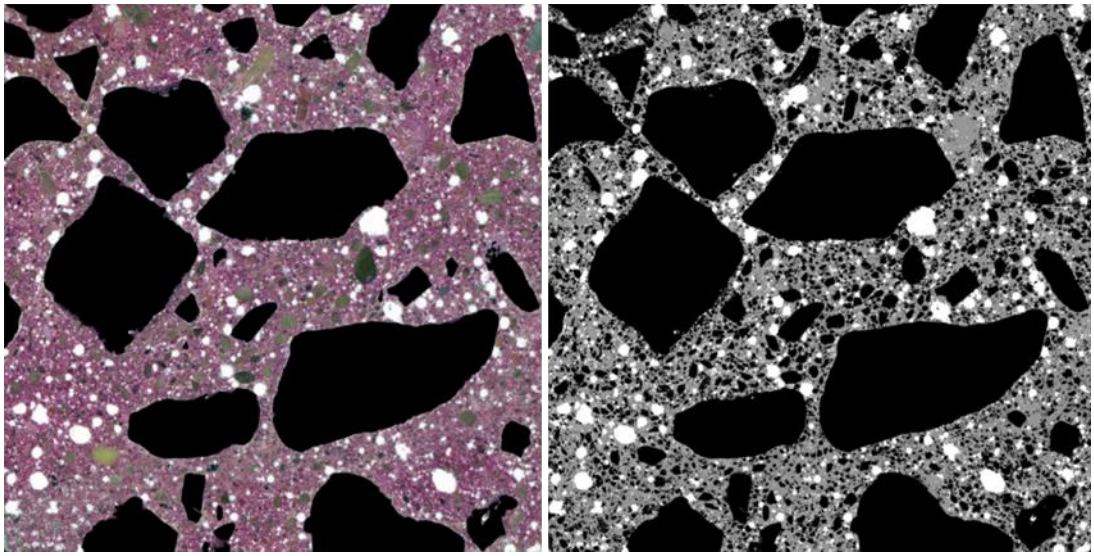

Figure 84. (Left) Source and (right) multilevel images of LWAC specimen with black filled LWA.

6.1.2 Image Analysis Results

The images were analyzed at traverse lengths of 63.5 mm (2.5 in.), line spacing of 0.762 mm (0.03 in.), and a traversed length of more than 5000 mm. The total traversed lengths satisfied the minimum requirements of ASTM C457, 2413 mm and 2286 mm for concrete specimens with maximum aggregate sizes of 25.0 mm and 19.0 mm, respectively. The traversed lines and the total times a void intersected in the image analysis are listed in Table 47. A high number of air void intersects was recorded for the LWAC due to the highly porous coarse aggregate. Of the 7626 air voids intersects, only 2987 were attributed to the cement paste.

Table 47

Total Length of Traverse during Image Analysis

Specimen	Total traversed, Tt (mm)	Total traversed in air, Ta (mm)	Total traversed in paste, Tp (mm)	Total air voids intersect, N
0.48-NWAC	5290.81	278.17	1295.96	2075
0.38-RCA1	5290.81	268.48	2113.93	1646
0.38-RCA3	5290.81	266.41	1643.56	1954
0.48-RCA2	5290.81	443.24	2071.69	3319
0.38-RCA5	5291.25	374.85	2172.81	2063
0.38-RCA8	5290.81	345.89	2363.6	2216
0.48-LWAC	5291.67	855.99	1707.78	7626
0.48-LWAC*	5290.81	485.05	1696.14	2987

*Air voids from the mortar only

6.1.3 Air Void Structure

Using the equations provided in ASTM C457, as also presented in Chapter 3, the concrete air void parameters consist of the air content, void frequency, specific surface of the voids, paste content, paste-air ratio, and the spacing factor. The calculated air void parameters are listed in Table 48. The following interpretation of results was based on the ASTM C457 [108] Appendix:

1. The air void parameters determined from the specimens were in the usual range of values for the air-entrained concretes designed according to ACI 201.2R and ACI 211.1, which are 4~10 paste-air ratio, 25~45 mm^{-1} specific surface, and 0.1 to 0.2 mm spacing factor.
2. Based on the usual evaluation of the spacing factor, most concrete mixtures analyzed can be considered durable to freeze-thaw damage at moderate exposure (max. 200 μm). Three RAC mixtures have more than 200 μm

spacing factor and can be evaluated as adequate for mild exposure. However, the spacing factors of those three RAC specimens are not too far from the 200 μm limit and could be because of sampling and between laboratory variations.

3. The void frequencies measured satisfied the requirements of more than 0.30/mm for satisfactory values of specific surface and spacing factor.

Table 48

Concrete Air Void Parameters

Specimen	Air Content, A (%)	Void frequency, n (mm^{-1})	Specific surface, α (mm^{-1})	Paste content, ρ (%)	Paste-air ratio, ρ/A	Spacing factor, L (μm)
0.48-NWAC	5.26	0.39	29.84	24.49	4.66	150.29
0.38-RCA1	5.07	0.31	24.52	39.95	7.87	232.24
0.38-RCA3	5.04	0.37	29.34	31.06	6.17	173.79
0.48-RCA2	8.38	0.63	29.95	39.16	4.67	149.94
0.38-RCA5	7.08	0.39	22.01	41.06	5.80	225.11
0.38-RCA8	6.54	0.42	25.63	44.67	6.83	208.43
0.48-LWAC	16.18	1.44	35.64	32.27	2.00	55.99
0.48-LWAC*	9.17	0.56	24.63	32.06	3.50	141.96

* Air voids from the mortar only

The air void distributions of the specimens analyzed are shown in Figure *82* to Figure *84*. The small-sized air void sections were detected, which is essential for correctly evaluating air void parameters. The entrained air voids are usually 50 to 200 μm, while the entrapped air voids are larger [7]. Most of the air voids detected are entrained air voids. A high amount of entrapped air voids at 0.5 to 1 mm can be noticed in the specimens. Entrapped air voids as large as 4mm were also found in some concrete mixtures. These large air voids possibly affected the concrete permeability adversely. In

the LWAC48 specimen, the air void distributions with and without the LWA voids were presented. It can be observed from the histogram that more than half of the total number of voids detected were from LWA. If only the mortar is considered, the air void distribution in LWAC is similar to that of NWAC.

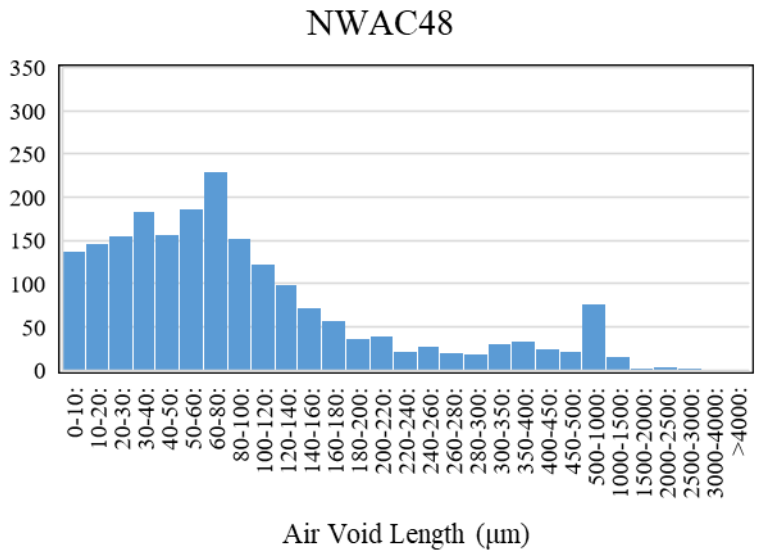

Figure 85. Air voids distribution of NWAC48 specimen.

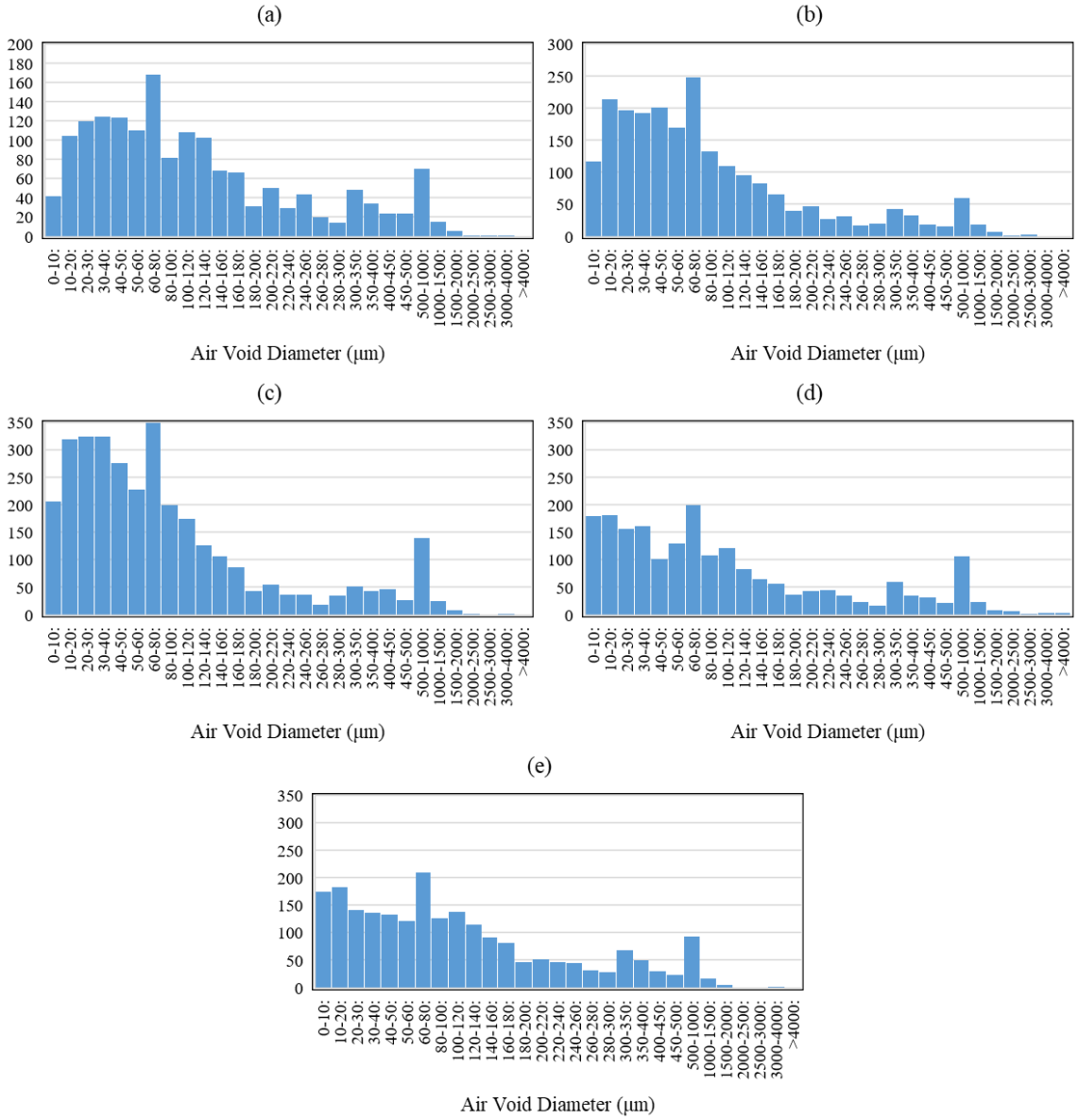

Figure 86. Air voids distribution of RAC specimens: (a) 0.38-RCA1, (b) 0.38-RCA3, (c) 0.48-RCA2, (d) 0.38-RCA5, and (d) 0.38-RCA8.

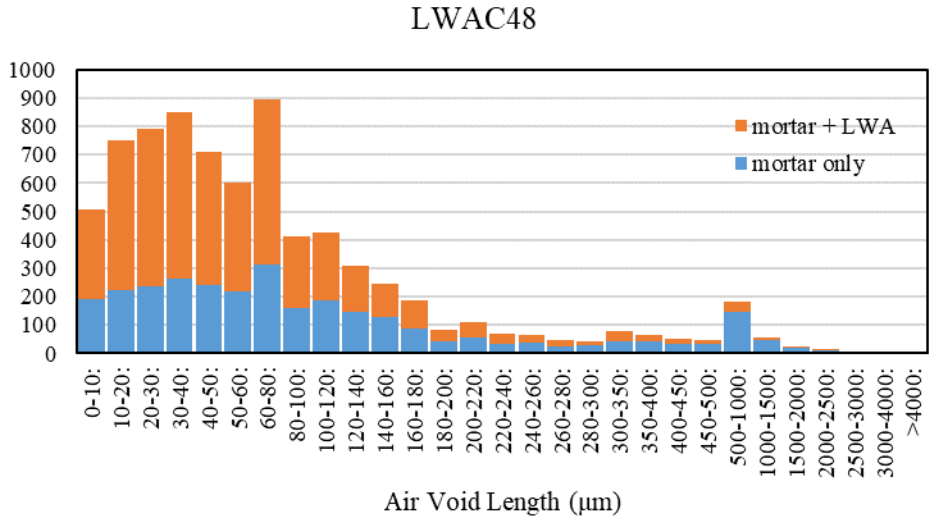

Figure 87. Air voids distribution of LWAC48 specimen considering the total air voids (mortar + LWA) and the air voids in mortar only.

6.1.4 Adjusted Air Void Parameters for LWAC

In the LWAC specimens, there are numerous voids observed inside the aggregates. Identifying the air void parameters by ignoring the voids from the LWA might be adequate to evaluate the performance of cement paste against the freeze-thaw cycle. However, a satisfactory air void structure in the cement paste of LWAC does not mean sufficient freeze-thaw durability in the concrete itself. During the freeze-thaw cycle, the water inside the LWA also expands and develops stress in the LWA pores. As a result, the concrete damage can start from the LWA and propagate to the adjacent mortar causing expansion and damage to the concrete [126].

No studies found suggesting a process for adjustment of air void structure calculations for concrete with coarse LWA. For this study relating the air void structure to the concrete permeability, the spacing factor was adjusted based on the total permeable

area, including the paste and the LWA. Using Equations (*40*) or (*41*), the spacing factor for LWAC48 increased from 55.99μm to 108.71μm. Furthermore, the paste + LWA to air ratio of 3.87 is within the typical values for air-entrained concretes. This adjusted spacing factor was used in the subsequent discussions.

$$\boldsymbol{if}\ (\boldsymbol{p}\&\boldsymbol{L})/\boldsymbol{A}\ <=\ \mathbf{4.342}:$$

$$\boldsymbol{spacing\ factor}\ (\bar{\boldsymbol{L}}), \boldsymbol{in\ mm}\ =\ \frac{(\boldsymbol{p}\&\boldsymbol{L}) \times \boldsymbol{T_t}/\mathbf{100}}{(\mathbf{4}\boldsymbol{N})} \tag{40}$$

$$\boldsymbol{else}:$$

$$\bar{\boldsymbol{L}} = \frac{\mathbf{3}}{\boldsymbol{\alpha}} \times [\mathbf{1.4}\left(\mathbf{1} + \frac{\boldsymbol{p}\&\boldsymbol{L}}{\boldsymbol{A}}\right)^{\frac{\mathbf{1}}{\mathbf{3}}} - \mathbf{1}] \tag{41}$$

where: ρ = paste content (%), L = LWA content (%), A = air content (%), T_t = total traverse length in the image analysis (mm), and N = total voids intersect.

6.1.5 Air Content Determined using Linear Traverse Method

After image scanning, the air voids in the 0.38-RAC1 specimen were also counted under a microscope using the linear traverse machine. The pitch or distance of measurements along the line was set to 0.0254 mm (0.001 in.), and the distance between lines was set to 1.27 mm (0.05 in.). The line spacing was spaced enough to cover the major area of the concrete surface and meet the required traverse length. Tallying the traversed lines in paste was skipped to speed up the process.

The specimen's image was reanalyzed using the same line spacing of 1.27 mm to match the total traversed length in the linear-traverse method. The results of the two methods are shown in Table 49. The air contents calculated in the two methods only

differ by 0.71%, but the number of air voids encountered during the image analysis is much larger than in the linear traverse. The significant difference in air voids intersect could be due to the difference in the pitch along each line. In the linear traverse, the pitch is 25.4 μm, while in the image analysis, where a high-resolution image with 4800 dpi was used, the pitch is equivalent to 5.29 μm. The smaller spacing in the image analysis enables the detection of tiny voids and more precise void edge recognition.

Table 49

Comparison of Linear-Traverse and Image Analysis Results

Method	Total traversed, Tt (mm)	Total traversed in air, Ta (mm)	Total air voids intersect, N	Air Content, A (%)	Void frequency, n (mm^{-1})
Linear-traverse	2844.8	117.7	566	4.14	0.20
Image analysis	3174.48	153.9	963	4.85	0.30

Challenges were encountered in the linear-traverse method. The test method is very tedious and time-consuming. For each tiny movement of the specimen, the user must actuate the tally counter of either void, paste, or aggregate. Since the pitch is small at only 0.0254 mm, a lot of time is needed to satisfy the required traverse of more than 2200 mm. At least 86,615 points are needed to be tallied.

Furthermore, even with the already very small pitch, it is still not enough to accurately tally the length of the air voids. The void edge often fell between the two succeeding index points, and therefore the void edge was not counted. Many small voids,

less than 20 μm, were also not tallied because the pitch was larger. These challenges can be solved using the image analysis method with a high-resolution image of the concrete surface, like in this study.

6.2 Air Void Structure and its Relationship with Concrete Permeability

Several types of concrete permeability were measured in this study, and air content was determined to be a significant factor in the permeability measurements. The relation of the concrete permeability with the air void parameters was determined. All permeability measurements strongly correlate with the hardened concrete's air content determined from the image analysis method. Unlike in the fresh concrete, where only the air voids from the new mortar were considered, the air content determined from the image analysis includes the air voids from the porous aggregates, RCA and LWA. It, therefore, is a better indicator of concrete permeability than the measurements made from fresh concrete. The other air void parameters that showed a strong correlation with concrete permeability are also discussed in this section.

6.2.1 Relation to Formation Factor

The relation of the formation factor with the air content, void frequency, and paste-air ratio are shown in Figure *88*. The formation factor decreases as the air content and void frequency increase. On the other hand, it increases with an increase in the paste-air ratio. The data point for the NWAC in the first plot (a) is below the trendline for RAC. Only the total volume or area of air voids in the concrete was considered in that air content parameter. In the other plots, (b) and (c), the NWAC data point is close to the RAC trendlines. Therefore, it can be inferred that the formation factor can be explained

better by the air void structure, mainly the void frequency and paste-air ratio. Even with the high air content, the formation factor could be higher when the air voids are not closely spaced.

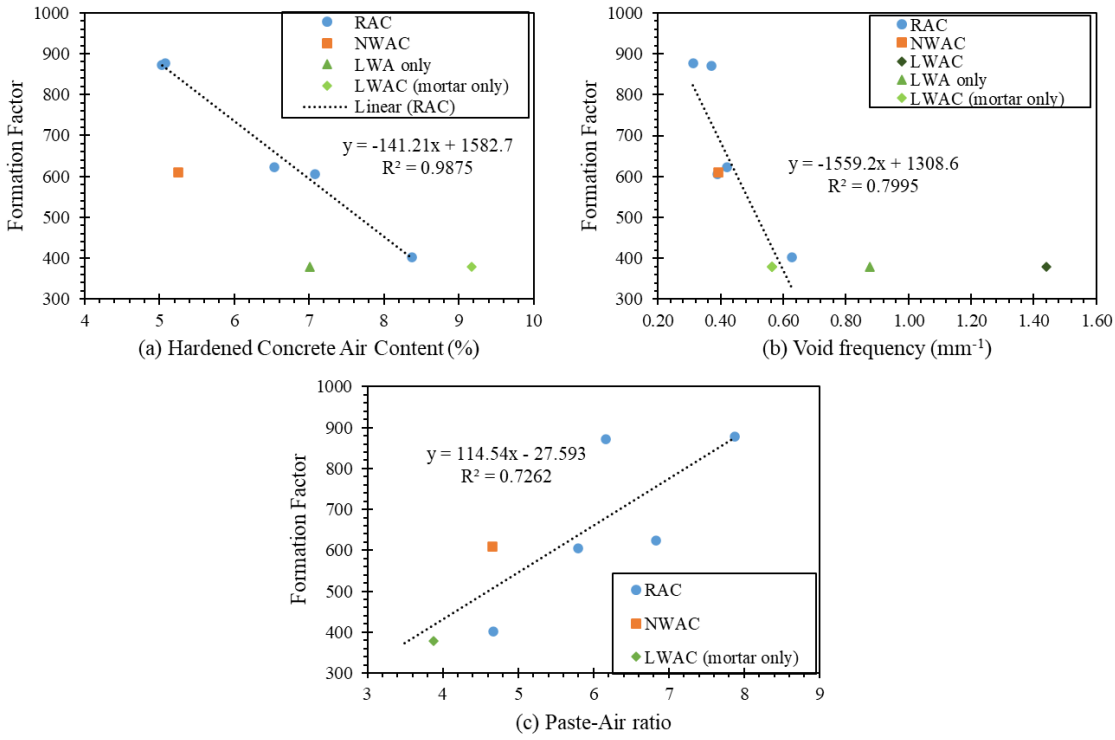

Figure 88. Relation to the formation factor of the (a) hardened concrete air content, (b) void frequency, and (c) paste-air ratio. Trendline shown is for (a) RCA only, (b)(c) RCA, NWAC, and LWAC mortar.

The paste-air ratio parameter also normalized the results of the RAC specimens as the old cement paste in the RCA was considered. Even when the air content in the RAC is higher than NWAC, if the concretes' void frequency and paste-to-cement ratio are the same, their formation factors could be the same too. The data points of LWAC when only

the air voids in the mortar were considered in the calculation are close to the trendline with the RAC data points. On the other hand, the total air content in the LWAC (16.18%) is far from the other data points. It seems that the air void structure in the new mortar can be used to explain the formation factor of LWAC.

6.2.2 Relation to Germann Water Permeability of Air Void Structure

The relationships between the GWT measurements and air void parameters are shown in Figure *89*. A strong linear relationship between the GWT measurements and air content was observed. As discussed in Chapter 4, the LWAC mixtures exhibited very high-water permeability due to the large pores in the LWA. These large pores in LWA were detected in the concrete image analysis and were included in the hardened concrete air content. Based on the plots, it can be inferred that the GWT measurements are dependent on the large voids, more than 5μm, in the concrete, including the air voids in the cement paste and the pores in the aggregates. Furthermore, the GWT measurement increases as the air void frequency increases, suggesting that the water permeability depends not only on the total volume of voids but also on the number of air voids.

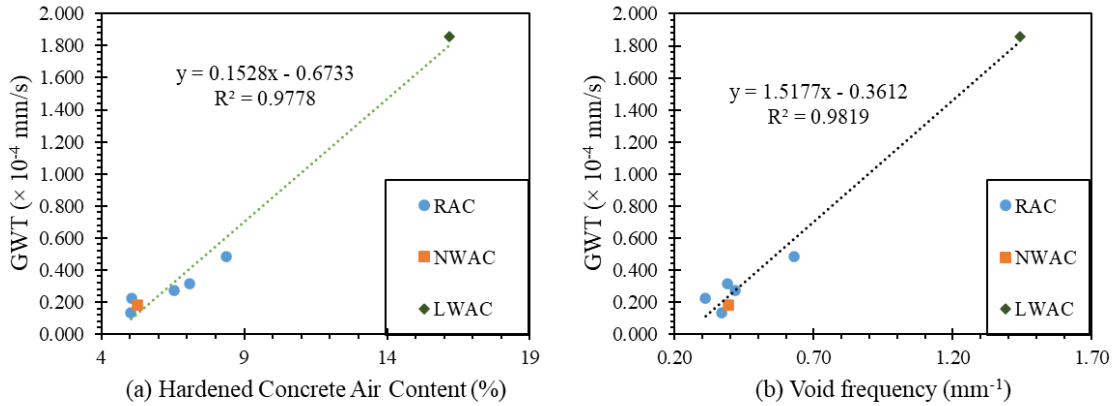

Figure 89. Relation to GWT measurements of the (a) hardened concrete air content and (b) void frequency.

6.2.3 Relation to Rapid Chloride Permeability of Air Void Structure

The relations of the total charge passed in RCPT with the air content, void frequency, and paste-air ratio are shown in Figure *90*. Strong correlations were observed between the RCPT measurements and some of the air void parameters of the RAC specimens. However, the data points for both NWAC and LWAC are far from the RAC trendline. Furthermore, unlike other permeability measurements, the trends in the RCPT measurements with changes in air void parameters are not definite. It seems that the air void structure, including the air voids from the cement paste and the aggregates, is still not enough to explain the variance in RCPT measurements. In plot (d), the paste content measured from image analysis of RAC, NWAC, and LWAC specimens with the same water-cement ratio (0.48) were plotted against their RCPT measurements. It was observed that the RCPT measurements increased linearly with the paste content. The paste content could have represented the amount of capillary voids. Capillary voids are smaller voids in cement paste that were not detected in the image analysis, but still

significantly affects the concrete pore structure. The large capillary voids, larger than 50 nm, could be influential in the strength and permeability of concrete [7].

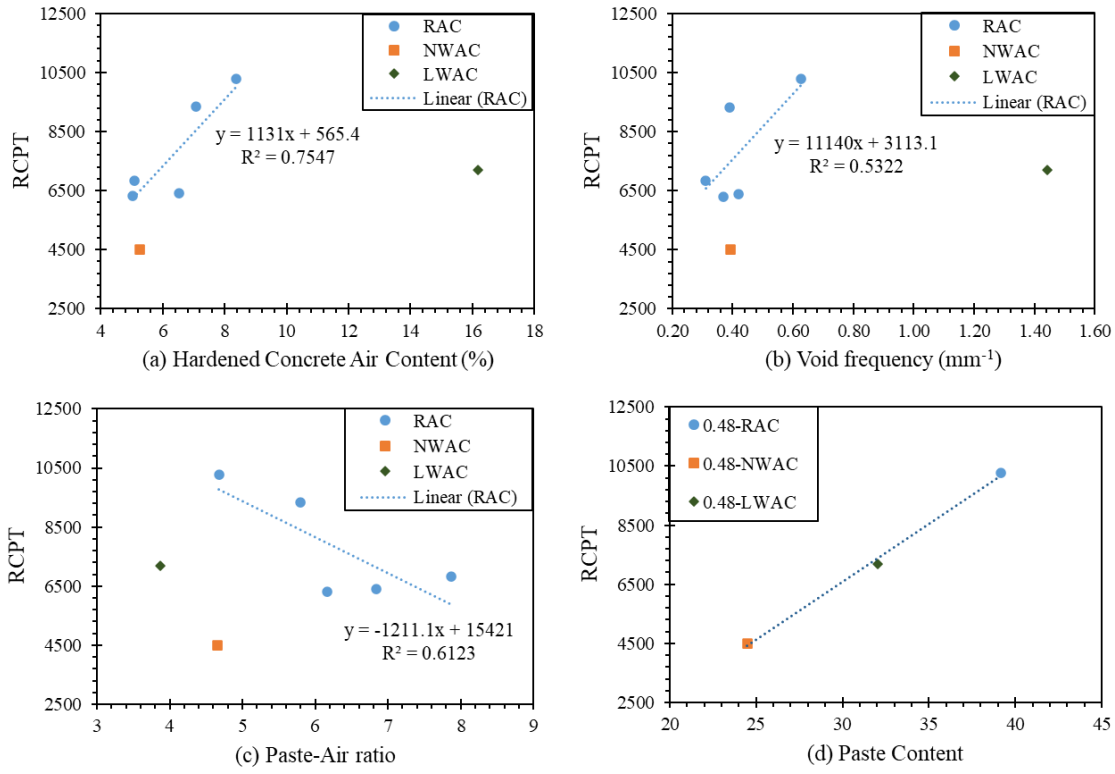

Figure 90. Relation to RCPT measurements of the (a) hardened concrete air content, (b) void frequency, (c) paste-air ratio, and (d) paste content.

6.2.4 Relation to Sorptivity and Rate of Saturation of Air Void Structure

Figure *91* and Figure *92* show the relationship of the sorptivity-based concrete parameters with the air void parameters. High air content and void frequency resulted in higher sorptivity measurements. Similar to the GWT, very high sorptivity measurements were observed in LWAC specimens because of the highly porous LWA. Because of the

voids in LWA, very high air content and void frequency were calculated in LWAC. On the other hand, the sorptivity and saturation rate decreases as the paste-air ratio and spacing factor increase. Even with a higher air content, if the paste content of a particular concrete specimen is also high, like in the RAC specimens, the sorptivity measurement could be lower. Meanwhile, the spacing factor and air content are considered the most important indicators of freeze-thaw durability among the air-void parameters calculated. With their strong correlation to the sorptivity measurements, it supports the findings from the other studies [55, 127] that sorptivity can be used to evaluate the performance of concrete against freezing and thawing exposure.

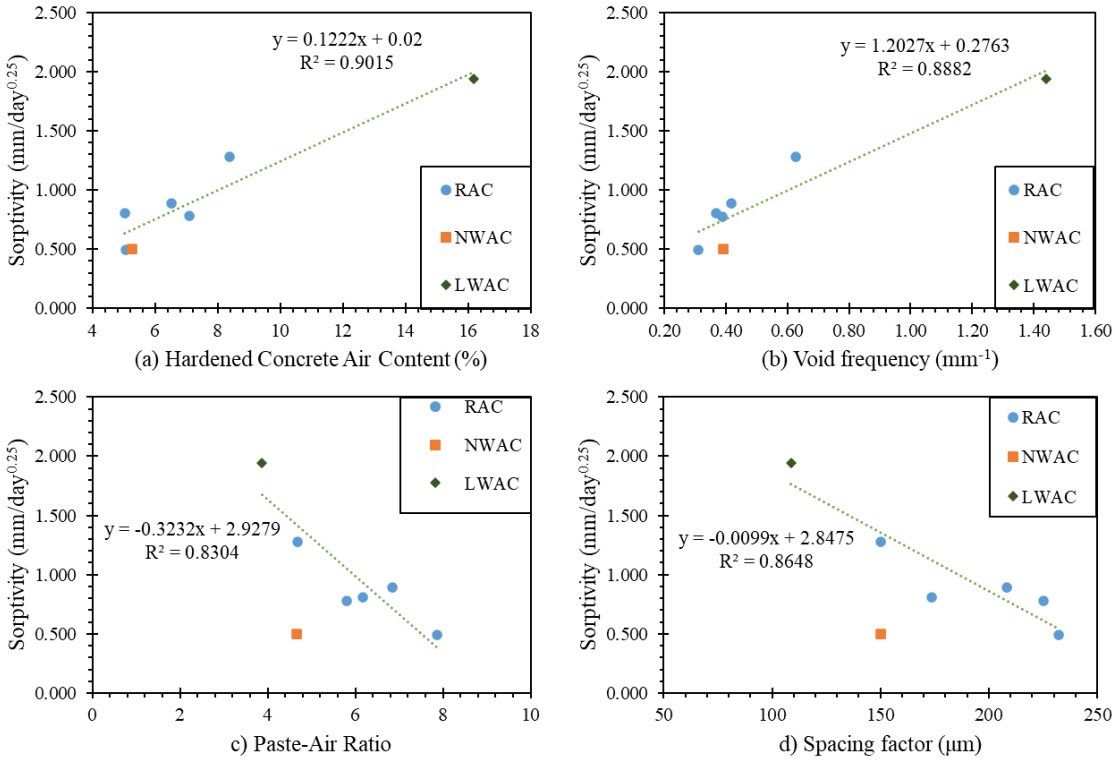

Figure 91. Relation to water sorptivity of the (a) hardened concrete air content, (b) void frequency, (c) paste-air ratio, and (d) spacing factor. NWAC is not included in the trendlines of the (c) and (d) plots.

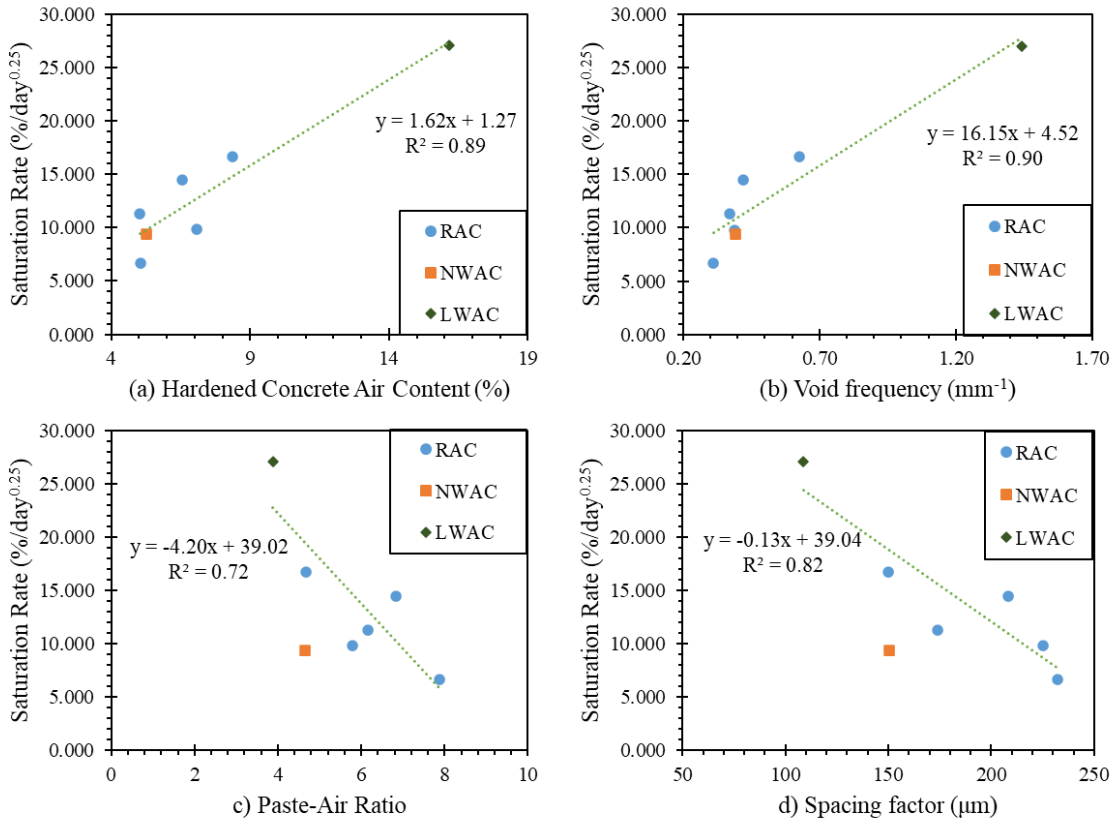

Figure 92. Relation to water saturation rate of the (a) hardened concrete air content, (b) void frequency, (c) paste-air ratio, and (d) spacing factor. NWAC is not included in the trendlines of the (c) and (d) plots.

6.2.5 Water Sorptivity Normalized Based on Total Cement Paste

The mixture proportions of the parent concrete used to produce RCAs in this study are provided in Chapter 3. However, the proportion of the materials in the RCA could be different from its parent concrete due to the removal of fine mortar particles during RCA production. As a result, it is hard to calculate the amount of residual cement paste in RCA and, consequently, the total cement paste in the new concrete, RAC. The image analysis method was able to determine the total cement paste or paste content in RAC specimens, as included in Table 48.

As previously discussed, while the porous aggregate concretes exhibited high permeability, it does not necessarily mean higher fluid penetration, as the aggregates can absorb the fluids or ions. In Figure *93*, the sorptivity measurements were adjusted based on the total permeable area in concrete: the total cement paste for RAC and the cement paste + LWA for LWAC. It can be observed that the increase in sorptivity measurements was reduced when the sorptivity was based on the total permeable area in concrete. The results provide a reason to suspect that the depth of fluid penetration in porous aggregate concretes could be lower than in regular concrete with the same sorptivity.

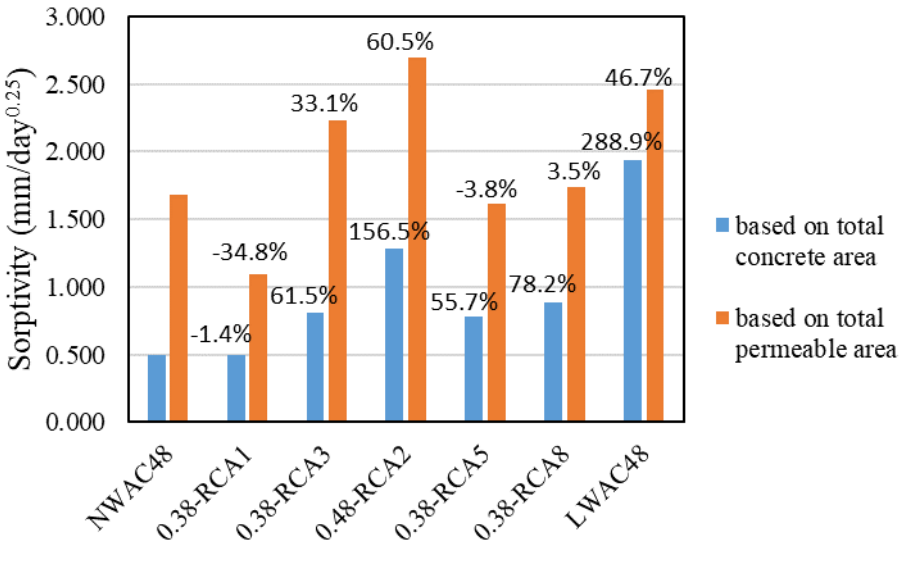

Figure 93. Adjusted water sorptivity based on the total cement paste (NWAC and RAC) and cement paste + LWA (LWAC). Data labels show the percent increase (decrease) compared to NWAC48.

6.3 RCA Residual Cement Paste and Air Content

The established methods of concrete air void analysis in concrete cannot characterize the air void structure and the composition of RAC. RAC is made from recycled concrete aggregates (RCA) and has a more complicated microstructure than conventional concretes. The RAC composition can be divided into five sections: the new cement paste, air voids from the new cement paste, old cement paste from RCA, air voids from RCA, and natural aggregates. The presented method in Chapter 3, which involves digitally editing the concrete images, can calculate the RAC volume components, including RCA's paste and air contents. The estimated RAC components from the image analysis results are summarized in Table 50. The results show that about 1~2.6% of the total air voids of 5~8.5% came from the coarse RCA. Furthermore, 4.9~10.4% of the total cement paste of 31~45% is the residual cement paste from the RCA. On average, about 25% of the total air content and 22% of the total cement paste in RAC are attributed to the RCA.

Table 50

RAC Components Calculated from Image Analysis Results

Specimen	RCA content (%)	A_{RCA} (%)	P_{RCA} (%)	RCA air content	RCA paste content
0.38-RCA1	43.13	1.24	8.70	2.88	20.16
0.38-RCA3	45.16	0.96	6.02	2.12	13.33
0.48-RCA2	39.53	1.52	4.90	3.85	12.40
0.38-RCA5	43.81	2.64	10.38	6.03	23.70
0.38-RCA8	37.20	1.57	9.32	4.21	25.05

Note: A_{RCA} & P_{RCA} = percent of air and paste in the new concrete contributed by the RCA, RCA air & paste content = amount of paste and air per unit volume of RCA.

The values of the RAC components were estimated based on the RCA particles recognized from the RAC images due to their discoloration. The major volume of RCA was determined. The RCA content calculated from the image analysis is compared to the RCA content from the mixture proportion, as shown in Figure *94*. The results from the image analysis are all higher than the RCA content in the mixture proportion by around 17%. This difference could be because of the scanned surface location, around 125mm from the top of the 200mm high concrete cylinders. Due to the difference in the material density, the aggregates tend to settle while the water rises in the concrete specimen. As a result, more aggregates could be present in the bottom part of the concrete specimens.

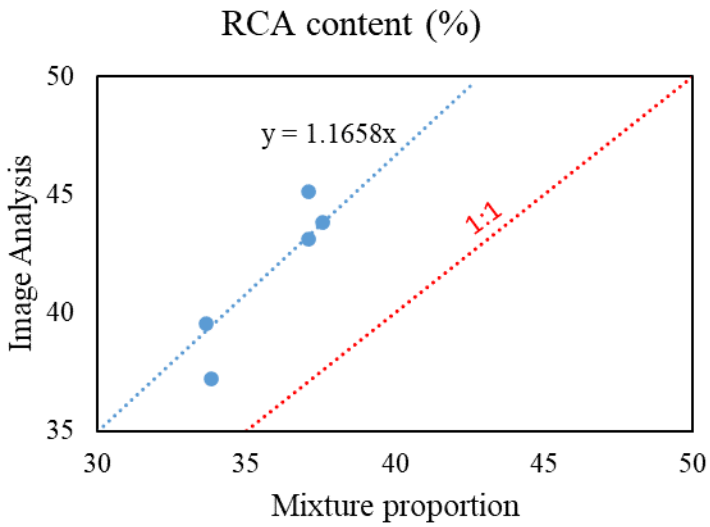

Figure 94. Comparison of RCA content (% Volume) determined from the image analysis and the mixture proportion.

The image analysis results were also compared from the mixture proportion of the RCA's parent concrete, as shown in Figure *95* and Figure *96*. All air and paste contents determined from the image analysis are lower than their respective percent volume in the mixture proportion. Comparing the RCA compositions determined from image analysis to the mixture proportion of their parent concretes, the air and paste contents are lower by about 61% and 67%, respectively. These results support the assumption that the percent of paste and air in the RCA is lower than in the RCA's parent concrete. The decrease in the paste and air content can be attributed to RCA production and screening, where the fine particles of mortar were removed from the bulk of RCA.

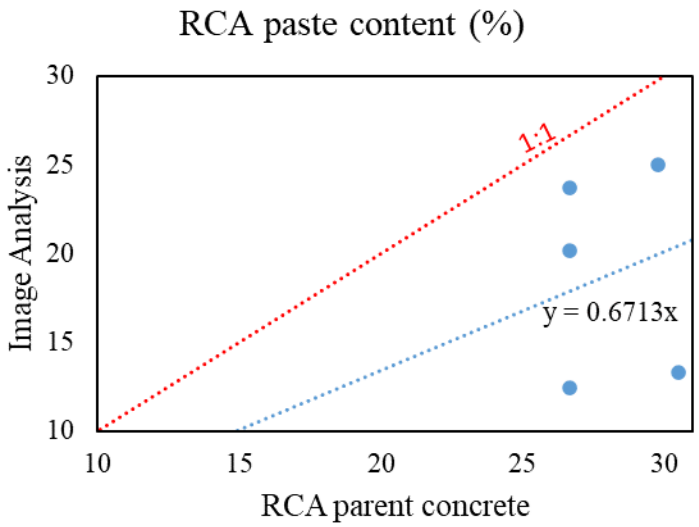

Figure 95. Comparison of RCA paste content determined from the image analysis and the mixture proportion.

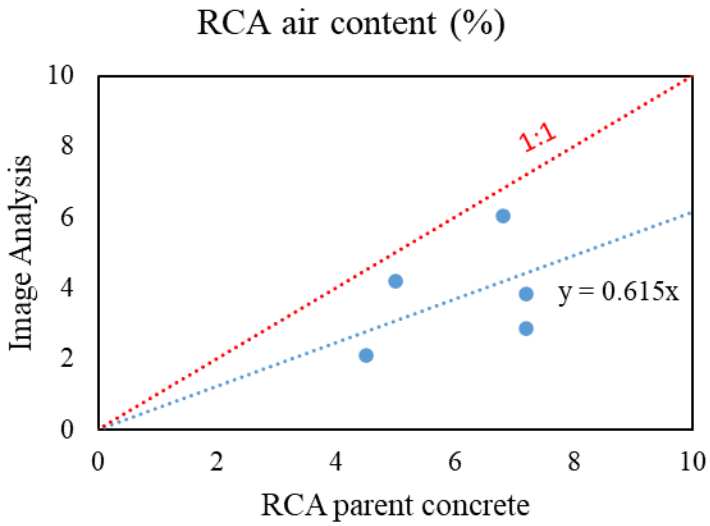

Figure 96. Comparison of RCA air content determined from the image analysis and the mixture proportion.

Chapter 7

Conclusions and Recommendations for Future Work[5]

Sixteen concrete mixtures with 100% recycled concrete coarse aggregate (RAC), three concrete mixtures with 100% coarse lightweight aggregates (LWAC), three concrete mixtures with 50% coarse lightweight aggregates by volume (50LWAC), and three concrete mixtures with all natural and normalweight aggregates (NWAC), were prepared and subjected to different permeability tests. The testing included surface resistivity, bulk resistivity, formation factor, water permeability, rapid chloride permeability, and water sorptivity. Regression analyses were performed to determine if the electrical resistivity-based measurements (surface resistivity, bulk resistivity, and formation factor) could be used to estimate the water permeability, rapid chloride permeability, water sorptivity, and saturation rate of the concrete mixtures. Furthermore, the air void structure of some specimens was analyzed using image analysis. Based on the test results and observations, several conclusions were made. Recommendations based on the results and limitations of this dissertation are provided in this section.

7.1 Conclusions

7.1.1 RAC Permeability

The water-cement ratio and RCA variation significantly affected RAC specimens' electrical resistivity (surface and bulk), formation factor, rapid chloride permeability, water sorptivity, and water saturation rate. RAC can achieve low water permeability

[5] Some parts of this chapter are published in [129, 130, 131]

when a low water-cement ratio is used. However, the effect of RCA variation in GWT measurements was insignificant. The average water flux in RAC specimens measured by GWT is 2.3 to 2.5 times higher than in NWAC.

Very high RCPT measurements were recorded in RAC specimens, which were 2.2~2.6 times higher than NWACs. Due to the very high total charge passed during RCPT, the RAC specimens are considered to have low resistance against chloride ion penetration and, therefore, have a high risk of reinforcement corrosion.

High water absorption, water sorptivity, and saturation rate measurements were observed in RAC specimens. The water sorptivity on RAC specimens was about 1.5~2.4 times higher, while the rate of water saturation was about 1.1~1.7 times higher than that of NWAC specimens. The total cement paste and air content of some RAC specimens were determined using image analysis. It was observed that the differences between the water sorptivity of the RAC and NWAC specimens when adjusted based on the total permeable area (cement paste + air), were significantly reduced. Therefore, there is a good reason to suspect that the fluid penetration in RAC could be lower than in NWAC with the same water sorptivity.

7.1.2 LWAC Permeability

The water-cement ratio and coarse LWA replacement significantly affected LWAC specimens' electrical resistivity (surface and bulk), formation factor, rapid chloride permeability, and water sorptivity. As the percent of porous aggregates, water-cement ratio, or both increases, the average electrical resistivity and formation factor decrease while the average water and chloride permeability increase.

The coarse LWA replacement significantly affected the GWT measurements, but the water-cement ratio was insignificant due to the high variation in measured flux. Very high water permeabilities were measured for concretes with coarse LWA. The water permeability in concretes with 100% coarse LWA was 10% to more than 100% higher than NWAC. As the water-cement ratio decreases, the difference in water permeability of LWAC and NWAC increases. There was only a slight improvement in water permeability when the volume of LWA was reduced to 50%. Therefore, concretes with coarse LWA are not recommended for use in structures subjected to high hydrostatic forces.

High RCPT measurements were also recorded on the LWAC specimens. Compared to NWACs of the same water-cement ratio, concretes with 100% coarse LWA was 1.6~2.7 times higher. The concretes with 50% LWA volume replacement were less permeable and only 1.2~1.6 times higher than NWAC. Most LWACs were evaluated to have low resistance against chloride ion penetration. Still, the chloride permeability decreased when the cement paste was improved by lowering the water-cement ratio to as low as 0.28.

The LWAC specimens recorded the highest sorptivity measurements among the three concrete types. The water sorptivity on LWAC specimens was about 1.8~3.9 times higher, while the rate of water saturation was about 1.2~2.9 times higher than that of NWAC specimens. Significant improvements in water sorptivity-based measurements were observed when the coarse LWA replacement was reduced to 50%. The water sorptivity and saturation rate of concretes with 50% LWA volume replacement were only 0~1.9 and 0~1.5 times higher than of NWAC. The difference in the sorptivity

measurements of LWAC and NWAC decreases as the water-cement ratio decreases. Like in the RAC, the high absorption of LWA suggests that there could be lower fluid penetration in LWAC than in NWAC with the same sorptivity.

7.1.3 Relations of Permeability to Electrical Resistivity-Based Properties

There is a very strong correlation between surface and bulk resistivity, where the surface resistivity measurements are about 1.84 times higher than bulk resistivity measurements. Moderate to strong negative linear relationships were observed between the permeability measurements and electrical resistivity/formation factor. Based on the correlation coefficients, the formation factor is a better indicator of the concrete's water permeability, sorptivity, and saturation rate than the electrical resistivity (surface or bulk). However, the differences in their correlation coefficients were minimal. Considering the additional work required to determine the formation factor, the electrical resistivity measurements are still a good and a more practical indicator of concrete's permeability. Moreover, the electrical resistivity measurements are still better indicators of rapid chloride permeability than the formation factor.

Differences in linear regressions of permeability with the electrical resistivity/formation factor of the three concrete types were observed. At the same formation factor, the water permeability of concretes with LWA is significantly higher than concretes with RCA. While both aggregates are porous, the larger pores of LWA made fluid flow into concrete easier. On the other hand, the tiny and tortuous pore structure of the RCA's adhered mortar resulted in lower water permeability.

While the LWAC and NWAC have a similar trend for the increase in RCPT measurement per unit increase of surface conductivity, the trend for RAC is higher. At the same electrical resistivity, the RCPT measurement of RAC is higher than the lightweight and normalweight concretes. The higher results were attributed to the increased total mortar in RAC, which may have provided more flow paths for the ionic migration.

The linear regression of the water sorptivity and saturation rate of all concrete types with the electrical resistivity/formation factor can be expressed on a single trendline. For every unit increase of the inverse of the formation factor (1000/FF), the water sorptivity increases by about 0.60 $mm/day^{0.25}$, while the rate of saturation increases by about 7.27 $\%/day^{0.25}$.

7.1.4 Permeability Regression Models

The permeability regression models with the electrical resistivity-based measurements as primary predictors improved when multiple linear regression was performed. For RAC regression models, the RCA parent concrete properties, RCA properties, and fresh concrete properties of RAC were considered as additional explanatory variables. The GWT measurements in RAC can be estimated using the formation factor/surface resistivity, RAC air content, and residual mortar (mortar in the RCA parent concrete) air content. On the other hand, the bulk resistivity and the RAC fresh concrete properties, including the slump, air content, and density, can estimate the RCPT measurements in RAC. Lastly, the sorptivity and saturation rate of RAC can be

calculated using the formation factor/bulk resistivity, RAC air content, RCA residual mortar air content, and the volume of RCA in the new RAC mixture.

For the other concretes investigated, with 0%, 50%, and 100% coarse LWA replacement by volume, the permeability regression models, except GWT, improved when the weighted coarse aggregate porosity and water-cement ratio were added as explanatory variables. The RCPT measurements can be estimated using surface resistivity and weighted coarse aggregate porosity. The sorptivity and saturation rate can be calculated using the formation factor/bulk resistivity, weighted coarse aggregate porosity, and water-cement ratio. On the other hand, the regression model for GWT measurements did not improve even with the addition of explanatory variables. It can be attributed to the high variability of GWT measurements within each group.

The multiple regression models generated in this study can be used to quickly estimate the Germann water permeability, rapid chloride permeability, water sorptivity, and water saturation rate in porous aggregate concretes. The estimated values can be used to compare or evaluate the permeability of concrete mixtures with RCA or LWA.

7.1.5 Concrete Air Void Structure

The image processing method developed in this dissertation was able to quantify the air void structure of the porous aggregate concretes. Air voids were found in the residual mortar of RCA. Large voids were also observed in LWA, affecting LWAC specimens' permeability. The air content of the hardened concrete determined from image analysis included the air voids from the RCA and the large voids from the LWA.

The air content (percent area of air voids in the concrete) and the void frequency (number of air voids per unit length of concrete) had strong positive linear relationships with the GWT, RCPT, sorptivity, and saturation rate. Therefore, the number of air voids significantly affects the concrete permeability. The paste-air ratio was also strongly correlated with the RCPT measurements. The RCPT measurements increased linearly with the paste content, which explains why very high RCPT measurements were observed in RAC specimens.

Based on the typical values of the spacing factor in air-entrained concretes, most concrete mixtures analyzed, including RAC and LWAC specimens, can be considered durable to freeze-thaw damage at moderate exposure. The spacing factors have strong negative linear relationships with the sorptivity and saturation rate. Their strong correlation supports the findings from the literature that the sorptivity measurements are related to concrete durability against freeze-thaw damage.

7.2 Recommendations for Future Work

Based on the results and limitations of this study, recommendations for future work are discussed below.

7.2.1 RAC and LWAC with Reduced Permeability

The concrete mixtures in this study were produced at varying water-cement ratios resulting in a range of permeability measurements. Expectedly, the permeability of RAC and LWAC mixtures was higher than in NWAC. Several studies have already shown how to improve the permeability of RAC and LWAC mixtures. The permeability of porous

aggregate concretes can be decreased by improving the cement paste quality using superplasticizers and SCMs [24, 25, 92, 23, 128]. The RAC permeability can also be enhanced by several RCA treatments, such as carbonation [26] and soaking in pozzolan slurry [29]. Developing another permeability regression model, including the porous aggregate concretes with lower permeability than what was measured in this study, is recommended.

7.2.2 Relation of Permeability to Fluid Penetration Tests

Another limitation of this research is that the liquid penetration was not physically measured. While the permeability measurements can be used to compare the quality of the same types of concrete, the durability of RAC and LWAC specimens is not directly comparable to that of NWAC. This study shows that some relationships between the permeability measurements of RAC and LWAC differ from those of NWAC. The equivalent fluid penetration at the same permeability between the three concrete types might differ. There is a good reason to suspect that the penetration depth of fluid in RAC and LWAC will be lower when compared to NWAC with the same permeability. Therefore, a study relating permeability to fluid penetration is highly suggested. This recommended study will be able to evaluate the porous aggregate concrete's durability.

7.2.3 Machine Learning on Image Analysis

The image analysis software developed for this dissertation was able to calculate the percent of voids, cement paste, and aggregates in the concrete. The color values of the components were used as the basis for image segmentation. However, this method was challenging. The results depend on how accurately the user can threshold the images as

close to the original. Furthermore, some cement paste did not significantly change its color to pink, while some aggregates were stained by the pigment. As a result, it was hard to separate the paste from the aggregates based on color values, and the image needed to be edited digitally.

Machine learning-based image processing is recommended for a simpler and more accurate calculation of hardened concrete components, including the air void structure. The air voids can be determined by their circular shape and depth. The aggregates come in different colors depending on the rock origin but can be recognized by their angular shape. On the other hand, the shape of cement paste is irregular as the boundaries are not well-defined. The machine can be trained with segmented images of air voids and aggregates. If the air voids and aggregates can be recognized, the image's remaining parts can be considered cement paste. With machine learning-based image analysis, pigmenting the cement paste and filling air voids with white powder might not be necessary.

References

[1] Concrete Institute of Australia, "Concrete Durability Series Z7/07 Performance Tests to Assess Concrete Durability," Concrete Institute of Australia, North Sydney, Australia, 2015.

[2] H. Beushausen and L. Fernandez Luco, Eds., Performance-Based Specifications and Control of Concrete Durability: State-of-the-Art Report RILEM TC 230-PSC, 1st ed., Dordrecht: Springer Netherlands, 2016.

[3] F. Andrews-Phaedonos, "Test methods for the assessment of durability of concrete," in *23rd ARRB Conference – Research Partnering with Practitioners*, Adelaide Australia, 2008.

[4] L. Basheer, J. Kropp and D. J. Cleland, "Assessment of the durability of concrete from its permeation properties: a review," *Construction and Building Materials,* vol. 15, pp. 93-103, 2001.

[5] P. M. Basheer, "16 - Permeation Analysis," in *Handbook of Analytical Techniques in Concrete Science and Technology*, William Andrew Publishing/Noyes, 2001, p. 658–737.

[6] D. Whiting, "Permeability of Selected Concrete," *ACI Special Publication SP-108 Permeability of Concrete,* pp. 195-222, 1987.

[7] P. K. Mehta and P. J. M. Monteiro, Concrete: microstructure, properties, and materials, 4th ed. ed., New York: McGraw-Hill Professional, 2014.

[8] American Association of State Highway and Transportation Officials, "Standard Method of Test for Surface Resistivity Indication of Concrete's Ability to Resist Chloride Ion Penetration (AASHTO T358-15)," AASHTO, Washington, D.C., 2015.

[9] American Association of State Highway and Transportation Officials, "Standard Method of Test for Electrical Resistivity of a Concrete Cylinder Tested in a Uniaxial Resistance Test (AASHTO TP 119-15)," AASHTO, Washington, D.C., 2015.

[10] J. Gudimettla and G. Crawford, "Resistivity Tests for Concrete—Recent Field Experience," *ACI Materials Journal*, vol. 113, no. 4, pp. 505-512, July-August 2016.

[11] C. M. Tibbetts, J. M. Paris, C. C. Ferraro, K. A. Riding and T. G. Townsend, "Relating water permeability to electrical resistivity and chloride penetrability of concrete containing different supplementary cementitious materials," *Cement and Concrete Composites,* vol. 107, 2020.

[12] A. A. Ramezanianpour, A. Pilvar, M. Mahdikhani and F. Moodi, "Practical Evaluation of Relationship Between Concrete Resistivity, Water Penetration, Rapid Chloride Penetration and Compressive Strength," *Construction and Building Materials*, vol. 25, no. 5, p. 2472–2479, 2011.

[13] A. Jenkins, "Surface Resistivity as an Alternative for Rapid Chloride Permeability Test of Hardened Concrete," Report No.: FHWA-KS-14-15. Kansas Department of Transportation. Bureau of Materials & Research, Topeka, 2015.

[14] M. Almarshoud, H. Mosavi, R. Alrashidi, M. H. M. Alyami, C. C. Ferraro, H. D. DeFord and K. A. Riding, "Use of Electrical Resistivity-Based Tests for Concrete Penetrability Measurement," *ACI Materials Journal*, vol. 118, no. 1, pp. 21-30, 2021.

[15] J. Tanesi, L. Montanari and A. Ardani, "Formation Factor Demystified and its Relationship to Durability," Federal Highway Administration, 2019.

[16] W. J. Weiss, R. P. Spragg, O. B. Isgor, M. T. Ley and T. Van Dam, "Toward Performance Specifications for Concrete: Linking Resistivity, RCPT and Diffusion Predictions Using the Formation Factor for Use in Specifications," in *High Tech Concrete: Where Technology and Engineering Meet*, 2017.

[17] G. E. Archie, "The Electrical Resistivity Log as an Aid in Determining Some Reservoir Characteristics," *Transactions of American Institute of Mining Metallurgical Engineers*, vol. 146, p. 54–62, 1942.

[18] ASTM C1876, "Standard Test Method for Bulk Electrical Resistivity or Bulk Conductivity of Concrete," ASTM International, West Conshohocken, PA, 2019.

[19] National Institute of Standards and Technology, "Estimation of Pore Solution Conductivity," 15 February 2022. [Online]. Available: https://www.nist.gov/el/materials-and-structural-systems-division-73100/inorganic-materials-group-73103/estimation-pore.

[20] C. Qiao, M. K. Moradllo, H. Hall, M. T. Ley and J. Weiss, "Electrical Resistivity and Formation Factor of Air-Entrained Concrete," *ACI MATERIALS JOURNAL*, vol. 116, no. 3, pp. 85-93, 2019.

[21] J. Xiao, Recycled Aggregate Concrete Structures, Berlin, Germany: Springer Tracts in Civil Engineering, 2018.

[22] R. Zaharieva, F. Buyle-Bodin, F. Skoczylas and E. Wirquin, "Assessment of the surface permeation properties of recycled aggregate concrete," *Cement & Concrete Composites*, vol. 25, pp. 223-232, 2003.

[23] R. Majhi and A. Nayak, "Bond, durability and microstructural characteristics of ground granulated blast furnace slag based recycled aggregate concrete," *Construction and Building Materials,* vol. 212, p. 578–595, 2019.

[24] D. Pedro, J. de Brito and L. Evangelista, "Durability performance of high-performance concrete made with recycled aggregates, fly ash and densified silica fume," *Cement and Concrete Composites,* vol. 93, p. 63–74, 2018.

[25] R. Somna, C. Jaturapitakkul and A. Amde, "Effect of ground fly ash and ground bagasse ash on the durability of recycled aggregate concrete," *Cement & Concrete Composites,* vol. 34, p. 848–854, 2012.

[26] D. Xuan, B. Zhan and C. S. Poon, "Durability of recycled aggregate concrete prepared with carbonated recycled concrete aggregates," *Cement and Concrete Composites,* vol. 84, pp. 214-221, 2017.

[27] V. Spaeth and A. D. Tegguer, "Improvement of recycled concrete aggregate properties by polymer treatments," *International Journal of Sustainable Built Environment,* vol. 2, no. 2, pp. 143-152, 2013.

[28] A. M. Grabiec, J. Klama, D. Zawal and D. Krupa, "Modification of recycled concrete aggregate by calcium carbonate biodeposition," *Construction and Building Materials,* vol. 34, pp. 145-150, 2012.

[29] W. M. Shaban, J. Yang, H. Su, Q.-f. Liu, D. C. Tsang, L. Wang, J. Xie and L. Li, "Properties of recycled concrete aggregates strengthened by different types of pozzolan slurry," *Construction and Building Materials,* vol. 216, pp. 632-647, 2019.

[30] Standard Terminology Relating to Concrete and Concrete Aggregates, "ASTM C125 − 19," ASTM International, West Conshohocken, PA, 2019.

[31] W. H. Wolfe, "Designing with Lightweight Concrete," *STRUCTURE magazine,* pp. 10-12, April 2008.

[32] T. Lo and H. Cui, "Effect of porous lightweight aggregate on strength of concrete," *Materials Letters,* vol. 58, no. 6, pp. 916-919, February 2004.

[33] H. Satpathy, S. Patel and A. Nayak, "Development of sustainable lightweight concrete using fly ash cenosphere and sintered fly ash aggregate," *Construction and Building Materials,* vol. 202, p. 636–655, 2019.

[34] S. Real and J. A. Bogas, "Oxygen permeability of structural lightweight aggregate concrete," *Construction and Building Materials,* p. 21–34, 2017.

[35] K. S. Chia and M.-H. Zhang, "Water permeability and chloride penetrability of high-strength lightweight aggregate concrete," *Cement and Concrete Research,* vol. 32, p. 639–645, 2002.

[36] K.-S. Youm, J. Moon, J.-Y. Cho and J. J. Kim, "Experimental study on strength and durability of lightweight aggregate concrete containing silica fume," *Construction & Building Materials,* vol. 114, pp. 517-527, 2016.

[37] S. Chandra and L. Berntsson, Lightweight Aggregate Concrete Science, Technology, and Applications, Norwich, New York: William Andrew Publishing / Noyes, 2003.

[38] T. Holm, T. Bremner and J. Newman, "Concrete Bridge Decks: Lightweight Aggregate Concrete Subject to Severe Weathering," *Concrete International,* vol. 6, no. 6, pp. 49-54, 1984.

[39] X. Liu, K. S. Chia and M.-H. Zhang, "Water absorption, permeability, and resistance to chloride-ion penetration of lightweight aggregate concrete," *Construction and Building Materials,* vol. 25, no. 1, pp. 335-343, January 2011.

[40] M. Gesoğlu, E. Güneyisi, T. Özturan, H. Ö. Öz and D. S. Asaad, "Permeation characteristics of self compacting concrete made with partially substitution of natural aggregates with rounded lightweight aggregates," *Construction and Building Materials,* pp. 1-9, 2014.

[41] J. F. Young, "Review of the Pore Structure of Cement Paste and Concrete and its Influence on Permeability," *ACI Symposium Publication,* vol. 108, pp. 1-18, 1988.

[42] S. Patel, R. Majhi, H. Satpathy and A. Nayak, "Durability and microstructural properties of lightweight concrete manufactured with fly ash cenosphere and sintered fly ash aggregate," *Construction and Building Materials,* vol. 226, p. 579–590, 2019.

[43] M. Almarshoud, H. Mosavi, R. Alrashidi, M. H. M. Alyami, C. C. Ferraro, H. D. DeFord and K. A. Riding, "Use of Electrical Resistivity-Based Tests for Concrete Penetrability Measurement," *ACI Materials Journal,* vol. 118, no. 1, pp. 21-30, 2021.

[44] C. M. Tibbetts, J. M. Paris, C. C. Ferraro, K. A. Riding and T. G. Townsend, "Relating water permeability to electrical resistivity and chloride penetrability of concrete containing different supplementary cementitious materials," *Cement and Concrete Composites,* vol. 107, 2020.

[45] American Concrete Institute, "ACI Concrete Terminology (ACI CT-21)," American Concrete Institute, Farmington Hills, MI, 2021.

[46] T. C. Powers, "The Physical Structure and Engineering Properties of Concrete," *Portland Cement Association,* 1958.

[47] J. Weiss, "Relating Transport Properties to Performance in Concrete Pavements," 2014.

[48] P. Mehta, "Mechanism of sulfate attack on portland cement concrete — Another look," *Cement and Concrete Research,* vol. 13, no. 3, pp. 401-406, 1983.

[49] ACI Committee 318, "Building Code Requirements for Structural Concrete (ACI 318-14)," American Concrete Institute, 2014.

[50] Y. Bu, R. Spragg and W. Weiss, "Comparison of the Pore Volume in Concrete as Determined Using ASTM C642 and Vacuum Saturation," *Advances in Civil Engineering Materials,* vol. 3, 2014.

[51] T. D. Long, C. Franck and M. Michel, "Impact of the Porosity of Coarse Aggregates on the Structuration of the Paste-Aggregate Interface: Elementary Model Study," in *Ha-Minh, C., Dao, D., Benboudjema, F., Derrible, S., Huynh, D., Tang, A. (eds) CIGOS 2019, Innovation for Sustainable Infrastructure. Lecture Notes in Civil Engineering, vol 54*, Springer, Singapore, 2020.

[52] ASTM C1585, "Standard Specification for Measurement of Rate of Absorption of Water by Hydraulic-Cement Concretes," ASTM International, West Conshohocken, PA, 2013.

[53] R. J. Rohne, "Effect of Concrete Materials on Permeability of Concrete Mixes Used in Mn/DOT Paving Projects," Minnesota Department of Transportation, St. Paul, Minnesota, 2009.

[54] ASTM C642, "Standard Test Method for Density, Absorption, and Voids in Hardened Concrete," ASTM International, West Conshohocken, PA, 2013.

[55] W. Li, M. Pour-Ghaz, J. Castro and J. Weiss, "Water Absorption and Critical Degree of Saturation Relating to Freeze-Thaw Damage in Concrete Pavement Joints," *Journal of Materials in Civil Engineering,* vol. 24, no. 3, pp. 299-307, 2012.

[56] C. L. Lucero, D. P. Bentz, D. S. Hussey, D. L. Jacobson and J. Weiss, "Using Neutron Radiography to Quantify Water Transport and the Degree of Saturation in Entrained Air Cement Based Mortar," *Physics Procedia,* vol. 69, pp. 542-550, 2015.

[57] G. Fagerlund, "The critical degree of saturation method of assessing the freeze/thaw resistance of concrete," *Materials and Structures,* pp. 217-229, 1977.

[58] British Standards Institution, "BS 1881 : Part 208. Reccomendations for the determination of the initial surface absorption of concrete," BSI Publications, London, 1996.

[59] F. R. Montgometry and A. Adams, "Early experience with a new concrete permeability apparatus," in *2nd International Conference on Structural Faults and Repairs*, 1985.

[60] G. D. Henderson, P. A. M. Basheer and A. E. Long, "Pull-Off Test and Permeation Tests," in *Handbook on Nondestructive Testing of Concrete*, 2nd ed., West Conshohocken, PA, CRC Press LLC, 2004, pp. 149-160.

[61] P. A. M. Basheer, "“Clam” Permeability Tests for Assessing the Durability of Concrete," Queen’s University of Belfast, 1991.

[62] NDT James Instruments Inc., *C-P-6000, C-P-6050 Porosiscope Operator’s Manual,* Chicago, IL: James Instruments Inc., 2018.

[63] A. Moczko and M. Moczko, "GWT – New Testing System for “in-situ” Measurements of Concrete Water Permeability," *Procedia Engineering,* vol. 153, pp. 483-489, 2016.

[64] British Standards Institution, "BS EN 12390-8: Testing hardened concrete - Part 8: Depth of penetration of," British Standards Institution, London, 2000.

[65] AASHTO T 259-02, "Standard Method of Test for Resistance of Concrete to Chloride Ion Penetration," American Association of State Highway and Transportation Officials, Washington, D.C., 2012.

[66] ASTM C1556, "Standard Test Method for Determining the Apparent Chloride Diffusion Coefficient of Cementitious Mixtures by Bulk Diffusion," ASTM International, West Conshohocken, PA, 2016.

[67] AASHTO T 277-07, "Standard Method of Test for Electrical Indication of Concrete’s Ability to Resist Chloride Ion Penetration," American Association of State Highway and Transportation Officials, Washington, D.C., 2011.

[68] ASTM C1202, "Standard Test Method for Electrical Indication of Concrete’s Ability to Resist Chloride Ion Penetration," ASTM International, West Conshohocken, PA, 2019.

[69] AASHTO TP 119, "Standard Method of Test for Electrical Resistivity of a Concrete Cylinder Tested in a Uniaxial Resistance Test," American Association of State Highway and Transportation Officials, Washington, D.C., 2015.

[70] ASTM C1876, "Standard Test Method for Bulk Electrical Resistivity or Bulk Conductivity of Concrete," ASTM International, West Conshohocken, PA, 2019.

[71] AASHTO T358, "Standard Method of Test for Surface Resistivity Indication of Concrete's Ability to Resist Chloride Ion Penetration," American Association of State Highway and Transportation Officials, Washington, D.C., 2015.

[72] N. S. Berke, D. W. Pfeifer and T. G. Weil, "Protection against chloride-induced corrosion," *Concrete International,* vol. 10, no. 12, pp. 45-55, 1988.

[73] E. Vivas, A. J. Boyd, H. R. Hamilton and M. Bergin, "Permeability of Concrete – Comparison of Conductivity and Diffusion Methods.," National Technical Information Service, Springfield, VA, 2007.

[74] ASTM C1760, "Standard Test Method for Bulk Electrical Conductivity of Hardened Concrete," ASTM International, West Conshohocken, PA, 2012.

[75] AASHTO PP 84, "Standard Practice for Developing Performance Engineered Concrete Pavement Mixtures," American Association of State Highway and Transportation Officials, Washington, D.C., 2018.

[76] W. Weiss, T. Barrett, C. Qiao and H. Todak, "Toward a Specification for Transport Properties of Concrete Based on the Formation Factor of a Sealed Specimen," *Advances in Civil Engineering Materials,* vol. 5, no. 1, 2016.

[77] K. Snyder, X. Feng, B. Keen and T. Mason, "Estimating the electrical conductivity of cement paste pore solutions from OH-, K+ and Na+ concentrations," *Cement and Concrete Research,* vol. 33, p. 793–798, 2003.

[78] T. J. Barrett, "Improving Service Life of Concrete Structures Through the Use of Internal Curing: Impact on Practice," Purdue University, West Lafayette, IN, 2015.

[79] R. Spragg, Y. Bu, K. Snyder, D. Bentz and J. Weiss, "Electrical Testing of Cement-Based Materials: Role of Testing Techniques, Sample Conditioning, and Accelerated Curing," Publication FHWA/IN/JTRP-2013/28. Joint Transportation Research Program, Indiana Department of Transportation and Purdue University, West Lafayette, Indiana, 2013.

[80] P. Ghosh and Q. Tran, "Correlation Between Bulk and Surface Resistivity of Concrete," *International Journal of Concrete Structures and Materials,* vol. 9, no. 1, pp. 119-132, 2015.

[81] M. K. Moradllo, C. Qiao, B. Isgor, S. Reese and W. J. Weiss, "Relating Formation Factor of Concrete to Water Absorption," *ACI Materials Journal*, vol. 115, no. 6, pp. 887-898, 2018.

[82] U.S. Environmental Protection Agency (EPA), "Construction and Demolition Debris: Material-Specific Data," 21 December 2021. [Online]. Available: https://www.epa.gov/facts-and-figures-about-materials-waste-and-recycling/construction-and-demolition-debris-material#:~:text=Construction%20and%20Demolition%20%28C%26D%29%20debris%20is%20a%20type,clay%20tile%2C%20asphalt%20shingles%2C%20concrete%2C%20and. [Accessed 06 August 2022].

[83] U.S. Environmental Protection Agency (EPA), "Construction and Demolition Debris Generation in the United States, 2015," 2020.

[84] N. Otsuki, S.-i. Miyazato and W. Yodsudjai, "Influence of Recycled Aggregate on Interfacial Transition Zone, Strength, Chloride Penetration and Carbonation of Concrete," *Journal of Materials in Civil Engineering*, vol. 15, no. 5, pp. 443-451, 2003.

[85] Q. Gao, Z. Ma, J. Xiao and F. Li, "Effects of Imposed Damage on the Capillary Water Absorption of Recycled Aggregate Concrete," *Advances in Materials Science and Engineering*, vol. 2018, 2018.

[86] J. Bao, S. Li, P. Zhang, X. Ding, S. Xue, Y. Cui and T. Zhao, "Influence of the incorporation of recycled coarse aggregate on water absorption and chloride penetration into concrete," *Construction and Building Materials*, vol. 239, 2020.

[87] B. Cantero, I. Sáez del Bosque, A. Matías, M. Sánchez de Rojas and C. Medina, "Water transport mechanisms in concretes bearing mixed recycled aggregates," *Cement and Concrete Composites*, vol. 107, 2020.

[88] S. C. Paul, "Data on optimum recycle aggregate content in production of new structural concrete," *Data in Brief*, vol. 15, pp. 987-992, 2017.

[89] C. Faella, C. Lima, E. Martinelli, M. Pepe and R. Realfonzo, "Mechanical and durability performance of sustainable structural concretes: An experimental study," *Cement and Concrete Composites*, vol. 71, pp. 85-96, 2016.

[90] R. Jaskulski, O. A. Waszak and Wojciech Kubissa, "Model for Forecasting the Sorptivity of Concretes with Recycled Concrete Aggregate," *Procedia Engineering*, vol. 153, pp. 240-247, 2016.

[91] R. Kurda, J. d. Brito and J. D. Silvestre, "Water absorption and electrical resistivity of concrete with recycled concrete aggregates and fly ash," *Cement and Concrete Composites,* vol. 95, pp. 169-182, 2019.

[92] V. Corinaldesi and G. Moriconi, "Influence of mineral additions on the performance of 100% recycled aggregate concrete," *Construction and Building Materials,* vol. 23, no. 2869–2876, 2009.

[93] S. Chandra and L. Berntsson, Lightweight aggregate concrete science, technology. and applications, New York: Noyes Publications, 2002.

[94] M. Hornakova, P. Konecny, P. Lehner, J. Katzer, E. Kormaníková, K. Kotrasová and S. Kmeť, "Durability of structural lightweight waste aggregate concrete – electrical resistivity," *MATEC Web of Conferences,* vol. 310, p. 15, 2020.

[95] ASTM C33/C33M − 18, "Standard Specification for Concrete Aggregates," ASTM International, West Conshohocken, PA, 2018.

[96] ASTM C29/C29M − 17a, "Standard Test Method for Bulk Density (“Unit Weight”) and Voids in Aggregate," ASTM International, West Conshohocken, PA, 2017.

[97] ASTM C127 − 15, "Standard Test Method for Relative Density (Specific Gravity) and Absorption of Coarse Aggregate," ASTM International, West Conshohocken, PA, 2015.

[98] ASTM C330/C330M − 17a, "Standard Specification for Lightweight Aggregates for Structural Concrete," ASTM International, West Conshohocken, PA, 2017.

[99] Northeast Solite Corporation, "Solite® (USA)," 2021. [Online]. Available: https://northeastsolite.com/?page_id=831. [Accessed 29 January 2023].

[100] ACI Committee 211, "Standard Practice for Selecting Proportions for Normal, Heavyweight, and Mass Concrete (ACI 211.1-91)," American Concrete Institute, 1991.

[101] ACI Committee 211, "Standard Practice for Selecting Proportions for Structural Lightweight Concrete (ACI 211.2-98)," American Concrete Institute, 1998.

[102] ASTM C143/C143M, "Standard Test Method for Slump of Hydraulic-Cement Concrete," ASTM International, West Conshohocken, PA, 2016.

[103] ASTM C1064/C1064M, "Standard Test Method for Temperature of Freshly Mixed Hydraulic-Cement Concrete," ASTM International, West Conshohocken, PA, 2017.

[104] ASTM C173/C173M, "Standard Test Method for Air Content of Freshly Mixed Concrete by the Volumetric Method," ASTM International, West Conshohocken, PA, 2016.

[105] ASTM C231/C231M, "Standard Test Method for Air Content of Freshly Mixed Concrete by the Pressure Method," ASTM International, West Conshohocken, PA, 2017.

[106] H. Layssi, P. Ghods, A. Alizadeh and M. Salehi, "Electrical Resistivity of Concrete," *Concrete International,* vol. 37, pp. 41-46, 2015.

[107] D. Bentz, "A virtual rapid chloride permeability test," *Cement & Concrete Composites,* vol. 29, p. 723–731, 2007.

[108] ASTM C457/C457M − 16, "Standard Test Method for Microscopical Determination of Parameters of the Air-Void System in Hardened Concrete," ASTM International, West Conshohocken, PA, 2017.

[109] R Core Team, "R: A language and environment for statistical computing," R Foundation for Statistical Computing, Vienna, Austria, 2020. URL https://www.R-project.org/.

[110] D. S. Young, Handbook of Regression Methods, First Edition ed., Boca Raton, FL : Chapman and Hall/CRC, 2017.

[111] J. Fox and S. Weisberg, An {R} Companion to Applied Regression, Third ed., Thousand Oaks, CA: Sage, 2019. URL: https://socialsciences.mcmaster.ca/jfox/Books/Companion/.

[112] A. Hebbali, "olsrr: Tools for Building OLS Regression Models. R package version 0.5.3," 2020. URL: https://CRAN.R-project.org/package=olsrr.

[113] A. Zeileis and T. Hothorn, "Diagnostic Checking in Regression Relationships," *R News,* vol. 2, no. 3, pp. 7-10, 2002. URL https://CRAN.R-project.org/doc/Rnews/.

[114] S. H. Chu, "Effect of paste volume on fresh and hardened properties of concrete," *Construction & building materials,* vol. 218, p. 284–294, 2019.

[115] H. Yiğiter, H. Yazıcı and S. Aydın, "Effects of cement type, water/cement ratio and cement content on sea water resistance of concrete," *Building and Environment,* vol. 42, no. 4, pp. 1770-1776, 2007.

[116] Y. Jiang, S. Liu, B. Li, J. He and A. G. Hernandez, "Effects of aggregate packing optimization and cement paste volume on the properties of natural and recycled aggregate concrete," *Structural Concrete : Journal of the FIB 23,* vol. 23, no. 4, pp. 2260-2273, 2022.

[117] K. G. Trezos, I. P. Sfikas and D. Pavlou, "Water Permeability of Self Compacting Concrete," in *3rd fib International Congress,* 2010.

[118] H. Luan, J. Wu and J. Pan, "Saline water absorption behavior and critical saturation degree of recycled aggregate concrete during freeze-thaw cycles," *Construction & building materials,* vol. 258, p. 119640, 2020.

[119] Z. Liu and W. Hansen, "Effect of hydrophobic surface treatment on freeze-thaw durability of concrete," *Cement and Concrete Composites,* vol. 69, pp. 49-60, 2016.

[120] Y. Wei, Z. Wei, K. Xue, W. Yao, C. Wang and Y. Hong, "Automated detection and segmentation of concrete air voids using zero-angle light source and deep learning," *Automation in Construction,* vol. 130, 2021.

[121] B. Hilloulin, I. Bekrine, E. Schmitt and A. Loukili, "Open-source deep learning-based air-void detection algorithm for concrete microscopic images," *Journal of Microscopy,* vol. 286, no. 2, pp. 179-184, 2022.

[122] U. Jakobsen, C. Pade, N. Thaulow, D. Brown, S. Sahu, O. Magnusson, S. D. Buck and G. D. Schutter, "Automated air void analysis of hardened concrete — a Round Robin study," *Cement and Concrete Research,* vol. 36, no. 8, pp. 1444-1452, 2006.

[123] Z. Zhang, F. Ansari and N. Vitillo, "Automated Determination of Entrained Air-Void Parameters in Hardened Concrete," *ACI Materials Journal,* vol. 102, no. 1, pp. 42-48, 2005.

[124] J. Wawrzeńczyk and W. Kozak, "A Method of Analyzing the Porous Microstructure in Air-Entrained Concrete on the Basis on 2D Image Analysis," *Procedia Engineering,* vol. 108, pp. 102-107, 2015.

[125] P. C. Fonseca and G. W. Scherer, "An image analysis procedure to quantify the air void system of mortar and concrete," *Materials and Structures,* vol. 45, no. 10, pp. 3087-3098, 2015.

[126] J. Mao, K. Ayuta, H. Qi and Z. Liu, "Experimental Study on Freeze-Thaw Damage Mechanism of Lightweight Aggregate Concrete," *Journal of ASTM International,* vol. 7, no. 1, pp. 1-12, 2010.

[127] D. P. Bentz, M. A. Ehlen, C. F. Ferraris and E. J. Garboczi, "Sorptivity-Based Service Life Predictions For Concrete Pavements," in *7th International Society for Concrete Pavements*, Orlando, Florida, 2001.

[128] R. K. Majhi, A. Nayak and B. Mukharjee, "Development of sustainable concrete using recycled coarse aggregate and ground granulated blast furnace slag," *Construction and Building Materials,* vol. 159, pp. 417-430, 2018.

[129] A. M. M. Aragoncillo, D. B. Cleary and G. R. Lomboy, "Estimating the permeability of porous aggregate concretes using electrical resistivity based tests," *Construction and Building Materials,* vol. 364, p. 129909, 2023.

[130] A. M. M. Aragoncillo and G. R. Lomboy, "Correlation of Electrical Resistivity and Formation Factor with Chloride and Water Permeability of Recycled Aggregate Concrete," *Transportation Research Record,* vol. 2676, no. 6, pp. 788-796, 2022.

[131] A. M. Aragoncillo, D. Cleary, U. Thayasivam and G. Lomboy, "Water sorptivity prediction model for concrete with all coarse recycled concrete aggregates," *Construction and Building Materials,* vol. 394, 2023.

Appendix A

Sample Calculation of Coarse Aggregate Properties

Bulk Unit Weight, γ_{bulk}:

$$\gamma_{bulk} = \frac{(G - T)}{V}$$

where:

G = mass of the aggregate plus the measure, kg,

T = mass of the measure, kg, and

V = volume of the measure, m^3

$$\gamma_{bulk} = \frac{(31.88 - 8.32)}{0.0141584} = 1664.03\ kg/m^3 \quad \text{(NWA)}$$

$$\gamma_{bulk} = \frac{(16.68 - 5.42)}{0.0141584} = 795.29\ kg/m^3 \quad \text{(LWA)}$$

$$\gamma_{bulk} = \frac{(23.894 - 5.43)}{0.0141584} = 1303.89\ kg/m^3 \quad \text{(RCA1)}$$

Specific gravity (SG), Absorption, and Porosity:

$$SG = \frac{B}{(B - C)}$$

$$Absorption = \frac{(B - A)}{A} \times 100$$

$$Porosity = \frac{(B - A)}{(B - C)} \times 100$$

where:

A = mass of oven-dry test sample in air, kg,

B = mass of saturated-surface-dry test sample in air, kg, and

C = apparent mass of saturated test sample in water, kg.

$$SG = \frac{6.374}{(6.374 - 4.053)} = 2.746 \quad \text{(NWA)}$$

$$SG = \frac{4.915}{(4.915 - 1.851)} = 1.604 \quad \text{(LWA)}$$

$$SG = \frac{4.949}{(4.949 - 2.877)} = 2.389 \quad \text{(RCA1)}$$

$$Absorption = \frac{(6.374 - 6.36)}{6.36} \times 100 = 0.22\% \quad \text{(NWA)}$$

$$Absorption = \frac{(4.915 - 4.276)}{4.276} \times 100 = 14.94\% \quad \text{(LWA)}$$

$$Absorption = \frac{(4.949 - 4.744)}{4.744} \times 100 = 4.32\% \quad \text{(RCA1)}$$

$$Porosity = \frac{(6.374 - 6.36)}{(6.374 - 4.053)} \times 100 = 0.60\% \quad \text{(NWA)}$$

$$Porosity = \frac{(4.915 - 4.276)}{(4.915 - 1.851)} \times 100 = 20.86\% \quad \text{(LWA)}$$

$$Porosity = \frac{(4.949 - 4.744)}{(4.949 - 2.877)} \times 100 = 9.89\% \quad \text{(RCA1)}$$

Appendix B

Sample Mixture Proportion Designs

0.48-RCA1 Mixture Design:

Water content = 163 kg/m^3 of concrete (for 25mm NMAS & 50mm slump)

Cement content = Water content / (w/c) = 163 / 0.48 = 339.58 kg/m^3 of concrete

Dry bulk volume of CA per unit volume of concrete = 0.67 (for 2.8 FM & 25mm NMAS)

RCA content = $0.67 \times \gamma_{bulk} = 0.67 \times 1303.89 = 873.61$ kg/m^3 of concrete

Water content (Volume) = mass / density = 163 / 1000 = 0.163

Cement content (Volume) = mass / $(SG \times \gamma_{water}) = 339.58 / (3.14 \times 1000) = 0.108$

RCA content (Volume) = mass / $(SG \times \gamma_{water}) = 873.61 / (2.39 \times 1000) = 0.366$

Air content (Volume) = 0.06

FA content (Volume) = 1 – 0.163 – 0.108 – 0.366 – 0.06 = 0.303

FA content = $V \times SG \times \gamma_{water} = 0.303 \times 2.62 \times 1000 = 794.315$ kg/m^3 of concrete

0.48-NWAC Mixture Design:

Water content = 163 kg/m^3 of concrete (for 25mm NMAS & 50mm slump)

Cement content = Water content / (w/c) = 163 / 0.48 = 339.58 kg/m^3 of concrete

Dry bulk volume of CA per unit volume of concrete = 0.67 (for 2.8 FM & 25mm NMAS)

CA content = $0.67 \times \gamma_{bulk} = 0.67 \times 1664.03 = 1114.90$ kg/m^3 of concrete

Water content (Volume) = mass / density = 163 / 1000 = 0.163

Cement content (Volume) = mass / (SG × γ_{water}) = 339.58 / (3.14 × 1000) = 0.108

CA content (Volume) = mass / (SG × γ_{water}) = 1114.90 / (2.75 × 1000) = 0.406

Air content (Volume) = 0.06

FA content (Volume) = 1 – 0.163 – 0.108 – 0.406 – 0.06 = 0.263

FA content = V × SG × γ_{water} = 0.263 × 2.62 × 1000 = 688.65 kg/m^3 of concrete

0.48-LWAC Mixture Design:

Water content = 169.83 kg/m^3 of concrete (for 19mm NMAS & 50mm slump)

Cement content = Water content / (w/c) = 169.83 / 0.48 = 353.80 kg/m^3 of concrete

Dry bulk volume of CA per unit volume of concrete = 0.7 (for 2.8 FM & 19mm NMAS)

LWA content = $0.7 \times \gamma_{bulk} = 0.7 \times 793.55 = 555.49$ kg/m^3 of concrete

First estimate of LWAC weight = 1780 kg/m^3

FA content = 1780 – 169.83 – 353.80 – 555.49 = 700.71 kg/m^3 of concrete

Water content (Volume) = mass / density = 169.83 / 1000 = 0.11

Cement content (Volume) = mass / (SG × γ_{water}) = 353.80 / (3.14 × 1000) = 0.17

LWA content (Volume) = mass / (SG × γ_{water}) = 555.49 / (1.60 × 1000) = 0.35

FA content (Volume) = mass / (SG × γ_{water}) = 700.71 / (2.62 × 1000) = 0.27

Appendix C

Test for Equality of Means in RAC Mixtures

Table C1

Two-Way ANOVA on the Inverse of RAC Mixture's Surface Resistivity (1/SR)

Source of Variation	Df	SS	MS	F	p-value
water-cement ratio	1	0.015191	0.015191	437.05	< 2e-16
RCA variation	7	0.007060	0.001009	29.02	5.08e-15
Interaction (RAC Mixture)	7	0.004520	0.000646	18.58	1.35e-11
Residuals	47	0.001634	0.000035		

Table C2

Two-Way ANOVA on the Inverse of RAC Mixture's Bulk Resistivity (1/BR)

Source of Variation	Df	SS	MS	F	p-value
water-cement ratio	1	0.05561	0.05561	1737.6	< 2e-16
RCA variation	7	0.02322	0.00332	29.02	<2e-16
Interaction (RAC Mixture)	7	0.01104	0.00158	18.58	<2e-16
Residuals	47	0.00150	0.00003		

Table C3

Two-Way ANOVA on GWT Measurements of RAC

Source of Variation	Df	SS	MS	F	p-value
water-cement ratio	1	0.2467	0.24666	18.280	0.000104
RCA variation	7	0.1876	0.02679	1.986	0.079330
Interaction (RAC Mixture)	7	0.3394	0.04848	3.593	0.003937
Residuals	32	0.5802	0.01349		

Table C4

Two-Way ANOVA on RCPT Measurements of RAC

Source of Variation	Df	SS	MS	F	p-value
water-cement ratio	1	51196394	51196394	102.46	1.68e-11
RCA variation	7	57259900	8179986	16.37	5.96e-09
Interaction (RAC Mixture)	7	36400871	5200124	10.41	9.70e-07
Residuals	32	15988906	499653		

Table C5

Two-Way ANOVA on the Sorptivity Measurements of RAC

Source of Variation	Df	SS	MS	F	p-value
water-cement ratio	1	2.1639	2.1639	393.58	< 2e-16
RCA variation	7	2.2425	0.3204	58.27	< 2e-16
Interaction (RAC Mixture)	7	0.7312	0.1045	19.00	9.66e-10
Residuals	32	0.1759	0.0055		

Table C6

Two-Way ANOVA on the Rate of Saturation Values of RAC

Source of Variation	Df	SS	MS	F	p-value
water-cement ratio	1	320.9	320.9	151.299	1.14e-13
RCA variation	7	389.8	55.7	26.255	1.50e-11
Interaction (RAC Mixture)	7	69.6	9.9	4.691	0.00104
Residuals	32	67.9	2.1		

Appendix D

Test for Equality of Means in LWAC, 50LWAC, and NWAC Mixtures

Table D1

Two-Way ANOVA on the LWAC, 50LWAC, and NWAC mixtures' Surface Resistivity (SR)

Source of Variation	Df	SS	MS	F	p-value
water-cement ratio	2	131.2	65.58	258.19	< 2e-16
RCA variation	2	427.1	213.57	840.85	< 2e-16
Interaction (Mixture)	4	18.0	4.49	17.69	3.07e-07
Residuals	27	6.9	0.25		

Table D2

Welch-ANOVA on the LWAC, 50LWAC, and NWAC Mixtures' Bulk Resistivity (BR)

Source of Variation	num df	denom df	F	p-value
Mixture	8.00	10.99	498.24	5.814e-13

Table D3

Two-Way ANOVA on the LWAC, 50LWAC, and NWAC Mixtures' GWT

Source of Variation	Df	SS	MS	F	p-value
water-cement ratio	2	3.128	1.564	5.137	0.0132
RCA variation	2	16.854	8.427	27.681	3.62e-07
Interaction (RAC Mixture)	4	0.849	0.212	0.697	0.6009
Residuals	26	7.915	0.304		

Table D4

Two-Way ANOVA on the LWAC, 50LWAC, and NWAC Mixtures' RCPT

Source of Variation	Df	SS	MS	F	p-value
water-cement ratio	2	27039178	13519589	46.339	7.96e-08
RCA variation	2	55951972	27975986	95.888	2.52e-10
Interaction (RAC Mixture)	4	6244287	1561072	5.351	0.0051
Residuals	18	5251606	291756		

Table D5

Two-Way ANOVA on the Inverse of Sorptivity (1/S) of LWAC, 50LWAC, and NWAC Mixtures

Source of Variation	Df	SS	MS	F	p-value
water-cement ratio	2	20.237	10.119	156.787	< 2e-16
RCA variation	2	9.225	4.613	71.471	< 2e-16
Interaction (RAC Mixture)	4	2.010	0.503	7.787	9.66e-10
Residuals	18	1.162	0.065		

Table D6

Two-Way ANOVA on the LWAC, 50LWAC, and NWAC Mixtures' Rate of Saturation

Source of Variation	Df	SS	MS	F	p-value
water-cement ratio	2	577.7	288.86	220.98	2.15e-13
RCA variation	2	280.2	140.10	107.17	1.01e-10
Interaction (RAC Mixture)	4	284.4	71.10	54.39	8.27e-10
Residuals	18	23.5	1.31		